UNIVERSITÀ DEGLI STUDI DI TRIESTE
e
UNIVERSITÀ CA' FOSCARI DI VENEZIA

XXXI CICLO DEL DOTTORATO DI RICERCA IN CHIMICA

Funded by AIRC5x1000 grant 12214 "Application of Advanced Nanotechnology in the Development of Innovative Cancer Diagnostics Tools"

FLUORESCENT MOLECULARLY IMPRINTED POLYMERS AS SENSORS FOR ANTICANCER DRUGS

CHIM/06 (Chimica Organica)

Ph.D. Student
Martina Tommasini

Ph.D. Program Coordinator
Prof. Barbara Milani

Thesis Supervisor
Prof. Federico Berti

Anno accademico 2017/2018

UNIVERSITÀ DEGLI STUDI DI TRIESTE
e
UNIVERSITÀ CA' FOSCARI DI VENEZIA

XXXI CICLO DEL DOTTORATO DI RICERCA IN CHIMICA

Finanziato da AIRC5x1000 grant 12214 "Application of Advanced Nanotechnology in the Development of Innovative Cancer Diagnostics Tools"

FLUORESCENT MOLECULARLY IMPRINTED POLYMERS AS SENSORS FOR ANTICANCER DRUGS

Settore scientifico-disciplinare: **CHIM/06 (Chimica Organica)**

DOTTORANDA
MARTINA TOMMASINI

COORDINATORE
PROF. BARBARA MILANI

SUPERVISORE DI TESI
PROF. FEDERICO BERTI

ANNO ACCADEMICO 2017/2018

A Gabriele e Giacomo

Man finds God behind every door

that science manages to open.[*]

Albert Einstein

* L'uomo incontra Dio dietro ogni porta

che la scienza riesce ad aprire

Table of Contents

University of Trieste

PhD School in Chemistry (XXXI cycle)

Fluorescent Molecularly Imprinted Polymers as sensors for anticancer drugs

PhD Thesis

PhD candidate: *Martina Tommasini*

Supervisor: *Prof. Federico Berti*

Abstract

Chemotherapy is a medical treatment mainly aimed at damaging solid and haematological tumors, by the administration of specific drugs able to target cancer cells and preventing their proliferation. These drugs, however, often show many secondary effects and present variable inter-individual pharmacokinetics. Hence, the ideal optimization of the therapy would consist of continuously monitoring, in each patient, drug absorption in blood circulation, in order to adjust the daily dose regimen, decreasing therefore its side effects and improving the whole treatment. This methodology is known as Therapeutic Drug Monitoring (TDM), and it can be applied to drugs that meet specific criteria, as a significant inter- or intra-individual pharmacokinetic variability, a narrower therapeutic window and the availability of a defined and accurate method for drug quantification in biological fluids. TDM, indeed, requires the determination of drug concentration in various biological matrix, as blood, plasma, urine or saliva, and interpretation of these concentrations in terms of relevant clinical parameters. The main goal of TDM consists of individualization of therapeutic treatment of the patient.

However, TDM application usually involves the support of specific instrumentations, as HPLC-MS (or HPLC-UV) or LC-MS, that allow to perform an accurate and precise analysis of the samples, but they result time consuming, expensive and require trained personnel. Thanks to the recent technological developments, it is possible to miniaturize all of this, towards the design of specific Point-of-Care (POC) devices, able to perform a rapid quantification of the sample, without requirement of clinical

support. The main advantages of using POC devices are portability, inexpensiveness and easiness to handle, hence to be used directly from patients themselves.

This work is part of the project "*Application of Advanced Nanotechnology in the development of innovative cancer diagnostic tools*", funded by Associazione Italiana Ricerca Cancro (AIRC) and coordinated by Centro di Riferimento Oncologico di Aviano (CRO); one of its aims consists of the development of Point-of-Care devices to be used for the Therapeutic Drug Monitoring of several anticancer drugs, included irinotecan and imatinib.

This thesis project is focused, in particular, on the development of artificial receptors, named Molecularly Imprinted Polymers (MIPs), that can act as sensors for antitumor agents irinotecan and imatinib detection in human plasma samples. MIPs have been prepared by incorporating various fluorescent functional monomers in the polymer matrix, in order to obtain a fluorescent sensor, acting as recognition element and transducer at the same time. Different fluorescent 1,8-naphtalimide and a polymerisable EDANS derivatives have been synthesized; the interactions of these monomers and of fluorescein O-acrylate (commercially available) with each anticancer drug were investigated through NMR experiments. After selection of the best monomer-drug match, several MIPs have been prepared for each target molecule, following a high dilution radical polymerization protocol, and characterized by Dynamic Laser Light Scattering (DLS) and Transmission Electron Microscopy (TEM); nanoparticles with an average diameter of 15 nm were obtained. The MIPs rebinding capacity and specificity were studied through HPLC assays in water, and, exploiting their intrinsic fluorescence properties, it was possible to investigate on their rebinding capabilities in different media, by observing the eventual quenching of fluorescence upon binding.

A MIP designed for irinotecan, in particular, containing a naphtalimide fluorescent dye, showed very promising results, as best specificity in water and an optimal drug sensitivity within its therapeutic concentrations range (17 nM – 17 µM), also in samples of plasma treated with acetonitrile (LOD 9.4 nM with within-run variability 10% and day to day variability 13%).

The best MIP for imatinib, instead, was obtained by incorporation of EDANS fluorophore in the polymeric matrix; at fluorescence measurements, MIP showed both a good specificity and rebinding capacity toward the imatinib in water (LOD of 1.7 µM and within-run variability 4.4%).

Publications:

- Pellizzoni E., Tommasini M., Marangon E., Rizzolio F., Saito G., Benedetti B., Toffoli G., Resmini M., Berti F., Fluorescent molecularly imprinted nanogels for the detection of anticancer drugs in human plasma, Biosensors and Bioelectronics (2016) 86: 913–919

- Tommasini, Martina; Pellizzoni, Elena; Iacuzzi, Valentina; Marangon, Elena; Posocco, Paola; Forzato, Cristina; et al. (2019): Monitoring of Irinotecan in Human Plasma: Sensitive Fluorescent Nanogels by Molecular Imprinting. ChemRxiv. Preprint. https://doi.org/10.26434/chemrxiv.8256695.v1

Università degli Studi di Trieste

Scuola di dottorato in Chimica (XXXI ciclo)

Polimeri fluorescenti ad Imprinting Molecolare come sensori per farmaci antitumorali

Tesi di Dottorato

Dottoranda: *Martina Tommasini*

Relatore: *Prof. Federico Berti*

Riassunto

La chemioterapia è una pratica medica rivolta principalmente a colpire tumori solidi ed ematologici, avvalendosi della somministrazione di specifici farmaci in grado di bersagliare tali cellule tumorali, impedendone la proliferazione. Tali farmaci, tuttavia, presentano spesso numerosi effetti collaterali e possiedono una farmacocinetica inter-individuale molto variabile. Pertanto, l'ideale ottimizzazione della terapia consisterebbe nel poter monitorare continuamente, in ogni singolo paziente, l'assorbimento di tale farmaco nel circolo sanguigno, in modo da aggiustarne quotidianamente la dose, riducendone così gli effetti collaterali e migliorando di conseguenza l'intero trattamento. Tale metodologia è conosciuta come Therapeutic Drug Monitoring (TDM), e può esser applicata a farmaci che soddisfino alcuni specifici criteri, come una significativa variabilità farmacocinetica inter- o intra-individuale, una ristretta finestra terapeutica e la disponibilità di un metodo definito e accurato per la quantificazione del farmaco in fluidi biologici. Il TDM prevede, infatti, la determinazione della concentrazione di farmaco in vari matrici biologiche come sangue, plasma, urina o saliva, e nella conseguente interpretazione di tali valori in termini di parametri clinici rilevanti. Lo scopo finale del TDM consiste nell'individualizzare il più possibile il trattamento terapeutico del paziente.

Tuttavia, l'attuazione del TDM richiede generalmente il supporto di strumenti specifici come l'HPLC-MS (o HPLC-UV) o LC-MS, che permettono di effettuare un'analisi accurata e precisa dei campioni, ma che richiedono tempo, costi e personale formato. Grazie ai recenti sviluppi tecnologici, è possibile miniaturizzare il tutto tramite la

progettazione di specifici dispositivi Point-of-Care (POC), capaci di effettuare una misura rapida del campione, senza la necessità di un supporto clinico. I principali vantaggi nell'utilizzare dispositivi POC consistono nell'essere portatili, poco costosi e facilmente maneggiabili, da potere esser quindi usati direttamente dai pazienti stessi.

Questo lavoro di tesi prende parte al progetto "*Application of Advanced Nanotechnology in the development of innovative cancer diagnostic tools*", finanziato dall'Associazione Italiana Ricerca Cancro (AIRC) e coordinato dal Centro di Riferimento Oncologico di Aviano (CRO); uno degli obiettivi di tale progetto consiste nello sviluppo di dispositivi Point-of-Care da poter utilizzare per il Therapeutic Drug Monitoring di diversi farmaci antitumorali, tra cui l'irinotecano e l'imatinib.

Questo progetto di tesi si è occupato, in particolare, dello sviluppo di specifici recettori artificiali, chiamati polimeri ad imprinting molecolare (MIPs), che possono trovar applicazione come sensori nel rilevare, in campioni di plasma umano, gli antitumorali imatinib ed irinotecano. Tali MIPs sono stati preparati incorporando nella matrice polimerica diversi monomeri funzionali fluorescenti in modo da ottenere un sensore fluorescente, che comprende perciò sia l'elemento di riconoscimento che il trasduttore del segnale. Si sono sintetizzati diversi derivati fluorescenti dell'1,8-naftalimide e un derivato polimerizzabile dell'EDANS; le interazioni di tali monomeri e della fluoresceina O-acrilata (commercialmente disponibile), con ciascun agente antitumorale sono state studiate mediante titolazioni NMR. Dopo aver selezionato le migliori combinazioni monomero-antitumorale, diversi MIPs per ciascun agente chemioterapico sono stati preparati, mediante polimerizzazione radicalica ad alta diluizione, e caratterizzati mediante Dynamic Laser Light Scattering (DLS) e microscopia elettronica a trasmissione (TEM); sono state ottenute nanoparticelle solubili, aventi un diametro medio di 15 nm. La capacità di legame in acqua e la specificità di ciascun polimero sono state determinate mediante test di recupero all'HPLC, e sfruttando le proprietà fluorescenti di ciascun polimero, è stato anche possibile studiarne la capacità di cattura del farmaco osservandone l'eventuale spegnimento della fluorescenza, in diversi solventi o miscele di solventi.

In particolare, un MIP progettato per l'irinotecano e contenente un monomero fluorescente naftalimidico, ha mostrato i risultati più promettenti, ossia la migliore specificità in acqua e un'ottima sensibilità nei confronti del farmaco antitumorale, all'interno del suo intervallo terapeutico di concentrazioni (17 nM – 17 μM), anche in campioni di plasma trattato con acetonitrile (LOD 9.4 nM), con una precisione intra-serie del 10% e inter-serie (riproducibilità) del 13%.

Per l'imatinib, invece, il migliore MIP è stato ottenuto incorporando nella matrice polimerica il fluoroforo EDANS; da misure di fluorescenza, tale polimero ha mostrato sia una buona specificità per l'agente antitumorale, sia una buona capacità di legame alle

concentrazioni terapeutiche dell'imatinib, mostrando in acqua un LOD pari a 1.7 µM ed una precisione intra-serie del 4.4%.

Pubblicazioni:

- Pellizzoni E., Tommasini M., Marangon E., Rizzolio F., Saito G., Benedetti B., Toffoli G., Resmini M., Berti F., *Fluorescent molecularly imprinted nanogels for the detection of anticancer drugs in human plasma*, Biosensors and Bioelectronics (2016) 86: 913–919

- Tommasini, Martina; Pellizzoni, Elena; Iacuzzi, Valentina; Marangon, Elena; Posocco, Paola; Forzato, Cristina; et al. (2019*): Monitoring of Irinotecan in Human Plasma: Sensitive Fluorescent Nanogels by Molecular Imprinting*. ChemRxiv. Preprint. https://doi.org/10.26434/chemrxiv.8256695.v1

List of Abbreviations

AA	Acrylamide
Abl	Abelson kinase
AIBN	azobisisobutyronitrile
Accn	Acetonitrile
AFM	Atomic Force Microscopy
AIRC	Associazione Italiana Ricerca Cancro
a.u.	arbitrary unit
ATP	Adenosine triphosphate
Boc	Ter-Butilossicarbonile
BPO	Benzoylperoxide
C_m	Critical monomer concentration
CML	Chronic myeloid leukemia
CPT	Camptothecin
CRO	Centro di Riferimento Oncologico
DCM	Dichloromethane
DLS (or DLLS)	Dynamic Laser Light SCattering
DMF	Dimethylformamide
DMSO	Dimethyl sulfoxide
DMSO-d_6	Deuterated Dimethyl sulfoxide
DPV	Differential pulse voltammetry
DVB	Divinylbenezene
EBA	N,N'-ethylenebisacrylamide
EDTA	Ethylene diaminetetraacetic acid
EGDMA	Ethylene glycol dimethacrylate
Et_3N	Triethylamine
EtOH	Ethanol
ESI-MS	Electronspary Ionization Mass Spectrometry
FDA	Food and Drug Administration
GIST	Gastrointestinal stromal tumors

HPLC	High-performance Liquid Cromatography
HPLC-MS	High-performance Liquid Chromatography coupled to Mass detection
HPLC-UV	High-performance liquid chromatography coupled to ultraviolet
KPS	Potassium persulfate
MAA	Methacrylic acid
MBA	N,N'-methylenebisacrylamide
MALDI MS	Matrix-assisted laser desorption/ionization Mass Spectrometry
MeOH	Methanol
NIPAM	N-Isopropylacrylamide
LC–ESI–MS/MS	Liquid chromatography electrospray-tandem mass spectrometry
LC-MS/MS	Liquid chromatography-tandem mass spectrometry
LOD	Limit of Detection
LOQ	Limit of Quantification
MIP	Molecularly Imprinted Polymer
MISPE	Molecularly Imprinted Solid Phase Extraction
NIP	Non Imprinted Polymer
nm	nanometers
NMR	Nuclear Magnetic Resonance
PDA	Photodiode array
PDI	PolyDispersion Index
PETA	Pentaerythritol triacrylate
POC	Point of Care
PTK	Protein Tyrosine Kinase
SERS	Surface Enhanced Raman Spectroscopy
SPE	selective solid-phase extraction
SPR	Surface Plasmon Resonance
TDM	Therapeutic Drug Monitoring
TEM	Transmission Electron Microscopy
TFA	Trifluoroacetic acid
THF	Tetrahydrofuran
TLC	Thin Layer Chromatography

TRIM	Trimethylpropane trimethacrylate
UDP	Uridine DiPhosphate
VEGF	Vascular Endothelial Growth Factor

1. Introduction

1.1 Target molecules

Irinotecan

Irinotecan (CPT11, Camptosar®, **Scheme 1.1a**) is a chemotherapeutic drug mainly used for the treatment of colon-rectal and advanced pancreatic cancer. It is a synthetic analogue of the natural pentacyclic alkaloid camptothecin (CPT).[1,2] It is a prodrug as it undergoes enzymatic cleavage of the bispiperidino-side chain by carboxylesterase to form 7-ethyl-10-hydroxycamptothecin (SN-38, **Scheme 1.1b**), a potent inhibitor of Topoisomerase I, an enzyme involved in DNA replication. SN-38 is 100- to 1000-fold more cytotoxic than irinotecan, and its exposure is highly variable.[3]

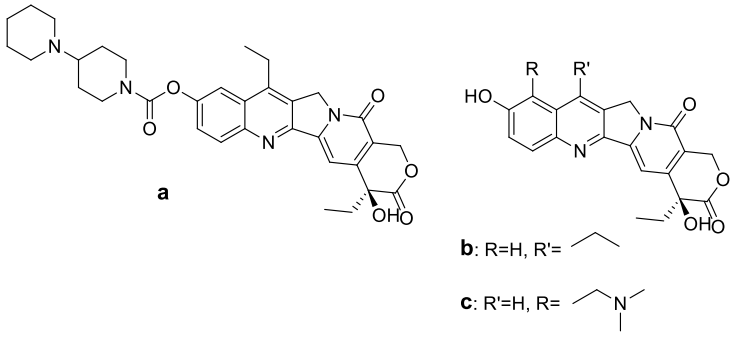

Scheme 1.1: Chemical structure of irinotecan (**a**), its active metabolite SN-28 (**b**) and topotecan (**c**).

History

Irinotecan belongs to a class of cytotoxic alkaloid compounds named Camptothecins (CPT), first isolated from extracts of the Chinese tree *Captotheca acuminata* by Wall and co-workers in the 1960s; these molecules showed an interesting antitumor activity against leukemia.[4] Since camptothecin is insoluble in water, it was converted to its ring-opened carboxylate sodium salt; in the early 1970s phase I trials were carried out with this water soluble salt, but unfortunately, this form caused many toxic effects and seemed to decrease its anticancer activity, leading to discontinuance of phase II trials. However, the interest in camptothecin was improved in 1985, when it was discovered its capability to inhibit the enzyme Topoisomerase I,[5] involved in DNA overwinding or underwinding, during transcription, replication and other nuclear processes.

Many camptothecins derivatives have been prepared in the last decades, mostly keeping intact the lactone, after the discover in 1980 by Wani et Wall, that

camptothecin was about ten-fold more potent than the carboxylate sodium salt in antitumor assay, confirming that lactone is a crucial structural feature for the anticancer activity.[6]

In 1989 Giovanella et al found that camptothecin and some of its derivatives showed anticancer activity against advanced human colon cancer xenografts in nude mice;[7] since then, two groups of camptothecins were led to the clinical trials: the water-soluble and the water insoluble compounds. The first group included Irinotecan and topotecan (**Scheme 1.1c**), both commercially available and administered intravenously. The water insoluble compounds, instead, included camptothecin and two semisynthetic derivatives: 9-aminocamptothecin and its pro-drug 9-nitrocamptothecin, which were orally administered.[7]

At present, FDA has been approved (from 1996) two topoisomerase I inhibitors as second-line agents for the treatment of ovarian carcinoma and colorectal cancer: the water soluble compounds topotecan and irinotecan (**Scheme 1.1**). Topotecan has been shown to be active in the treatment of Myelodysplastic Syndrome (MDS) and inactive in the treatment of Chronic Lymphocytic Leukemia (CLL). Responses to topotecan have also been seen in refractory multiple myeloma, refractory acute leukemia, and refractory large-cell lymphoma. The lactone forms of topotecan and SN-38 (the active form of irinotecan) are as much as 1000-fold more active inhibitors of DNA topoisomerase I than are their carboxylate forms.[7]

Chemistry

Camptothecin (**Scheme 1.2**) has a pentacyclic structure that includes a pyrrolo[3,4-b]quinolone moiety (rings A, B and C), and a six-membered lactone (ring E) with an α–hydroxyl group,[8] containing an α-hydroxy-gamma-lactone moiety (ring E), which is the main responsible of the antitumor activity.[9] In aqueous solutions this lactone ring undergoes reversible hydrolysis to the less active carboxylate form. This reaction is pH dependent: at equilibrium the lactone form is predominant at acidic pH, the ring opened form, instead, is mainly present at neutral and alkaline conditions.[1] Substitutions at the level of rings A and B do not affect either the extent or the rate of this reaction in aqueous solutions,[10] and under physiological conditions (at pH 7.4 and 37 °C) 50% conversion of many camptothecin analogues to the corresponding carboxylates occurs in 10-20 min.[11,12] This fast lactone hydrolysis has been attributed to the α-hydroxyl group, which is believed to accelerate this reaction through intermolecular hydrogen bonding.[13] To overcome this drawback that favours the not biologically active carboxylate, during the last decades, many structural modifications of camptothecins were made aimed to get more stable-ring analogues, as 20-deoxycamptothecins or 21-lactam camptothecins. Unfortunately, the absence of the C-

20 hydroxyl group resulted in a total loss of activity in vitro and in vivo.[14,15] This suggested that a ring-opening reaction is involved in the interaction between CPT and Topoisomerase I, and consequence of lactonolysis reaction is that continuous interchange of the two forms happens in vivo.[16]

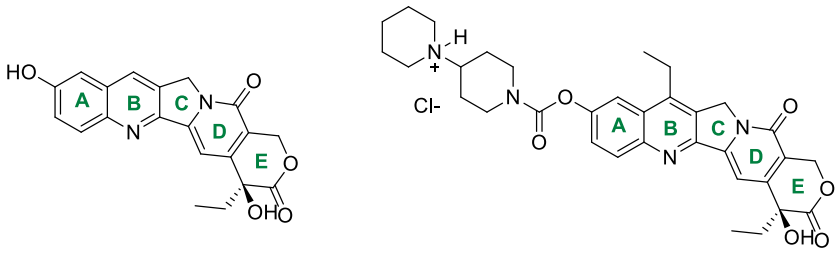

Scheme 1.2: Chemical structure of camptothecin (left) and irinotecan hydrochloride salt (right).

Irinotecan is a water soluble derivative of camptothecin, that was first prepared in 1991 by Sawada et al. by bonding the hydroxyl phenolic group of 7-ethyl-10-hydroxy campothecin with a bispiperidino moiety through a carbamate linkage; its antitumor activity was evaluated in vivo and an excellent result was obtained against L-1210 leukemia and other murine tumors.[17]

Another important structural feature of irinotecan is the stereogenic center in ring E at position 20 with S configuration; natural form of camptothecin, the 20(S) isomer, is the active form against Topoisomerase I enzyme, whilst the 20(R) isomer does not show any antitumor activity.[15] Irinotecan is also a very fluorescent molecule, thanks to the high conjugation of its chromophores; when excited at 368 nm, an emission band is observed at 426 nm (in water). The fluorescence intensity is dependent on the pH; it increases with pH until it reaches a maximum between pH 3 and 7. At higher values of pH fluorescence intensity decreases and it completely disappears at strongly basic pH (pH 13). From pH 10, irinotecan hydrolysis process occurs.[18]

Mechanism of action

Camptothecins are cytotoxic molecules able to inhibit the enzyme Topoisomerase I. Topoisomerases are a group of enzymes responsible for solving the complex topological problems encountered during DNA processing (replication, transcription).[19] Topoisomerase I is in particular involved in the unwinding of DNA supercoiling that foregoes the advancing replication fork. This relaxation is carried out by nicking a single strand of DNA duplex, rotation of one strand and religation. This enzyme-single strand intermediate, also known as “cleavable” complex, is generally a transient species because religation then occurs fast. Camptothecins react with a subset of these intermediates and not with Topo I or DNA alone.[20] The camptothecin binding to the

transient intermediate leads to a stable complex, and since the stabilized complex features single-stand discontinuities, the advancing replication fork is arrested and double-stranded DNA breaks are generated (**Figure 1.1**).[20] It is also suspected that the generated DNA fragments are able to recombine at other sites of the arrested fork, leading to illegitimate recombination.[21] Irinotecan and its active metabolite SN-38 both stabilize the "cleavable" complex, although the activity of the metabolite is greater than the relative pro-drug.

It remains unknown if the arrest of the replication fork is in itself a sufficient damage that induces cell death or if illegitimate recombination in vital genes is also required. In any case, the formation of persistent double-strand breaks by themselves could represent a lethal lesion.[22]

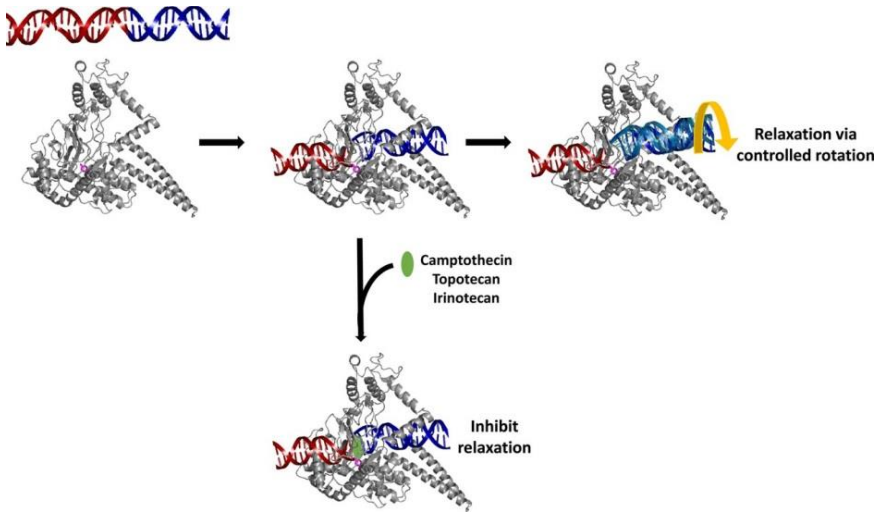

Figure 1.1: DNA relaxation reaction catalysed by human Topoisomerase 1 and the effect of camptothecins.[23]

Pharmacokinetic and pharmacodynamics

Irinotecan is administered intravenously as Camptosar® formulation, which is supplied as a sterile aqueous solution. One milliliter of the solution contains 20 mg of irinotecan hydrochloride (on the basis of the trihydrate salt), 45 mg of sorbitol, NF, and 0.9 mg of lactic acid, USP. The pH of the solution has to be adjusted to 3.5 (range, 3.0 to 3.8) with sodium hydroxide or hydrochloric acid.[24]

The therapeutic concentrations of irinotecan usually found in human plasma are within the range 10-10000 μgL^{-1} (17 nM – 17 µM).[25]

As already mentioned, at physiological pH the lactone-ring of irinotecan and SN-38 can be hydrolysed to the carboxylate form. In plasma the carboxylate form of irinotecan and the lactone-form of SN-28 dominate. Conversion of irinotecan lactone to carboxylate within the circulation is rapid, with an initial half-life of between 9 and 14 min, which results in a 50% reduction in irinotecan lactone concentration after 2.5 hours, compared with end of infusion (66 vs. 35%).[26]

After drug infusion ends, a rapid decrease of irinotecan plasma concentrations is observed; peak concentrations of SN-38 are reached within 2 hours after infusion.[27] In plasma, most part of irinotecan and SN-38 is bound to albumin, which has a stronger binding capacity for the more hydrophobic active metabolite; albumin also stabilizes the lactone forms of irinotecan and SN-38.[28]

In blood, SN-38 is almost completely bound, with two/thirds located in platelets and, predominantly, red blood cells. Various population pharmacokinetic models of irinotecan have been developed. All models confirmed the large inter-individual variability in pharmacokinetic parameters of approximately 30%. A mean SN-38 distribution half-life was estimated to be very short (approximately 8 minutes).[13]

Irinotecan metabolism is highly complex because many enzymes and transporters are involved; several phase I and II enzymes, including cytochrome P450 (CYP) 3A4 and uridine diphosphate glucuronosyltransferase (UGT) 1A, form inactive metabolites, making its metabolism prone to environmental and genetic influences. Patient characteristics, lifestyle and the concomitant use of other drugs also influence irinotecan pharmacokinetics. Other factors, including dietary restriction, are currently being studied.[3]

Elimination of irinotecan is mainly biliary (66%) and dose independent. All metabolites, except SN-38G, are largely excreted in faeces, although they are also detectable in urine.[29] However the wide inter-individual variability in irinotecan clearance is still not completely understood.

Irinotecan in known for its dose-limiting adverse effects; diarrhoea and myelosuppression are the most clinically significant and common toxicities of this drug.[30] Two types of diarrhoea caused by irinotecan can be distinguished: early- and late-onset diarrhoea. The early-onset one starts during, or immediately after, drug infusion and is often part of an acute cholinergic syndrome that includes diaphoresis and abdominal pain.[3] With the aid of premedication, by administration of anticholinergic agents (as atropine), the incidence of this syndrome is reduced from 70% to 9%, before irinotecan infusion.[31] Late-onset diarrhoea appears approximately 8-10 days after drug infusion and is characterized by a more severe course; it is

recommended to treat the late-onset diarrhoea with loperamide or, alternatively, octreotide.[32]

Irinotecan is efficient in a wide range of cancers; it is mainly used in the treatment of metastatic colon rectal cancer (mCRC) as monotherapy or within combination therapy. It is also used in the treatment of small cell lung cancer (SCLC) and non-SCLC, combined with other chemotherapeutic agents. Furthermore, irinotecan has demonstrated anticancer activity in phase II trials in a wide range of other solid tumors (i.e. mesothelioma, glioblastoma, gynaecological cancers, and head and neck cancer), although no phase III data are available.[3]

Imatinib

Imatinib (commercially available as Gleevec® or Glivec®) is a competitive inhibitor of specific tyrosine kinases, used for the treatment of chronic myeloid leukemia (CML), gastrointestinal stromal tumors (GISTs) and other malignant pathologies.[33,34] Chemically, imatinib is 4-[(4-methyl-1-piperazinyl)methyl]-N-[4-methyl-3-[[4-(3-pyrimidinyl)-2-pyrimidinyl]amino]-phenyl]benzamide (**Scheme 1.3**).

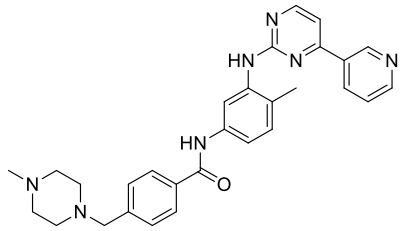

Scheme 1.3: Chemical structure of the anticancer agent imatinib.

History

Imatinib was prepared by rational drug design in 1990 by a scientists team of Ciba-Geigy (which merged with Sandoz in 1996 to become Novartis), headed by the biochemist Nicholas Lydon, and its activity against chronic myeloid leukemia (CML) was studied by Brian Druker, an oncologist who led the clinical trials confirming its efficacy in CML.[35] The first clinical trials of imatinib took place in 1998 and the drug was approved by FDA in 2001. Lydon, Druker, and other colleagues were awarded in 2009 for "converting a fatal cancer into a manageable condition" and the Japan Prize in 2012 for their part in "the development of a new therapeutic drug targeting cancer-specific molecules." Encouraged by the success of Imatinib in treating CML patients, scientists

explored its effect in other cancers and it was found to produce a similar impressive effect in other cancers where tyrosine kinases were overexpressed.[36]

Chemistry

Imatinib is a 2-phenyl amino pyrimidine derivative. Under physiological conditions (at 37 °C, pH 7.4) imatinib exists predominantly in its neutral and mono-protonated form (33%). Protonation occurs at the piperazine nitrogen atom N7, bound to the methyl group (**Scheme 1.4**).[37] Lin and co-workers[38] studied the specific imatinib binding to the Abelson tyrosine kinase; they reported that the drug carries a net positive charge in the bound complex, allowing to interact through hydrogen-bonding with the backbone carbonyl of specific residues (Ile360 and His361) of the kinase.

Imatinib can add up to four protons, according to the acidity of the medium; the sequence of protonation is the following: N7 (pKa 7.7), N1 (pKa 3.9), N6 (pKa 3.1), N4 (pKa 1.7), as determined by potentiometric and NMR titrations.[39]

As Imatinib base is insoluble in water, it is orally administered as mesylate salt form.

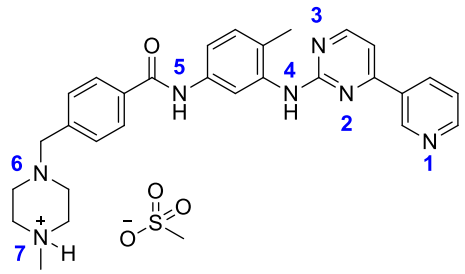

Scheme 1.4: Chemical structure of imatinib mesylate.

Mechanism of action

Protein kinases are a large family of homologous proteins comprising two significant subfamilies, the protein serine/threonine kinases and protein tyrosine kinases (PTKs). Protein kinases are components of signal transduction pathways, playing a central role in various biological processes such as control of cell growth, metabolism, differentiation, and apoptosis.[40] During early development, imatinib was named STI57, where STI stands for “Signal Transduction Inhibitor” and represented the drug ability to inhibit enzymes PTKs.[35]

Tyrosine kinases have an active site for ATP binding; they modify other proteins by transferring a phosphate group from ATP to a tyrosine sidechain, resulting in a functional change of the target protein and a cellular signal. Irregular kinase activity can lead to excessive cell division and cause many forms of cancer, such as chronic myeloid leukemia, where the kinase Abelson (Abl) is improperly activated.[41] Imatinib mesylate selectively inhibits BCR-ABL (BCR: breakpoint cluster), ABL1, Abl2, and other kinases including KIT, a receptor tyrosine kinase that imatinib targets for the treatment of gastrointestinal stromal tumor.[42]

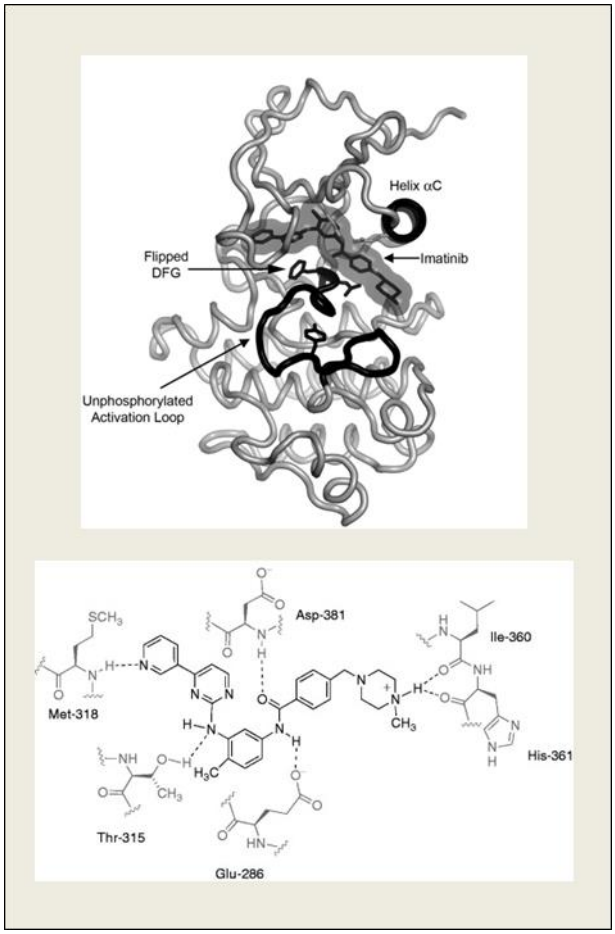

Figure 1.2: Crystal structure of the kinase domain of Abl1 in complex with imatinib (top)[1]; Abl1 binding site residues involved in the interaction with imatinib (bottom).[41]

Kuriyan and coworkers,[43] using X-ray crystallography, found that imatinib binds to an inactive conformation of Abl1. It binds in the cleft between the amino- and carboxy-terminal lobes of the kinase domain; the pyridine and pyrimidine moieties are found in the site where the adenine base of ATP normally binds. The rest of the compound instead penetrates into the hydrophobic core of the kinase, between the activation loop and αC helix, keeping the kinase in an inactive conformation.[44] Overall, imatinib establishes six hydrogen bond contacts (**Figure 1.2**), with a large number of complementary van der Waals interactions. The fact that imatinib binds to an unusual conformation of the kinase may explain its high selectivity.[45]

Recent steady-state kinetic studies indicated that imatinib is a competitive inhibitor of ATP,[46] which is consistent with the X-ray studies showing that the drug binds to the ATP-binding site.

Pharmacokinetic and pharmacodynamics

Imatinib mesylate is administered orally and the recommended dose ranges between 400 and 800 mg daily. After oral intake, the drug is rapidly adsorbed from the gut, because of its rapid dissolution at acidic pH. After repeated administration of 400 mg of imatinib per day, the mean plasma concentration in steady state is ≥1 $\mu molL^{-1}$ after 24 hours.[47] Imatinib is highly bound to proteins (approximately 95%) and mostly binds to albumin.[48]

The drug is metabolized by the cytochrome P450 (CYP) isoenzymes in the gut wall and liver; the main metabolite is the N-demethylated piperazine derivative, which has potency comparable to that of the parent compound.[47]

On average, 75% of imatinib dose undergoes biotransformation; fecal elimination takes place via the bile, 68% as metabolites and 20% as parent compound. Renal elimination instead is low, as only 13% of metabolites and 5% of parent compound are excreted via kidneys. The main secondary effects of imatinib are mild nausea, vomiting, edema, muscle cramps, liver dysfunction and bone marrow toxicity.[47]

The level of 1000 $ngmL^{-1}$ was established as the minimal concentration value threshold to predict molecular response.[49]

---

[1] Hahna R.Z., Arnhold P.C., Andriguetti N.B., Schneider A., Klück H.M., dos Reis S.L., Bastiani M.F., Kael I., Cezimbra da Silva A.C., Schwartsmann G., Antunes Marina V., Linden R., *Determination of irinotecan and its metabolite SN-38 in dried bloodspots using high-performance liquid-chromatography with fluorescence detection*, J. of Pharm. and Biomed. Anal. (2018) 150: 51–58

[2] Rivory L.P., Robert J., *Molecular, cellular, and clinical aspects of the pharmacology of 20(S)Camptothecin and its derivatives*, Pharmac. Ther. (1995) 68(2): 269-296

[3] De Man F.M., Goey A.K.L., van Schaik R.H.N., Mathijssen R.H.J., Bins S., *Individualization of Irinotecan Treatment: A Review of Pharmacokinetics, Pharmacodynamics, and Pharmacogenetics*, Clin. Pharmacokin. (2018) 57:1229–1254

[4] Wall M.E., Wani M.C., Cook C.E., Palmer K.H., McPhail A.T., Sim G.A., *Plant Antitumor Agents. The Isolation and Structure of Camptothecin, a Novel Alkaloidal Leukemia and Tumor Inhibitor from Camptotheca acuminate*, J. of the Am. Chem. Soc. (1966) 86: 16

[5] Hsiang Y.H., Hertzberg R., Hecht S., Liu L.F., *Camptothecin induces protein-linked DNA breaks via mammalian DNA topoisomerase I*, J Biol Chem (1985) 260 (27): 14873-8

[6] Wall M.E., *Alkaloids with antitumor activity*, International Symposium on Biochemistry and Physiology of the Alkaloids (1969), Berlin: Academic-Verlag 77–87

[7] Giovanella B.C., Stehlin J.S., Wall M.E., Wani M.C., Nicholas A.W., Liu L.F., Silber R., Potmesil M., *DNA topoisomerase I--targeted chemotherapy of human colon cancer in xenografts*, Science (1989) 24, 246 (4933): 1046-8

[8] Cao Z., Harris N., Kozielski A., Vardeman D., Stehlin J. S., and Giovanella B., *Alkyl Esters of Camptothecin and 9-Nitrocamptothecin: Synthesis, in Vitro Pharmacokinetics, Toxicity, and Antitumor Activity*, J. Med. Chem. (1998) 41, 31-37

[9] Wani M.C., Ronman P.E., Lindley J. T., and Wall M. E., *Plant Antitumor Agents. 18.1 Synthesis and Biological Activity of Camptothecin Analogues*, J. Med. Chem. (1980) 23, 554-560

[10] Fassberg J., Stella V.J., *A kinetic and mechanistic study of the hydrolysis of camptothecin and some analogues*, J. Pharm. Sci. (1992) 81(7): 676-84

[11] Mi Z., Burke T.G., *Differential interactions of camptothecin lactone and carboxylate forms with human blood components*, Biochemistry (1994) 30, 33(34): 10325-36

[12] Scott D.O., Bindra D.S., Stella V.J., *Plasma pharmacokinetics of the lactone and carboxylate forms of 20(S)-camptothecin in anesthetized rats*, Pharm. Res. (1993) 10: 1451-1457

[13] Bom D., Curran D.P., Chavan A.J., Kruszewski S., Zimmer S.G., Fraley K.A., and Burke T.G., *Novel A,B,E-Ring-Modified Camptothecins Displaying High Lipophilicity and Markedly Improved Human Blood Stabilities*, J. Med. Chem. (1999) 42, 16: 3018–3022

[14] Jaxel C., Kohn K.W., Wani M.C., Wall M.E., Pommier Y., *Structure- activity study of the actions of camptothecin derivatives on mammalian topoisomerase I. Evidence for a specific receptor site and relation to antitumor activity*, Cancer Res. (1989) 49: 1465-1469

[15] Wall M.E., Wani M .C., *Antineoplastic agents from plants*, Ann. Rev. Pharmacol. Toxicol. (1977) 17: 117-132

[16] Tobin P., Rivory L., Clarke S., *Inhibition of acetylcholinesterase in patients receiving irinotecan (camptothecin-11)*, Pharmacology and Therapeutics (2004) 76(5): 505-506

[17] Sawada S1, Okajima S, Aiyama R, Nokata K, Furuta T, Yokokura T, Sugino E, Yamaguchi K, Miyasaka T., *Synthesis and antitumor activity of 20(S)-camptothecin derivatives: carbamate-linked, water-soluble derivatives of 7-ethyl-10-hydroxycamptothecin*, Chem Pharm Bull Tokyo (1991) 39(6):1446-50

[18] M.I. Rodriguez Caceres, Duran-Meras I., Ornelas Soto N.E., Lopez de Alba P.L., Lopez Martinez L., *Spectrofluorimetric determination of irinotecan in the presence of oxidant agents and metal ions*, Talanta (2008) 74: 1484–1491

[19] Rivory L.P., *Irinotecan (CPT-11): a brief overview*, Clin. Exp. Pharm. Physiol. (1996) 23: 1000-1004

[20] Hsiang Y-H, Lihou MG, Liu LF., *Arrest of replication forks by drug-stabilized topoisomerase I-DNA cleavable complexes as a mechanism of cell killing by camptothecin*, Cancer Res. (1989) 49:5077-82

[21] Christiansen K., Dirac Svejstrup A.B., Andersen A.H., Westergaard O., *Eukaryotic topoisomerase I-mediated cleavage requires bipartite DNA interaction. Cleavage of DNA substrates containing strand interruptions implicates a role for topoisomerase I in illegitimate recombination*, J. Biol. Chem. (1993) 268: 9690-9701

[22] Ryan A. J., Squires S., Strutt H.L., Johnson R.T., *Camptothecin cytotoxicity in mammalian cells is associated with the induction of persistent double strand breaks in replicating DNA*, Nucl. Acids Res. (1991) 19: 3295-3300

[23] Delgado J.L., Hsieh C.M., Chan N.L., Hiasa H., *Topoisomerases as anticancer targets*, Biochem. J. (2018) 475(2): 373-398

[24] From RxList: https://www.rxlist.com/camptosar-inj-drug.htm#description

[25] Marangon E., Posocco B., Mazzega E., Toffoli G., *Development and Validation of a High-Performance Liquid Chromatography– Tandem Mass Spectrometry Method for the Simultaneous Determination of Irinotecan and Its Main Metabolites in Human Plasma and Its Application in a Clinical Pharmacokinetic Study*, Pone (2015) DOI:10.1371/journal.pone.0118194

[26] Rivory LP, Chatelut E, Canal P, Mathieu-Boue A, Robert J., *Kinetics of the in vivo interconversion of the carboxylate and lactone forms of irinotecan (CPT-11) and of its metabolite SN-38 in patients*, Cancer Res. (1994) 54(24): 6330–6333

[27] Sasaki Y, Yoshida Y, Sudoh K, Hakusui H, Fujii H, Ohtsu T, et al., *Pharmacological correlation between total drug concentration and lactones of CPT-11 and SN-38 in patients treated with CPT-11*, Jpn J Cancer Res. (1995) 86(1): 111–116

[28] Burke T.G., Mi Z., *The structural basis of camptothecin interactions with human serum albumin: impact on drug stability*, J. Med Chem. (1994) 37(1): 40–46

[29] Xie R, Mathijssen RH, Sparreboom A, Verweij J, Karlsson M.O., *Clinical pharmacokinetics of irinotecan and its metabolites: a population analysis*, J Clin Oncol. (2002) 20(15): 3293–3301

[30] Rothenberg M.L., *Irinotecan (CPT-11): Recent Developments and Future Directions–Colorectal Cancer and Beyond*, The Oncologist (2001) 6: 66-80

[31] Yumuk P.F., Aydin S.Z., Dane F., Gumus M., Ekenel M., Aliustaoglu M., et al., *The absence of early diarrhea with atropine premedication during irinotecan therapy in metastatic colorectal patients*, Int. J. Colorectal Dis. (2004) 19(6): 609–610

[32] Peterson D.E., Bensadoun R.J., Roila F., Group EGW, *Management of oral and gastrointestinal mucositis: ESMO. Clinical Practice Guidelines*, *Ann. Oncol*. (2011) 22(6): 78–84

[33] Capdeville R., Buchdunger E., Zimmermann J., Matter A., *Glivec (STI571, imatinib), a rationally developed, targeted anticancer drug*, Nat Rev Drug Discov. (2002) 1(7): 493-502

[34] Demetri G.D., von Mehren M., Blanke C.D., Van den Abbeele A.D., Eisenberg B., Roberts P.J., Heinrich M.C., Tuveson D.A., Singer S., Janicek M., Fletcher J.A., Silverman S.G., Silberman S.L., Capdeville R., Kiese B., Peng B., Dimitrijevic S., Druker B.J., Corless C., Fletcher C.D., Joensuu H., *Efficacy and safety of imatinib mesylate in advanced gastrointestinal stromal tumors*, N. Engl. J. Med. (2002) 15, 347(7):472-480

[35] Iram H., Iram F., Husain A., *A Review on Imatinib: A wonder drug in Oncology*, Adv. Biomed. Pharma. (2016) 3(4): 227-244

[36] Iqbal N., *Imatinib: A Breakthrough of Targeted Therapy in Cancer*, Chemother. Res. and Pract. (2014) 1-9

[37] Grante I., Actins A., Orola L., *Protonation effects on the UV/Vis absorption spectra of imatinib: A theoretical and experimental study*, Spectrochim. Acta Part A: Mol. and Biomol. Spectr. (2014) 129: 326–332

[38] Lin Y.L., Meng Y., Jiang W., and Roux B., *Explaining why Gleevec is a specific and potent inhibitor of Abl kinase*, PNAS (2013) 110 (5): 1664–1669

[39] Szakács Z., Béni S., Varga Z., Örfi L., Kéri G., and Noszál B., *Acid–Base Profiling of Imatinib (Gleevec) and Its Fragments*, J. Med. Chem. (2005) 48(1): 249–255

[40] Druker B.J., Lydon N.B., *Lessons learned from the development of an Abl tyrosine kinase inhibitor for chronic myelogenous leukemia*, J Clin Invest. (2000) 105(1): 3-7

[41] Aleksandrov A., Simonson T., *A Molecular Mechanics Model for Imatinib and Imatinib:Kinase Binding*, J. Comput. Chem. (2010) 31: 1550–1560

[42] Salah E., Ugochukwu E., Barr A.J., von Delft F., Knapp S., and Elkins J.M., *Crystal Structures of ABL-Related Gene (ABL2) in Complex with Imatinib, Tozasertib (VX-680), and a Type I Inhibitor of the Triazole Carbothioamide Class*, J. Med. Chem. (2011) 54 (7): 2359–2367

[43] Schindler T., Bornmann W., Pellicena P., Miller W.T., Clarkson B., Kuriyan J., *Structural Mechanism for STI-571 Inhibition of Abelson Tyrosine Kinase*, Science (2000) 289 (5486): 1938-1942

[44] Roskoski Jr. R., *STI-571: an anticancer protein-tyrosine kinase inhibitor*, Biochemical and Biophysical Research Communications (2003) 309(4): 709–717

[45] Avendaño C., Menéndez J.C, *Drugs That Inhibit Signalling Pathways for Tumor Cell Growth and Proliferation*, Med. Chem. of Anticancer Drugs (2008), Chapter 9: 271-272.

[46] Cowan-Jacob S.W., Guez V., Fendrich G., Fabbro D., Furet P., Liebetanz J., Mestan J., Manley P.W., *Imatinib (STI571) resistance in chronic myelogenous leukemia: molecular basis of the underlying mechanisms and potential strategies for treatment*, Mini Rev. Med. Chem. (2004) 4(3): 285-99.

[47] De Kogel C.E., Schellens J.H.M., *Imatinib*, The Oncologist (2007) 12: 1390–1394

[48] Peng B., Lloyd P., Schran H., *Clinical pharmacokinetics of imatinib*, Clin. Pharmacokinet. (2005) 44(9): 879-94

[49] Picard S., Titier K., Etienne G., Teilhet E., Ducint D., Bernard M.A., Lassalle R., Marit G., Reiffers J., Begaud B., Moore N., Molimard M., Mahon F.X., *Trough imatinib plasma levels are associated with both cytogenetic and molecular responses to standard-dose imatinib in chronic myeloid leukemia*, Blood (2007) 109(8): 3496-3499

1.2 Therapeutic Drug Monitoring

Therapeutic drug monitoring (TDM) is generally defined as "the clinical laboratory measurement of a chemical parameter that, with appropriate medical interpretation, will directly influence drug prescribing procedures". TDM involves the quantification of drug concentrations in various biological fluids, as blood, urine or saliva, and interpretation of these concentrations in terms of relevant clinical parameters. The main goal of this process is to individualize therapeutic regimens for optimal patient benefit.[1]

Therapeutic Drug Monitoring has been developed since the early 1960s, when a new aspect of this science was introduced with the publication of pharmacokinetic studies linking mathematical theories to patients outcomes. Pioneers of drug monitoring in the 1970s focused on adverse drug reactions and demonstrated clearly that by constructing therapeutic ranges, the incidence of toxicity to drugs such as digoxin, phenytoin, lithium, and theophylline could be reduced.[2]

TDM is limited to a small fraction of available drugs, that should satisfy several criteria: presence of significant inter- or intra-individual pharmacokinetic variability, existence of a defined relationship between drug concentration and pharmacological (toxic or therapeutic) effects, a narrow therapeutic window, and the availability of a defined and accurate method for drug quantification in biological fluids.[3]

TDM can be and has been successfully applied to optimize anticancer treatments.[4] Despite some limitations can restrict the clinical value of TDM for antineoplastic agents, as imperfect understanding of pharmacology and pharmacokinetics of some antitumor drugs, potential benefits are related to TDM of cancer chemotherapy: improving therapy efficacy and avoid toxicities, minimization of pharmacokinetic variability among patients, dose adjustment and detection of drug interactions.[3] Anticancer agents, indeed, satisfy the criteria of TDM and defining a therapeutic range for efficacy concentrations and toxicity concentrations would have enormous clinical utility.

The appropriate application of TDM to antineoplastic agents requires a correct administration of drug, correct collection and processing of blood samples, precise and accurate measurement of drug or active metabolite concentration, and appropriate interpretation of results. This whole multidisciplinary process involves skills and knowledge of different professionals, including scientists (as clinical chemists), pharmacists, nurses, technicians, and physicians.[5]

As an intervention method, TDM implicates to improve patient responses to important life-sustaining drugs and to decrease adverse drug reactions.[3] Furthermore, the resources consumed by TDM methods will likely be regained by positive outcomes, including decreased hospitalizations, and thus TDM is an appropriate candidate for an economic outcomes evaluation.[1]

TDM for irinotecan and imatinib

Rousselot et al.[6] demonstrated the efficacy of TDM for the optimization of daily doses of imatinib in patients with chronic myeloid leukemia (CML); monitoring the minimal imatinib concentration levels by chromatography-tandem mass-mass spectrometry, it came out that only one-third of patients treated with the standard 400 mg per day were correctly dosed and may not require systematic higher doses. On the contrary, two-thirds of the patients were not exposed enough to imatinib at standard dose and may benefit from individualized strategies. A dose adjustment based on pharmacology resulted in higher major molecular response rate at 12 months (63% vs 37%), a magnitude in line with the results previously reported with second generation tyrosine kinase inhibitors or high dose imatinib front line. A cost-effectiveness analysis of Therapeutic Drug Monitoring of generic imatinib for the treatment of CML was performed by Salamone *et al.*,[7] comparing first-line imatinib TDM versus first-line imatinib alone in terms of costs, quality-adjusted life-years (QALYs), and cost-effectiveness. The model found that imatinib TDM dominates imatinib alone with $15,452 to $36,940 in savings and 0.25 higher QALYs. Therefore imatinib TDM is both a clinically and economically practicable first-line treatment option for CML.

The level of evidence for imatinib TDM is classified between potentially useful and recommended.[8] Monitoring the plasma level of imatinib may help to optimize therapy, reduce the cost of treating CML and GIST and improve population health.[9]

Irinotecan could be a good candidate for TDM, because of the occurrence of side effects due to the large interpatient variability in drug metabolism. Furthermore, pharmacogenetics studies clearly identified a functional polymorphism in the UGT1A1 gene (UDP glucuronosyltransferase 1A1 catalyses the clearance of the active metabolite SN-38 of irinotecan) which significantly impacts on the incidence of toxicities in patients. These findings led the FDA to include a recommendation to UGT1A1 genetic testing; this test should be used by clinicians to identify patients with the risk to suffer from severe toxicities, who must therefore be treated with lower starting irinotecan doses.[10] However FDA did not included specific dosing recommendations, therefore limiting the use of this genetic test.[11] Irinotecan preliminary studies suggest that TDM approaches may be beneficial, but further investigations need to be carried out.

Practical issues to perform TDM[8]

The currently preferred analytical method for measuring concentrations of irinotecan and imatinib in biological fluids are the rapid and efficient liquid chromatography-tandem mass spectrometry (LC-MS/MS)[12,13] and liquid chromatography electrospray-tandem mass spectrometry (LC–ESI–MS/MS).[14] High-performance liquid chromatography coupled to ultraviolet (HPLC-UV)[15] or mass detections (HPLC-MS)[16] can also constitute an alternative for laboratories not equipped with the more sophisticated and expensive LC-MS/MS. Recently, also MALDI mass spectrometry has been applied to TDM of imatinib and other anticancer agents.[17,18,19] All these techniques, however, are time consuming, expensive, require bulky instrument and trained personnel. The financial costs related to instrumental operation and maintenance, and the time required for the preparation and analysis of samples, for processing the results, severely affects the application of TDM in medical practices.[20] Technological developments towards the miniaturisation of monitoring tests and their delivery at point-of-care represent a future approach to make TDM in cancer more feasible.

---

[1] Kang J.S., Lee M.H., *Overview of Therapeutic Drug Monitoring*, The Kor. J. of Int. Med. (2009) 24(1): 1-10

[2] Tange S.M., Grey V.L., Senecal P.E., *Therapeutic drug monitoring in pediatrics: a need for improvement*, J. Clin. Pharmacol. (1994) 34: 200-214

[3] Alnaim L., *Therapeutic drug monitoring of cancer chemotherapy*, J.Oncol. Pharm. Practice (2007) 13: 207-221

[4] Galpin A.J., Evans W.E., *Therapeutic Drug Monitoring in Cancer Management*, Clin. Chem. (1993) 39, 11(B): 2419-2430

[5] Reynolds D.J.M, Aronson J.K., *Making the most of plasma drug concentration measurements*, Br. Med. J. (1993), 306: 48-51

[6] Rousselot P. et al, *Personalized Daily Doses of Imatinib By Therapeutic Drug Monitoring Increase the Rates of Molecular Responses in Patients with Chronic Myeloid Leukemia. Final Results of the Randomized OPTIM Imatinib Study*, Blood (2015) 126(23): 133

[7] Salamone S., Becker R., Padula W. and Conti R.M., *The Cost-Effectiveness of Therapeutic Drug Monitoring (TDM) of Generic Imatinib for the Treatment of Chronic Myelogenous Leukemia*, Blood (2017) 130: 4701

[8] Widmer N., Bardin C., Chatelut E., Paci A., Beijeng J., Leveque D., Veal G., Astier A., *Review of therapeutic drug monitoring of anticancer drugs part two – Targeted therapies*, Eur. J. of Cancer (2014) 50: 2020–2036

[9] Guilhot F., Hughes T.P., Cortes J., Druker B.J., Baccarani M., Gathmann I., Hayes M., Granvil C., Wang Y., *Plasma exposure of imatinib and its correlation with clinical response in the Tyrosine Kinase Inhibitor Optimization and Selectivity Trial*, Haematologica (2012) 97(5): 731-738

[10] Paci A., Veal G., Bardin C., Leveque D., Widmer N., Beijnen J., Astier A., Chatelut E., *Review of therapeutic drug monitoring of anticancer drugs part 1 – Cytotoxics*, Eur. J. of Cancer (2014) 50: 2010–2019

[11] Clinically Available Pharmacogenomics Tests at https://doi.org/10.1038/clpt.2009.39

[12] Haouala A., Zanolari B., Rochat B., et al., *Therapeutic drug monitoring of the new targeted anticancer agents imatinib, nilotinib, dasatinib, sunitinib, sorafenib and lapatinib by LC tandem mass spectrometry*, J. Chromatogr. B. Analyt. Technol. Biomed. Life Sci. (2009) 877: 1982–1996

[13] Marangon E., Posocco B., Mazzega E., Toffoli G., *Development and Validation of a High-Performance Liquid Chromatography–Tandem Mass Spectrometry Method for the Simultaneous Determination of Irinotecan and Its Main Metabolites in Human Plasma and Its Application in a Clinical Pharmacokinetic Study*, PLoS ONE (2015) 10(2): e0118194

[14] Negreira N., Mastroianni N., López de Alda M., Barceló D., *Multianalyte determination of 24 cytostatics and metabolites by liquid chromatography–electrospray–tandem mass spectrometry and study of their stability and optimum storage conditions in aqueous solution*, Talanta (2013) 116: 290–299

[15] Guetens G., Prenen H., De Boeck G., van Oosterom A., Schoffski P., Highley M., de Bruijn E.A., *Simultaneous determination of AMN107 and Imatinib (Gleevec®, Glivec®, STI571) in cultured tumour cells using an isocratic high-performance liquid chromatography procedure with UV detection*, J. Chromatogr. B (2007) 846: 341–345

[16] De Francia S., D'Avolio A., De Martino F., Pirro E., Baietto L., Siccardi M., Simiele M., Racca S., Saglio G., Di Carlo F., Di Perri G., *New HPLC–MS method for the simultaneous quantification of the antileukemia drugs imatinib, dasatinib, and nilotinib in human plasma*, J. Chromatogr. B (2009) 877: 1721–1726

[17] D'Aronco S., Dall'Armi M., Crotti S., Calandra E., Traldi P., Di Marco V., Buonadonna A., Corona G., Giodini L., Marangon E., Posocco B., Toffoli G., Agostini M., *Field-assisted paper spray mass spectrometry for therapeutic drug monitoring: 1. the case of imatinib in plasma*, J. Mass Spectrom. (2017) 52(5): 283-289

[18] D'Aronco S., Calandra E., Crotti S., Toffoli G., Marangon E., Posocco B., Traldi P., Agostini M., *Field-assisted paper spray mass spectrometry for the quantitative evaluation of imatinib levels in plasma*, Eur. J. Mass Spectrom. (Chichester) (2016) 22(5): 217-228

[19] D'Aronco S, D'Angelo E., Crotti S., Traldi P., Agostini M., *New Mass Spectrometric Approaches for the Quantitative Evaluation of Anticancer Drug Levels in Treated Patients*, Ther. Drug Monit. (2019) 41(1): 1-10

[20] Polo F., Toffoli G., *Point-of-Care for Therapeutic Drug Monitoring of Antineoplastic Drugs*, Med. Chem. (Los Angeles) (2016) 6: 6

1.3 Sensors and Point-Of-Care devices

Sensors and Biosensors

A sensor is a device whose purpose is to detect events or changes in its environment and send the information to other electronics, usually a computer processor. It is constituted by three items: a recognition element, a transducer and a data processor, as a computer or smartphone (**Figure 1.3**).[1]

A chemical sensor is a tool able to provide real-time analytical information, usually the concentration, of a test sample. The target species is commonly named *analyte*. First, the analyte interacts with the recognition (or sensing) element, which shows affinity for the target molecule. As a result of this interaction, certain physical or chemical properties of the sensing element vary as a function of the analyte concentration. In order to allow the user to assess this variation, a chemical sensor converts the above change into a measurable physical quantity. This process is called signal transduction (or simply transduction) or signalling. The sensing element and the transducer can be distinct components packaged together, in direct spatial contact, in the same unit or, as in certain types of chemical sensor, no physical distinction between the sensing element and the transducer occurs.[2]

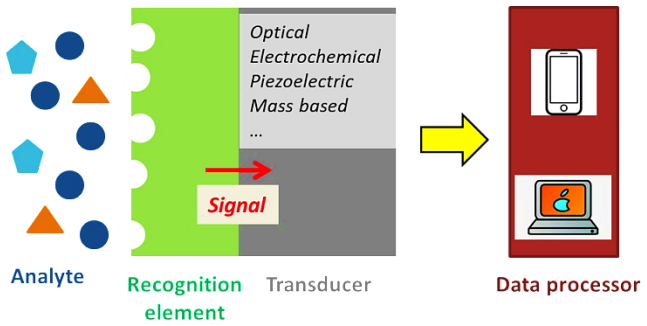

Figure 1.3: General scheme of a sensor.

A biosensor is a bioanalytical device incorporating a biological element (as antibodies, enzymes, nucleic acids, peptides) associated with or integrated within a physicochemical transducer or transducing microsystems, which can be optical, thermometric, electrochemical, piezoelectric or magnetic.[3] Biosensors have been applied in many fields namely food industry, medical field, environment and marine sector etc., and they provide better stability and sensitivity as compared with the traditional methods.[4]

The process of analyte recognition usually occurs by affinity interactions, which involve reversible multiple binding of two chemical species through non covalent bonds, such as hydrogen bonds, ionic bonds, and van der Waals interactions. The product of an affinity interaction is a molecular association complex. In order for such a complex to form, the involved species should be complementary with respect to shape and chemical reactivity.[2]

Examples of biosensors for irinotecan detection have been developed by some research groups involved in our same project funded by *AIRC*. Alvau *et al.*[5] described an enzymatic biosensor able to quantify irinotecan (**Figure 1.4**); this biosensor is based on acetylcholine esterase (AChE), an enzyme involved in neuromuscular junction, and choline oxidase (ChOx). Acetylcholine (ACh) substrate is converted to choline, which is subsequently metabolized by ChOx to give betaine aldehyde and hydrogen peroxide. The latter one is then oxidized at a suitably polarized platinum electrode, providing a current transient proportional to the amount of ACh. This process is hindered by irinotecan. The biosensor showed a about 60% of maximal inhibition toward AChE activity within the irinotecan therapeutic concentration range 10–10 000 ngmL^{-1} in both phosphate buffer and fetal bovine serum matrix.

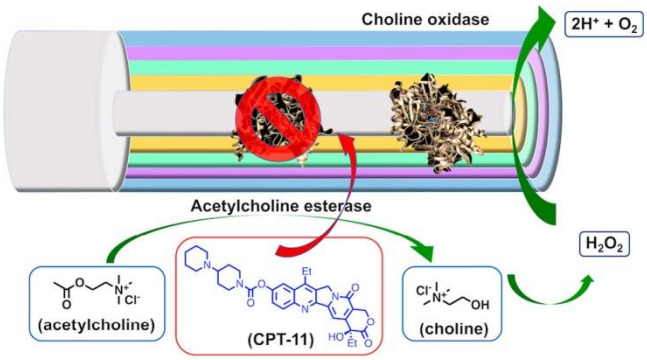

Figure 1.4: Schematic representation of the enzymatic biosensor for irinotecan developed by Alvau *et al*.5

A very sensitive electrochemical sensor was developed for imatinib detection in spiked human urine samples;[6] the anticancer drug was oxidized on anodically pretreated boron doped diamond electrode (BDDE), and using differential pulse voltammetry (DPV), a well-shaped oxidation peak was obtained at positive potential, at pH 2. The results showed a limit of detection (LOD) of 6.3×10^{-9}mol L^{-1}and a limit of quantification (LOQ) of 2.1 × 10^{-8}mol L^{-1}.

Point-of-care (POC) devices

Point-of-Care (POC) systems are considered as integrated systems that can process clinical samples in a variety of settings, such as clinical laboratories, doctors' offices and eventually, at home. Basically, POC systems make state-of-the-art technology platforms accessible to a large population pool. The development of POC technologies will provide opportunities for better screening of at-risk patients, tighter surveillance of disease recurrence and better monitoring of treatment, particularly in cancer therapies. Finally POC technologies are low cost in their implementation making large scale screening for disease prevention more attractive to health care insurers.[3]

When all the data are collected by this tiny device, in a few minutes the patient can decide either by himself or by immediate communication with a specialist or medical doctor, which action is required, with everything done at home or even in the field without requiring any kind of medical knowledge by the user. POC devices are portable, easy-to-use, and able to monitor several parameters and variables similar to a portable laboratory; these are the main advantages of the POC technology.[7]

POC devices are used for prevention, control of disease outbreaks, and monitoring of health conditions in remote areas or non-laboratory settings, where lack of professional technicians and sophisticated laboratory infrastructures reduces the healthcare parameters.[3]

Nowadays, some portable devices that can monitor and diagnose the condition of the user are already available. A well-known example is the glucose meter (**Figure 1.5**), which with a few microliters of blood, can determine the glucose concentration in the sample and notify the diabetes patient if there is any action required, such as the injection of insulin or the intake of food. Probably, the most popular POC devices are optical- or electrochemical-based; with the development of nanotechnology many types of devices exploit the advantages of nanomaterials by integrating them in different parts of existing sensing platforms or offering quite innovative detection system.[7]

Figure 5: Two examples of commercially available point of care devices; left: the electrochemical-based glucose meter; right: *iBreastExam*, a handle, mobile connected device which can detect

tumour tissues as small as 3-5 mm while emitting no harmful radiation (developed by the startup UE LifeSciences and already approved by FDA).[8]

Point of Care devices in cancer research

There has been a significant technological progress in POC devices in recent years and new categories of POC devices have been introduced.[9] Most of the Point-of-Care devices developed for cancer are aimed at diagnosis or early prognosis of the disease. Various point-of-care approaches such as lab-on-chip, lateral flow assays and electrochemical test strips have been assessed.[10] In particular, strategies using nano-sized biosensor technology have shown great results for early prognosis and diagnosis of cancer; the advanced nano-scaled sensors can achieve higher sensitivity, specificity and multiplexing for complete elucidation of stage and type of cancer.[11] The identification and detection of biomarkers related to a specific cancer can help in early diagnosis and monitoring disease progression. Biomarkers are molecules which undergo prominent alterations during cancer; they may be nucleic acids, metabolites, proteins, isoenzymes and hormones, and are classified as diagnostic, prognostic and predictive. Diagnostic biomarkers are related to the detection of the disease, prognostic biomarkers offer information about the course of recurrence of the disease, and predictive biomarkers estimate the response to treatment.[12]

Biosensor-based point-of-care monitoring can aid cancer management and facilitate earlier diagnosis. The systems developed are numerous, mostly on simple detection, although there are few platforms for multiplex analysis. The detection limits achieved range between femto- and nano-scales, depending on the biosensor components used; antigen- and antibody-based biological systems are generally preferred due to the high specificity of antibody-antigen interactions.[13]

For example, Stern *et al*.[14] developed a label-free nanosensor to detect from whole blood the prostate-specific antigen (PSA) and carbohydrate antigen 15.3 (CA15.3), that are standard clinical diagnostic biomarkers for prostate and breast cancer, respectively. Thanks to a microfluidic purification chip multiple biomarkers can be captured simultaneously from blood samples using specific antibodies, and released, after washing, into purified buffer for sensing by a silicon nanoribbon detector. This two-stage approach isolated the detector from the complex environment of whole blood, and reduced its minimum required sensitivity by pre-concentrating the biomarkers. They demonstrated specific and quantitative detection of the two model cancer antigens from a 10 μL sample of whole blood in less than 20 minutes. The portability and versatility of this method can suggest its application in POC technology.

An aptasensor (**Figure 1.6**) based on carbon–gold nanocomposite-modified screen-printed electrode has been recently fabricated for the detection of vascular endothelial growth factor (VEGF165) in the serum of patients with lung cancer.[15] The electrochemical behaviour of the biosensor was investigated by cyclic voltammetry and electrochemical impedance spectroscopy. The aptasensor principle of operation is based on the changes in the interfacial properties of the electrode due to interaction of the immobilized antiVEGF165aptamer at the electrode surface with VEGF165 tumor marker in the sample solution, which results in a change in the interfacial charge transfer resistance as detected by electrochemical impedance spectroscopy. The calibration curve for VEGF165 determination was linear over 10.0–300.0 $pgmL^{-1}$ with a limit of detection of 1.0 $pgmL^{-1}$. The prepared aptasensor exhibited high sensitivity, good selectivity and reproducibility.

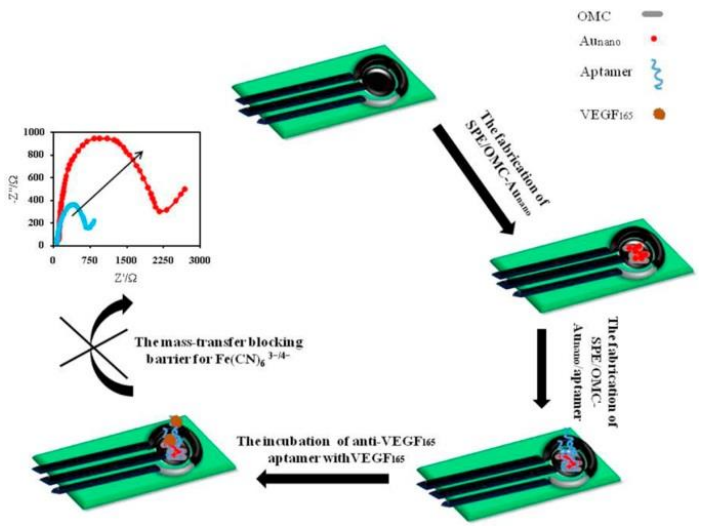

Figure 1.6: Schematic illustration of fabrication and sensing mechanism of aptasensor proposed by Tabrizia *et al*.15

Point-of-Care devices for TDM application

Very few examples report the use of sensors for the TDM application, and almost none are ready for POC testing (except for the glucose sensor, even though it may not be strictly considered a TDM sensor).[16]

One example is the multi-channel portable device developed by Zhao *et al*.[17] for monitoring the anticancer drug methotrexate in clinical samples by SPR (Surface Plasmon Resonance). In the assay, the human dihydrofolate reductase (hDHFR, which is inhibited by methotrexate) was immobilized on the SPR sensor chip and constituted the

bioreceptor; a competition test was then performed between folic acid-functionalized gold nanoparticles (FA-AuNP) and methotrexate (**Figure 1.7**). The results obtained for human plasma samples were in good agreement with fluorescence polarization immunoassay and LC-MS/MS.

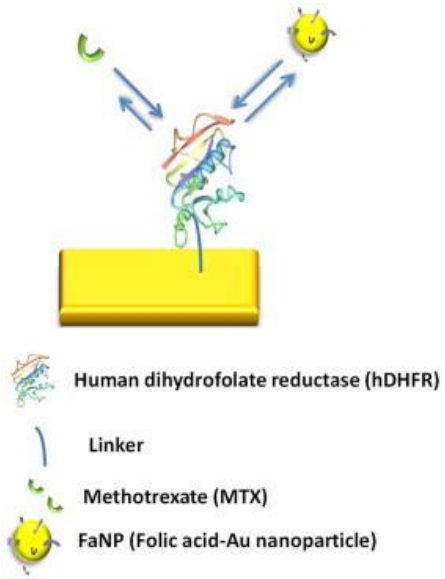

Figure 1.7: Schematic illustration of the SPR competitive assay for methotrexate detection.

Another example of a point-of-care device for therapeutic drug monitoring of the antiepileptic drug phenytoin was developed by Huang and co-workers;[18] a miniaturized and electrically measured piezoresistive microcantilever biosensor was integrated into a microfluidic channel with a system for label-free detection. The phenytoin detection by the biosensor was tested in water and fetal bovine serum; The concentration sensitivity was 2.94×10^{-6} ($\mu g mL^{-1}$) and the calculated binding affinity (K_D) resulted equal to 58 $\mu g mL^{-1}$. The results showed a solid correlation of phenytoin drug detection with that in the clinically used fluorescence polarization immunoassay (FPIA).

[1] Janata J., Bezegh A., *Chemical sensors*, Anal. Chem. (1988) 60 (12): 62–74

[2] Banica F.G., *Chemical Sensors and Biosensors. Fundamentals and Applications*, Wiley (2012), ISBN 978-0-470-71066-1

[3] Soper S.A. et al., *Point-of-care biosensor systems for cancer diagnostics/prognostics*, Biosensors and Bioelectronics (2006) 21: 1932–1942

[4] Mehrotra P, *Biosensors and their applications – A review*, J. of Biol. and Craniofacial Res. (2016) 6: 153-159

[5] Alvau M.D., Tartaggia S., Meneghello A., Casetta B., Calia G., Serra P.A., Polo F., Toffoli G., *Enzyme-Based Electrochemical Biosensor for Therapeutic Drug Monitoring of Anticancer Drug Irinotecan*, Anal. Chem. (2018) 90 (10): 6012–6019

[6] Brycht M., Kaczmarska K., Uslu B., Ozkan S.A., Skrzypek S., *Sensitive determination of anticancer drug imatinib in spiked human urine samples by differential pulse voltammetry on anodically pretreatedboron-doped diamond electrode*, Diamond & Related Materials (2016) 68: 13–22

[7] Quesada-Gonzalez D., Merkoçi A., *Nanomaterial-based devices for point-of-care diagnostic applications*, Chem. Soc. Rev. (2018) 47: 4697-4709

[8] Broach R.B., Geha R., Englander B.S., DeLaCruz L., Thrash H., Brooks A.D., *A cost-effective handheld breast scanner for use in low-resource environments: a validation study*, World J. Surg. Oncol. (2016) 14: 277

[9] Zarei M., *Portable biosensing devices for point-of-care diagnostics: Recent developments and applications*, Trends in Analytical Chemistry (2017) 91: 26-41

[10] Campbell J.M., Balhoff J.B., Landwehr G.M., Rahman S.M., Vaithiyanathan M., Melvin A.T., *Microfluidic and paper-based devices for disease detection and diagnostic research*, Int. J. Mol. Sci. (2018) 19, E2731.

[11] Shandilya R., Bhargava A., Bunkar N., Tiwari R., Goryachev I.Y., Mishra P.K., *Nanobiosensors: Point-of-care approaches for cancer diagnostics*, Biosens. and Bioelectr. (2019) 130: 147–165

[12] Sankara Aditya Jayanthi V.S.P.K., Bikas Das A., Saxena U., *Recent advances in biosensor development for the detection of cancer biomarkers*, Biosensors and Bioelectronics (2017) 91: 15–23

[13] Siontorou C.G., Nikoleli G.P.D., Nikolelis D.P., Karapetis S., Tzamtzis N., Bratakou S., *Point-of-Care and Implantable Biosensors in Cancer Research and Diagnosis*, Next Generation Point-of-care Biomedical Sensors Technologies for Cancer Diagnosis, DOI 10.1007/978-981-10-4726-8_5

[14] Stern E., Vacic A., Rajan N.K., Criscione J.M., Park J.,. Ilic B.R., Mooney D.J., Reed M.A., Fahmy T.M., *Label-free biomarker detection from whole blood*, Nature Nanotechnol. (2010) 5(2): 138–142

[15] Tabrizia M.A., Shamsipura M., Farzin L., *A high sensitive electrochemical aptasensor for the determination of VEGF165 in serum of lung cancer patient*, Biosensors and Bioelectronics (2015) 74: 764–769

[16] Polo F., Toffoli G., *Point-of-Care for Therapeutic Drug Monitoring of Antineoplastic Drugs*, Med. Chem. (Los Angeles) (2016) 6 (6)

[17] Zhao S.S., Bukar N., Toulouse J.L., Pelechacz D., Robitaille R., Pelletier J.N., Masson J.F., *Miniature multi-channel SPR instrument for methotrexate monitoring in clinical samples*, Biosens Bioelectron. (2015) 64: 664-670

[18] Huang L.S., Pheanpanitporn Y., Yen Y.K, Chang K.F, Lin L.Y., Lai D.M., *Detection of the antiepileptic drug phenytoin using a single free-standing piezoresistive microcantilever for therapeutic drug monitoring*, Biosens. And Bioelectr. (2014) 59: 233–238

1.4 Molecularly Imprinted Technology

Molecular recognition plays an important role in any biochemical process. It is fascinating how nature controls complex, specific and selective interactions such as substrate-enzyme, antigen-antibody or hormone-receptor, leading to an attractive interest in mimicking these natural processes and reproduce them artificially.

Molecular imprinting allows to easily obtain artificial receptors; in 1972 Wulff and Sarhan introduced the technique of molecular imprinting, using enzyme-analogous polymer matrix for the resolution of racemates.[1] This technique achieved scientific breakthrough in the early 1980s thanks to the work developed by the research group of Wulff, Shea and Mosbach, who were among the first to underline the role and utility of organic polymer networks acting as matrices for molecular imprinting. The field of research of molecular imprinting has been rapidly growing and is still of increasing interest, thanks to its wide application fields, as enzyme mimicking catalysis, imprinted membranes, sensor devices, antibody mimicking pseudo-immunoassays and drug delivery.[2] Furthermore, selective separation using MIP as stationary phases includes liquid chromatography (LC),[3] capillary electro-chromatography (CEC),[4] and molecularly imprinted solid phase extraction (MISPE).[5]

The main advantages of using Molecularly imprinted polymers (MIPs) are long-term stability, the ability to work under harsh conditions, as high temperature, extreme pH values, and in the presence of organic solvents, and the economical reagents and procedure necessary for their synthesis.

Fundamentals of molecular imprinting

The general idea behind molecular imprinting involves the creation of selective recognition sites for a target molecule (template), within a synthetic polymer network. The recognition process in molecular imprinting may be considered as the analogue of the mechanism found in enzyme-substrate complexes, the “lock-and-key” principle of Fischer (**Figure 1.8**).[6] Before starting the molecularly imprinted polymer (MIP) synthesis, it is necessary to select specific functional monomers, which are responsible for the introduction of complementary functionality into the polymer matrix. It is important that these functional monomers are able to bind the template molecule trough non-covalent or covalent interactions, establishing the formation of the so-called pre-polymerization complex. To keep this tri-dimensional arrangement, the pre-polymerization complex is then copolymerized with a great amount of cross-linker,

which provides the polymer backbone. After the polymerization, the template is removed in order to get a highly cross-linked matrix containing binding cavities complementary in terms of size and shape to the template molecule, and available for selective rebinding.

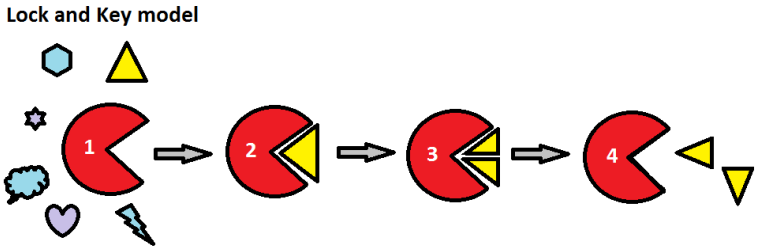

Figure 1.8: Schematic representation of Fischer's Lock and Key model.

There are two general approaches for preparing MIPs, based on the type of interactions between the functional monomers and the template molecule, during the formation of the pre-polymerization complex: the non-covalent and covalent approaches. In addition, some derivatives of these approaches have been reported in the literature, as the semi-covalent process.

Mosbach *et al.*[7] have introduced the non-covalent approach (also known as self-assembly approach, **Figure 1.9**), which resembles the mechanism of molecular recognition present in nature. This process provides formation of the self-assembled complex, obtained towards non-covalent weak interactions established between the template and the functional monomers, as hydrogen bonding, electrostatic interactions, van der Waals forces and hydrophobic interactions (e.g. π-π stacking). Within the pre-polymerization solution the functional monomer is usually introduced in molar excess compared to the template molecule,[8] because non-covalent interactions only provide weak binding strengths. According to the principle of Le Chatelier, the equilibrium is therefore shifted toward the formation of the pre-polymerization complex. On the other side, the probability of generating non-selective binding sites caused by an excess of functional monomers randomly incorporated into the polymer matrix, and which are not associated with the template, is increased.[9] In general, the non-covalent approach is the mainly used technique, because it does not require synthetic steps toward the pre-polymerization complex, the template removal is much easier, typically achieved by continuous extraction by dialysis or Soxhlet, and a greater variety of functional groups can be introduced in the MIP binding sites.[10]

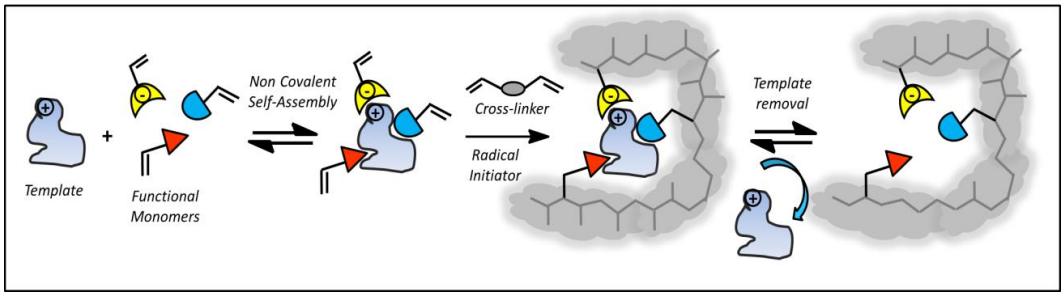

Figure 1.9: Schematic illustration of non-covalent imprinting approach.

The covalent imprinting approach (also known as pre-organized approach, **Figure 1.10**), first realized by Wulff and Sarhan,[11] provides the formation of the pre-polymerization complex toward covalent bonds between the template and functional monomers; after polymerization occurs, these bonds must be cleaved to remove the template from the binding pocket. The rebinding of the template then occurs by re-establishing this covalent bond, or by non-covalent interactions. In this latter case the approach is known as the "semi-covalent" process, a combination of the covalent and non-covalent approaches, developed by Sellergren and Andersson.[12] The main advantage of the covalent imprinting consists of the stoichiometric interactions between template and functional monomer, which provide a narrower affinity distribution of the binding sites, reducing the non-specific interactions.[13] On the other hand, in this approaches more synthetic chemistry is required and the higher binding energy of covalent bonds results in slower template rebinding kinetics, if rebinding is based on covalent interactions.[2] The semi-covalent imprinting exploit the benefits of the two approaches: the stoichiometry interactions in the pre-polymerization complex, thanks to covalent bonds, and the accelerated rebinding kinetics governed by non-covalent interactions.

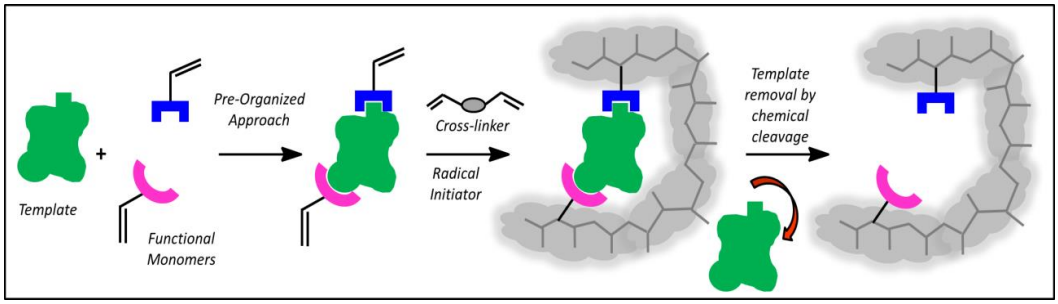

Figure 1.10: Schematic illustration of covalent imprinting approach.

The choice of the imprinting technique strongly depends on the template molecule (some compounds cannot establish covalent bonds that have to be cleaved after polymerization) and the final application of the MIP.

Components of MIPs

The elements necessary for building a molecularly imprinted matrix are the following: template molecule, functional monomer(s), cross-linker(s), initiator, and porogen solvent.

The **functional monomer** greatly affects the final performance of the MIP; it is usually selected for a certain template through studies of stoichiometry and strength of monomer-template interactions, by means of for example, nuclear magnetic resonance (NMR)[14] or spectroscopic measurements.[15] Particularly in the non-covalent approach, the choice of the proper functional monomer is crucial for a successfully development of MIPs. Functional monomers has to expose at least one polymerisable group, as vinyl or acryloyl functions, allowing the covalent incorporation in the polymer matrix. Nowadays, most of the functional monomers are commercially available, and one of the mainly used is methacrylic acid (MAA), because it can be both an hydrogen bond donor and acceptor; there are also many examples in literature where functional monomers are designed and synthesized for a specific template molecule.[16]

The **cross-linker** has the role to provide rigidity to the polymer matrix, allowing the creation of binding cavities determined by the pre-polymerization complex. To establish a rigid network, the cross-linker is usually added in very higher amounts rather than the functional monomers and template molecule, affecting morphology, binding capacity, chemical and physical properties of the final polymer.[17] Di-functional cross-linkers are predominant in MIP formulations, however also tri- and tetra-functional cross-linker are employed, as trimethylolpropane triacrylate (TRIM) or pentaerythritol triacrylate (PETA), to ensure even more rigidity of the polymer matrix.13

Ethyleneglycole dimethacrylate (EGDMA) is the most commonly used cross-linker, which contains a reactive and prochiral methacrylate ester and a short spacer, allowing a lot of conformation possibilities and a good degree of rigidity in the final polymer. Ethylene- and methylene- bis-acrylamide (EBA and MBA) are also very common, furthermore thanks to their solubility in water, allowing to perform the imprinting process in water, particularly for water soluble templates, as peptides or aminoacids.[2] Generally, an optimum cross-linker percentage can be found in the range of 50% to 80%, depending on the functional monomers used.[10]

The methods to initiate polymerization are mainly divided into radical, electrochemical and radiation polymerization.[17] Radical polymerization is the most common technique employed to prepare molecularly imprinted polymers; a **radical initiator** is activated by heat or UV light to induce free radical polymerization. Azobis-nitriles are the most common compounds employed as sources of free radicals, especially 2,2'-azobis-

(isobutyronitrile) (AIBN), which appears very often in literature papers and can be decomposed by thermolysis (at 70 °C) or by photolysis (UV). The choice of the radical initiator depends on the properties of template molecule and the environment in which the polymerization occurs. For example, for a template that undergoes thermal decomposition, the photo-initiation at 0 °C is favourable; if polymerization is performed in water media, water soluble initiators are required, as persulfates (as ammonium persulfates, APS) or hydrogen peroxide.[17] Normally, radical initiators are used in small amounts, e.g. 1 wt.% or 1 mol% compared to the total number of moles of polymerisable double bonds.[18] To ensure the polymerization reaction, removal of the dissolved oxygen from polymerization solutions immediately prior to proliferation is very important.

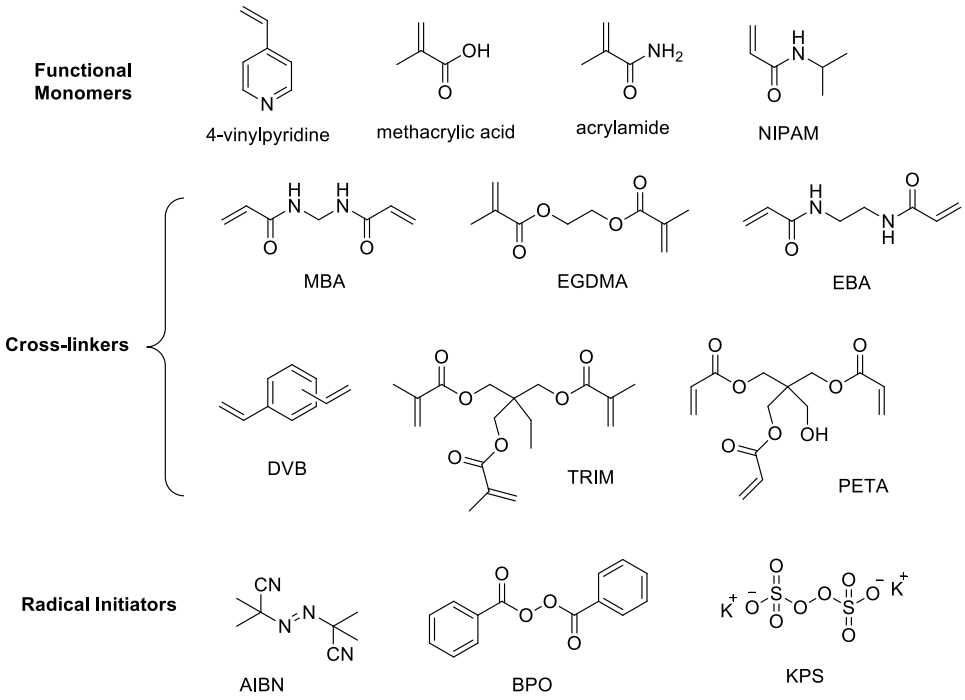

Scheme 1.5: Chemical structures of common functional monomers, cross-linkers, radical initiators. MBA: N,N'-methylenebisacrylamide, EGDMA: Ethylene glycol dimethacrylate, EBA: N,N'-ethylenebisacrylamide, DVB: divinylbenezene, TRIM: trimethylpropane trimethacrylate, PETA: pentaerythritol triacrylate, AIBN: azobisisobutyronitrile, BPO: benzoylperoxide, KPS: potassium persulfate.

The solvent in which polymerization occurs, plays an important role in molecular imprinting, and is usually known as **porogenic solvent** or simply porogen. As the cross-

linker, the choice of the solvent affects the final morphology of the polymer, determining not only MIP porosity, but also the MIP format (bulk polymers, microparticles, nanoparticles, film, etc.). A porous MIP can benefit because presence of pores ensures fast binding kinetics and rapid transfer of the template molecule from and toward the binding cavities.[2] The choice of the porogen is also determining in non-covalent imprinting, as it affects the stability of the pre-polymerization complex; high polar protic solvents, as water or methanol, tend to disrupt the hydrogen bonds established between template and functional monomers, dissociating the pre-prolymerisation complex, apolar solvents, on the other hands, will improve complex formation, favouring non-covalent interactions, as ionic strengths or hydrogen bonding. The study of the influence of porogen solvents on the stability of the pre-polymerization complex was performed by Sellergren and Shea.[19] Polar protic solvents, as water, are chosen when hydrophobic interactions (as π-π stacking) drive the formation of the pre-polymerization complex.[18] Polar aprotic solvents, as DMSO, favour ionic pairs and other strong dipolar interactions.[13] In general, a compromise between template solubility and solvent polarity is usually required.[13] In general, after polymerization, optimum rebinding performance is achieved when it is performed in the same or similar solvent used as porogen for imprinting.[20]

Finally, it is important to notice that an ideal template molecule should have the following features: contain functional group not able to inhibit polymerization, have excellent chemical stability during polymerization reaction, and expose functional groups able to form complexes with the functional monomers employed.

Polymerization methods and MIPS formats

The methods developed to prepare molecularly imprinted polymers are various and selected according to the final MIP format desired, for its application. Free-radical polymerization is the mainly used process to obtain MIPs, and the most popular method is bulk polymerization, which requires a quite simple procedure, as MIPs are synthesized in bulk, then grinded in particles and finally sieved into the desired size range. However, some specific cavities of the polymers can be destroyed during the smashing process, decreasing MIP's loading capacity, particles size and shape are often not uniform, and the process usually requires a large amount of template, not always available. This method has been often applied for preparing stationary phases for chromatographic columns.[21] To overcome the drawbacks of this technique, other polymerization methods have been developed to obtain many different formats of MIPs, as MIP films, membranes, particles or *in situ* prepared monoliths.

Monolithic MIPs, for example, have been prepared by a simple one-step *in situ* polymerization, directly inside a chromatographic column, avoiding the grinding and column packing steps. Lin *et al.*[22] prepared an hybrid silica-based monolithic MIP monolith in a column by a sol-gel process and was imprinted with proteins, as Bovine Serum Albumine (BSA) or Lysozime. This MIP monoliths showed good recognition capacities and selectivity.

MIP membranes and films are usually formed on planar or corrugated surfaces, and find application, for example, in sensing devices. Belmont *et al.*[23] developed a reflectometric spectroscopic sensor to detect the herbicide atrazine; they deposited MIP films on glass transducers by two different methods: spin-coating followed by thin films *in situ* polymerisation, and MIP nanoparticles auto-assembly using an associative linear polymer. The sensor was able to detect atrazine at very low concentrations (1.7 ppm) and the results showed good reproducibility.

Particles can be prepared by various polymerization methods, as emulsion polymerization, precipitation polymerization, suspension polymerization, in situ polymerization, seed polymerization, or surface imprinting.[24]

The precipitation method allows to obtain more regular microspheres, simply by increasing the amount of the porogenic solvent to the same mixture employed in the bulk polymerization, favouring the growing of individual polymer chains and avoiding coalescence. Polymers will precipitate when they will become large enough to be insoluble in the reaction mixture. Compared to bulk polymerization, these polymerization requires a larger amount of organic solvent and a strict control of reaction conditions, as temperature and stirring speed.[25] Spherical MIPs have been prepared *in situ* also by a multi-step swelling method, also known as seed polymerization; quite monodispersed particles are obtained using this method and they well suit for chromatographic application.[26]

MIP nanoparticles and nanogel

In recent years, particular attention of many research groups has focused on obtaining regularly shaped imprinted particles, especially in the nanoscale; MIP nanoparticles have the advantage of exposing higher surface-to-volume ratios, making binding cavities more accessible to the template and improving MIPs binding kinetics. This format is also easier to handle, as MIP nanoparticles are able to dissolve in stable colloidal solution and are simpler to dose.[27]

Fabrication of regular MIP nanoparticles is not easy by conventional radical polymerization, because it is difficult to control the rate of chain propagation; the

resultant polymers have generally a broad size distribution due to the various side reactions.[28] Many strategic pathways have been developed to prepare imprinted nanoparticles, as precipitation polymerization, mini- and micro-emulsion polymerization or core-shell approaches.

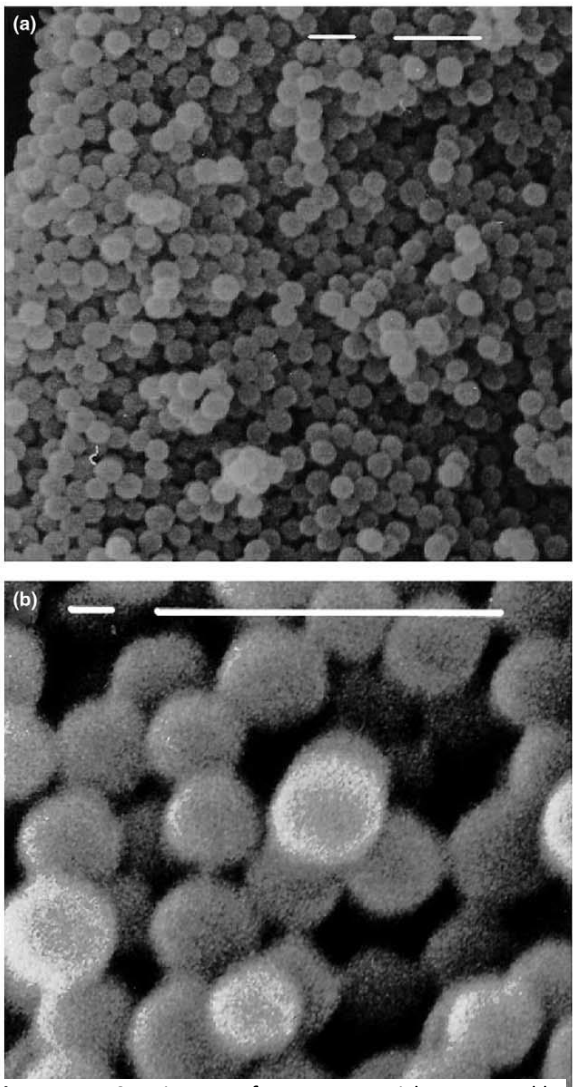

Figure 1.11: SEM images of MIP nanoparticles prepared by precipitation polymerization.[29] a) 7500x magnification; b) 30000x magnification. Scale bar: 1 µm.

Nanoparticles obtained by precipitation polymerization were first prepared by Ye *et al.* in 1999;[29] in this study spherical imprinted polymer nanoparticles were prepared against theophylline and 17β-estradiol (**Figure 1.11**). To obtain nanoparticles by precipitation, first monomers, cross-linkers and radical initiator are mixed in a dilute solution of the porogenic solvent, forming an homogeneous phase; as polymerization starts, oligomers and monomers aggregate into particles and when the growing polymer becomes insoluble in the reaction medium, precipitation occurs without coagulation of polymer chains. This technique is easy, provides good yields and is less time consuming than bulk polymerization.[27] Various imprinted nanoparticles have been prepared in the last decades using this method and tailoring the technique to the final application, in fields as sensing[30] or drug delivery.[31]

Emulsion polymerization have also been used to prepare MIP nanoparticles, and, in contrast to precipitation polymerization, this approach emulsify the organic reaction mixture (containing monomers, cross-linker, template and initiator) with an aqueous

phase containing a surfactant, by sonication or magnetic stirring. A co-stabilizer, as Sodium Dodecyl Sulfate (SDS), is added to the emulsion to avoid diffusion processes in the continuous phase. The so-called mini-emulsion polymerization allows to obtain stable emulsions with homogeneous droplet size; the particles are generated in a disperse phase constituted by liquid polymers or polymers solution, and have sizes around 50-1000 nm.[32] The first example using this technique is reported by the study of Vaihinger *et al*.,[33] who prepared imprinted nanospheres using MAA as functional monomer, EGDMA as cross-linker, SDS as surfactant and hexadecane as hydrophobic agent to prevent the Ostwald ripening of the mini-emulsion; these nanospheres were prepared using the chiral amino acid derivatives L- or D-Boc-phenylalanine anilid as template. The nanoparticles obtained had an hydrodynamic radius around 200 nm and enantioselective rebinding of the templates was observed. Micro-emulsion, instead, takes place in a dispersion made of water, oil and surfactant(s) with dispersed particles diameter varying from 1 to 100 nm, usually 10 to 50 nm.[34] In general, even if mini- and micro-emulsion techniques can produce very small nanoparticles, the need of various chemicals, as surfactants and co-stabilizers, may interfere with the imprinting process, reducing the MIP affinity for the template, and also the purification steps required can result very long and difficult.[27]

Other interesting formats are obtained by the "core-shell" approaches, used to synthesize particles with more complex architectures; some core-shell nanoparticles are prepared by deposition of MIP layers (shell) on the surface of nanospheres (core), acting as supports and formed using several materials, as silica, magnetite, gold or polymers. Otherwise, it is possible to prepare imprinted core particles (MIP core) containing specific binding sites, and attach on their surface, for example, charged functional groups that can be used to covalently immobilize the nanoparticles on silica or metal surfaces, exploiting the exposing groups of the shell.[35]

Finally, a valid alternative to the natural antibodies and enzymes is represented by MIP nanogels, very interesting materials for the development of synthetic receptors, thanks to their good solubility and flexibility.[36] The term "nanogel" refers to cross-linked polymer particles having dimensions around 100 nm, comparable to the size of biological receptors, and that can form stable colloidal solutions in suitable solvents, without attending precipitation.[37] MIP nanogels find application in various fields, as sensing, catalysis, separation and also drug delivery or diagnostics. An example of water-soluble MIP nanogel is reported in the work by Carboni *et al*.,[38] who prepared nanogel with aldolase type I activity, following a high dilution polymerization approach developed by Graham and Cameron.[37] This catalytic MIP nanogel showed good enantioselectivity and a homogeneous affinity distribution of the catalytic sites, proving that MIP nanoparticles can replace enzymes under conditions in which they become unstable, as extreme pH or organic environment. Moreover, a "post-dilution method"

to prepare MIP nanogels has been developed by Wulff *et al.*;[39] this technique involved first thermal polymerization at high monomer concentrations in an appropriate solvent and then early termination of polymerization by diluting the solution, therefore avoiding to reach the macrogelation point. This yielded soluble nanoparticles of 40 kDalton with, on average, one catalytic site per particle, showing Michaelis-Menten kinetics comparable to natural enzymes.

MIPs in sensors

As already mentioned, MIPs technology can be applied to various fields, including sensing. Imprinted polymers indeed can be employed as synthetic receptors in sensors, namely MIP-based sensors, first introduced by Mosbach to detect the vitamin K1 binding to an imprinted silicon surface using optical surface ellipsometry.[40] The main feature of most MIP-based sensors is that MIPs can both bind specifically the target and generate output signals, constituting the recognition element and transducer of a sensor. The most common output signals can be electrochemical, optical or piezoelectric.[24]

Optical sensing systems include chemiluminescence, fluorescence, colorimetric/UV-Vis, surface plasmon resonance (SPR), infrared and SERS detections. Fluorescence sensing, in particular, has attracted great interest, because of its high sensitivity and fast response; several approaches can be followed using this technique in MIP-based sensors, for example direct or indirect fluorescence detection of the target molecule. If analyte is intrinsically fluorescent active, it is possible to perform quantitative and qualitative analysis of the binding to the MIP, directly studying the variation of target's fluorescence intensity upon interaction with MIP; Moreno-Bondi *et al.*,[41] for example, reported the first MIP patterned by electron beam lithography (EBL) direct writing (**Figure 1.12**), designed for the detection of the fluorescent template Rhodamine 123. The polymeric mixture was based on a linear co-polymer, and the analyte binding experiments were carried out by fluorescence confocal microscopy. However, direct fluorescence detection is limited to very few analytes.

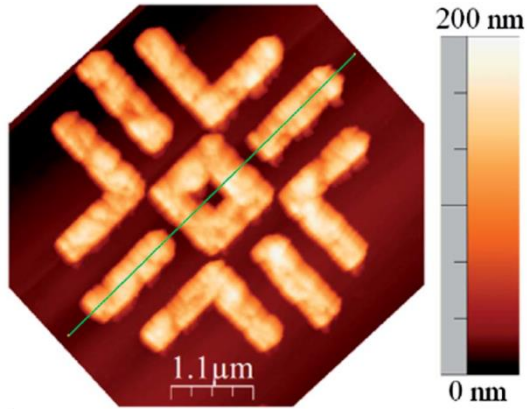

Figure 1.12: AFM image of a MIP nanostructure fabricated by EBL for Rhodamine 123 detection.

More common is the indirect fluorescence detection of non-fluorescent analytes, that can be performed following three different methods: using a labelled template or a fluorescent analogue derivative in a competitive or displacement assay for a MIP-based sensor, using a polymerisable fluorescent functional monomer that can be incorporated in the MIP matrix, or embedding a fluorescent signal sources in the MIP network, as organic fluorescent compounds or quantum dots.[24] An example of a fluorescent competitive assay has been reported by Sellergren *et al*.,[42] who prepared an automatic molecularly imprinted sorbent based assay (MIA) for the detection of penicillin-type β-lactam antibiotics in urine samples. A fluorescent analyte analogue was synthesized and employed in the competitive assay; upon desorption from the MIP, the fluorescent signal emitted by the analogue was measured and related to the amount of the antibiotic in the sample. The sensor showed a limit of detection of 0.197 µM and a dynamic range from 0.680 to 7.21 µM for penicillin G. An example of fluorescent molecularly imprinted polymer (FMIP) containing 1,8-naphtalimide dye is described by Rouhani,[43] who developed a FMIP-based optical sensor for the detection of caffeine; FMIP fluorescence emission was switched off in the presence of the target molecule, leading to a linear correlation between fluorescence intensity and caffeine concentration. The dynamic range investigated was from 1.94 to 194 μgmL^{-1}, with a sensor detection limit of 1.22 μgmL^{-1}.

The surface-enhanced Raman scattering (SERS) spectroscopy technique has also been used in combination with the molecularly imprinting technology; in 2003 Wulff *et al.*[44] proposed a MIP-based SERS sensor for the uptake and release of N-benzyloxycarbonyl-(L)-aspartic acid in aqueous solutions, but MIP layers stability was not high enough without the presence of an additional lubricant. It is not easy, indeed, to keep the SERS metal surface active after deposition of MIP particles or layers. However, in 2010 Haupt *et al.*[45] developed chemical nanosensors with a core-shell design, based on a polymer core, an imprinted (MIP) shell for β-blocker (S)-propanolol recognition, and an

interlayer of gold nanoparticles for signal enhancement. This was the first example of target detection by SERS measurements on single MIP-based particles, and the limit of detection of (S)-propanolol was 0.1 μM.

MIPs for irinotecan and imatinib

To our knowledge, only few examples on MIPs for irinotecan or imatinib have been reported in literature and not any of them finds application in sensors development.

A very interesting MIP for selective solid-phase extraction (SPE) of irinotecan from human serum samples was prepared by Roy *et al*.[46] The MIP was synthesized by non-covalent bulk polymerization, using methacrylic acid and vinylpyridine as functional monomers, EGDMA as cross-linker and AIBN as radical initiator. A MISPE column was packed with 50 μg of MIP into cartidges and was coupled to LC-PDA (photodiode array) to perform the extraction analysis. The extraction recovery was 88% from human serum spiked samples with 10 $\mu g \cdot mL^{-1}$ of irinotecan, demonstrating the MIP high selectivity for this anticancer drug.

In 2011 Zhou et al. have been developed a MIP for imatinib mesylate, for solid-phase extraction (SPE). The imprinted polymer was obtained by bulk polymerization.[47]

---

[1] Wulff G., Sarhan A., *Use of polymers with enzyme-analogous structures for the resolution of racemates*, Angew. Chem. (1972), 84: 364

[2] Meier F., Mizaikoff B., *Molecularly Imprinted Polymers as Artificial Receptors*, Artificial Receptors for Chemical Sensors (2011) Chapter 13, ISBN: 978-3-527-32357-9

[3] Hoshina K., Horiyama S., Matsunaga H., Haginaka J., *Molecularly imprinted polymers for simultaneous determination of antiepileptics in river water samples by liquid chromatography-tandem mass spectrometry*, J.l of Chrom. A (2009) 1216(25):4957-4962

[4] Cacho C., Schweitz L., Turiel E., Pérez-Conde C., *Molecularly imprinted capillary electrochromatography for selective determination of thiabendazole in citrus samples*, J. of Chrom.A (2007) 1179(2):216-223

[5] Benito-Pena E., Martins S., Orellana G., Moreno-Bondi M. C., *Water-compatible molecularly imprinted polymer for the selective recognition of fluoroquinolone antibiotics in biological samples*, Anal. Bioanal. Chem. (2008) 393: 235–245

[6] Fischer E., *Einfluss der Configuration auf die Wirkung der Enzyme*, Ber. Deutsch. Chem. Ges. (1894) 27, 2985–2993

[7] Arshady R., Mosbach, K., *Synthesis of substrate-selective polymers by host-guest polymerization*, Macromol. Chem. and Phys. (1981) 182(2): 687–692

[8] Wulff G., *Enzyme-like catalysis by molecularly imprinted polymers*, Chem. Rev. (2002) 102(1): 1–27

[9] Andersson H.S., Nicholls I.A., *Spectroscopic evaluation of molecular imprinting polymerization systems*, Bioorg. Chem. (1997) 25 (3): 203–211

[10] D.A. Spivak, *Optimization, evaluation, and characterization of molecularly imprinted polymers*, Adv. Drug Del. Rev. (2005) 57: 1779-1794

[11] Wulff G., Sarhan A., *The use of polymers with enzyme-analogous structures for the resolution of racemates*, Angew. Chem. Int. Ed. Engl. (1972) 11(4): 341-344

[12] Sellergren B., Andersson L., *Molecular recognition in macroporous polymers prepared by a substrate analog imprinting strategy*, J. Org. Chem. (1990) 55(10): 3381–3383

[13] Mayes A.G., Whitcombe M.J., *Synthetic strategies for the generation of molecularly imprinted organic polymers*, Adv. Drug Del. Rev. (2005) 57: 1742-1778

[14] Withcombe M.J., Martin L., Vulfson E.N., *Predicting the selectivity of imprinted polymers*, Chrom. (1998) 47(7-8): 457-464

[15] Lu Y., Li C.X., Zhang H.S., Liu X.H., *Study on the mechanism of chiral recognition with molecularly imprinted polymers*, Anal. Chim. Acta (2003) 489: 33-43

[16] Karim K., Breton F., Rouillon R., Piletska E.V., Guerreiro A., Chianella I., Piletsky S.A., *How to find effective functional monomers for effective molecularly imprinted polymers?*, Adv. Drug Deliv. Rev. (2005) 57: 1795-1808

[17] Li S., Ge Y., Piletsky S.A., Lunec J., *Molecularly Imprinted Sensors: Overview and Applications* (2012) Chapter 2, ISBN: 9780444563316

[18] Cormack A.P.G., Elorza A.Z., *Molecularly imprinted polymers: synthesis and characterisation*, J. of Chrom. B (2004) 804: 173-182

[19] Sellergren B., Shea K.J., *Influence of polymer morphology on the ability of imprinted network polymers to resolve enantiomers*, J. Chromatogr. (1993) 635: 31-49

[20] Kempe M., Mosbach K., *Binding studies on substrate- and enantio-selective molecularly imprinted polymers*, Anal. Lett. (1991) 24: 1137-1145

[21] Vasapollo G., Del Sole R., Mergola L., Lazzoi M.R., Scardino A., Scorrano S., Mele G., *Molecularly Imprinted Polymers: Present and Future Prospective*, Int. J. Mol. Sci. (2011) 12: 5908-5945

[22] Lin Z., Yang F., He X., Zhao X., Zhang Y., *Preparation and evaluation of a macroporous molecularly imprinted hybrid silica monolithic column for recognition of proteins by high performance liquid chromatography*, J. of Chrom. A (2009) 1216(49): 8612-8622

[23] Belmont A.S., Jaeger S., Knopp D., Niessner R., Gauglitz G., Haupt K., *Molecularly imprinted polymer films for reflectometric interference spectroscopic sensors*, Biosens. Bioelectron. (2007) 22(12): 3267-3272

[24] Chen L., Wang X., Lu W., Wu X., Li J., *Molecular imprinting: perspectives and applications*, Chem. Soc. Rev. (2016) 45: 2137-2211

[25] Liu Y., Hoshina K., Haginaka J., *Monodispersed, molecularly imprinted polymers for cinchonidine by precipitation polymerization*, Talanta (2010) 80(5): 1713-1718

[26] Hiratsuka Y., Funaya N., Matsunaga, H., Haginaka J., *Preparation of magnetic molecularly imprinted polymers for bisphenol A and its analogues and their application to the assay of bisphenol A in river water*, Pharm. Biomed. Anal. (2013) 75: 180-185

[27] Poma A., Turner A.P.F., Piletsky S.A, *Advances in the manufacture of MIP nanoparticles*, Trends in Biotechn. (2012) 28(12): 629-637

[28] Li Y., Li X., Dong C., Li Y., Jin P., Qi J., *Selective recognition and removal of chlorophenols from aqueous solution using molecularly imprinted polymer prepared by reversible addition-fragmentation chain transfer polymerization*, Biosens. Bioelectron. (2009) 25(2): 306–312

[29] Ye L., Cormack P.A.G., Mosbach K., *Molecularly imprinted monodisperse microspheres for competitive radioassay*, Anal. Commun. (1999) 36(2):35–38

[30] Ye L., Mosbach K., *Polymers Recognizing Biomolecules Based on a Combination of Molecular Imprinting and Proximity Scintillation: A New Sensor Concept*, J. Am. Chem. Soc. (2001) 123(12): 2901–2902

[31] Ciardelli G., Cioni B., Cristallini C., Barbani N., Silvestri D., Giusti P., *Acrylic polymeric nanospheres for the release and recognition of molecules of clinical interest*, Biosens. Bioelectron. (2004) 20(6): 1083–1090

[32] Wackerlig J., Lieberzeit P.A., *Molecularly imprinted polymer nanoparticles in chemical sensing – Synthesis, characterisation and application*, Sens. and Act. B (2015) 207: 144–157

[33] Vaihinger D., Landfester K., Krauter I., Brunner H., Tovar G.E.M., *Molecularly imprinted polymer nanospheres as synthetic affinity receptors obtained by miniemulsion polymerisation*, Macromol. Chem. Phys. (2002) 203: 1965–1973

[34] Slomkowski S., Alemán J.V., Gilbert R.G., Hess M., Horie K., Jones R.G., Kubisa P., Meisel I., Mormann W., Penczek S., Stepto R.F.T., *Terminology of polymers and polymerization processes in dispersed systems (IUPAC Recommendations 2011)*, Pure and Appl. Chem. (2011) 83(12): 2229–2259

[35] Kamra T., Chaudhary S., Xu C., Montelius L., Schnadt J., Ye L., *Covalent immobilization of molecularly imprinted polymer nanoparticles on a gold surface using carbodiimide coupling for chemical sensing*, J. of Coll. and Interf. Science (2016) 461: 1–8

[36] Flavin K., Resmini M., *Imprinted nanomaterials: a new class of synthetic receptors*, Anal. Bioanal. Chem. (2009) 393: 437-444

[37] Graham N.B., Cameron A., *Nanogels and microgels: The new polymeric materials playground*, Pure and Appl. Chem. (1998) 70(6): 1271-1275

[38] Carboni D., Flavin K., Servant A., Gouverneur V., Resmini M., *The first example of molecularly imprinted nanogels with aldolase type I activity*, Chem. Eur. J. (2008) 14: 7059–7065

[39] Wulff G., Chong B.O., Kolb U*., Soluble Single-Molecule Nanogels of Controlled Structure as a Matrix for Efficient Artificial Enzymes*, Angew. Chem. Int. Ed. 2006, 45, 2955 –2958

[40] Lars I., Andersson C., Mandenius F., Mosbach K., *Studies on guest selective molecular recognition on an octadecyl silylated silicon surface using ellipsometry*, Tetr. Lett. (1988) 29(42): 5437-5440

[41] Carrasco S., Canalejas-Tejero V., Navarro-Villoslada F., Barrios C. A., Moreno-Bondi M. C*., Cross-linkable linear copolymer with double functionality: resist for electron beam nanolithography and molecular imprinting*, J. of Mat. Chem. C (2014) 2(8): 1400-1403

[42] Urraca J.L., Moreno-Bondi M.C., Orellana G., Sellergren B., Hall A.J., *Molecularly imprinted polymers as antibody mimics in automated on-line fluorescent competitive assays*, Anal Chem. (2007) 79(13):4915-4923

[43] Rouhani S., Nahavandifard F., *Molecular imprinting-based fluorescent optosensor using apolymerizable 1,8-naphthalimide dye as a florescence functional monomer*, Sens. and Act. B (2014) 197: 185–192

[44] Kostrewa S., Emgenbroich M., Klockow D., Wulff G., *Surface-Enhanced Raman Scattering on Molecularly Imprinted Polymers in Water*, Macrom. Chem. and Phys. (2003) 204(3): 481-487

[45] Bompart M., De Wilde Y., Haupt K., *Chemical Nanosensors Based on Composite Molecularly Imprinted Polymer Particles and Surface-Enhanced Raman Scattering*, Adv. Mat. (2010) 22(21): 2343-2348

[46] Roy B., Vo Duy S., Puy J.Y., Martin C., Guitton J., Dumontet C., Périgaud C., Lefebvre-Tournier I., *Synthesis and Evaluation of a Molecularly Imprinted Polymer for Selective Solid-Phase Extraction of Irinotecan from Human Serum Samples*, J. Funct. Biomater. (2012) 3: 131-142

[47] Zhou J., Rao Y., Wu B., *Preparation of imatinib mesylate-MIP and its selective recognition ability*, Chin. Pharm. J. (2011) 46(17): 1330-1333

2. Aim of the Project

As already mentioned, this thesis takes part to a large project funded by "Associazione Italiana per la Ricerca sul Cancro (AIRC)" and coordinated by "Centro di Riferimento Oncologico di Aviano (CRO)", designed for the development of innovative cancer diagnostic tools, employing the latest Nanotechnology advances.

One of the aims of this project concerns the development of Point Of Care (POC) devices for the Therapeutic Drug Monitoring of specific anticancer drugs, including irinotecan and imatinib, widely administered at CRO of Aviano to numerous patients. Both these antitumor agents show many secondary effects and a significant inter- and intra-individual pharmacokinetic variability, hence monitoring the therapy can allow dose adjustments, reduced toxicities and improved treatment efficacy. The sensor devices should operate on a very small volume of blood; blood samples, indeed, could be directly taken by patients themselves, using for example a finger prick (as for glucose sensor used by diabetics), and after extraction of the plasma matrix, this processed sample could be analysed by a recognition element incorporated in the sensor, able to quickly quantify the drug. This is a very ambitious goal, also because no POC devices have been already commercialized for antitumor drugs.

The main challenges on achieving this target are related to the complexity of human plasma matrix, which contains many proteins and molecules that can interfere with the drug recognition process, carried out by a specific receptor, and to the necessity to develop a handle miniaturized sensor tool, easy to use and cheap, in order to obtain a stable device than can be directly used by patients, without the need of a clinical support.

This thesis project was focused on the development of fluorescent molecularly imprinted nanoparticles (MIPs) to be used as recognition elements in POC sensor devices for the anticancer agents irinotecan and imatinib. The advantage of working with nanoparticles is mainly due to their higher surface-to-volume ratio, favouring the accessibility to the binding sites, but also the facility to handle them, as they can dissolve in stable colloidal solution, allowing to perform many investigations on them. Both the target templates (irinotecan and imatinib) contain various aromatic rings and some polar moieties, that can be exploited for their recognition by imprinted polymers.

MIPs imprinted with irinotecan were designed employing various fluorescent 1,8-naphtalimide derivatives, and many other fluorophores had to be discarded, since this anticancer drug is a very fluorescent molecule. The naphtalimide molecules have proven to be a valid alternative, as they emit at wavelengths around 520 nm, far from irinotecan's emission spectrum, avoiding therefore to interfere with the anticancer agent fluorescence.

For the imatinib, instead, the use of also two other fluorescent dyes, EDANS and fluorescein, was planned, as it does not show any fluorescence activity. The functional monomers employed for MIPs preparation were suitably synthesized and evaluated on their ability to establish interactions with each specific anticancer drug; such interactions were studied through NMR experiments, and, after identification and selection of the best ones, molecularly imprinted polymers were prepared, their synthesis was optimized and, finally, polymers characterization was carried out. Investigations on MIPs rebinding capabilities were performed through HPLC and fluorescence experiments in different media; many issues were encountered while carrying out the fluorescence studies of MIPs rebinding capabilities, related to the little solubility of the anticancer drugs or aggregation of some imprinted polymers in some organic media or mixtures. The best MIP for each anticancer drug was then preliminary tested in human plasma samples, to obtain a proof of concept on the potential of such approach for the TDM of anticancer drugs.

In cooperation with Cobik, a Centre of Excellence on optical sensors (located in Slovenia), a first prototype sensor incorporating a MIP has been developed for the detection of irinotecan.

3. Results and Discussion

Fluorescent MIPs for Irinotecan

3.1 Synthesis of polymerisable monomers

Irinotecan is a very fluorescent molecule[1] and it is possible to exploit its intrinsic emission to produce a sensor. Its direct quantification from various biological matrices has been already proposed by many research groups.[2,3,4] Puojol *et al*.[5] developed one of the most sensitive HPLC-Fluorescence method for irinotecan quantification in human plasma and saliva, with a limit of quantification of 0.5 μgL^{-1} (about 0.7 nM) in both media. Hence, it would be possible to develop a not fluorescent MIP able to bind irinotecan and directly quantify the drug bound to the MIP through its fluorescence emission. However, its fluorescence intensity could be not enough for lowering the limit of detection and, moreover, the drug wavelengths could be easily affected by plasma interferences. Consequently, a set of dyes emitting fluorescence within a wavelength range far from the emission of the anticancer agent was considered. The attention was focused on some naphtalimide derivatives, able to emit around 520 nm when excited at 450 nm, and fluorescein O-acrylate (monomer **11**), emitting at about 515 nm when excited at 450 nm (differently to free fluorescein which is usually excited at 490 nm in water) (**Figure 3.1**).[6,7]

The 1,8-naphtalimide derivatives have been already employed as fluorescent monomers for the synthesis of various fluorescent MIPs;[8,9,10] for example, monomer **2** (reported in **Scheme 3.1**) was employed by Rouhani *et al.*[11] to develop a fluorescent MIP imprinted with caffeine, which showed a quenching of its fluorescence upon binding to the template with a limit of detection of 1.22×10^{-6} gmL^{-1} (6.28 µM). These very fluorescent molecules have been also used as probes for the detection of acidic drugs and biomolecules[12], anions,[13] and even as anti-cancer molecules.[14]

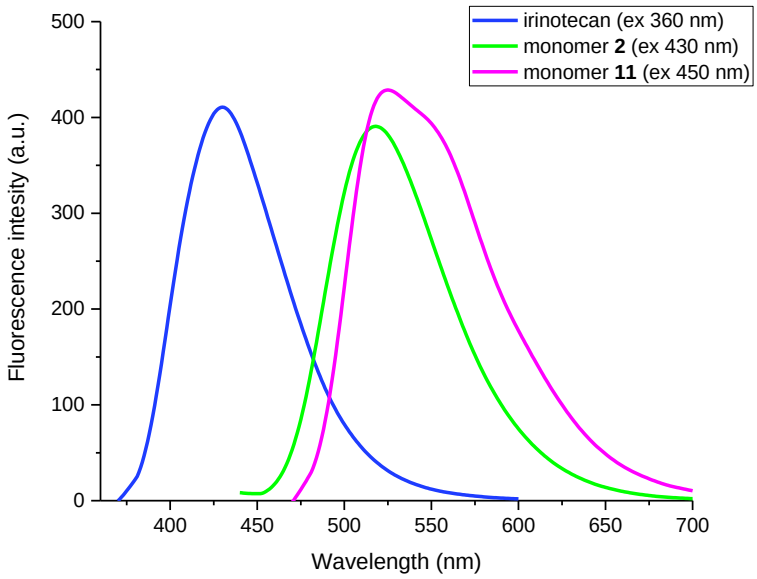

Figure 3.1: Fluorescence emission spectra of 250 nM irinotecan in methanol (excitation wavelength 360 nm), 1 µM of a naphtalimide derivative (monomer **2**) in 3:1 methanol:water mixture (excitation wavelength 430 nm), and 7 µM fluorescein O-acrylate (monomer **11**) in water (excitation wavelength 450 nm).

These 1,8-naphtalimide dyes show very interesting fluorescent properties, and thanks to their high sensitivity to solvents effect or upon interaction with other molecules,[15] they can be incorporated inside artificial receptors as peptides or molecularly imprinted polymers, and act as probes for sensors.

Synthesis of naphtalimide derivatives

4-amino-1,8-naphtalimide compounds are well known dyes able to emit in the green spectrum field. Since the '70s they have been employed for the preparation of coloured synthetic polymers and the synthesis of many derivatives are reported in literature.[16]

Different naphalimide dyes have been prepared for this project, aimed at obtaining fluorescent MIPs for both irinotecan and imatinib (**Scheme 3.1**).

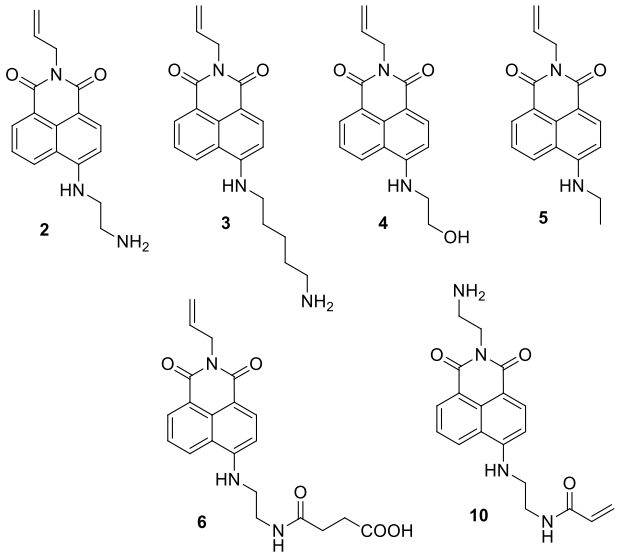

Scheme 3.1: Chemical structure of the synthesized naphtalimide derivatives.

The fluorescent monomers **2**, **3**, **4**, **5** and **6**, reported in **Scheme 3.1**, all contain the same N-allyl polymerisable group, besides the naphtalimide scaffold, but different chains at the anilino position 4. These different amines were chosen in order to investigate if interactions with irinotecan are favoured when chains have an amino (and if increasing the amino terminal distance from the naphtalimide moiety affects these interactions – comparing compound **2** with **3**), an hydroxyl, a methyl or a carboxyl terminal group. Compound **10**, instead, was synthesized properly to study if incorporation of N-acryloyl, rather than N-allyl group, was favoured for MIPs imprinted with irinotecan, and if exchanging the position of the amino terminal chain with the polymerizable domain could influence as well MIP fluorescence performance.

Comparing all these functional monomers interactions with irinotecan, it is possible to identify the best monomer-template match for the pre-polymerization complex.

To incorporate a polymerisable moiety inside the 1,8-naphtalimide dye, both 4-Chloro-1,8-naphtalic anhydride and 4-Bromo-1,8-naphtalic anhydride were used in the reaction with N-allylamine (**Scheme 3.2**). The reaction was performed according to literature.[17]

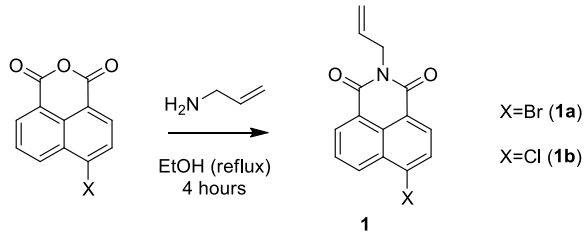

Scheme 3.2: Synthesis of compounds **1a** and **1b**.

The products **1a** and **1b** were obtained with a similar yield, around 60%. However, the best performance in the next synthetic step was observed using compound **1b**, when it has been used as the reactant of a nucleophilic aromatic substitution of the halogen atom with ethylenediamine (**Scheme 3.3**).[18]

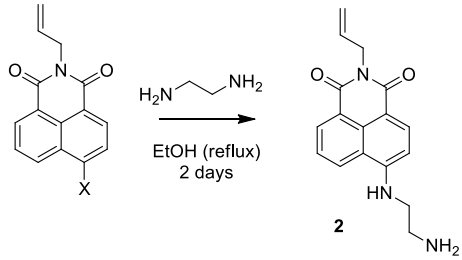

Scheme 3.3: Synthesis of compound **2**.

Using reagent **1a**, the obtained yield of product **2** was 49%, while using reagent **1b**, it turned out 97%. This result confirmed that chlorine leaving group, rather than bromide, favours the nucleophilic aromatic substitution, making the reaction faster and increasing yields.

Nucleophilic aromatic substitutions of activated aromatic compounds show a mechanism of addition-elimination, kinetically similar to the bimolecular nucleophilic substitution (S_N2) of aliphatic systems, having a second-order kinetic;[19] however, in contrast to S_N2 mechanism, where a transition state is formed after attack of the nucleophilic reagent, an intermediate is observed in nucleophilic aromatic substitution. The rate of reaction, hence, increases when stronger nucleophilic reagents are employed, substituents of the aromatic compound withdraw electrons from the site of substitution, and leaving groups facilitate/ help the site of attack to become more positively charged. For this reason, the halogens in activated aromatic systems can be easily substituted in the following order: F >> Cl > Br > I.[20]

To synthesize other 1,8-naphtalimide derivatives compound **1b** was used as precursor (**Scheme 3.4**). The only disadvantage of this reaction was the long time required. To overcome this drawback, the synthesis was repeated by the support of microwaves,

avoiding the adding of a solvent.[21] In **Table 3.1**, time, yield and conditions of reactions between **1b** and different primary amines are reported.

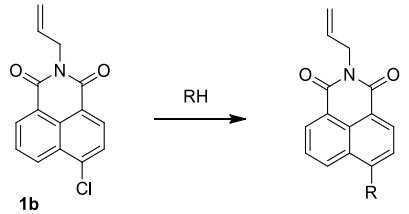

Scheme 3.4: Nucleophilic aromatic substitution of **1b** with various primary amines (RH).

RH	*Product*	*Reaction Time (hours)*	*Yield (%)*	*Conditions*
H_2N NH_2	**2**	51	97	Δ, EtOH reflux
		2	92	microwave assisted, 85 °C
H_2N NH_2	**3**	96	92	Δ, EtOH reflux
HO NH_2	**4**	96	99	Δ, EtOH reflux
NH_2	**5**	4	82	microwave assisted, 85 °C

Table 3.1: Time, yield and conditions followed for the nucleophilic aromatic substitution reported in Scheme 3.3 between compound **1b** and different primary amines (RH).

Comparing the reactions to obtain compounds **2**, **3** and **4**, performed in ethanol at reflux, using ethylenediamine, the time required for total conversion was shorter, probably because of its higher nucleophilicity. To our knowledge, the examples found in literature where microwaves were used for aromatic nucleophilic substitutions of naphtalimide moieties, performed the reaction with various amines in ethanol[22] or in solvent free conditions, with the aid of a catalyst (KF/Al_2O_3)[21] or without.[23] The yields obtained were lower (between 50 and 90 %) when solvent or catalyst were used, while in solvent free conditions without the adding of any catalyst the yields resulted higher, between 70 and 95%. Hence, the yields that we obtained using the microwaves were consistent with these values. Reaction time required using the microwaves were longer if compared to the times reported by literature, because we employed variable microwaves power keeping fixed the temperature at 85 °C during the reaction. However, there are not references in literature reporting the aromatic nucleophilic substitution of the substrate **1b** using the amines listed in **Table 3.1**, except for compound **2**.

*Synthesis of compound **6***

Using product **2**, obtained by nucleophilic aromatic substitution, it was possible to prepare a compound containing a terminal carboxylic group in place of an amino or hydroxyl moiety. The reaction of **2** with succinic anhydride in a basic environment, in anhydrous THF yielded indeed product **6** with a 73% yield.

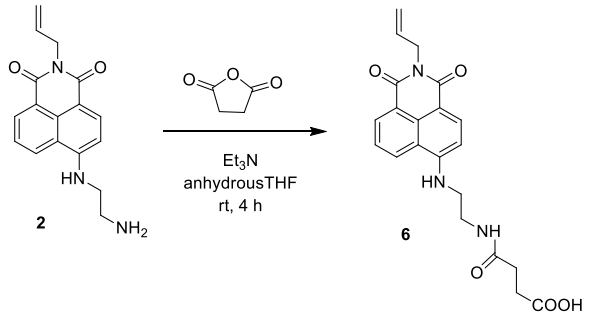

Scheme 3.5: Synthesis of compound **6**.

*Synthesis of compound **10***

Another synthetic strategy was considered to prepare a 1,8-naphtalimide derivative bearing a different polymerisable group, namely an acrylamide, at a different position respect to the N-allyl group of the above mentioned products. The reaction steps are reported in **Scheme 3.6**.

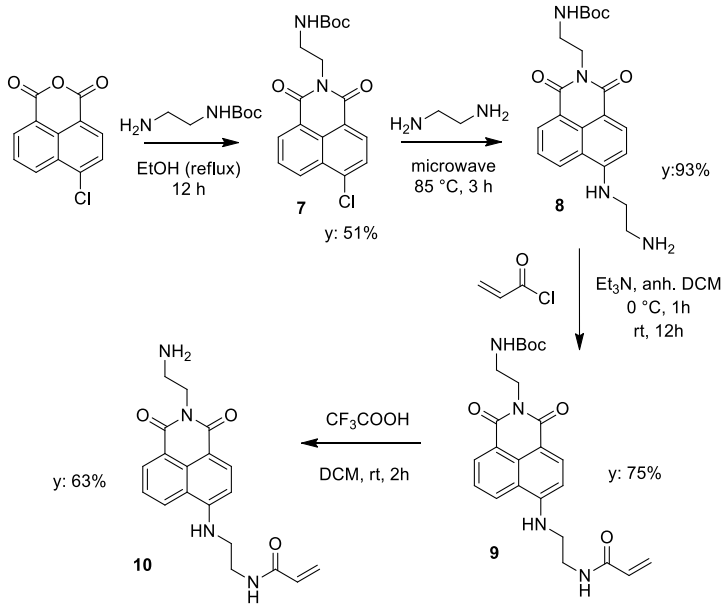

Scheme 3.6: Synthesis of compound **10**.

The first step of the synthesis consisted of the reaction between 4-Chloro-1,8-naphtalic anhydride and N-Boc-ethylenediamine, previously prepared. The Boc protection of one amino terminal of ethylenediamine allowed to avoid, in the following third step, the N-acrylation of both amino sites, leading to a bis acrylated monomer without containing any free amino group available to interact with irinotecan. The yield of the first step of the synthesis was quite low (51%), as previously noticed for the reaction reported in **Scheme 3.2**. The second step was the nucleophilic aromatic substitution of compound **7** with ethylenediamine in solvent free conditions, employing microwaves irradiation, that yielded compound 8 with 93%, result consistent with previous observed values of yields. The third step was the acryloylation reaction of the free amino group of compound **8**, that was performed in anhydrous dichloromethane, using triethylamine and acryloyl chloride, stirring at 0 °C for one hour and at room temperature overnight. Compound **9** was obtained with 75% yield. Last step was the deprotection of the amino terminal group, performed using trifluoroacetic acid in dichloromethane at room temperature, that yielded compound 10 at 63%.

The overall synthesis yield was 22%.

3.2 ^{1}H-NMR titrations of irinotecan with the functional monomers

In 1988 Sellergren *et al.* presented a study on the nature of the template molecule-functional monomer complex, formed by non-covalent interactions, using NMR spectroscopy.[24] Performing ^{1}H-NMR titrations of the template molecule with increasing equivalents of a potential functional monomer, in the porogen solvents selected for MIPs synthesis, it is possible to identify if non-covalent interactions, as hydrogen bonds, π-π stacking, ionic or hydrophobic interactions, are established and which groups of the template molecule are mainly involved in complex formation.

By acquiring multiple NMR spectra, while a titration of the template with increasing amounts of the functional monomer is performed, it is possible to get information about monomer-template complex formation, expressed by the equilibrium exchange:

$$T + M \underset{}{\overset{K_A}{\rightleftharpoons}} T\text{-}M$$

Where T, M and T-M are respectively template, monomer and template - monomer complex, and K_A is the equilibrium association constant, expressed by the **Equation 3.1**:

$$K_A = \frac{[T-M]}{[T][M]} = \frac{k_{ass}}{k_{diss}}$$

(**Eq. 3.1**)

Where *[T-M]*, *[T]* and *[M]* are the molar concentrations of template-monomer complex, template free and monomer free, respectively. The association constant K_A can be also expressed by the ratio between the kinetic constant related to the association (k_{ass}) process and the one related to the dissociation process (k_{diss}), as complex formation is a dynamic process.[25]

The exchange rate between free and bound template will have influence on the aspect of the NMR spectra, and three exchange systems, based on interconversion rate, can be distinguished: slow exchange, intermediate exchange, and fast exchange (represented in **Figure 3.2**). These exchange systems are also strongly affected by template binding affinity (K_A), because a tighter binding complex yields a longer-lived bound state, hence slower exchange between free and bound states will occur. Intermediate exchange (or coalescence) is, instead, present when the rate of the equilibrium process is similar to the NMR time scale. A single intermediate broadened signal is therefore observed, due to the interference of interconversion between the two species. When a fast exchange occurs, interconversion of the two species is faster than NMR time scale, hence just one averaged peak is shown in the NMR spectra.

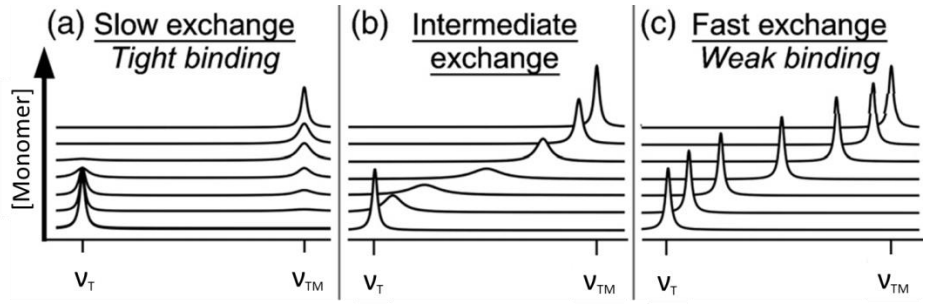

Figure 3.2: Representations of the three exchange regime (slow, intermediate or fast), strongly affected by template affinity for the functional monomer; ν_T and ν_{TM} are the chemical shifts of signals related to template and template-monomer complex, respectively. (a) Strong binding yields slow exchange because template-monomer complex rarely dissociates during the detection period of the NMR experiment. (b) Intermediate exchange is observed when the rate of the dynamic process is similar to the NMR time scale. (c) Weak binding yields fast exchange because interconversion between the two species is very rapid during the detection period of NMR experiment.[26]

During ^{1}H-NMR titration, if a complex is formed, template protons can undergo variation of their chemical shift to higher or lower fields, and entities and trends of these shifts can give information about the energy of interactions established with template and how the equilibrium of free and bound template species is shifted while the functional monomer is added.

Proton NMR titrations of 4 mM irinotecan with increasing amounts of the synthesized fluorescent functional monomers **2**, **3**, **5**, **6** and **10** (from 2 mM to 40 mM, except for monomer **10** added from 1 mM to 10 mM) were performed in DMSO-d_6. ^{1}H-NMR titration of irinotecan with the commercially available fluorescein-O-acrylate (monomer **11**) was also carried out.

In **Figure 3.3** the entities of chemical shifts of observed irinotecan protons are reported and correspond to the variation observed between irinotecan before starting the titration and after the adding of ten equivalents of each functional monomer (the titration with compound **10** is reported in the third set of polymers for irinotecan). The type of exchange observed in all titrations is mainly fast, suggesting that weak interactions are established between the drug and the functional monomers. Some protons, for example the ones involved in hydrogen bonds, showed instead an intermediate exchange with the typical broadened signals.

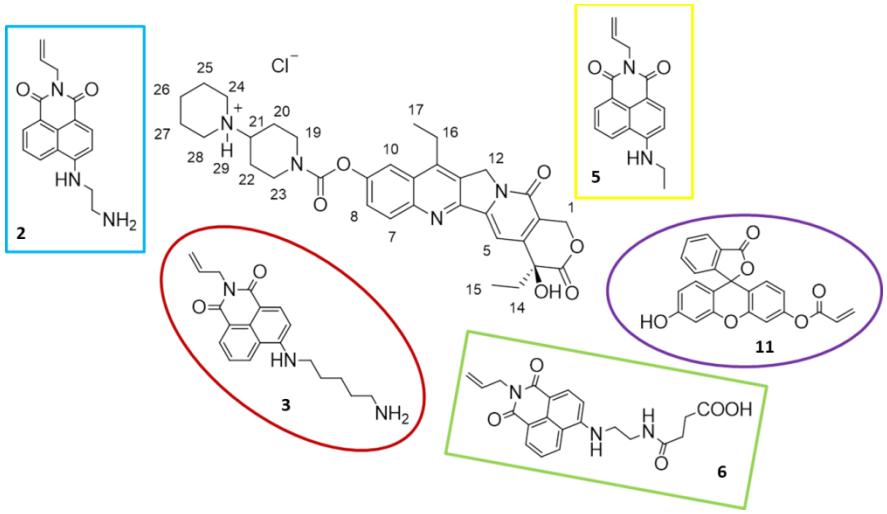

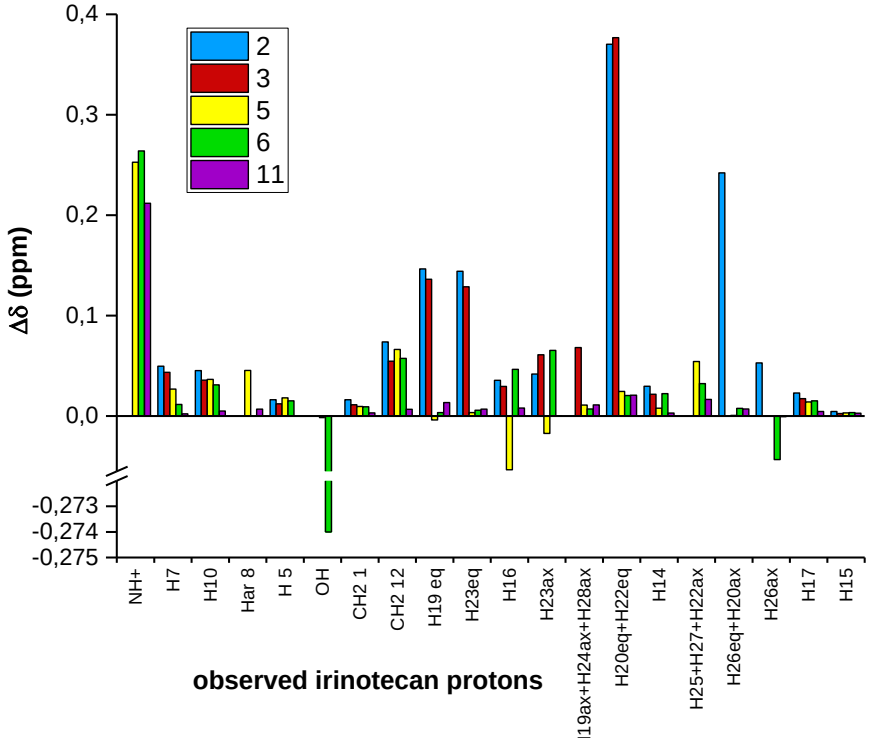

Figure 3.3: Variation of chemical shift of irinotecan protons before and after the adding of 10 equivalents of the functional monomers **2**, **3**, **5**, **6** and **11** (fluorescein O-acrylate).

Not all irinotecan protons are reported in **Figure 3.3** because signals becomes overlapped during titration or disappear. In general, upon monomers adding, most of irinotecan protons were shifted to higher fields, suggesting a shielding due to the close presence of the monomer. Fluorescein O-acrylate (**11**) and compound **5** did not interact significantly with the drug, while 1,8-naphtalimide derivatives **2**, **3** and **6** showed the largest proton shifts. In particular, compounds **2** and **3** showed a very similar behaviour towards irinotecan, as they are very similar molecules, both exposing an amino terminal group.

The irinotecan portion mainly involved in the interactions with **2** and **3** was the bis-piperidino moiety, as its corresponding protons showed the largest variation of chemical shift, suggesting the possibility to assist at the deprotonation of the irinotecan piperidinium group (NH^+) by the amino functional monomers. This can be confirmed also by the apparent disappearance of this piperidinium proton, that occurred after addition of 0.5 equivalents of functional monomer, as shown in **Figure 3.4** (right).

While monomers were added, it was possible to assist also to a high shift of methylene protons *13* and *16* of respective compounds **2** and **3**, to lower fields, probably due to the adjacent amino group protonation (**Figure 3.4**).

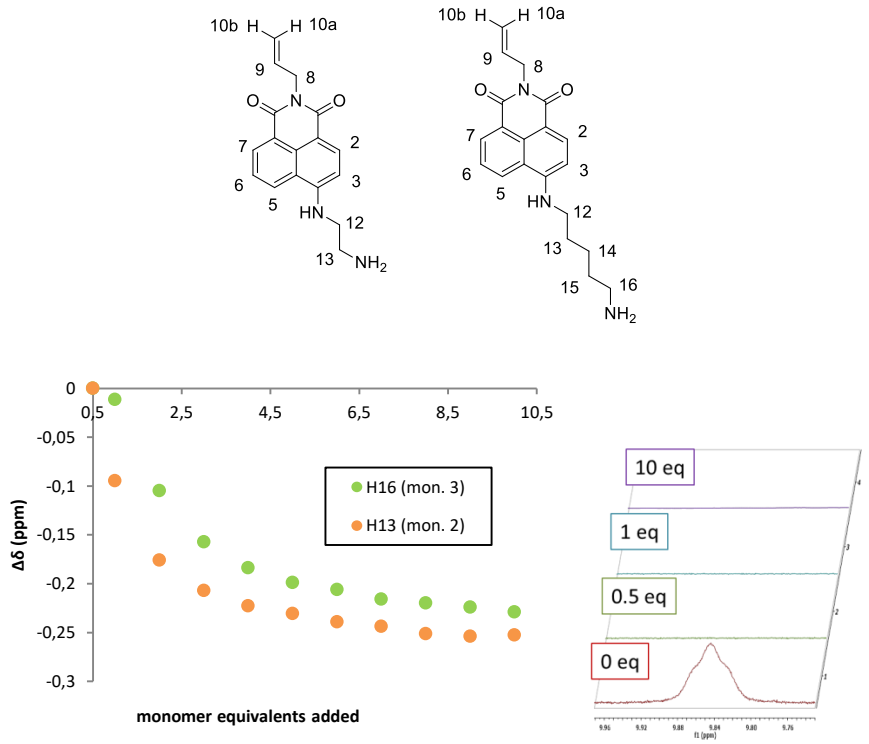

Figure 3.4: Variation of chemical shift of protons H16 (of monomer **3**) and H13 (of monomer **3**) during the irinotecan NMR titration (left); apparent disappearance of piperidinium proton of irinotecan after the adding of monomer **2** (the same behaviour was observed with monomer **3**).

Such probable proton transfer led also to chemical shifts variation of adjacent protons. Large proton shift was, indeed, observed for equatorials *H19*, *H20*, *H22*, *H23*, *H26* and axial *H20* (**Figure 3.5**), all belonging to the bis-piperidino moiety of irinotecan. The corresponding trends reached a plateau after the addition of one equivalent of monomer **2**, confirming that a strong interaction occurred between the drug and the functional monomer. Finally π-π-staking interactions also occurred between the aromatic structure of napthalimide and the quinoline moiety of the anticancer agent.

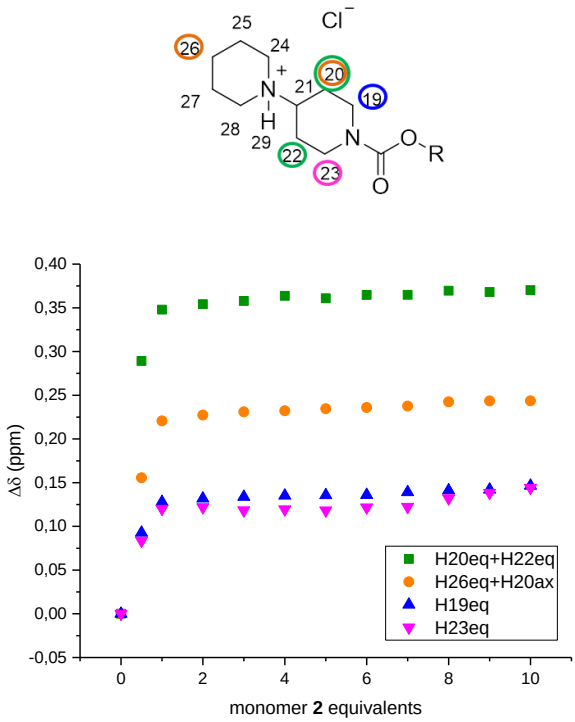

Figure 3.5: Variation of proton chemical shift of irinotecan protons *H20eq+H22eq*, *H26eq+H20ax*, *H19eq* and *H23eq* upon interaction with monomer **2**.

It is interesting also to notice that, during titrations with monomers **5**, **6** and **11**, the piperidinium NH^+ signal of irinotecan did not disappear, but was moved to higher fields, indicating that the equilibrium between free and bound irinotecan was continuously shifted to the bound form, without reaching a plateau (**Figure 3.6(a)**).

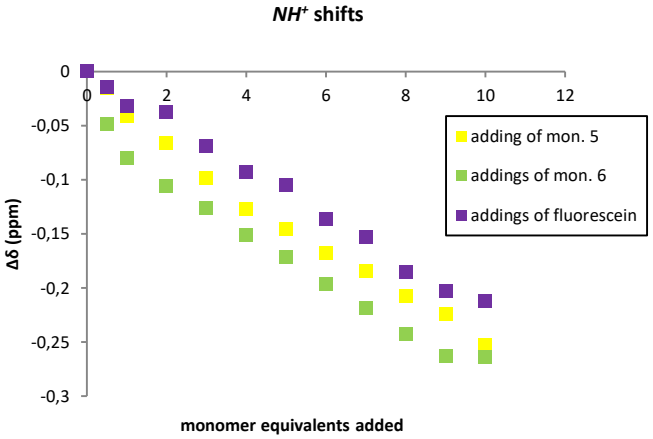

(a)

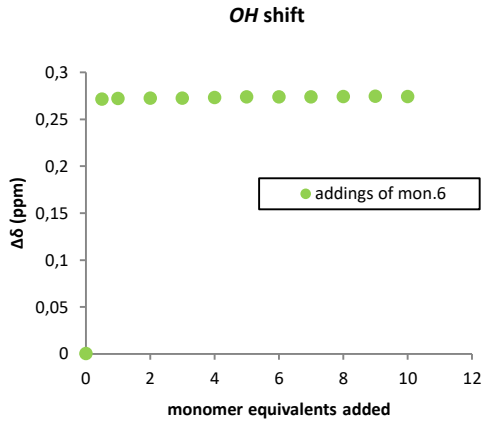

(b)

Figure 3.6: Variation of chemical shifts of some irinotecan protons: (a) NH^+ in titrations with monomer **5**, **6** and fluorescein O-acrylate; (b) hydroxyl upon during titration with monomer **6**.

Finally, the signal of irinotecan hydroxyl group was clearly shifted during the NMR titration with monomer **6** (**Figure 3.6(b)**). The proton signal, while the adding of functional monomer, was shifted to lower fields, suggesting that an hydrogen bond was probably established with compound **6**.

3.3 Synthesis, characterization and binding studies of fluorescent MIPs for irinotecan

The synthesis of imprinted nanoparticles was performed following the non-covalent high dilution radical polymerization protocol developed by Prof. Resmini[27] (in cooperation with her and her group members at Queen Mary University of London) and already employed by our research group in the preparations of materials for the recognition of sunitinib.[28] According to this method, stabilization of the growing polymer is achieved through steric control when the total monomer concentration is kept below a certain value, known as "critical monomer concentration" (C_m), which is determined experimentally for each system.[29] Working at monomer concentrations below the C_m, high dilution radical polymerization can be performed aimed at obtaining nanoparticles, stabilized by the porogen itself and avoiding that macrogelation occurs.[30] In this project, the value of the C_m was usually fixed at 1% (in weight), while the porogen solvent constituted the 99% (in weight) of the total mixture, since this C_m value gave good results in previous works, executed by our research group;[31] DMSO was chosen as the porogenic solvent, as it can dissolve the template and all the synthesized functional monomers; it is a polar solvent, somewhat similar to the aqueous environment of blood samples, in which the final MIPs will have to operate. Another advantage of DMSO is its capacity to favour ionic pair formation and other strong dipolar interactions, less interfering in hydrogen bonds formation rather than water.[32]

The mass of the porogen solvent was calculated using the following **Equation 3.2**:

$$m(S) = \frac{[m(fm) + m(com) + m(cl)] \cdot solvent\ \%}{tot.monomer\ \%\ (C_M)}$$

(**Eq. 3.2**)

Where *m(fm)*, *m(com)* and *m(cl)* are respectively the mass of the functional monomer, the co-monomer and the cross-linker.[33]

The amount of radical initiator was decided on the basis of our previous experience,[31] according to which we concluded that 18% percentage of AIBN was necessary to obtain MIPs with good yields, using irinotecan as template molecule.[1a] However, also different percentage of AIBN were explored in this Ph.D. project. The number of moles

[1a] The percentage (in mol) of AIBN employed does not correspond to the real amount of initiator involved in the reaction, as we ascertained that its efficiency was not at 100%, despite we recrystallized it before the utilization.

corresponding to a certain percentage of AIBN was calculated using the following **Equation 3.3**:

$$n\,(ri) = [n(fm) + n(com) + 2n(cl)] \cdot \frac{\%(ri)}{100}$$

(**Eq. 3.3**)

Where *n(ri)* stays for the moles or radical initiator to be calculated, and *n(fm)*, *n(com)* and *n(cl)* are respectively the moles of radical initiator, functional monomer, co-monomer and cross-linker, each one multiplied for the number of polymerisable bonds contained by each molecule; *%(ri)* is the percentage of radical initiator, previously decided.

Before initiating the reaction, the pre-polymerization complex was formed by stirring in DMSO the template and the functional monomer for one hour. Then a co-monomer, high amounts of cross-linker (70% mol) and radical initiator were added to the mixture. Polymerization was carried out at 70 °C for 96 or 24 hours.

Three steps of the radical polymerisation process can be distinguished (**Scheme 3.7**): *initiation*, *propagation* and *termination*. The *initiation* step concerns the first radicals formation, from homolytic dissociation of the radical initiator (AIBN), and addition of each first radical to the polymerisable double bond of the monomers employed. The second step consists of chain *propagation*, by successive addition of monomers in sequence, allowing growing of polymer chain. Finally, termination step concerns the stop of polymer growing, achieved by *combination* (*coupling*) of two radical chains, through formation of a covalent bond between each other, or, more rarely, by *disproportion*, where a hydrogen in beta position respect to a radical center is transferred to another radical center, producing two polymer molecules, one unsaturated and another one saturated.

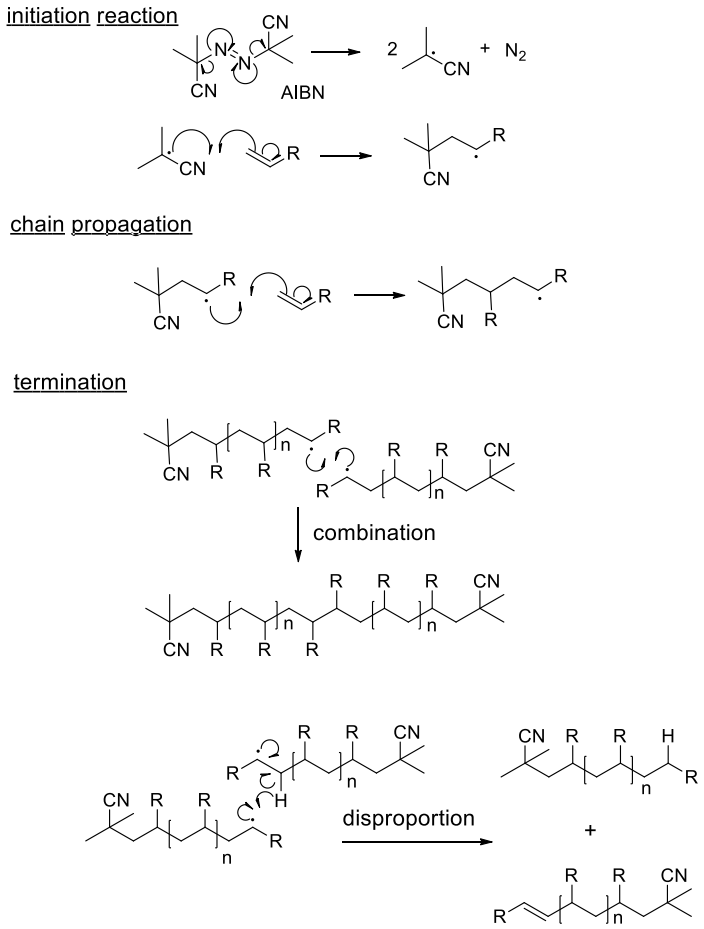

Scheme 3.7: Reaction steps of radical polymerisation using AIBN as initiator.

At the end of polymerisation, a highly viscous clear solution was obtained, suggesting the formation of a nanogel. The template was then removed from the polymer matrix by dialysis in water first and then in a 7:3 mixture of methanol : acetic acid.[34] In water, swelling of the polymer matrix occurred, favouring the opening of the pores and cavities formed in the imprinted polymer; in methanol, instead, shrinking of the polymer was observed, favouring as well the release of the template because of constriction of the polymer matrix.[35]

After template removal, the polymer was freeze-dried from water suspension, and a solid highly cross-linked material was obtained. For each MIP synthesized, an analogous non imprinted polymer (NIP) was prepared, following the same general protocol described above, except for the adding of the template. Finally, the yields of the MIPs

and NIPs obtained were calculated using the following **Equation 3.4**, which does not take into account the incorporation of the fraction of radical initiator.

$$\%\ yield = \frac{mass\ (polymer)}{\sum mass\ (monomers)}$$

(**Eq. 3.4**)

A very common technique employed to characterize MIPs is Dynamic Laser Light Scattering (DLLS or DLS);[36] this method measures Brownian motion of the particles and relates this to their size, by illuminating particles with a laser and analysing the intensity fluctuations of the scattered light. Brownian motion is defined as "the random movement of particles in a liquid due to the bombardment by the molecules that surround them"; it is known that small particles move or diffuse in a liquid more quickly than larger particles. Hence, if "two pictures" of the sample are taken in a short interval of time, it is possible to see how much the particles have moved and therefore calculate their size. Particle size can be determined using the relationship between diffusion speed and size.

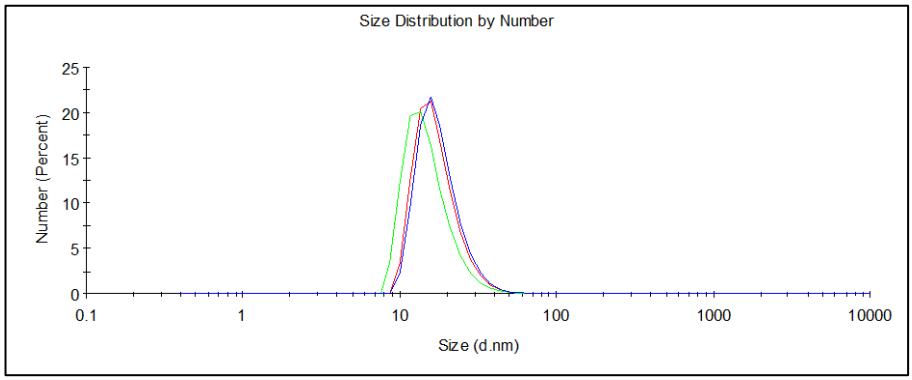

Figure 3.7: Example of a graph reporting size distribution by number obtained by DLS measurements of MIP nanoparticles, showing a mean diameter of 16.9 nm.

First set of fluorescent MIPs for irinotecan

A first set of molecularly imprinted polymers for irinotecan was designed using the fluorescent functional monomer **2**, which showed very promising results at NMR investigations, and different percentage (in mol) of methacrylic acid (MAA) as co-monomer. Carboxylic acid-base monomers, indeed, are actually the most successful

functional monomers employed in non-covalent imprinting. This probably is due to the fact that they have quite few atoms able to interact with template in different ways and with rotational degrees of freedom. Moreover, methacrylic acid also benefits from the hydrophobic methyl group, which provides additional van der Waals interactions and perhaps limits the conformational and rotational flexibility of the polymeric side chains.[32] Finally, using MAA as co-monomer could increase MIPs solubility in water and methanol environment, favouring their rebinding in plasma treated.

The cross-linkers chosen were EGDMA or MBA, both slightly water soluble and commercially available. The molar ratio between the template and functional monomer was fixed at respectively 1.2 : 1; using a small excess of template ensures that all the functional monomer molecules were involved in the interaction with the irinotecan, reducing the possibility to have non-specific binding sites. In **Table 3.2** compositions, yields and nanoparticles dimensions of *MIPs* and *NIPs A*, *B* and *C*, measured by DLS, are reported.

Polymer	Funct. Mon.	Co-monomer	Cross-linker	Reaction Time	Yield	DLS Size Distr. By Number (nm)	PDI
MIP A	**2** (10%)	MAA (20%)	EGDMA (70%)	96 h	92%	16.1±1.0	0.256
MIP B	**2** (10%)	MAA (30%)	EGDMA (60%)	24 h	93%	40.9±2.3	0.242
MIP C	**2** (30%)	MAA (20%)	MBA (50%)	24 h	79%	8.3±1.9	0.466
NIP A	**2** (10%)	MAA (20%)	EGDMA (70%)	96 h	98%	12.2±1.8	0.434
NIP B	**2** (10%)	MAA (30%)	EGDMA (60%)	24 h	80%	15.1±0.8	0.157
NIP C	**2** (30%)	MAA (20%)	MBA (50%)	24 h	63%	7.0 ± 1.8	0.579

Table 3.2: Compositions, yields and particles dimensions of MIPs and NIPs of the first set of fluorescent polymers for irinotecan. Time of polymerization is also reported for each nanogel. *MIP* and *NIP A* were prepared using 18% of AIBN, while *MIPs* and *NIPs B* and *C* using only 5% Particles hydrodynamic diameters were measured by DLS using 0.25 mg/mL nanogel solutions in DMSO, after sonication and filtration on 0.45 µm PTFE filters.

The reaction yields became higher by decreasing the percentage of monomer **2**, probably because functional monomer **2** contains the less reactive allyl group rather than N- or O-acryloyl moieties of MAA and cross-linkers. The particles size were all in the tenth nanometers range. However, decreasing the amount of EGDMA from 70% to 60% the nanoparticles dimensions slightly increased, maybe due to a decrease of

rigidity. Employing MBA as cross-linker, instead, even at low percentage, gave nanoparticles smaller than 10 nm (*MIP C* and *NIP C*). Comparing *MIP A* with *MIP B*, having very similar polymer composition, it seems that reducing reaction time from 96 to 24 hours had no effect on the final polymer yields.

Uv-Visible measurements

To evaluate the amount of monomer **2** incorporated during polymerisation, UV-Visible absorbance measurements of polymer solutions in DMSO were performed. A calibration curve of monomer **2** was previously performed in DMSO, in order to define its molar extinction absorptivity coefficient (ε) at 442 nm, obtained using Beer-Lambert Law. A value of ε_{442nm} 12504 $Lmol^{-1}cm^{-1}$ was obtained and then employed to calculate the concentration of fluorophore **2** inside the polymer matrix. In **Table 3.3** the nanomoles of monomer **2** per mg of polymer and the percentage of fluorophore incorporated during polymerization are reported.

Nanogel	Amount of mon. 2 incorporated/mg polymer ($nmol \cdot mg^{-1}$)	Percentage of mon. 2 incorporated during polymerisation
MIP A	33.0	5.5%
MIP B	39.2	3.4%
MIP C	211	13%
NIP A	97.3	19%
NIP B	88.7	7.6%
NIP C	262	16%

Table 3.3: Percentage of monomer **2** incorporated by the first set of fluorescent imprinting polymers for irinotecan ($nmolmg^{-1}$) and percentage of monomer **2** incorporated by each nanogel during polymerization.

Comparing *MIP A* with *MIP B*, both prepared using 10% of monomer **2**, *MIP B* incorporated more fluorophore than *MIP A*, indicating that probably a higher amount of cross-linker can be disadvantageous from the reactivity point of view, because it surely reacts faster than functional monomer **2**. On the other side, using higher amount of cross-linker increases the rigidity of the matrix, favouring the binding pockets formation. Hence, a compromise between the amount of functional monomer and cross-linker has always to be found. *MIP C* incorporated the largest amount of fluorophore **2**, as it was prepared using 30% of it. The percentage of compound **2** contained by *MIP C* and *NIP C* is, indeed, about three folds higher than *MIPs A* and *B*.

HPLC rebinding assay

One of the most common methods for evaluating MIPs binding capacity is *batch rebinding* (**Figure 3.8**), where each polymer is suspended in a known concentration of template (irinotecan) in water; after certain times a small amount of the mixture is taken, the polymer is separated by centrifugation and the supernatant analysed by HPLC, in order to define the amount of drug not absorbed by the polymer (concentration of free irinotecan). The amount of bound irinotecan (C_b) is then calculated by subtraction of the analysed free template concentration (C_f) from the total drug concentration (C_t) used to suspend the polymer (**Equation 3.5**).[37]

$$C_b = C_t - C_f$$

(**Eq. 3.5**)

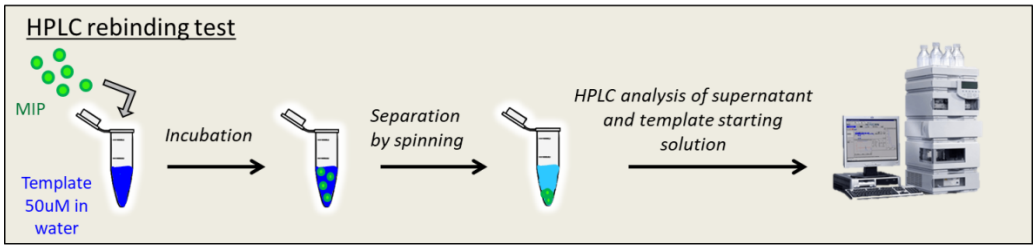

Figure 3.8: Schematic illustration of batch rebinding assay performed using HPLC.

1 mgmL^{-1} suspensions of *MIPs* and *NIPs A*, *B* and *C* in a 50 µM irinotecan solution in water were incubated for 24 hours at room temperature. A sample of each suspension was collected after 10, 30, 60, 90, 180 and 1440 minutes, centrifuged to separate polymer from unbound irinotecan and analysed at HPLC. The rebinding experiment was carried out in the same way, except for the centrifugation step. Samples were collected over time from the solution outside the dialysis tube, corresponding to the unbound drug. The amount of drug rebound by each polymer is reported in **Figure 3.9**.

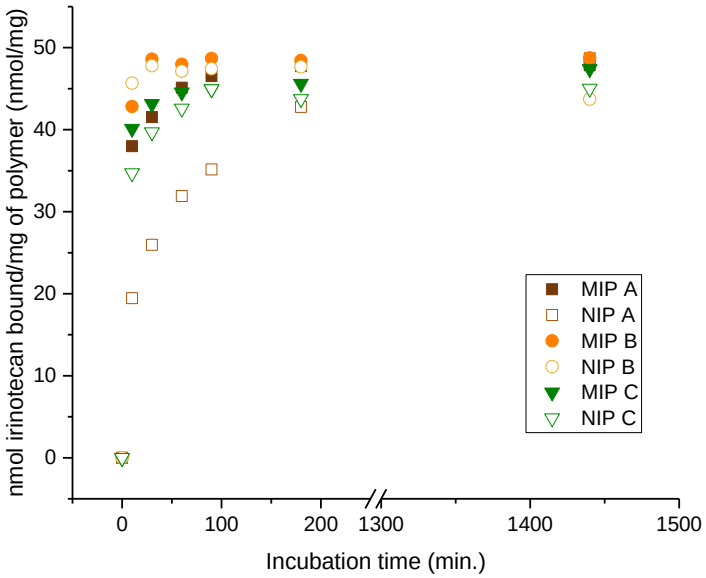

Figure 3.9: Binding kinetics of *MIPs* and *NIPs A*, *B* and *C*, obtained by HPLC rebinding assays in water.

All the analysed MIPs and NIPs showed very high rebinding of irinotecan in water, capturing almost all the drug available, already after 10 minutes of incubation. Binding kinetics of these MIPs, hence, were very fast. Only *MIP A*, however, showed good specificity for the anticancer agent and only at short incubation times, while *MIP B* and *MIP C* demonstrated very low specificity, capturing quite the same amount of corresponding NIPs, throughout the 24 hours of incubation. After 24 hours, unfortunately, specificity was not achieved by any MIP. This unsatisfactory result is probably due to the presence of MAA, which increases the polymers rebinding capacity, as it is both donor and acceptor of hydrogen bonds and can establish formal ion-pair or weaker dipole-dipole interactions, making it known as an "universal functional monomer" largely employed;[38] it was also shown that high percentage of MAA in MIPs compositions would result in large pore size inside the polymer matrix, further enhancing their binding capabilities.[39] On the other side, it has been demonstrated that an excess of MAA increases the amount of non-specific binding, lowering the overall specificity and selectivity of MIPs.[32]

Fluorescence measurements

The fluorescence phenomenon consists of the emission of light from a substance named "fluorophore", from electronically excited states. Fluorescence emission rates are usually in the field of 10^8 s^{-1}, therefore a typical fluorescence lifetime (τ_0, the average time between the excitation and the return to the ground state of a fluorophore) is around 10 ns.[40] The main important features of fluorescence as an analytical technique are its high sensitivity, facility and rapidity of measurements.

Various processes can lead to a decrease of fluorescence intensity; this phenomenon is known as "fluorescence quenching". Different mechanisms can cause a quenching, for example molecular processes that bring to static or collisional quenching, or non-molecular mechanisms, such as attenuation of the incident light by absorbing species (causing the so called "inner filter effect") or by the fluorophore itself.

Collisional quenching

Collisional quenching is a type of dynamic quenching that occurs when the excited-state fluorophore is deactivated upon impact with other molecules in solutions, named quenchers, and the fluorophore returns to the ground state during a diffusive contact with the quenchers. The collisional quenching is well described by the Stern-Volmer equation (**Eq. 3.6**):[40]

$$\frac{F_0}{F} = 1 + k_q\tau_0[Q] = 1 + K_D[Q] \qquad \textbf{(Eq. 3.6)}$$

In **Equation 3.6** F_0 and F are the fluorescence intensities measured in the absence and the presence of the quencher, respectively; k_q is called bimolecular quenching constant and reflects quenching efficiency or fluorophores availability to the quencher; τ_0 is the characteristic lifetime of the fluorophore in the absence of the quencher and $[Q]$ is the molar concentration of the quencher. K_D corresponds to the Stern-Volmer Dynamic quenching constant, given by $K_D = k_q\tau_0$.

The fluorescence quenching data are usually reported as linear plots of F_0/F versus $[Q]$, where the intercept is equal to 1 and the slope corresponds to the K_D of the process observed. Linearity of the Stern-Volmer plot indicates that a single class of fluorophores is present and are equally available to the quencher. Deviations from linearity are observed when two or more populations of fluorophores are present in solution, showing different accessibilities to the quencher. This result can be found, for example, in proteins, where different tryptophan molecules can be available to the quenchers, some on the surface of the protein and some inside the protein pockets.

Values of k_q up to $1x10^{10}$ $Lmol^{-1}s^{-1}$ typically indicate diffusion-controlled quenching, that is a time-dependent process.

Static quenching

k_q values larger than the diffusion-controlled limit, instead, usually suggest that some binding interactions are established. When the quencher and the fluorophore create a non-fluorescent ground-state complex, a static quenching can be observed, since the absorbance of light by the non-fluorescent complex does not produce photon emission when it returns to the ground-state. The association constant K_S related to a complex formation is defined by the **Equation 3.7**:

$$F + Q \overset{Ks}{\rightleftharpoons} FQ$$

$$K_S = \frac{[FQ]}{[F][Q]}$$

(**Eq. 3.7**)

Where *[FQ]* is the molar concentration of the complex formed, *[F]* and *[Q]* are the molar concentrations of the free fluorophore and quencher, respectively.

The total fluorophore concentration (*[F_0]*) is obtained by adding the concentration of fluorophore involved in complex formation to the residual concentration of free fluorophore (**Eq. 3.8**).

$$[F_0] = [F] + [FQ]$$

(**Eq. 3.8**)

Substituting *[FQ]* with *[F_0]-[F]*, defined by **Eq. 3.8**, K_s can be expressed as **Equation 3.9**:

$$K_S = \frac{[F_0] - [F]}{[F][Q]} = \frac{[F_0]}{[F][Q]} - \frac{1}{[Q]}$$

(**Eq. 3.9**)

Finally, expressing the Stern-Volmer equation, using the arrangement of **Eq. 3.9**, **Equation 3.10** for static quenching is obtained:

$$\frac{F_0}{F} = 1 + K_S[Q]$$

(**Eq. 3.10**)

As for dynamic quenching, also for static quenching a linear correlation is observed between F_0/F and *[Q]*, except for the Stern-Volmer quenching constant (K_{SV}) that in **Equation 3.10** corresponds to the association constant of the complex (K_S).[40]

Different methods can be used to distinguish between static and collisional quenching:

- Measurements of fluorescence lifetimes (τ). Since in static quenching a non-fluorescent complex is formed, the fluorescence emission is only due to the uncomplexed fluorophores, so the measured lifetimes (τ) will correspond to fluorophore lifetime in the absence of the quencher (τ_0). Many values of τ_0 are known and reported in literature. For collisional quenching, fluorophore lifetime in the presence (τ) and the absence (τ_0) of the quencher are different, because collisions depopulate the excited state, determining a decrease of both fluorescence intensity and lifetime.
- Observance of fluorescence quenching behaviour upon temperature variation. Higher temperatures will result in faster diffusion, causing larger amounts of collisions between fluorophore and quencher, inducing an increase of quenching efficiency. By contrast, higher temperature will usually favour dissociation of weakly bound complexes, determining a smaller efficiency of static quenching.
- Observance of quenching behaviour upon variation of solvent viscosity. Diffusive process slows down in more viscous environment, static quenching instead is not influenced by solvent viscosity.
- Careful examination of the absorbance fluorophore spectra in the absence and the presence of the quencher. Collisional quenching has only influence on the excited state of the fluorophore, leaving unchanged its ground state, hence the absorbance spectrum remains unaltered. Complex formation, instead, also affects the ground-state, producing alteration of fluorophore absorbance spectrum.
- Calculation of the bimolecular quenching constant (k_q) from the values of the Stern-Volmer plots slopes obtained and fluorophore lifetime (τ_0); values larger that diffusion limit ($1x10^{10}$ $Lmol^{-1}s^{-1}$) can indicate that static quenching occurs.

To be sure that the observed quenching is only static and not a combination of collisional and static, the best approach is to employ more than one method above mentioned to distinguish between the two kind of quenching, excluding also the occurrence of the inner-filter effect.[41]

Fluorescence study of MIPs prepared for irinotecan were performed thanks to the incorporation of the aromatic naphtalimide moiety in the polymer matrix, able to emit fluorescence in the visible around 520 nm, when excited at 448 nm. The fluorescence

lifetime (τ_0) related to compound **2** is 8.3 ns in polar solvents, as reported in literature.[42]

The capacity of MIPs to report binding of irinotecan by a change in fluorescence was investigated through fluorescence titrations of each nanogel with increasing amounts of the drug, in different media. DMSO was chosen because it is the porogen solvent for MIPs synthesis, and 3:1 methanol:water mixtures, because each plasma sample will be treated with three volumes of methanol in order to precipitate proteins and extract the drug, normally highly bounded to albumin. The explored concentration range of irinotecan was within its therapeutic range (20 nM – 20 µM).[43] Quenching of the fluorescence of polymers was actually observed, due to the interaction between irinotecan and nanogel. The quenching was examined by Stern-Volmer analysis, plotting measured F_0/F (where F_0 stays for polymer fluorescence intensity in the absence of irinotecan and F in the presence of the drug) versus molar drug concentration. All the polymers showed not linear Stern-Volmer plots, but multimodal curve trends, indicating the presence of various heterogeneous binding sites. It was possible, however, to verify if a static quenching occurred and a complex between irinotecan and polymer was formed, analysing the value of the slope (K_{SV}) of the Stern-Volmer plots obtained. And it was also possible to identify the polymers with higher affinity for the drug, considering the values of the bimolecular quenching constants obtained using the following **Equation 3.11**, derived from Stern-Volmer equation (**Eq. 3.6**):[44]

$$k_q = \frac{K_{SV}}{\tau_0}$$

(**Eq. 3.11**)

To verify that irinotecan did not absorb light at the excitation wavelength of monomer **2** (around 450 nm), hence leading to a quenching caused by the inner filter effect, UV-Visible absorbance measurements of irinotecan (in the micromolar range) in water were performed: the anticancer drug did not show any absorbance at wavelengths higher than 400 nm, confirming that it cannot cause inner filter effect.

A fluorescence titration of 1 µM monomer **2** with increasing amount of irinotecan, from 0.5 to 10 equivalents, was also carried out in methanol, but no significant quenching of compound **2** fluorescence was observed upon adding of the anticancer drug, demonstrating that an eventual fluorescence quenching of MIPs containing dye **2**, in the presence of irinotecan can be safely attributed to binding phenomena.

Despite *MIPs A*, *B* and *C* did not show high specificity, to investigate the rebinding capacity of at least one MIP belonging to this first set of polymers (imprinted with irinotecan), a fluorescence titration of *MIP C* with the anticancer drug was performed, as this nanogel incorporated the highest amount of the fluorophore **2** during polymerization and a more efficient fluorescence quenching could be expected.

60 μgmL^{-1} *MIP C* were titrated in 3:1 DMSO:water mixture with increasing amounts of irinotecan, within its therapeutic range (20 nM – 20 µM), using an excitation wavelength of 448 nm and emission wavelength of 520 nm. The Stern-Volmer plot obtained is reported in **Figure 3.10**.

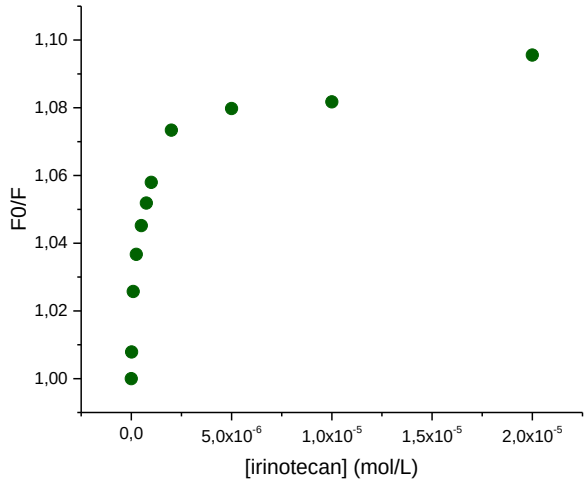

Figure 3.10: Stern-Volmer plot of 60 μgmL^{-1} *MIP C* titration with irinotecan in 3:1 DMSO:water. Inside box: zoom of the plot within concentrations range 0 – 1 µM.

In the *MIP C* Stern-Volmer plot, a bimodal trend was shown, suggesting that two populations of binding sites could be present in the polymer matrix. Since a more efficient fluorescent quenching occurred, a higher affinity for irinotecan was observed below 1 µM concentrations, that then decreased in the micromolar range, from 1 to 20 µM. The values of Stern-Volmer constants (K_{SV}) and related bimolecular quenching constants (k_q), reported in **Table 3.4**, confirmed that a static quenching occurred and a complex between *MIP C* and irinotecan was established. Good MIP sensitivity was observed at low irinotecan concentrations.

Nanogel	Concentration range	K_{SV} [10^4 $Lmol^{-1}$]	k_q [10^{12} $Lmol^{-1}s^{-1}$]
MIP C	0 – 1 µM	5.20	6.26
	1 µM – 20 µM	0.151	0.182

Table 3.4: Values of Stern-Volmer constant (K_{SV}) and related bimolecular quenching constants (k_q) obtained by Stern-Volmer analysis of fluorescence titrations of 60 $\mu g mL^{-1}$ *MIP C* with irinotecan in 3:1 DMSO:water mixture.

This low efficient quenching upon irinotecan adding was also observed for the other *MIP A* and *MIP B*, and despite *MIP C* incorporated the highest amount of monomer **2**, the fact that the quenching was not so efficient upon binding to the drug, suggested the idea that MAA could be the main responsible of *MIPs* drug rebinding, as very high rebinding capabilities were obtained at HPLC assays. Optimization of MIPs compositions, hence, had to be achieved.

MIP D synthesis

As previous MIPs containing 20 or 30% of MAA did not show specificity and efficient quenching for irinotecan, probably due to the too high amount of MAA, an imprinted polymer with irinotecan was designed decreasing the percentage of MAA to 15% and using compound **2** (15%) as fluorescent functional monomer, EGDMA as cross-linker (70%) and 18% of AIBN. The corresponding non imprinted polymer (*NIP D*) was as well synthesized.

Polymer	Funct. Mon. (15%)	Co-monomer (15%)	Cross-linker (70%)	Reaction Time	Yield	DLS Size Distr. By Number (nm)	PDI
MIP D	**2**	MAA	EGDMA	96 h	58%	19.0 ± 6.1	0.354
NIP D	**2**	MAA	EGDMA	96 h	45%	11.9 ± 3.7	0.199

Table 3.5: Compositions, yields and particles dimensions of *MIP D* and *NIP D*. Time of polymerization is also reported for each nanogel. Particles hydrodynamic diameters were measured by DLS using 0.25 mg/mL nanogel solutions in DMSO, after sonication and filtration on 0.45 µm PTFE filters. PDI stays for Poly Dispersion Index.

Uv-Visible measurements

The amount of monomer **2** incorporated by nanogels *D* was calculated by UV-Visible absorbance measurements in DMSO. In **Table 3.6** the nanomoles of monomer **2** per mg

of polymer and the amount of fluorophore incorporated during polymerization are reported.

Nanogel	Amount of mon. 2 incorporated/mg polymer ($nmol \cdot mg^{-1}$)	Percentage of mon. 2 incorporated during polymerization
MIP D	63.5	10%
NIP D	75.5	12%

Table 3.6.: Concentration of monomer **2** ($nmolmg^{-1}$) incorporated by *MIP D* and *NIP D*, measured by Uv-Visible measurements of polymers colloidal solutions in DMSO.

MIP and *NIP D* integrated almost twice the number of moles of compound **2** rather than previous polymers *MIP A* and *MIP B* (prepared with 10% of monomer **2**). As polymers *B* were designed with 15% of dye **2**, it seemed that increasing the percentage of the fluorophore in the pre-polymerization mixture, favoured its incorporation during the polymerisation, considering always that very low quantities of it will be then contained by the final polymer matrix, because of its lower reactivity compared to cross-linker or co-monomer ones.

HPLC rebinding assay

The rebinding capacities of *MIP D* and *NIP D* were investigated performing the HPLC assay, before mentioned, in 50 µM water solutions of irinotecan. In **Figure 3.11** corresponding binding kinetics are reported.

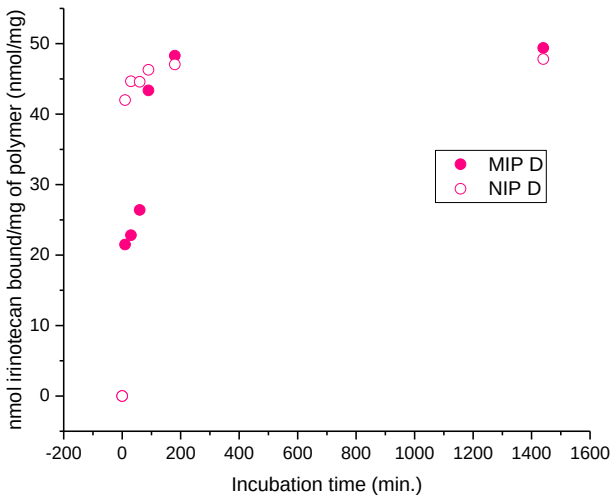

Figure 3.11: Binding kinetics of *MIP D* and *NIP D* in water obtained by HPLC rebinding experiments.

The amount of irinotecan absorbed in water by *MIP* and *NIP D* is similar to the one obtained in the previous HPLC results of the first set of polymers, probably because of MAA incorporation in the polymers matrix, even at lower percentage. It is interesting to note the different trend of the binding kinetics of *NIP D* and *MIP D*: the non-imprinted polymer showed a faster kinetic, absorbing already after 10 minutes most of the irinotecan available. *MIP D*, instead, exhibited a slower binding kinetic, that may indicate the presence of more specific binding sites, which require more time to be reached. However, after three hours of incubation, both *MIP* and *NIP D* showed a saturation of the binding sites available, and any different behaviour between them was not observed, suggesting the presence of many non-specific binding sites in both *B* nanogels.

Fluorescence measurements

Fluorescence titrations were performed also for 60 $\mu g mL^{-1}$ *MIP D* and *NIP D* in 3:1 DMSO:water, to further investigate *MIP D* specificity. The Stern-Volmer plots obtained, reported in **Figure 3.12**, showed also in this case a bimodal behaviour. At drug concentrations lower than 3 µM, a higher slope of the curve was remarked, while slope decreasing was observed for both *MIP D* and *NIP D* at concentrations higher than 3 µM. This change of inclination could be explained considering the existence of two

populations of binding sites in the polymers, one showing more affinity for the drug than the other one. However, specificity of *MIP D* was not observed, as *NIP D* showed even a more efficient fluorescence quenching than corresponding *MIP*. This behaviour is consistent with the results obtained at HPLC rebinding assays for these polymers.

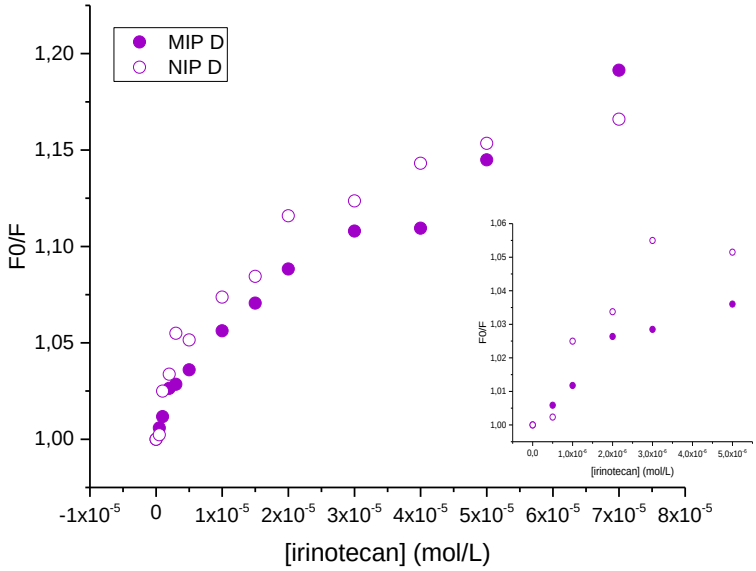

Figure 3.12: Stern-Volmer plots of 60 µgmL^{-1} *MIP D* and *NIP D* titrations with irinotecan 3:1 DMSO:water mixture. Inset: concentration range 0-2 µM.

In **Table 3.7** the values of the apparent Stern-Volmer constants (K_{SV}) corresponding to the plots slopes, and related apparent bimolecular quenching constants (kq) are reported.

Nanogel	Concentration range	K_{SV} [10^4 Lmol^{-1}]	k_q [10^{12} Lmol^{-1}s^{-1}]
MIP D	0 – 3µM	1.01	1.22
	3 – 20 µM	0.349	0.421
NIP D	0 – 3 µM	1.86	2.24
	3 – 20 µM	0.360	0.434

Table 3.7: Values of Stern-Volmer constants and bimolecular quenching constants obtained by Stern-Volmer analysis of *MIP D* and *NIP D* fluorescence titration with irinotecan 3:1 DMSO:water mixture.

A static quenching was observed, particularly at irinotecan concentrations below 3 µM, as K_{SV} values were larger than diffusion limit (1x10^{10} Lmol^{-1}s^{-1}). At concentrations higher

than 3 µM a decrease of the plot slope occurred, and the values of bimolecular quenching constants where in the order of 10^{11} $Lmol^{-1}s^{-1}$, anyway large enough to suggest static quenching.

MIP D rebinding capacity was also investigated in 3:1 methanol:water mixture. This medium was chosen properly, because the final environment in which the MIP should work will correspond to human plasma (aqueous portion) treated with a solvent (as methanol or acetonitrile) able to precipitate most of plasma proteins (which irinotecan binds to) and extract as much drug as possible. A methanol – plasma mixture is a very standard condition in clinical chemistry.[43] It is conversely important to note that, in general, as to the performance of molecularly imprinted polymers, a solvent as methanol is usually disadvantageous, as methanol promotes shrinking of polymer matrix, favouring probably the disclosure of some binding cavities, hence decreasing its binding capacity.[35]

60 μgmL^{-1} *MIP D* was titrated in 3:1 methanol:water with increasing amount of irinotecan. The concentrations explored was limited to 0 – 2.5 µM range. The resulting Stern-Volmer plot is reported in **Figure 3.13**.

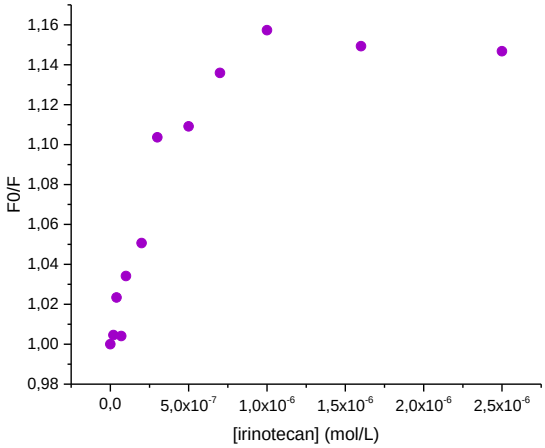

Figure 3.13: Stern-Volmer plot of 60 μgmL^{-1} *MIP D* fluorescence titration with irinotecan in 3:1 methanol:water mixture.

At concentrations below 1 µM a linear trend was observed in the Stern-Volmer plot of *MIP D* in 3:1 methanol:water, while a plateau was reached in the micromolar range, suggesting that a population of more specific *MIP D* binding sites was accessible for

irinotecan at concentrations in the nanomolar range, which showed the highest value of bimolecular quenching constant (**Table 3.8**) obtained until now, of 10^{13} $Lmol^{-1}s^{-1}$ order.

Nanogel	Concentration range	K_{SV} [10^4 $Lmol^{-1}$]	k_q [10^{12} $Lmol^{-1}s^{-1}$]
MIP D	0 – 1 µM	16.58	19.97
	1 µM – 2.5 µM	neg.	-

Table 3.8: Values of Stern-Volmer constants and bimolecular quenching constants obtained by Stern-Volmer analysis of *MIP D* fluorescence titration with irinotecan 3:1 methanol:water mixture.

Comparing these fluorescence results with the previous ones, a higher *MIP D* affinity for irinotecan was observed in a solvent as methanol rather than in DMSO, in the nanomolar range. The behaviour of this MIP in methanol was very promising for the future MIPs development, as they should operate in an aqueous environment containing mostly methanol.

However, at micromolar concentrations of the drug, a quenching of *MIP D* fluorescence was not observed, suggesting that the higher affinity of *MIP D* for irinotecan could probably due to the presence of MAA rather than naphtalimide monomer **2**, as in water it gave a very good drug rebinding (49 $nmolmg^{-1}$), but not very efficient quenching was observed at fluorescence measurements, confirming that the main interactions in the *MIP D* probably involved MAA rather than compound **2**.

The decrease of the MAA percentage from 20/30% (*MIPs A*, *B* and *C*) to 15% (*MIP D*) in MIPs design did not favour MIP specificity, despite very high drug rebinding capacities in water were obtained. Hence, this co-monomer, even at low concentrations, can act as a competitor to monomer **2**, favouring the formation of many non-specific binding sites in the polymers matrix. The interaction of this co-monomer (MAA) with irinotecan was also investigated through ^{1}H-NMR titration of the template with increasing amount of MAA. MAA was added to 4 mM irinotecan, from 0.5 to 10 equivalents (from 2 to 40 mM), in DMSO-d_6. Not any irinotecan proton was significantly shifted while functional monomer was added, indicating that interactions between the template and free MAA were not established in DMSO. In **Figure 3.14** some irinotecan signals (aromatic *H8* and equatorials *H19* and *H23*) shifts upon adding of MAA, are reported.

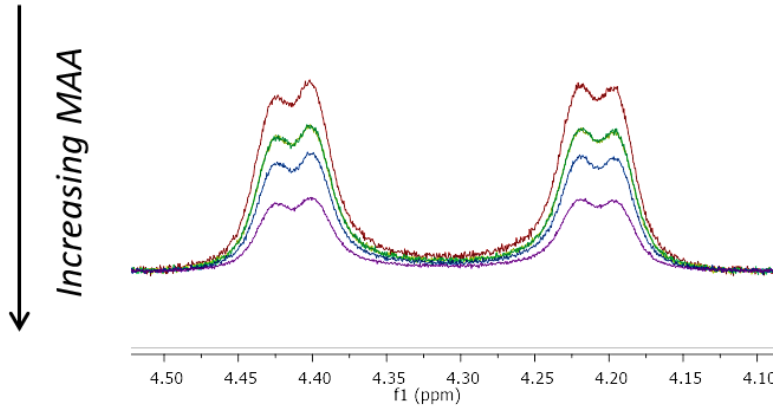

Figure 3.14: Chemical shifts variations of irinotecan equatorial *H19* and *H23* protons upon adding of MAA).

The NMR study confirmed that MAA was correctly considered as co-monomer, as it was not able to form the pre-polymerization complex with the anticancer drug in DMSO, that is a requirement of the non-covalent imprinting approach. However, the high rebinding capability obtained by MIPs containing MAA, suggested that incorporation of this monomer in a polymer matrix led to the formation of many non-specific interactions in water, lowering in general MIP specificity towards irinotecan.

Second set of fluorescent MIPs for irinotecan

Since the incorporation of MAA in the previous polymers did not lead to satisfying results, a second set of fluorescent imprinted polymers for irinotecan was designed using no longer MAA, but 15% (mol) of monomer **2**, and 15% (mol) of different commercially available co-monomers, as acrylamide and N-isopropyl acrylamide (NIPAM), in order to select the best for irinotecan imprinting. The chosen cross-linkers were EGDMA or MBA, both slightly water soluble and commercially available, and the AIBN amount was 18% for all the polymers. As previously, the molar ratio between the template and the functional monomer **2** was fixed at respectively 1.2 : 1; **Table 3.9** reports compositions, yields and mean hydrodynamic diameter of particles, obtained by DLS measurements.

Polymer	Funct. Mon. (15%)	Co-monomer (15%)	Cross-linker (70%)	Reaction Time	Yield	DLS Size Distr. By Number (nm)	PDI
MIP E	**2**	Acrylamide	EGDMA	96 h	54%	20.6 ± 2.8	1.00
MIP F	**2**	NIPAM	EGDMA	96 h	69%	15.7±1.4	0.382
MIP G	**2**	Acrylamide	EGDMA	24 h	73%	27.9 ± 2.6	0.370
MIP H	**2**	Acrylamide	MBA	24 h	74%	712 ± 103	0.762
NIP E	**2**	Acrylamide	EGDMA	96 h	41%	16.6 ± 5.0	0.357
NIP F	**2**	NIPAM	EGDMA	96 h	49%	19.5 ±2.6	1.00

Table 3.9: Compositions, yields and particles dimensions of *MIPs* and *NIPs* of the second set of fluorescent polymers for irinotecan. Time of polymerization is also reported for each nanogel. Particles hydrodynamic diameters were obtained by DLS measurements of 0.25 mg/mL nanogel solutions in DMSO, after sonication and filtration on 0.45 µm PTFE filters. PDI stays for Poly Dispersion Index.

As expected, nanoparticles of around 20 nm (hydrodynamic radius) were obtained, as confirmed by DLS measurements, except when MBA was used as cross-linker instead of EGDMA (*MIP H*). These nanoparticles dimension values are comparable to the ones obtained in our previous work, using the anticancer drug sunitinib as template molecule.[28] Since all the polymer samples were sonicated and filtered before performing DLS measurements on 0.45 µm filters, it followed that particles of *MIP H* highly aggregated in a very short time, resulting in very big particles hydrodynamic diameters (around 700 nm) measured at DLS. This result is not due to the presence of the cross-linker MBA, since the previously described *MIP C*, containing MBA as well, gave nanoparticles of 8 nm. Hence, it is not clear why *MIP H* highly aggregated in DMSO solution. Further investigations using MBA should be done, before excluding this cross-linker for irinotecan imprinted nanoparticles.

UV-Visible measurements

To evaluate the amount of monomer **2** incorporated during polymerization, UV-Visible absorbance measurements of polymer colloidal solutions in DMSO were carried out. In **Table 3.10** the nanomoles of monomer **2** per mg of polymer and the amount of fluorophore incorporated during polymerization are reported.

Polymer	Amount (mon. 2) incorporated/mg polymer (nmol·mg^{-1})	Percentage of mon. 2 incorporated during polymerisation
MIP E	44.4	5.6%
MIP F	47.1	6.2%
MIP G	31.9	4.0%
MIP H	-	-
NIP E	45.4	5.8%
NIP F	23.2	3%

Table 3.10: Concentration of monomer **2** (nmol mg^{-1}) incorporated by the second set of fluorescent MIPs and NIPs, measured by UV-Visible measurements in DMSO.

The results obtained by absorbance measurements demonstrated that *MIPs E*, *F* and *NIP E* incorporated quite the same amount of monomer **2**: about 6% of total initial monomer quantity, suggesting that N-allyl group is not so reactive, if compared with cross-linker and co-monomer. *MIP G* incorporated the lowest amount of the fluorophore **2** (4%), maybe because of the less time of polymerisation reaction. Finally, it was not possible to measure the absorbance of *MIP H* because of high turbidity of its suspension.

HPLC rebinding assay

The rebinding capacity of *MIPs* and *NIPs E*, *F*, G and *H* was investigated performing the HPLC assay before mentioned, in 50 µM water solutions of irinotecan. On the contrary of the "standard" assay, previously explained, *MIP H* was studied by equilibrium dialysis, because this polymer was partially soluble in water and it was not possible to separate it from the free drug solution simply by centrifugation.

The amount of drug absorbed by each polymer, after certain intervals of incubation time, is reported in **Figure 3.15**.

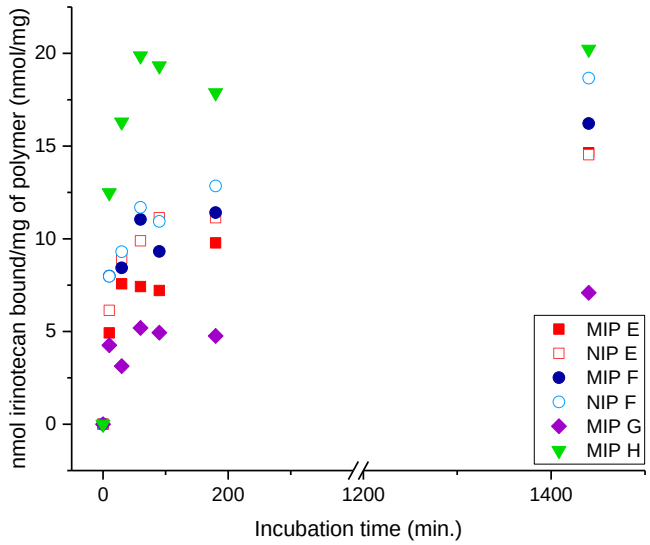

a)

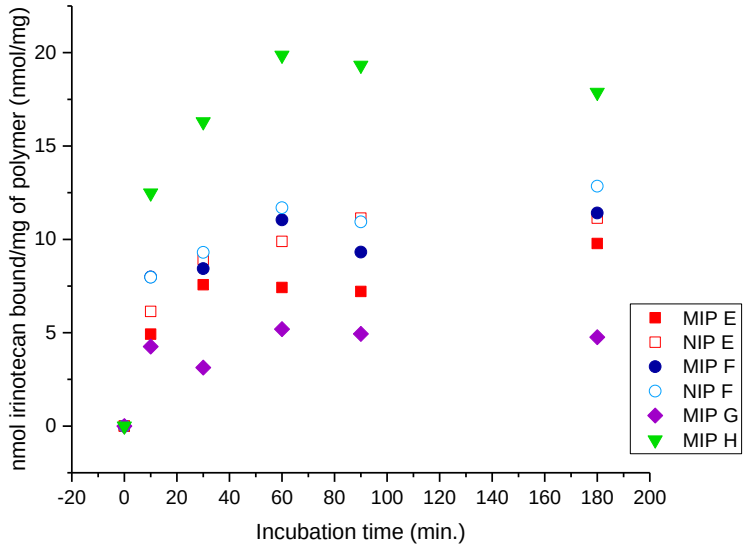

b)

Figure 3.15: Binding kinetics of MIPs and NIPs belonging to the second set of polymers for irinotecan, obtained by HPLC experiments in water. a): total incubation time range (0-24 h); b): short incubation time range (0-3 h).

The best rebinding capacity was observed for *MIP H*, despite its high aggregation in solution, that disfavoured its solubility in water and DMSO, leading to difficulties in performing many investigations on it. *MIPs E* and *G*, containing both acrylamide, did not show high absorbing capacity and rebinding kinetics resulted also quite slow. Moreover, no specificity in water was observed for *MIP E*, since the corresponding non imprinted polymer (*NIP E*) captured even more amount of irinotecan, suggesting the presence of many non-specific binding sites in *MIP E*. The use of NIPAM as co-monomer also did not lead to very high rebinding capacity in water and many non-specific binding sites were present within *MIP F*, as well.

Comparing the amount of irinotecan absorbed by these polymers with the ones of the first set of polymers, it is clear that the presence of MAA affected most of polymers rebinding capacity, leading to capturing almost the double number of irinotecan moles than this second set of *MIPs*. Hence, incorporation of co-monomers as acrylamide or NIPAM did not improve *MIPs* specificity and neither their rebinding capacity.

Study of MIP E specificity in DMSO through fluorescence

To further investigate *MIP E* specificity, fluorescence titrations of 60 μgmL^{-1} *MIP E* and *NIP E* were performed in DMSO with irinotecan, and the Stern-Volmer plots obtained are reported in **Figure 3.16**. Both titrations did not lead to a total quenching of nanogels fluorescence, however a decrease of their emission intensity was observed, and these variations were both detectable and reproducible.

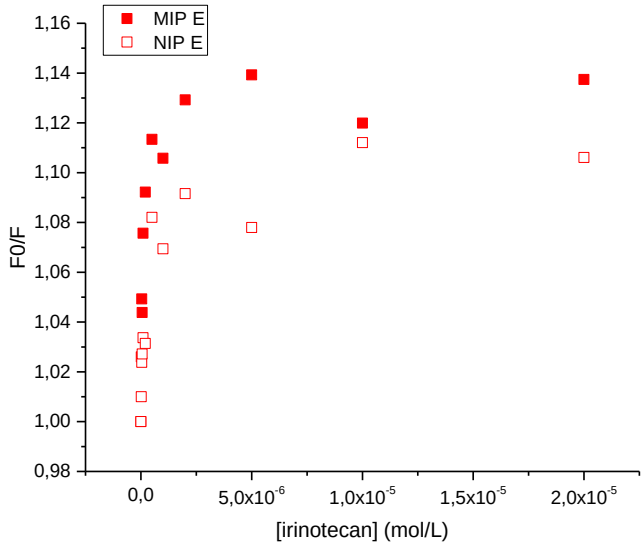

Figure 3.16: Stern-Volmer plots of 60 μgmL^{-1} *MIP E* and *NIP E* titrated with irinotecan in DMSO.

A linearity of both plots was observed at drug concentrations below 2 μM, while at higher concentrations a plateau was reached, suggesting the presence of specific binding sites population occupied only at irinotecan in the nanomolar range.

In **Table 3.11** the values of Stern-Volmer constants (K_{SV}) and related bimolecular quenching constants (k_q) are reported.

Nanogel	Concentration range	K_{SV} [10^4 Lmol^{-1}]	k_q [10^{12} Lmol^{-1}s^{-1}]
MIP E	0 – 2 μM	4.87	5.87
	2 – 20 μM	0.0104	0.0125
NIP E	0 – 2 μM	4.04	4.86
	2 – 20 μM	0.0250	0.0301

Table 3.11: Values of Stern-Volmer constants and bimolecular quenching constants obtained by Stern-Volmer analysis of *MIP E* and *NIP E* fluorescence titration with irinotecan in DMSO.

A static quenching was observed for both *MIP E* and *NIP E* within the concentrations range below 2 μM, as K_{SV} values were larger than diffusion limit (1x10^{10} Lmol^{-1}s^{-1}). However, the K_{SV} order of magnitude was the same, indicating that *MIP E* was not specific for the anticancer drug, hence the HPLC rebinding results previously obtained were confirmed by these fluorescence titrations. At drug concentrations higher than 2 μM, instead, the values of bimolecular quenching constants were not so far by the diffusion limit value, indicating that probably, fluorescence quenching observed was

also affected by a collisional contribute. As the Stern-Volmer constant (K_{SV}) can be considered as the association constant of template-MIP complex (**Equation 3.10**), if a static quenching occurs, it is possible to estimate the apparent dissociation constant for *MIP E* and *NIP E*, at concentrations below 2 µM, simply by calculating the inverse of Stern-Volmer constants (1 / K_{SV}). Therefore, values of apparent dissociation constants (K_D) of $20.5 \cdot 10^{-6}$ molL^{-1} and $22.7 \cdot 10^{-6}$ molL^{-1} for *MIP E* and *NIP E*, respectively, were obtained.

MIP E vs MIP F in 3:1 methanol:water

To compare the affinity of *MIPs E* and *F* for irinotecan, fluorescence titrations of both nanogels with the drug were then performed in 3:1 methanol:water mixture.

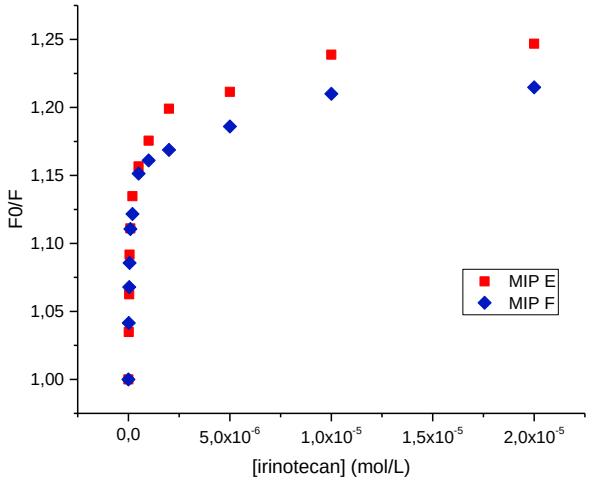

Figure 3.17: Stern-Volmer plots of 60 µgmL^{-1} *MIPs E* and *F* fluorescence titrations with irinotecan in 3:1 methanol:water mixture.

The Stern-Volmer plots obtained by these titrations in 3:1 methanol:water showed as usual a bimodal linear trend for both nanogel. A larger value of the slope was observed in the nanomolar range of irinotecan concentrations (0 – 1 µM), while a plateau was then reached by both polymers above 1 µM. Values of the related Stern-Volmer constants and bimolecular quenching constants are reported in **Table 3.12**.

Nanogel	Concentration range	K_{SV} [10^4 $Lmol^{-1}$]	k_q [10^{12} $Lmol^{-1}s^{-1}$]
MIP E	0 – 1 µM	13.80	16.6
	1 – 20 µM	0.337	0.405
MIP F	0 – 1 µM	12.21	14.70
	1 – 20 µM	0.280	0.336

Table 3.12: Values of Stern-Volmer constant (K_{SV}) and related bimolecular quenching constants (k_q) obtained by Stern-Volmer analysis of 60 μgmL^{-1} *MIPs E* and *F* fluorescence titrations with irinotecan in 3:1 methanol:water mixture.

MIP E and *MIP F* showed a similar behaviour in 3:1 methanol:water mixture. A very high affinity for the drug was observed at concentrations lower than 1 µM, with quenching constants in the order of 10^{13} $Lmol^{-1}s^{-1}$. At concentrations higher than 1 µM, instead, the values of the bimolecular quenching constants dramatically decreased and were not so far from the diffusion limit, indicating that probably a combination of both static and collisional quenching occurred at micromolar concentrations range. However, *MIP E* showed much higher sensitivity in methanol rather than in DMSO, even improving its performance in the micromolar concentration range. On the contrary of the expected MIP behaviour in methanol, it seemed that this solvent did not decrease MIP sensitivity, rather disfavoured accessibility to non-specific binding sites, leading to a more efficient quenching of fluorescence, within the irinotecan therapeutic range. This behaviour in methanol was very promising for future development of MIPs.

Third set of fluorescent MIPs for irinotecan: using different naphtalimides derivatives

A third set of fluorescent polymers imprinted with irinotecan was designed using different 1,8-naphtalimide derivatives, namely compounds **5**, **6** and **10**, previously synthesized, to see if incorporation of a different fluorescent dye than monomer **2** in the MIPs matrix, could improve their rebinding capability and specificity.

*^{1}H-NMR titration of irinotecan with compound **10***

The ^{1}H-NMR titration of 4 mM irinotecan with the synthetic monomer **10** was performed in DMSO-d_6 and increasing amounts of compound **10** were added from 0.25 (1 mM) to 2.5 equivalents (10 mM), because of low availability of monomer **10** and its low solubility in DMSO. The chemical shift variations of irinotecan's protons before and

after the adding of 2.5 equivalents of monomer **10** are reported in the histogram of **Figure 3.18**.

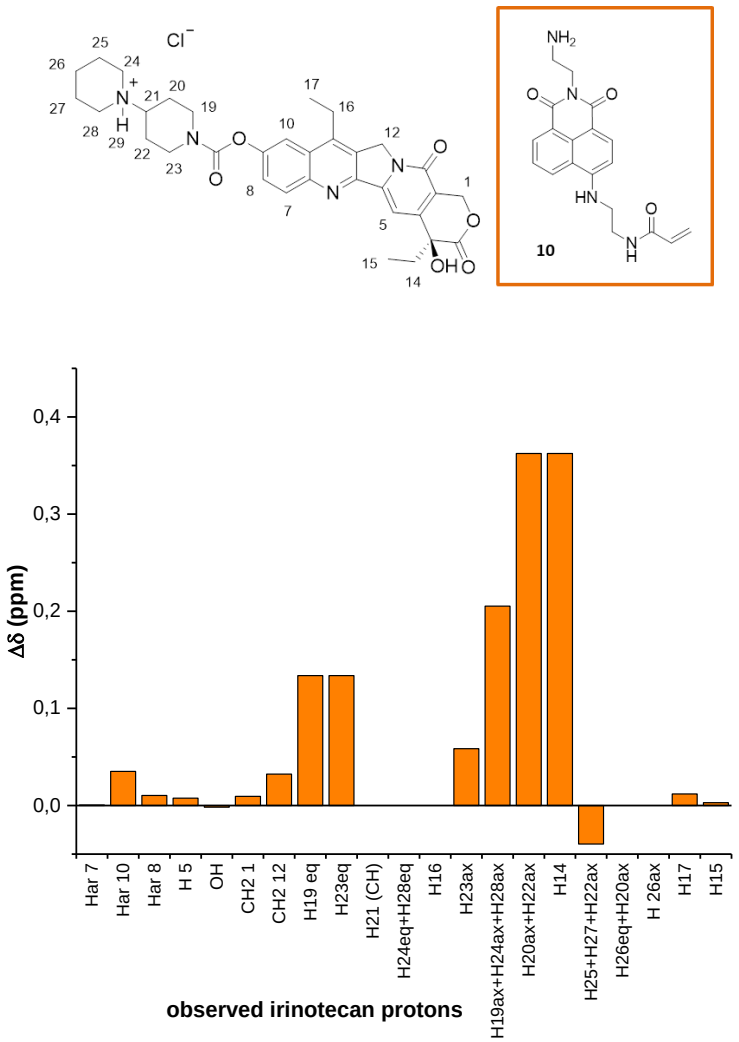

Figure 3.18: Chemical structures of irinotecan and monomer **10** and histogram reporting the variation of observed irinotecan protons chemical shift before and after the adding of 2.5 equivalents of compound **10**.

As previously seen in the titrations with monomers **2** and **3**, irinotecan piperidinium (*NH*$^+$) signal disappeared after the adding of 0.5 equivalents of compound **10**; it is also interesting to notice that irinotecan protons mainly shifted upon ^{1}H-NMR titration with functional monomer **10** belong to the bis-piperidino moiety, suggesting that the *NH*$^+$ proton could be transferred to the amino terminal group of the naphtalimide derivative. In **Figure 3.19** the chemical shifts variations of irinotecan protons observed upon binding to compound **10** are reported.

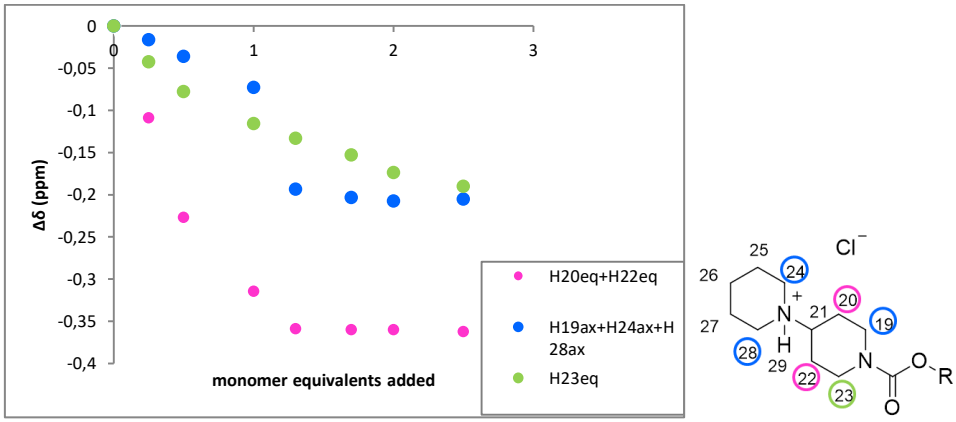

Figure 3.19: Variation of chemical shift of irinotecan protons *H20eq+H22eq*, *H19ax+H24ax+H28ax* and *H23eq*, all belonging to the bis-piperidino moiety of the drug, which chemical structure is reported right.

All the protons reported in **Figure 3.19**, except for equatorial *H23*, reached a plateau at 1.3 equivalents, suggesting that all available molecules of irinotecan were involved in establishing interactions with monomer **10**, and increasing amounts of compound **10** could not shift anymore the equilibrium from the free to the bound form. Equatorial protons *H20* and *H22* were more affected by the presence of the fluorophore, as they are found on the same plane of *NH*$^+$ proton.

MIPs I, *J* and *K* were designed in order to pair an appropriate co-monomer to the chosen functional monomer, on the basis of their chemical-physical properties. *MIP I* was prepared using 15% of compound **5**, which does not expose any amino or carboxyl terminal group, hence MAA was employed as co-monomer to increase MIP solubility in water and favour hydrogen bonds interactions. *MIP J*, instead, was prepared using 15% of monomer **6**, containing a terminal carboxylic group, and NIPAM as co-monomer, which could increase MIP solubility in water. Finally, *MIP K* was prepared using only 10% of compound **10** (because of its low availability), 30% of NIPAM as co-monomer, and MBA as cross-linker, as it is an acrylamide as monomer **10**, and similar reactivity of the polymerisable groups could probably favour fluorophore incorporation. The

amount of AIBN employed for the polymerization was 18% for *MIPs* and *NIPs I* and *J*, since monomers **5** and **6** should show similar reactivity to monomer **2**, while for *MIP K* and *NIP K* just 5%, because compound **10** was expected to be more reactive. Molar ratio of template and functional monomer used was fixed at 1.2 : 1, respectively.

Compositions, yields, reaction time and dimensions of MIPs and relative NIPs belonging to this third series of nanogels, designed for irinotecan, are reported in **Table 3.13**.

Polymer	Funct. Mon.	Co-monomer	Cross-linker	Reaction Time	Yield	DLS Size Distr. By Number (nm)	PDI
MIP I	**5** (15%)	MAA (15%)	EGDMA (70%)	96 h	78%	15.6±0.6	0.187
MIP J	**6** (15%)	NIPAM (15%)	EGDMA (70%)	96 h	71%	16.5±2.7	0.247
MIP K	**10** (20%)	NIPAM (30%)	MBA (50%)	24 h	69%	5.7±2.6	0.561
NIP I	**5** (15%)	MAA (15%)	EGDMA (70%)	96 h	77%	8.6±1.1	0.318
NIP J	**6** (15%)	NIPAM (15%)	EGDMA (70%)	96 h	67%	29.9±4.2	0.269
NIP K	**10** (20%)	NIPAM (30%)	MBA (50%)	24 h	56%	-	-

Table 3.13: Compositions, yields and particles dimensions of MIPs and NIPs of the third set of fluorescent polymers for irinotecan. Time of polymerisation is also reported for each nanogel. Particles hydrodynamic diameters of 0.25 mg/mL nanogel solutions in DMSO were measured by DLS, after sonication and filtration on 0.45 µm PTFE filters. DLS measurements of NIP K were not performed because of high aggregation. PDI indicates the Poly Dispersion Index measured at DLS.

The yields of the polymers prepared are quite similar and seemed not significantly affected by the time employed for polymerisation. The particles dimensions are all in the nanomolar range, and both *MIP K* and *NIP I* resulted particularly small. The different particles sizes observed, comparing each MIP with the corresponding NIP, could be due to the presence or absence of irinotecan during polymerisation, that maybe affected the final polymer morphology.

Uv-Visible measurements

To calculate the amount of the functional monomers **5**, **6** and **10** incorporated during polymerisation, UV-Visible absorbance measurements of each polymer solution in DMSO were carried out. The molar extinction coefficients were obtained performing

UV-Visible calibration curves of each dye in DMSO at their maximum absorbance wavelength.

In Table **3.14** concentrations of each monomer ($nmolmg^{-1}$) in polymer matrix and percentage of fluorophore incorporated during polymerization are reported.

Nanogel	Amount (mon.) incorporated/mg polymer ($nmol \cdot mg^{-1}$)	Percentage of mon. incorporated during polymerisation
MIP I	24.5 (mon. **5**)	3.2%
MIP J	17.4 (mon. **6**)	3.5%
MIP K	"163" (mon. **10**)	"15.7"%
NIP I	20.3 (mon. **5**)	2.1%
NIP J	22.3 (mon. **6**)	3.0%
NIP K	"365" (mon. **10**)	"33.9"%

Table 3.14: Concentrations ($nmolmg^{-1}$) of each functional monomer incorporated by the corresponding nanogel (of third set of fluorescent polymers for irinotecan) during polymerisation reaction, and residual percentage of each monomer inside polymers matrix. *MIP K* and *NIP K* values are approximate, as they were filtered on 0.45 µm PTFE filter, as high aggregates were presents even in diluted solutions.

As expected, Uv-Visible measurements confirmed that the N-allyl group resulted much less reactive than N-acryloyl, as incorporation of the fluorophore in *MIP K* and *NIP K* was at least six fold higher. The percentage of monomer incorporated in the polymers matrix was very low (around 3% of the total amount of monomer used for MIPs and NIPs synthesis), even if fluorophores **5** and **6** were different to the previously employed monomer **2**.

HPLC rebinding assays

Rebinding capability of each nanogel in water was studied by HPLC assays, previously mentioned. 1 $mgmL^{-1}$ polymers suspensions in 50 µM aqueous irinotecan were incubated for 24 hours. The amount of drug absorbed over time by each nanogel is reported in **Figure 3.20**.

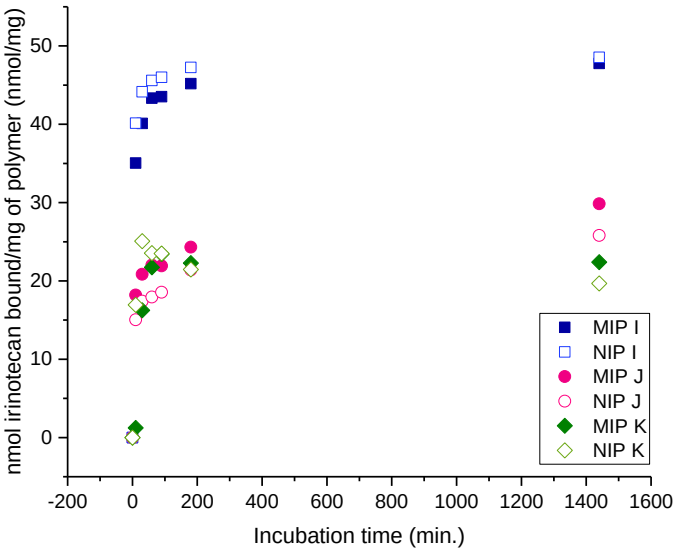

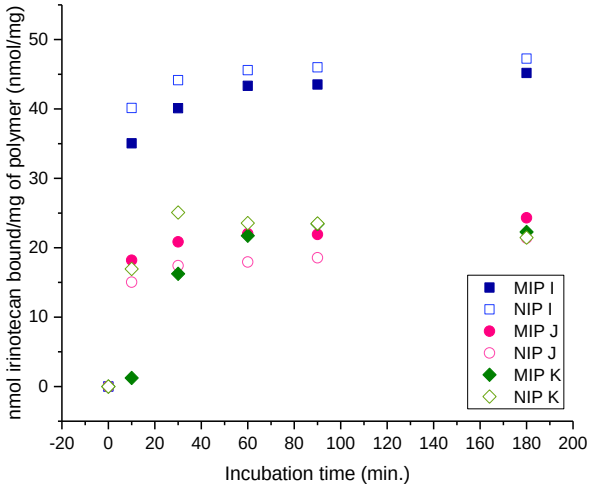

Figure 3.20: Binding kinetics of MIPs and NIPs belonging to the third set of polymers for irinotecan, obtained by HPLC experiments in water. a): total incubation time range (0-24 h); b): short incubation time range (0-3 h). All polymers were separated over time from unbound irinotecan solution by spinning, except for *MIP K* and *NIP K* that were kept in a dialysis tube during incubation, as these polymers were slightly soluble in water.

In general, no high specificity was observed for the MIPs belonging to the this series of polymers. *MIP I* and *NIP I* showed the highest affinity for irinotecan (capturing almost the total amount of irinotecan available after 24 hours), probably, as previously seen, thanks to the presence of MAA in their matrix. However, *MIP I* resulted not specific for irinotecan, neither after 24 hours, and saturation of binding sites was reached after one hour of incubation. *MIP J* showed the best specificity and over time it absorbed more and more amounts of irinotecan, up to catch 60% of total drug available, after 24 hours. *MIP K*, instead, showed the slowest kinetic at the beginning, absorbing around 30% of the drug after 30 minutes, but reaching a saturation of binding sites (corresponding to about 45% of irinotecan) already after one hour.

Fluorescence measurements

To investigate the quenching efficiency of *MIP I*, *J* and *K* in the presence of irinotecan, fluorescence titrations of these polymers were performed in DMSO or 3:1 DMSO:water mixture.

60 μgmL^{-1} *MIP I* was titrated with irinotecan in 3:1 mixture of DMSO:water, within its therapeutic range. A quenching of *MIP I* fluorescence was observed, particularly in the nanomolar range. At concentrations higher than 1 µM, however, *MIP I* fluorescence did not change significantly, and a sort of plateau of the corresponding Stern-Volmer plot was observed from 2 to 20 µM (**Figure 3.21**).

To 100 μgmL^{-1} solution of *MIP J* in DMSO increasing amounts of irinotecan were added, within the concentrations range 20 nM – 2 µM. Conversely to previous MIPs titrations, *MIP J* concentration was increased from 60 to 100 μgmL^{-1}, because no quenching was observed using the usual 60 μgmL^{-1} concentration. Unfortunately, though MIPs concentration was increased, only a slight quenching of its fluorescence after the adding of the drug, was observed. The corresponding Stern-Volmer plot is reported in **Figure 3.21**, and a linear trend can be seen only in the range 0 – 130 nM.

For *MIP K*, fluorescence titration of a 20 μgmL^{-1} nanogel solution was employed, as this imprinted polymer highly aggregated and a more dilute solution was necessary for the measurements. The titration was performed in 3:1 DMSO:water mixture, within irinotecan concentrations in the 20 nM – 20 µM range. The corresponding Stern-Volmer plot is reported in **Figure 3.21**. Despite the lower *MIP K* concentration, a better fluorescence quenching was observed, compared to *MIP J*. As previous MIPs, a decrease of trend linearity was observed at concentrations higher than 1 µM.

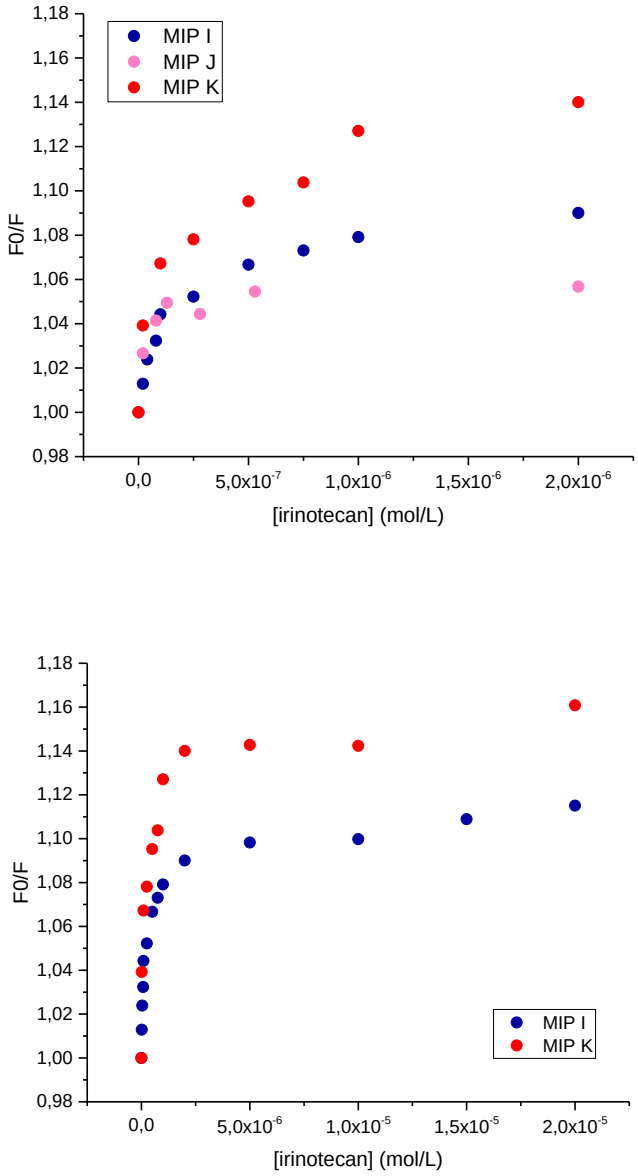

Figure 3.21: Top: Stern-Volmer plots of *MIPs J*, *I* and *K* fluorescence titrations with irinotecan in DMSO (*MIP J*) and 3:1 DMSO:water (*MIPs I* and *K*) within drug concentrations range 0 – 2 µM. Bottom: Stern-Volmer plot related to *MIPs I* and *K* titrations, within total concentration range 0 – 20 µM.

The Stern-Volmer constants and relative bimolecular quenching constants of these titrations are reported in **Table 3.15**.

Nanogel	Concentration range	K_{SV} [10^4 $Lmol^{-1}$]	k_q [10^{12} $Lmol^{-1}s^{-1}$]
MIP I	0 – 1 µM	6.75	8.13
	1 µM – 20 µM	0.161	0.194
MIP J	0 – 130 nM	33.6	40.5
	130 nM – 1 µM	not linear	-
MIP K	0 – 1 µM	9.77	11.8
	1 – 20 µM	0.142	0.171

Table 3.15: Stern-Volmer constants (K_{SV}) and corresponding bimolecular quenching constants values, related to *J* and *K* fluorescence titrations with irinotecan in DMSO and 3:1 DMSO:water, respectively. Values are expressed for concentrations ranges were linearity of the Stern-Volmer trend was observed. The lifetime value (τ_0) employed to calculate k_q was the one related to monomer **2**, as references were reported in literature about compounds **5**, **6** and **10**, and the instrument employed did not allow to measure fluorescence lifetimes.

The results obtained by Stern-Volmer analysis confirmed that a static quenching occurred and a MIP-irinotecan complex was formed with all *MIPs I*, *J* and *K*. In 0 - 1 µM concentrations range *MIPs I* and *K* showed very high affinity for the anticancer drug, and *MIP K* gave the highest value of the bimolecular quenching constant. However the values of the bimolecular quenching constants were all one order of magnitude lower than *MIP E* and *F*, and no linearity of the trend was present at concentrations higher than 1 µM. Therefore, employing different dyes than monomer **2** did not give very positive results and confirmed that compound **2** seems the best match for the synthesis of fluorescent MIPs, using a template as irinotecan.

In conclusion, substitution of fluorophore **2** with monomers **5**, **6** and **10**, demonstrated that the amino terminal group of the naphtalimide moiety is not essential to have a quenching of MIP fluorescence upon binding to irinotecan. *MIP I* and *MIP J*, containing respectively monomers **5** and **6**, indeed, gave a quite good Stern-Volmer plot, however none of them behaved as *MIP K* (containing compound **10**), which showed the best fluorescence quenching in the presence of the anticancer drug, indicating that, in any case, the amino terminal group increased MIP performance towards irinotecan. Despite these good results, the specificity was not improved, and the incorporation of compound **10** rather than monomer **2** did not increase MIP performance, but it rather favoured *MIP K* nanoparticles aggregation in DMSO. Finally, the use of MAA as co-monomer, as previously seen, ensured high irinotecan absorbance in water at HPLC rebinding assays, but again confirmed the presence of many non-specific binding sites in the polymers matrix. Hence, further investigations to improve the performance of the imprinted polymers for irinotecan had to be done.

Fourth set of fluorescent MIPs for irinotecan

As from previous results not any MIP imprinted with irinotecan showed good specificity, despite good rebinding capacities were observed, a new set of fluorescent MIPs was designed, using 30% of the functional monomer **2**, which gave the best results compared to the other fluorophores, and 70% of EGDMA as cross-linker. The amount of AIBN, the C_m, the time of polymerisation and also the kind of AIBN activation were changed one by one, in order to find the best combination of variables to get the more specific MIP for the anticancer drug irinotecan. The choice to avoid the adding of a co-monomer was due to the fact that it could interfere with template interaction with fluorophore, becoming even a competitor (as previously seen with MAA) of the fluorescent dye and favouring, for example, non-specific interactions. The molar ratio between template and functional monomer was fixed at respectively 1 : 2; this choice was done for two reasons, first because it was previously demonstrated that fluorophore **2** is not as reactive as the cross-linker, hence increasing the amount of functional monomer may favour its incorporation during polymerization, and second because a higher amount of monomer **2** shifts the equilibrium from the free monomer to the irinotecan-bound form, as previously showed at ^{1}H-NMR titration. The non-imprinted polymers (NIPs), obtained following the same MIPs procedure except for template adding, were prepared only for *MIPs L*, *M* and *O*, as *MIPs N*, *P* and *Q* were prepared just to investigate if decreasing the C_m from 1% to 0.1% (*MIP P*), decreasing the amount of AIBN from 18% to 5% (*MIP N*) and photo-initiating the reaction (*MIP Q*) were, in general, helpful for MIP performance at fluorescence. Composition, C_m, percentage of AIBN employed, time of polymerization, yield and size of particles obtained for each MIP and NIP prepared are reported in **Table 3.16**.

Polymer	Funct. Mon.	Cross-linker	AIBN	C_m	Reaction Time	Yield	DLS Size Distr. By Number (nm)	PDI
MIP L	**2** (30%)	EGDMA (70%)	18%	1%	96 h	77%	13.1±2.0	0.387
MIP M	**2** (30%)	EGDMA (70%)	18%	1%	24 h	42%	16.0±1.1	0.507
MIP N	**2** (30%)	EGDMA (70%)	5%	1%	96 h	48%	8.4±0.7	0.857
MIP O	**2** (30%)	EGDMA (70%)	10%	1%	96 h	65%	7.8±0.4	0.658
MIP P	**2** (30%)	EGDMA (70%)	18%	0.1%	96 h	34%	207±7.1	0.587
MIP L-UV	**2** (30%)	EGDMA (70%)	18%	1%	6 h (UV)	39%	21.7±3.0	0,867
NIP L	**2** (30%)	EGDMA (70%)	18%	1%	96 h	42%	16.1 ± 1.9	0.242
NIP M	**2** (30%)	EGDMA (70%)	18%	1%	24 h	42%	16.9±1.4	0.248
NIP O	**2** (30%)	EGDMA (70%)	10%	1%	96 h	66%	0.731±0.060	0.665

Table 3.16: Composition, percentage of AIBN, C_m, reaction time, yield and particles dimension of each nanogel belonging to the fourth set of MIPs for irinotecan. *MIP L-UV* was obtained using UV irradiation (360 nm) at 40 °C. Particles hydrodynamic diameter was obtained by DLS measurements of 0.25 $mgmL^{-1}$ DMSO solutions of each polymer, after sonication and filtration on 0.45 µm PTFE filter; PDI indicates the Poly Dispersion Index.

The reaction yields obtained were, in general, except for *MIP L*, not very high, particularly when the critical monomer concentration (C_m) employed was 0.1% (*MIP P*) and reaction time was reduced to 24 hours (*MIP M*) or 6 hours by photo-activation of the radical initiator AIBN (*MIP L-UV*). All *MIPs* and *NIPs* belonging to this fourth set of polymers showed dimensions in the nanometer scale, between 8 and 17 nm, as measured by DLS experiments. However only *MIP P* gave very large hydrodynamic particle diameters, around 200 nm, suggesting that maybe lowering the C_m higher aggregates were formed.

Transmission Electron Microscopy of MIP L

MIP L was also investigated by transmission electron microscopy, using a carbon coated grid. The relative images are reported in **Figure 3.22** and gave an average particle size of 6.2 ± 3.4 nm. This result was consistent with the one obtained by DLS, as in TEM measures the solvation sphere is obviously not present. The particles dimensions observed at TEM were comparable to the ones reported in the literature.[45]

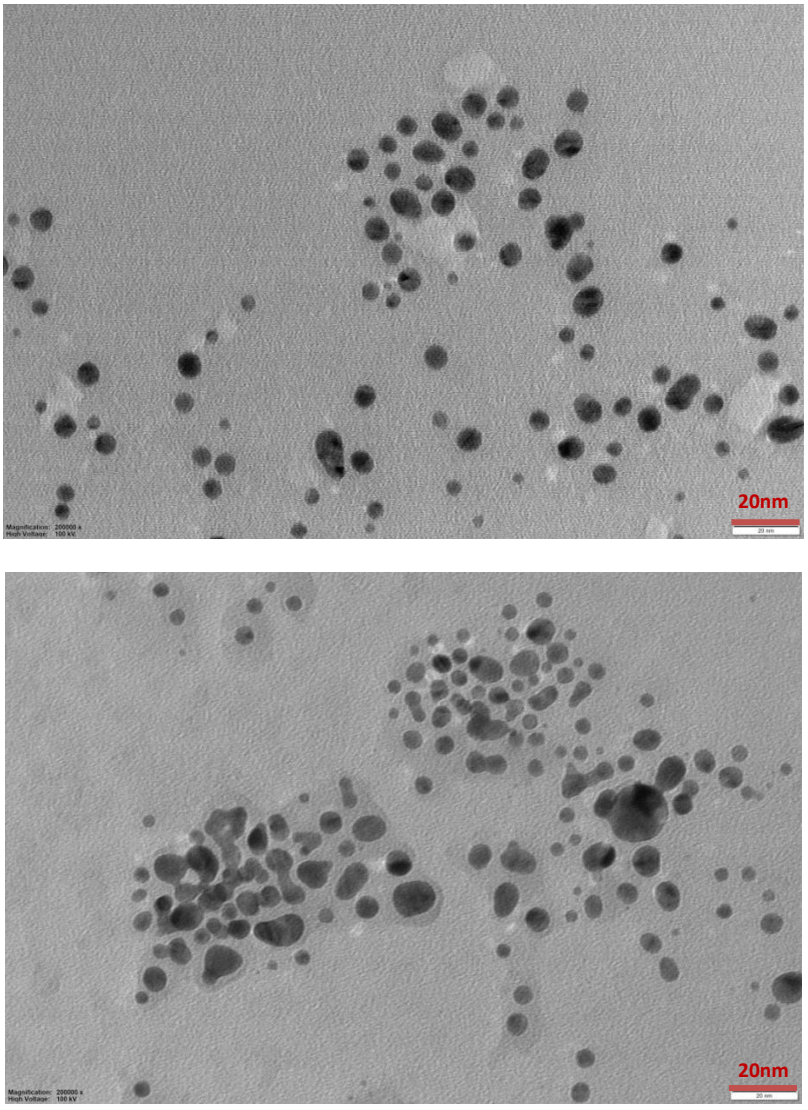

Figure 3.22: TEM images of *MIP L*.

Uv-Visible measurements

The amount of the functional monomer **2** incorporated during polymerisation was determined by UV-Visible absorbance measurements of each polymer solution in DMSO. In **Table 3.17** the nanomoles of each monomer per mg of polymer and the percentage of fluorophore incorporated during the reaction, are reported.

Nanogel	Amount of mon. 2 incorporated/mg polymer (nmol·mg^{-1})	Percentage of mon. 2 incorporated during polymerisation
MIP L	88.7	6.6%
MIP M	114.0	8.5%
MIP N	104.6	7.8%
MIP O	66.7	5.1%
MIP P	74.6	5.6%
MIP L-UV	51.6	3.8%
NIP L	90.2	6.8%
NIP M	93.6	7.0%
NIP O	83.3	6.3%

Table 3.17: Monomer **2** concentrations (nmolmg^{-1}) incorporated by each nanogel of the fourth set during polymerisation reaction, and residual percentage of each monomer inside polymers matrix.

Despite an higher percentage of monomer **2** was employed for this fourth set of MIPs design, the amount of incorporated dye resulted very low, just a little higher (around 6/7%) than MIPs of first and second sets, containing 15% of **2** (which showed percentage of monomer incorporation around 5%). These results underlined again the very low reactivity of compound **2**, that was investigated also through an NMR experiment.

*NMR investigations of monomer **2** conversion in MIP L and NIP L*

Two polymerisation mixtures, with or without irinotecan, were prepared on a small scale in DMSO-d_6, maintaining the same *MIP L* and *NIP L* compositions reported in **Table 3.16**. The ^{1}H-NMR spectra of each mixture were recorded before starting polymerization, after one hour and after 24 hours of reaction at 70 °C. An external standard (2-Bromo-6-methoxynaphtalene) was added to each mixture before recording the first NMR spectrum. Monomer **2** and EGDMA (cross-linker) conversions after one and 24 hours of polymerization, are reported in **Table 3.18**.

Nanogel	Polymerization time	Monomers	conversion (%)
MIP L	1 h	**2**	38
		EGDMA	53
	24 h	**2**	49
		EGDMA	99
NIP L	1 h	**2**	60
		EGDMA	66
	24 h	**2**	65
		EGDMA	99

Table 3.18: NMR conversions of monomer **2** and EGDMA after 1 and 24 hours of polymerisation at 70 °C, in presence (*MIP L*) and absence (*NIP L*) of irinotecan.

The experiment demonstrated that monomer **2** is effectively less reactive of the cross-linker, and, above all, it was not totally converted to radicals, even after 24 hours of polymerisation. Indeed, only 49% of compound **2** reacted in the presence of irinotecan (MIP L), while 65% in the absence of the template (*NIP L*), suggesting firstly, that the presence of irinotecan slightly hindered monomer **2** conversion, and secondly that dye incorporation in polymers matrix cannot be higher than circa 50% of initial employed amount. This investigation demonstrated that final composition of the polymers is affected by monomers reactivity and also by the presence of the template.[46]

However, the fact that a low amount of monomer **2** was incorporated in the polymer matrix did not mean that binding sites with low specificity were present in the polymers. As a matter of fact, a molar ratio between irinotecan and monomer **2** of 1 : 2 was respectively employed exactly to favour formation of more specific cavities, containing not only one molecule of fluorescent dye for each template molecule.

HPLC rebinding assays

The rebinding studies of this fourth series of MIPs were performed in water, following the already mentioned HPLC protocol. The results obtained for *MIPs* and *NIPs L*, *M* and *S* are reported in a histogram is **Figure 3.17**, to see if these MIPs showed specificity for irinotecan in water and identify the best MIP among them, in terms of affinity and specificity for irinotecan.

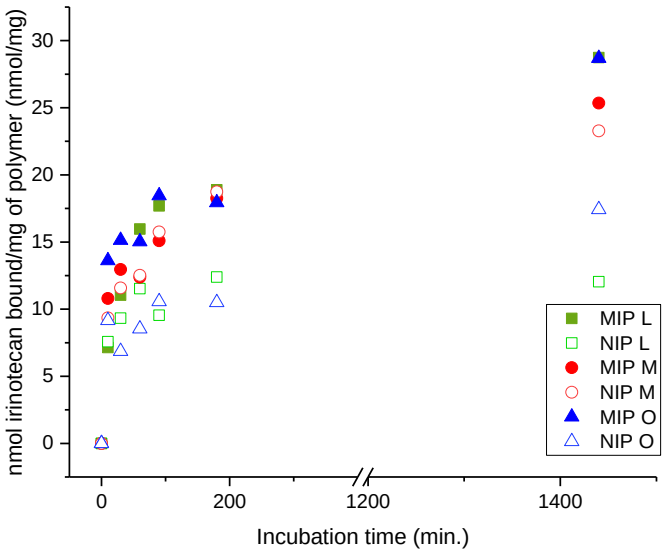

a)

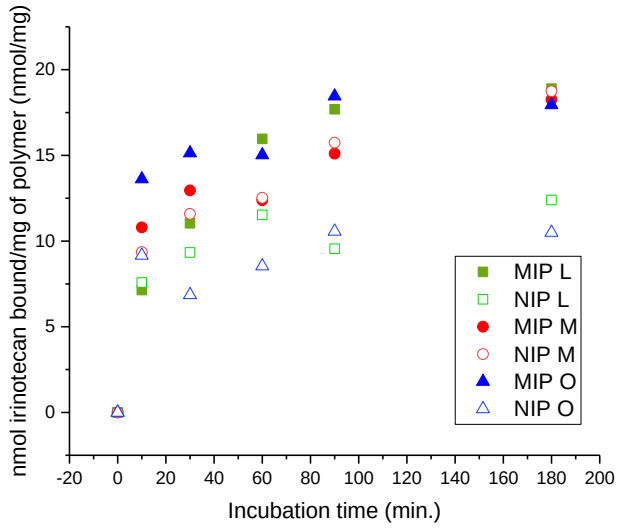

b)

Figure 3.23: Binding kinetics of *MIPs* and *NIPs L*, *M* and *O*, measured by HPLC analysis. a): total incubation time range (0-24 h); b): short incubation time range (0-3 h). All polymers were separated over time from unbound irinotecan solution by centrifugation.

From the kinetics in **Figure 3.23** it is possible to notice that *MIPs L* and *O* showed very good specificity and affinity for irinotecan, even after 24 hours of incubation. The

binding kinetics of *MIPs L* and *O* were both quite slow, perhaps because the more specific binding sites required more time to be reached, rather non-specific ones. *MIP M*, instead, did not show very high specificity and its binding capacity was very similar to the one of the corresponding *NIP M*. As *MIP L* and *MIP O* showed specificity towards irinotecan in water, it was possible to calculate their Imprinting Factor (I.F.), that is defined as the ratio between irinotecan concentration bound by each MIP and bound by corresponding NIP. For *MIP L* a 2.4 imprinting factor was obtained, after 24 hours of incubation in water, while for *MIP O* an I.F. of 1.6 was achieved.

To compare the binding affinity for irinotecan in water of this fourth set of imprinted polymers, the results obtained for all MIPs by HPLC measurements are reported in **Figure 3.24**.

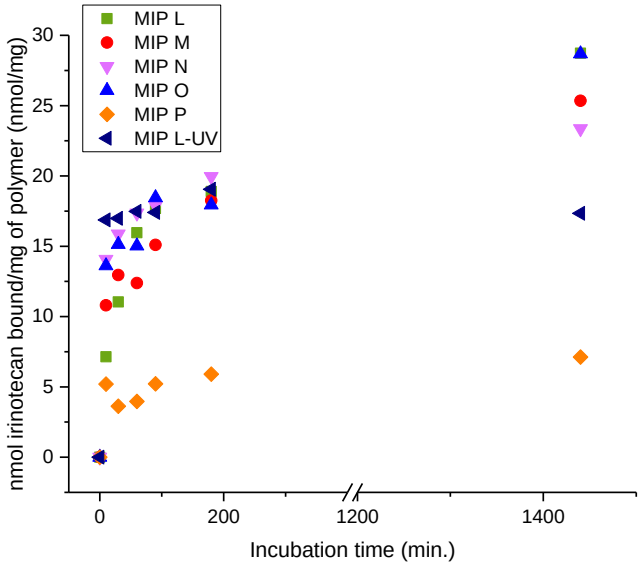

a)

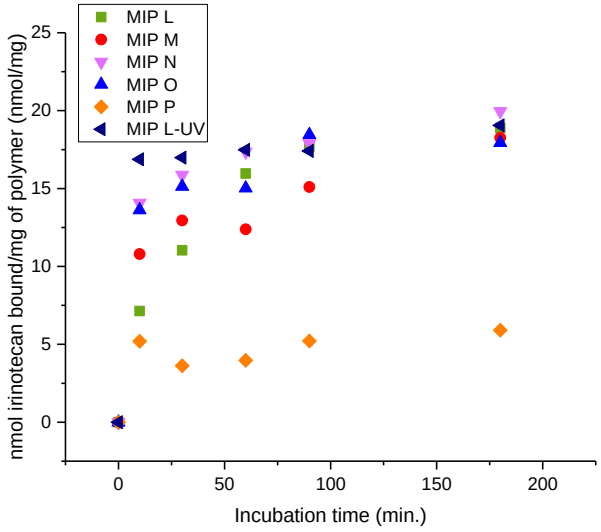

b)

Figure 3.24: Binding kinetics of M*IPs* and *NIPs L*, *M*, *N*, *O*, *P* and *L-UV*, belonging to the fourth series of fluorescent MIPs, obtained by HPLC rebinding assays in water. a): total incubation time range (0-24 h); b): short incubation time range (0-3 h).

Comparing the rebinding capabilities of MIPs prepared using 30% of monomer **2**, a similar behaviour of binding kinetics can be observed for *MIPs L*, *M*, *N* and *O*, while *MIP P*, prepared decreasing the C_m from 1 to 0.1%, showed the worst rebinding capacity for the anticancer drug in water, confirming that for a template as irinotecan, the best value of C_m was 1%. *MIP L-UV*, obtained by photo-activation of the radical initiator, showed the faster binding kinetic, absorbing 17 $nmolmg^{-1}$ of irinotecan already after 10 minutes of incubation, but its binding capacity did not increase over time, suggesting that a saturation of sites was probably already reached after 10 minutes.

MIPs N and *O*, prepared using 5% and 10% of AIBN, respectively, showed very similar binding kinetics from the beginning of the experiment until 180 minutes of incubation. Only after 24 hours, *MIP O* absorbed almost 10% more irinotecan than *MIP N*. Hence, the percentage of AIBN seemed not to affect the MIPs rebinding capabilities.

Fluorescence measurements

The fluorescence studies of MIPs belonging to the fourth set of polymers were performed directly in 3:1 methanol:water medium, as this environment is more similar to the final real samples of plasma treated.

Fluorescence titrations of 60 µgmL^{-1} *MIPs L*, *M* and *O* with irinotecan in 3:1 methanol:water mixtures were performed, in order to select the best MIP for further studies. The choice of these *MIPs* was due to the best rebinding results observed at HPLC experiments. The drug concentrations range investigated was between 20 nM and 100 µM. The Stern-Volmer plots are reported in **Figure 3.25**.

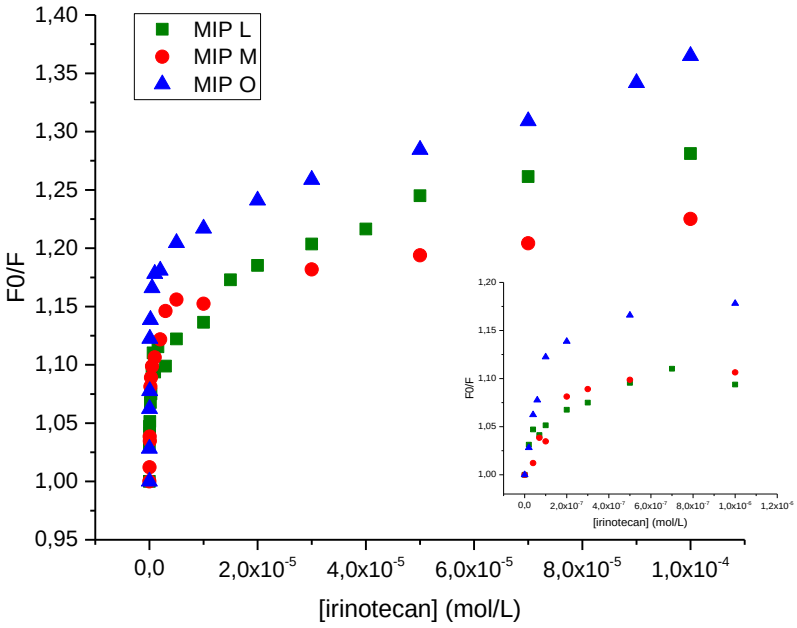

Figure 3.25: Stern-Volmer plots of 60 µgmL^{-1} *MIPs L*, *M* and *O* fluorescence titrations with irinotecan in 3:1 methanol:water mixture. Insert: lower concentrations range (0 – 1 µM).

In the Stern-Volmer plots of **Figure 3.25** we can observe that *MIP O* gave the more efficient fluorescence quenching, compared to *MIPs L* and *M*, both at nanomolar and micromolar concentrations of irinotecan. Considering the anticancer agent therapeutic range (20 nM – 20 µM), a quite similar trend behaviour is shown by *MIP L* and *MIP M*, while at very high concentrations, over 20 µM, *MIP L* demonstrated higher fluorescence quenching, hence affinity for irinotecan.

In general, the trend of the Stern-Volmer plots obtained were quite similar to the ones observed for the previous MIPs containing the fluorophore **2**. A good linearity was observed in the nanomolar range, indicating a very high MIPs sensitivity, and a decrease of the slope occurred in the micromolar range.

In **Table 3.19** the values of the Stern-Volmer constants and related bimolecular quenching constants calculated are reported for each nanogel analysed.

Nanogel	Concentration range	K_{SV} [10^4 $Lmol^{-1}$]	k_q [10^{12} $Lmol^{-1}s^{-1}$]
MIP L	0 – 700 nM	12.71	15.31
	700 nM – 10 µM	0.268	0.323
	10 µM – 70 µM	0.193	0.168
MIP M	0 – 3 µM	3.94	4.74
	3 µM – 100 µM	0.0792	0.0954
MIP O	0 – 500 nM	28.38	34.19
	500 nM – 100 µM	0.180	0.217

Table 3.19: Stern-Volmer constants (K_{SV}) and corresponding bimolecular quenching constants (k_q) values, calculated for *MIPs L*, *M* and *O* titrated with irinotecan in 3:1 methanol:water mixture. Values were evaluated in specific concentrations ranges, identified for each MIP based on the Stern-Volmer plot linearity.

All the bimolecular quenching constants resulted higher than the diffusion limit ($1x10^{10}$ $Lmol^{-1}s^{-1}$), in particular at drug concentrations in the nanomolar range, suggesting that a static quenching occurred and a complex MIP-irinotecan was formed. All *MIPs* showed a very high value of k_q at concentrations below 500 nM. Considering these values, *MIPs M* and *O* showed a very similar linear trend at low concentrations, showing very high sensitivity towards irinotecan.

In general, all these MIPs analysed showed very good fluorescence results, hence *MIP L* and *O* were selected for further investigations, as both of them showed at HPLC rebinding experiments the highest specificity for irinotecan.

The effect of MIP concentration

To study the behaviour of *MIP L* and *O* at different concentrations in 3:1 methanol:water mixtures, fluorescence titrations of both *MIPs* were performed at 30, 60 and 120 μgmL^{-1}. In **Figure 3.26** the corresponding Stern-Volmer plots are reported, except for 120 μgmL^{-1} *MIPs* titrations, because at this concentration both polymers started to aggregate, precipitation occurred and values of fluorescence intensities were not stable.

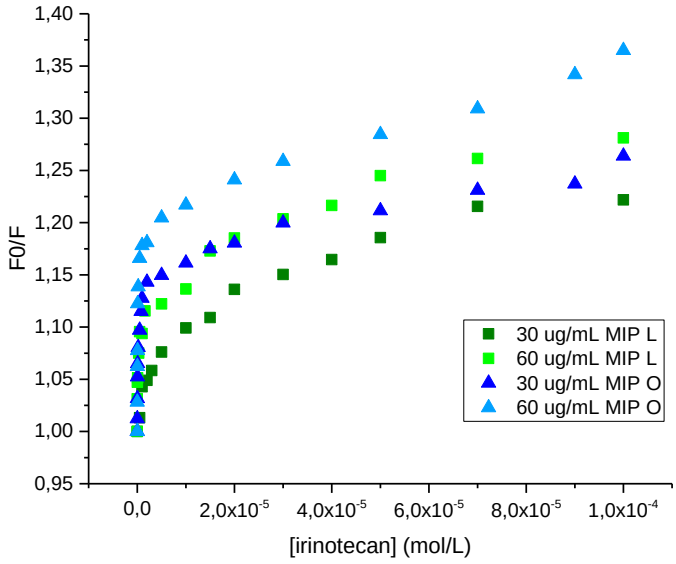

Figure 3.26: Stern-Volmer plots of 30 and 60 µgmL^{-1} *MIPs L* and *O* fluorescence titrations with irinotecan in 3:1 methanol:water.

Observing the curves obtained by the Stern-Volmer analysis (**Figure 3.26**) it was clear that for both *MIPs* the 60 µgmL^{-1} concentration was favoured in this medium rather than lower ones, as better fluorescence quenching was obtained, MIP aggregation was far from happening and good sensitivity for irinotecan was gained.

The 60 µgmL^{-1} concentration for *MIP O* and *MIP L* was chosen for further fluorescence studies in the human plasma matrix, reported in the following **Chapter 4**.

[1] Rodríguez Cáceres M., Durán-Merás I., Soto N.E., de Alba P.L., Martínez L.L., *Spectrofluorimetric determination of irinotecan in the presence of oxidant agents and metal ions*, Talanta (2008) 74(5) :1484-1491

[2] Hahn R.Z., Arnhold P.C., Andriguetti N.B., Schneider A., Klück H.M., Dos Reis S.L., Bastiani M.F., Kael I., da Silva A.C.C., Schwartsmann G., Antunes M.V., Linden R., *Determination of irinotecan and its metabolite SN-38 in dried blood spots using high-performance liquid-chromatography with fluorescence detection*, J Pharm Biomed Anal. (2018) 150: 51-58

[3] De Bruijn P., Verweij J., Loos W.J., Nooter K., Stoter G., Sparreboom A., *Determination of irinotecan (CPT-11) and its active metabolite SN-38 in human plasma by reversed-phase high-performance liquid chromatography with fluorescence detection*, J. Chromatogr. B Biomed. Sci. Appl. (1997) 698(1-2): 277-285

[4] Sai K., Kaniwa N., Ozawa S., Sawada J.I., *An analytical method for irinotecan (CPT-11) and its metabolites using a high-performance liquid chromatography: parallel detection with fluorescence and mass spectrometry*, Biomed. Chrom. (2002) 16(3): 209-218

[5] Poujol S., Inguet F., Malosse F., Astre C., Ychou M., Culine S., Bressolle F., *Sensitive HPLC-fluorescence method for irinotecan and four major metabolites in human plasma and saliva: application to pharmacokinetic studies*, Clin. Chem. (2003) 49(11): 1900-1908

[6] Alexiou M.S., Tychopoulos V., Ghorbanian S., Tyman J.H.P., Brown R.G., Brittain P., *The UV-Visible Absorption and Fluorescence of some Substituted 1,8-Naphthalimides and Naphthalic Anhydrides*, J. Chem. Soc. Perkin Trans. (1990) 2: 837-842

[7] Sjoback R., Nygren J., Kubista M., *Absorption and fluorescence properties of fluorescein*, Spectrochim. Acta Part A (1995) 51: L7-L21

[8] Ton X.A., Acha V., Bonomi P., Tse Sum Bui B., Haupt K., *A disposable evanescent wave fiber optic sensor coated with a Molecularly imprinted polymer as a selective fluorescence probe*, Bios. And Bioel. (2015) 64: 359–366

[9] Wagner Wei R., Wan M., Biyikal E., Benito-Peña, Moreno-Bondi M.C., Lazraq I., Rurack K., Sellergren B., *Synthesis, Spectroscopic, and Analyte-Responsive Behavior of a Polymerizable Naphthalimide-Based Carboxylate Probe and Molecularly Imprinted Polymers Prepared Thereof*, J. Org. Chem. (2013) 784: 1377-1389

[10] Ton X.A., Tse Sum Bui B., Resmini M., Bonomi P., Dika I., Soppera O., Haupt K., *A Versatile Fiber-Optic Fluorescence Sensor Based on Molecularly Imprinted Microstructures Polymerized in Situ*, Angew. Chem. Int. Ed. (2013) 52: 8317 –8321

[11] Rouhani Shohre, Nahavandifard F., *Molecular imprinting-based fluorescent optosensor using a polymerizable 1,8-naphthalimide dye as a florescence functional monomer*, Sens. and Act. B (2014) 197: 185–192

[12] Saito G., Velluto D., Resmini M., *Synthesis of 1,8-naphthalimide-based probes with fluorescent switch triggered by flufenamic acid*, http://dx.doi.org/10.1098/rsos.172137

[13] Dato Paduka Ali H., Kruger P.E., Gunnlaugsson T., *Colorimetric 'naked-eye' and fluorescent sensors for anions based on amidourea functionalised 1,8-naphthalimide structures: anion recognition via either deprotonation or hydrogen bonding in DMSO*, New J. Chem. (2008) 32: 1153–1161

[14] Meenakshi V., Vijay L., Kamaldeep., *Synthesis, in vitro evaluation and DNA interaction studies of N-allyl naphthalimide analogues as anticancer agents*, RSC Adv. (2015) 5: 41803–41813

[15] Callan J.F., Prasanna de Silva A., Magr D.C., *Luminescent sensors and switches in the early 21st century*, Tetrahedron (2005) 61: 8551–8588

[16] Peters A.T., Bide M.J., *Amino derivatives of 1,8-naphthalic anhydride and derived dyes for synthetic-polymer fibres*, Dyes and Pigm. (1985) 6 (5): 349-375

[17] Syu M.J., Hsu T.J., Lin Z.K., *Synthesis of Recognition Matrix from 4-Methylamino-N-Allylnaphthal-Imide with Fluorescent Effect for the Imprinting of Creatinine*, Anal. Chem. (2010) 82 (21): 8821–8829; Bojinov V., Konstantinova T., *Synthesis of polymerizable 1,8-naphtalimide dyes containing hindered amine fragment*, Dyes and Pigm. (2002) 54: 239-245

[18] Singh N., Kaur N., Dunn J., Behan R., Mulrooney R.C., Callan J.F., *A polymeric sensor for the chromogenic and luminescent detection of anions*, Eur. Polym. J. (2009) 45 (1): 272-277

[19] Huisgen R., Sauer J., *Nucleophile aromatische Substitutionen über Arine*, Angew. Chem. (1960) 72(3): 91-126

[20] Bunnett J.F., Zahler L.E., *Aromatic Nucleophilic Substitution Reactions*, Chem. Rev. (1951) 49(2): 273-412

[21] Bardajee G.R., *Microwave-assisted solvent-free synthesis of fluorescent naphthalimide dyes*, Dyes and Pigm. (2013) 99: 52-58

[22] Zhang Y., Feng S., Wu Q., Wang K., Yi X., Wang H., Pan Y., *Microwave-assisted synthesis and evaluation of naphthalimides derivatives as free radical scavengers*, Med. Chem. Res. (2011) 20: 752–759

[23] Wu Q., Qin W., *Solvent-Free Synthesis of 1,8-Naphthalimide Derivatives Under Microwaves Irradiation*, Asian J. of Chem. (2011) 23(10): 4713-4714

[24] Sellergren B., Lepistoe M., Mosbach K., *Highly enantioselective and substrate-selective polymers obtained by molecular imprinting utilizing noncovalent interactions. NMR and chromatographic studies on the nature of recognition*, J. Am. Chem. Soc. (1988) 110 (17): 5853–5860

[25] Kleckner I.R. , Foster M.P., *An introduction to NMR-based approaches for measuring protein dynamics*, Biochimica et Biophysica Acta (2011) 1814: 942–968

[26] Rule G.S., Hitchens T.K., *Fundamentals of Protein NMR Spectroscopy*, Springer Editor (2006), ISBN 978-1-4020-3500-5

[27] Maddock S.C., Pasetto P., Resmini M., *Novel imprinted soluble microgels with hydrolytic catalytic activity*, Chem. Commun. (2004) 5: 536–537

[28] Pellizzoni E., Tommasini M., Marangon E., Rizzolio F., Saito G., Benedetti B., Toffoli G., Resmini M., Berti F., *Fluorescent molecularly imprinted nanogels for the detection of anticancer drugs in human plasma*, Biosensors and Bioelectronics (2016) 86: 913–919

[29] Carboni D., Flavin K., Servant A., Gouverneur V., Resmini M., *The First Example of Molecularly Imprinted Nanogels with Aldolase Type I Activity*, Chem. Eur. J. (2008) 14: 7059 – 7065

[30] Graham N.B., Cameron A., *Nanogels and microgels: The new polymeric materials playground*, Pure and Appl. Chem. (1998) 70(6): 1271-1275

[31] Pellizzoni E., *Molecularly Imprinted polymeric nanoparticles for the Therapeutic Drug Monitoring of Anticancer Drugs*, PhD Thesis in Nanotechnology (2015)

[32] Mayes A.G., Whitcombe M.J., *Synthetic strategies for the generation of molecularly imprinted organic polymers*, Adv. Drug Deliv. Rev. (2005) 57: 1742-1778

[33] Wulff G., Chong B. O., Kolb U., *Soluble single-molecule nanogels of controlled structure as a matrix for efficient artificial enzymes*, Angew. Chem. Int. Ed. (2006) 45:2955- 2958

[34] Annamma K.M., Mathew B., *Design of 2,4-Dichlorophenoxyacetic Acid Imprinted Polymer with High Specificity and Selectivity*, Mater. Sci. Appl. (2011) 2: 131-140

[35] Lorenzo R.A., Carro A.M., Alvarez-Lorenzo C., Concheiro A., *To Remove or Not to Remove? The Challenge of Extracting the Template to Make the Cavities Available in Molecularly Imprinted Polymers (MIPs)*, Int. J. Mol. Sci. (2011) 12: 4327-4347

[36] Domingos R.F., Baalousha M.A., Nam Y., Reid M .M., Tufenkjy N., Lead J.R., Leppard G.G., Wilkinson K., *Characterizing Manufactured Nanoparticles in the Environment: Multimethod Determination of Particle Sizes*, Environ. Sci. Technol. (2009) 43: 7277–7284

[37] Spivak D.A., *Optimization, evaluation, and characterization of molecularly imprinted polymers*, Adv. Drug Del. Rev. (2005) 57: 1779-1794

[38] Chen L., Wang X., Lu W., Wu X., Li J., *Molecular imprinting: perspectives and applications*, Chem. Soc. Rev. (2016) 45: 2137-2211

[39] Golker K., Karlsson B.R.C., Olsson G.D., Rosengren A.M., Nicholls I.A., *Influence of Composition and Morphology on Template Recognition in Molecularly Imprinted Polymers*, Macromol. (2013) 46(4): 1408–1414

[40] Lakowicz J.R., *Principles of Fluorescence Spectroscopy*, Third Edition (2006) ISBN-10: 0-387-31278-1

[41] Van de Weert M., Stella L., *Fluorescence quenching and ligand binding: A critical discussion of a popular methodology*, J. of Mol. Struct. (2011) 998: 144-150

[42] May B., Poteau X., Yuan D., Brown R. G., *A study of a highly efficient resonance energy transfer between 7-N,N-diethylamino-4-methylcoumarin and 9-butyl-4-butylamino-1,8-naphthalimide*, Dyes Pigm. (1999) 42:79-84

[43] Marangon E., Posocco B., Mazzega E., Toffoli G., *Development and Validation of a High-Performance Liquid Chromatography–Tandem Mass Spectrometry Method for the Simultaneous Determination of Irinotecan and Its Main Metabolites in Human Plasma and Its Application in a Clinical Pharmacokinetic Study*, PLoS ONE (2015) 10(2): e0118194

[44] J.R. Albani, *Structure and Dynamics of Macromolecules: Absorption and Fluorescence Studies*, Chapt. 4 (141 – 192) First Edition (2004) ISBN: 9780444514493

[45] Servant A., Rogers S., Zarbakhsh A. and Resmini M., *Polymeric organic nanogels: structural studies and correlation between morphology and catalytic efficiency*, New J. Chem. (2013) 37: 4103-4109

[46] Liu P., Pearce C.M., Anastasiadi R.M., Resmini M., Castilla A.M., *Covalently Crosslinked Nanogels: An NMR Study of the Effect of Monomer Reactivity on Composition and Structure*, Polymers (Basel) (2019) doi: 10.3390/polym11020353

4. Results and Discussion

MIPs Investigations in human plasma: towards a prototype sensor for irinotecan

4.1 Plasma and MIPs

Most of MIPs operating in plasma have been prepared by bulk, sol-gel or precipitation polymerization, and have been usually developed for solid phase extraction (MISPE) of drugs.[1,2,3] For example, Da Silva *et al*.[4] developed a MIP for drug monitoring of lumefantrine, a drug used for the treatment of malaria. The MIP was prepared by precipitation polymerisation, using 4-vinylpiridine as monomer, EGDMA as cross-linker and AIBN as radical initiator. A MISPE-HPLC-UV method was applied to extract lumefantrine from human plasma samples. Drug recoveries ranging from 83.7% to 85.4% were obtained. Another example is reported in the work of Zhang and Chen,[5] who prepared a MIP monolith imprinted for berberine, using acrylamide as functional monomer and EGDMA as cross-linker. A molecularly imprinted micro solid-phase extraction (MI-μ-SPE) HPLC/UV method was developed for selective extraction of berberine from aqueous solutions, with a LOD of 1.0 $ngmL^{-1}$. The method was applied also for the pre-treatment of berberbine in human plasma and urine samples, showing recoveries larger than 90%. MISPE technique, however, is usually coupled to bulky instruments as HPLC or MS spectrometer for the analysis of the extracted sample.

To develop point-of-care sensor devices, employing smart materials as MIP nanoparticles can be very advantageous, as they are easier to handle and expose higher surface-to-volume ratio. The only example found in literature of MIP nanogel for the detection of the chemotherapeutic drug sunitinib in human plasma has been reported by our research group.[6] Fluorescent MIP nanoparticles were prepared using coumarin as functional monomer, acrylamide as co-monomer and MBA as cross-linker. High dilution radical polymerization was performed using AIBN (18%) as initiator and DMSO as porogen. MIP fluorescence quenching was observed upon binding to sunitinib in plasma samples, treated with DMSO, with a LOD of 400 $nmolL^{-1}$.

4.2 Plasma treatment protocol

Generally, for analytical measurements of drugs in plasma, serum, blood or urine, a sample preparation is required. The most common sample preparation procedure consists of protein precipitation (PP)/extraction, a very simple approach that requires minimal method development and removes the majority of the proteins from the sample.[7] Protein precipitation is usually performed with water miscible organic solvents, as acetonitrile or methanol. However, there are many other PP solvents (also inorganic) employed and the choice depends on the investigations that have to be done.[8]

The protocol followed to treat plasma was the one employed by the research group of Centro di Riferimento Oncologico (CRO), located in Aviano (PN, Italy),[9] involved in our same research project. Pooled plasma was collected at CRO from healthy donors.

Plasma samples were treated with an organic solvent to precipitate proteins. By adding three volumes of methanol or acetonitrile to one volume of plasma, precipitation occurred. After 2 minutes of vortexing and at least two centrifugation runs (10 min at 13000 rpm) at 4 °C the supernatants solutions were ready to be used or stored at -80 °C.

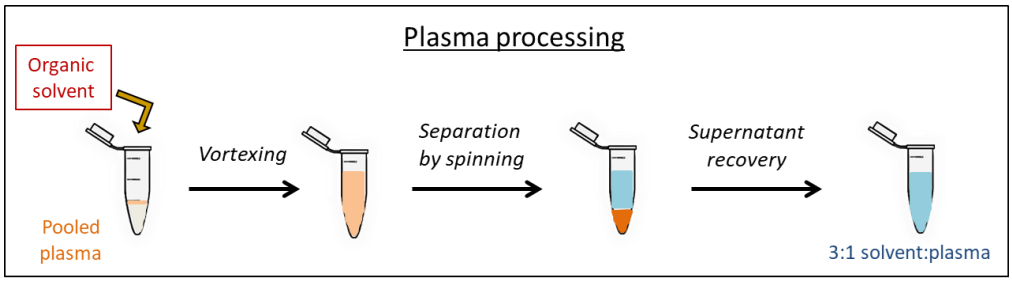

Figure 4.1: Schematic illustration of pooled plasma processing with organic solvents.

4.3 *MIP L* and *MIP O* fluorescence titration in 3:1 methanol:plasma mixture

To study *MIP L* and *MIP O* capacity to bind irinotecan in a complex matrix as human plasma, fluorescence titrations were performed on 60 μgmL^{-1} MIPs in 3:1 methanol:plasma with increasing amounts of irinotecan from solutions prepared in 3:1 methanol:water, investigating its therapeutic range (20 nM – 20 µM).

Unfortunately, *MIP O* fluorescence titration in 3:1 methanol:plasma could not be carried out, because the values of fluorescence intensities were not stable over time and *MIP* started to aggregate, hindering to perform the titration. Conversely, *MIP L* resulted relatively stable in this experiment.

The titration of 60 μgmL^{-1} *MIP L* was repeated three times during the same day. The corresponding Stern-Volmer plot is reported in **Figure 4.2**.

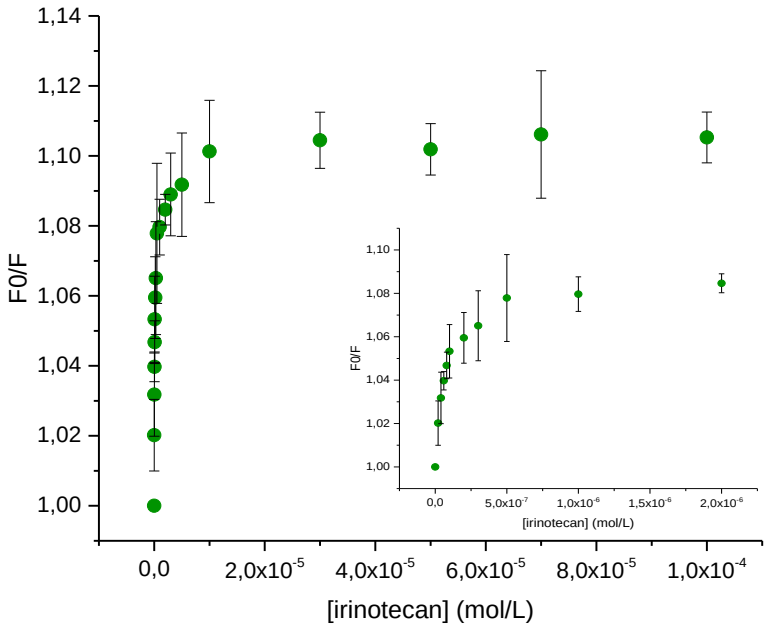

Figure 4.2: Stern-Volmer plots obtained by titrating 60 µgmL^{-1} *MIP L* with irinotecan in 3:1 methanol:plasma. Insert: lowest concentrations range investigated (0 – 2 µM).

The Stern-Volmer plot obtained in 3:1 methanol:plasma for *MIP L* showed a trend similar to the previous ones obtained in water, particularly with highest value of the slope and good linearity in the nanomolar range, indicating that *MIP L* sensitivity was kept also in a complex matrix as treated human plasma. At concentrations above 10 µM, the linearity decreased and further quenching of MIP fluorescence was no longer observed. Evaluating the overall range, however, quite large variability was observed, suggesting that *MIP L* is not very stable in this medium.

Moreover, comparing the Stern-Volmer plot in treated plasma with the previous one (**Chapter 3**) related to *MIP L* in 3:1 methanol:water (**Figure 4.3**), it is possible to notice that *MIP L* performance in human plasma dramatically decreased. At concentrations below 1 µM the trends were quite similar, while within the 1 – 5 µM concentrations range, the linearity decreased and a significant variation of *MIP L* fluorescence emission was not achieved at concentrations higher than 5 µM.

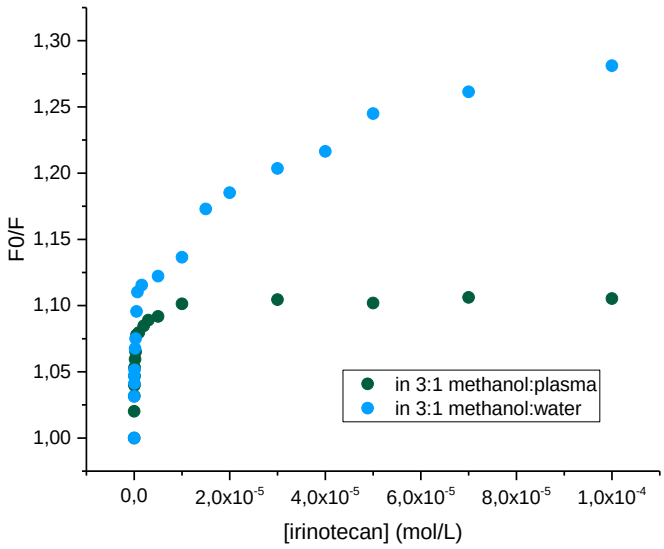

a)

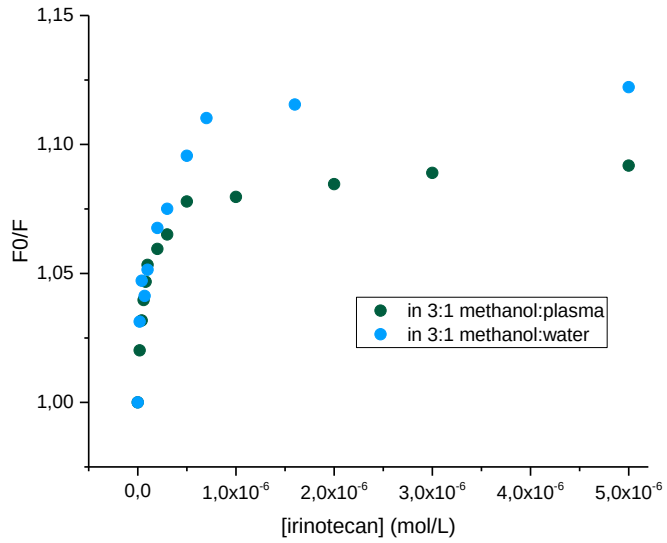

b)

Figure 4.3: Stern-Volmer plots related to 60 gmL^{-1} fluorescence titrations with irinotecan in 3:1 methanol:plasma and 3:1 methanol:water mixtures. a): total concentrations range investigated (0 – 100 µM); b): lower concentrations range (0 – 5 µM).

The values of the Stern-Volmer constants and the bimolecular quenching constants related to the plots of **Figure 4.3**, are reported in **Table 4.1**.

Nanogel	Concentrations range	K_{SV} [10^4 $Lmol^{-1}$]	k_q [10^{12} $Lmol^{-1}s^{-1}$]
***MIP L* (in 3:1 methanol:water)**	0 – 700 nM	12.71	15.31
	700 nM – 10 µM	0.268	0.323
	10 – 50 µM	0.235	0.283
***MIP L* (in 3:1 methanol:plasma)**	0 – 500 nM	12.39	14.93
	500 nM – 10 µM	0.238	0.287

Table 4.1: Values of Stern-Volmer constants and corresponding bimolecular quenching constants, related to the Graphs reported in **Figure 4.2**.

It is interesting to notice that the performance of *MIP L* seemed not affected by the presence of residual plasma at drug concentrations below 500 nM. A slightly decrease of its fluorescence quenching occurred between 500 nM and 10 µM, but a static quenching however was present, as the value of the corresponding bimolecular quenching constant calculated resulted in the order of 10^{11} $Lmol^{-1}s^{-1}$. The estimated values of the dissociation constants (K_D) were 7.9 µM and 8.1 µM in methanol:water and methanol:plasma, respectively, suggesting that *MIP L* affinity at low irinotecan concentrations was quite the same in these media. Unfortunately, a dramatic worsening of its performance occurred at concentrations higher than 10 µM.

In conclusion, results obtained by *MIP L* fluorescence titrations with irinotecan in treated human plasma showed that the performance of the nanogel was not completely lost in a disadvantageous environment as methanol:plasma mixture. However, the stability of the polymer was not very good (high variability of fluorescence intensities values) and the performance of MIP might be improved employing a different extracting solvent, as acetonitrile or DMSO.

4.4 *MIP L* in 3:1 DMSO:plasma and 3:1 acetonitrile:plasma

Different solvents, as acetonitrile and DMSO, able to extract the anticancer drug from human plasma, were thus taken into consideration to verify if *MIP L* performance in these environments, rather than in methanol, could be improved.

Acetonitrile, as methanol, is a common solvent used by clinicians to treat human plasma for proteins precipitation and extraction of substances (as drugs) soluble in this solvent.[8] DMSO, instead, leads to plasma proteins unfolding without precipitating them, but generating a different white precipitate, not absorbing UV at usual phenylalanine or tryptophan wavelengths;[10] such precipitate has been hypothetically identified as a fraction of the polysaccharides added to the blood sample at the collection time, acting as anticoagulant agents. To generate plasma, indeed, an anticoagulant supplement is needed, and the most commonly employed in the clinics are ethylene diaminetetraacetic acid (EDTA), heparin, citrate, and fluoride. Heparin is an anti-thrombin activator, whereas EDTA and citrate chelate calcium ions.[11] However, once this precipitate was separated by centrifugation DMSO:plasma mixtures still contained in solutions just unfolded proteins, which should not interfere with MIPs rebinding. Hence, investigations on *MIP L* performance in both 3:1 DMSO:plasma and 3:1 acetonitrile:plasma were done through fluorescence titrations.

60 µgmL^{-1} *MIP L* was titrated with increasing amount of irinotecan in both 3:1 DMSO:plasma and 3:1 acetonitrile:plasma. A quenching of *MIP L* fluorescence was observed and the results obtained by Stern-Volmer analysis are reported in **Figure 4.4**.

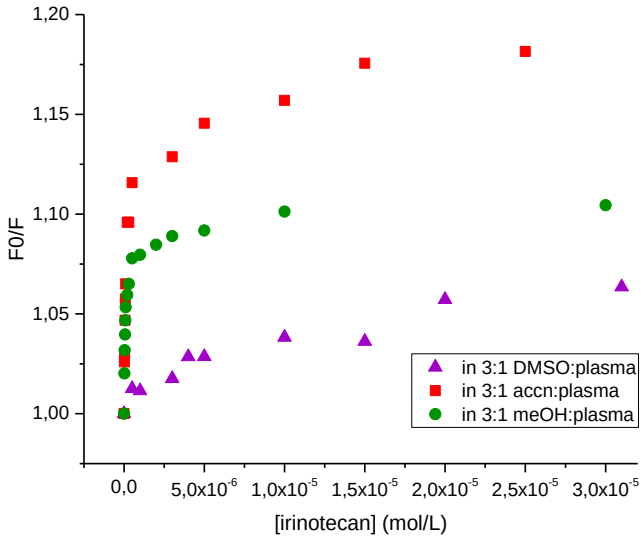

a)

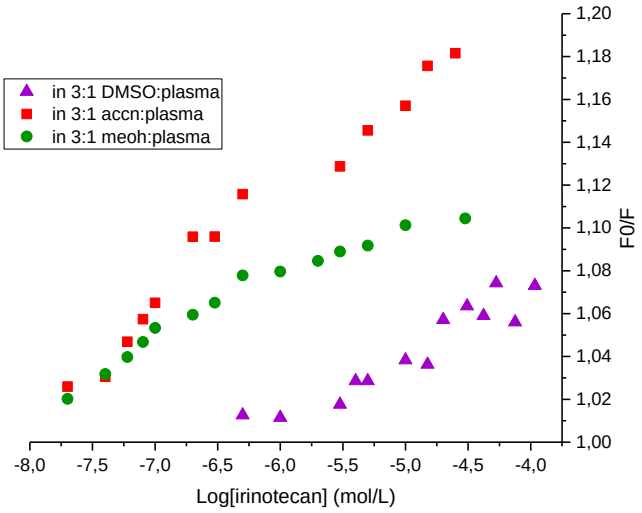

Figure 4.4: Stern-Volmer plots related to 60 μgmL^{-1} *MIP L* fluorescence titrations with irinotecan in 3:1 DMSO:plasma and 3:1 acetonitrile:plasma, compared with the one obtained in 3:1 methanol:plasma. a): linear scale; b): semiLog scale.

Comparing the Stern-Volmer plots of *MIP L* in **Figure 4.4**, it is clear that the presence of the proteins in DMSO negatively affected the MIP performance, as a not efficient fluorescence quenching even worse than in methanol was observed. *MIP L* behaviour in plasma treated with methanol and acetonitrile was very similar at drug concentrations below 100 nM, but acetonitrile seemed to favour irinotecan binding rather than methanol, as a more efficient quenching of fluorescence occurred within the whole therapeutic range of the anticancer drug.

The performance of *MIP L* in acetonitrile:plasma was therefore further characterized, with the aim to evaluate its potential in an analytical methodology exploiting its fluorescence.

First, we measured the Stern-Volmer constant (K_{SV}) and the bimolecular quenching constant (k_q) in 3:1 acetonitrile:water at low drug concentration, within the range 20 nM – 100 nM. The obtained values were $60.73 \cdot 10^4$ $Lmol^{-1}$ and $7.32 \cdot 10^{13}$ $Lmol^{-1}s^{-1}$ respectively, fully comparable with those obtained in water, equal to $60.64 \cdot 10^4$ $Lmol^{-1}$ and $5.7 \cdot 10^{13}$ $Lmol^{-1}s^{-1}$. Series of repeated titrations were then performed and reported in **Figure 4.5**.

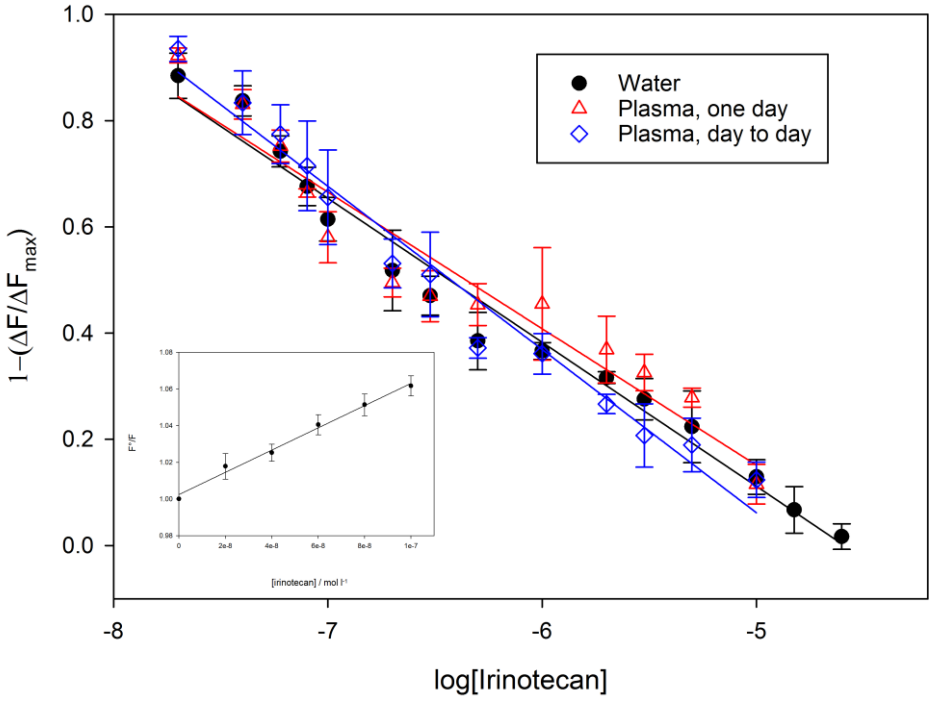

Figure 4.5: Fluorescence of *MIP L* at increasing concentrations of irinotecan. Black: in 3:1 acetonitrile:water mixture; red: in 3:1 acetonitrile:plasma; blue: average calibration over repeated measures carried out in three different days along one month. Error bars from the average of triplicates for the black and red series, from the average of the three replicas (each one triplicate) for the blue series. Insert: Stern-Volmer plot in 3:1 acetonitrile:water.

In this experiment, a potential calibration curve was built by plotting the relative fluorescence change vs the log of irinotecan concentration. In this way, a very high sensitivity for irinotecan was obtained in the absence of plasma (black series), with a LOD of 16 nM, estimated with the 3σ method. In 3:1 acetonitrile : plasma mixture after removal of plasma proteins (red and blue series), the trend was almost superimposable to that obtained in water. The LOD in plasma turned out 12 nM. The intra-assay precision on a single triplicated titration was 10.2% along the whole dynamic range.

The response of the MIP sensor was very stable and reproducible during time. The blue series in **Figure 4.5** reports the average outcome of repeated experiments carried out over one month. The sensitivity was not changed after this period, with an average LOD of 10 nM, while the inter – assay precision of the whole curve was 13.2%. However, it must be noted that the whole trend as reported in **Figure 4.5**, is not fully linear, despite the fact that all the series can be fitted to straight lines with $r^2 > 0.98$. A clear inflection

can be in fact observed between 500 nM and 1 µM irinotecan, in all the experiments. This is likely due to the presence of two populations of binding sites inside the MIP particles. A minority of binding sites has either higher affinity or higher sensitivity towards quenching from irinotecan and leads to the first linear region, while the less responsive major fraction of binding sites operates at higher concentrations. A similar bimodal behaviour have been observed by us also in our previous work on coumarin – based MIP for sunitinib.[6] Nevertheless, the dynamic range investigated is within the therapeutic range of irinotecan, which spans between 17 nM and 17 µM.

In conclusion, we have shown that *MIP L* can rebind irinotecan with good sensitivity. The fluorescence change upon rebinding actually allows the detection of irinotecan in spiked human plasma, in a tenth nM to tenth µM range, after simple treatment of plasma with acetonitrile and removal of the proteins. The proof of concept given with this result is encouraging as to the possibility of developing a portable device with sensors based on fluorescent imprinted nanogels for the detection of irinotecan.

4.5 Towards a prototype sensor

In collaboration with COBIK, a Research Center of Excellence on Biosensors, located in Slovenia, a fluorimetric sensor prototype for irinotecan detection has been developed (named "Fluorita"). This device incorporated *MIP L*, working as both recognition element and transducer, thanks to its intrinsic fluorescence activity. *MIP L* has been immobilized on 5 µL acrylic foil (plexiglass) wells using different organic solvents; DMF allowed to immobilize the imprinted polymer, without observing its removal after washings with mixtures of methanol and water, and to detect its residual fluorescence emission with good reproducibility. *MIP L*, hence, resulted very stable after immobilization on a surface. Images of this first prototype sensor for irinotecan detection are reported in **Figure 4.6**.

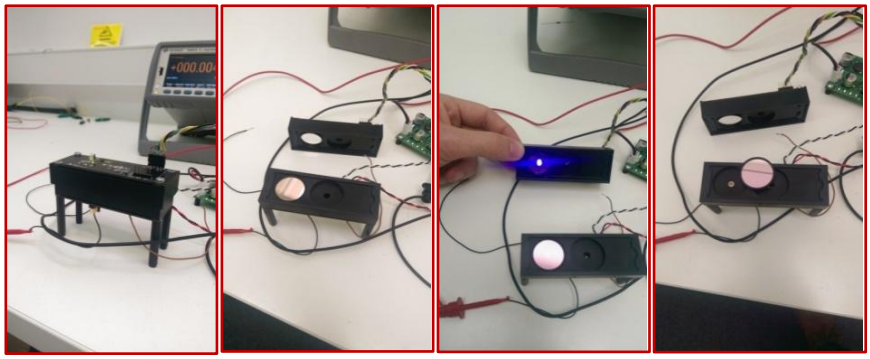

Figure 4.6: Fluorita sensor prototype.

MIP immobilization was optimised and the best results were obtained with polymer concentrations below 0.2 $mgmL^{-1}$. Some preliminary investigations on 0.1 $mgmL^{-1}$ *MIP* L and *NIP L* rebinding capacities were performed using Fluorita, by adding increasing concentrations of irinotecan in 3:1 methanol water mixture. A quenching of fluorescence very similar to the one observed in the titration of 60 μgmL^{-1} *MIP L* in 3:1 methanol:water solution with irinotecan, reported in **Figure 4.3**, was obtained and related Stern-Volmer plots are shown in **Figure 4.7**.

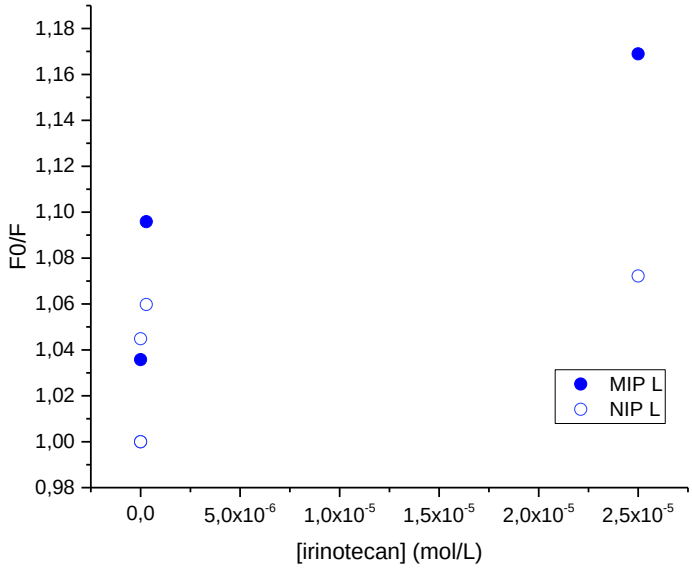

Figure 4.7: Stern-Volmer plots of 0.1 $mgmL^{-1}$ *MIP L* and *NIP L* preliminary titrations with irinotecan in 3:1 methanol:water, performed on Fluorita.

These preliminary measurements carried out on Fluorita prototype sensor shown very promising results. A good fluorescence quenching was observed, and *MIP L* was able to bind a higher amount of irinotecan rather than corresponding *NIP L*, hence confirming its specificity in 3:1 methanol:water mixtures.

By immobilizing *MIP L* on a surface and incorporating it in a sensor prototype, it will be possible to improve the sensitivity, by enhancing the fluorescence quenching observed upon interaction with irinotecan. This prototype could be employed as Point Of Care device for the TDM of this anticancer agent.

---

[1] Chassaing C., Stokes J., Venn R.F., Lanza F., Sellergren B., Holmberg A., Berggren C., *Molecularly imprinted polymers for the determination of a pharmaceutical development compound in plasma using 96-well MISPE technology*, J. Chromatogr. B Analyt. Technol. Biomed. Life Sci. (2004) 804(1): 71-81

[2] Attaran A.M., Mohammadi N., Javanbakht M., Akbari-Adergani B., *Molecularly Imprinted Solid-Phase Extraction for Selective Trace Analysis of Trifluoperazine*, J. of Chrom. Scie. (2014) 52: 730–738

[3] Abdollahi E., Abdouss M., Mohammadi A., *Synthesis of a nano molecularly imprinted polymeric sorbent for solid phase extraction and determination of phenytoin in plasma, urine, and wastewater by HPLC*, RSC Adv. (2016) 45(6): 39095-39105

[4] Da Silva P.H.R., Diniza Vieira M.L., Pianetti G.A., da Costa Cesar I., Scarpelli Ribeiro C.M.E., de Souza Freitas R.F., de Sousa R.G., Fernandes C., *Molecularly imprinted polymer for determination of lumefantrine in human plasma through chemometric-assisted solid-phase extraction and liquid chromatography*, Talanta (2018) 184: 173-183

[5] Zhang W., Chen Z., *Preparation of micropipette tip-based molecularly imprinted monolith for selective micro-solid phase extraction of berberine in plasma and urine samples*, Talanta (2013) 103: 103-109

[6] Pellizzoni E., Tommasini M., Marangon E., Rizzolio F., Saito G., Benedetti B., Toffoli G., Resmini M., Berti F., *Fluorescent molecularly imprinted nanogels for the detection of anticancer drugs in human plasma*, Biosensors and Bioelectronics (2016) 86: 913–919

[7] Alshammari T.M., Al-Hassan A.A., Hadda T.B., Aljofan M., *Comparison of different serum sample extraction methods and their suitability for mass spectrometry analysis*, Saudi Pharm J. (2015) 23(6): 689–697

[8] Bouzas N.F., Dresen S., Munz B., Weinmann W., *Determination of basic drugs of abuse in human serum by online extraction and LC-MS/MS*, Anal. Bioanal. Chem. (2009) 395(8): 2499–2507

[9] Marangon E., Posocco B., Mazzega E., Toffoli G., *Development and Validation of a High-Performance Liquid Chromatography–Tandem Mass Spectrometry Method for the Simultaneous Determination of Irinotecan and Its Main Metabolites in Human Plasma and Its Application in a Clinical Pharmacokinetic Study*, PLoS ONE (2015) 10(2): e0118194

[10] Pellizzoni E., *Molecularly Imprined Polymeric Nanoparticles for the Therapeutic Drug Monitoring of Anticancer Drugs*, Doctoral Thesis (2015)

[11] Yin P., Lehmann R., Xu G., *Effects of pre-analytical processes on blood samples used in metabolomics studies*, Anal. Bioanal. Chem. (2015) 407: 4879–4892

5. Results and discussion

Fluorescent MIPs for imatinib

5.1 Template and functional monomers synthesis

Synthesis of imatinib hydrochloride

Since imatinib is commercially available only as the free base, a salt form of the drug was prepared in order to get a water soluble compound. Imatinib, moreover, is orally administered as mesylate salt, and in the final real samples of plasma it should be mainly present as mono-protonated form, as the pK_a of the protonated piperazine nitrogen is 7.7.[1]

Imatinib hydrochloride salt was easily obtained by reaction of imatinib base with concentrated hydrochloric acid in ethanol, for twenty minutes.[2] After purification, the template was obtained with 62% yield. Its chemical structure is reported in **Scheme 5.1**.

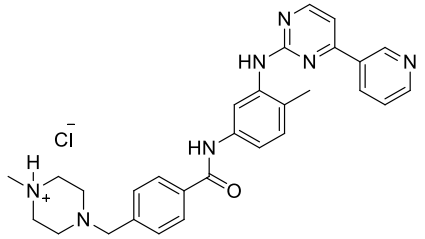

Scheme 5.1: Chemical structure of imatinib hydrochloride.

In the following experiments with the term "imatinib" we will always refer to imatinib hydrochloride.

In order to obtain fluorescent MIPs to imatinib, we have considered to use EDANS as the fluorescent reporter. EDANS is a very fluorescent molecule; when excited at 335 nm it emits light around 450 nm.[3] It is a very interesting compound, as it can perform a FRET quenching when coupled with the quencher DABCYL. Hence, EDANS was chosen for its fluorescence properties, in order to get fluorescent MIPs for imatinib, as this drug does not emit fluorescence. Such materials could be in principle exploited in two ways: in the first one, direct quenching of EDANS fluorescence by imatinib might be studied (trough an environmental change upon rebinding of the drug). In the second option, a DABCYL-labelled analogue of imatinib plays as a quencher in a competitive measure. Moreover, EDANS bears a strongly acidic sulphonic acid moiety, and is present as the anion at almost any pH, thus complementing the positive charge of imatinib.

Fluorescein was also considered as a potential fluorophore useful for imatinib MIPs, as well as the functional monomers already described in the previous chapter for irinotecan.

*Synthesis of N-acryloyl EDANS (**12**)*

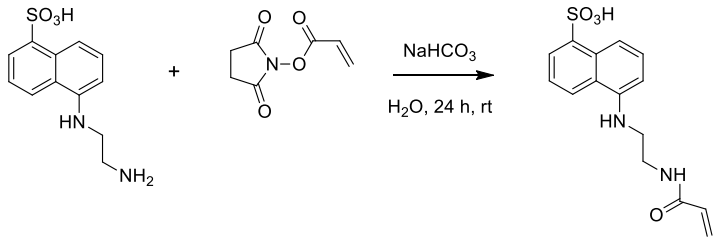

Scheme 5.2: Synthesis of N-acryloyl EDANS (**12**).

The functional monomer N-acryloyl EDANS was therefore obtained by reaction of EDANS with N-succinimidyl acrylate, previously prepared, in water, under basic conditions (**Scheme 5.2**). It was necessary to employ N-succinimidyl acrylate, a water soluble compound, rather than acryloyl chloride directly, because EDANS is not soluble in organic solvents, and the reaction had to be carried out in water. N-acryloyl EDANS (monomer **12**) was obtained with 86% yield, after purification by gravity chromatography.

5.2 ^{1}H-NMR titrations of imatinib with the functional monomers

To study if interactions between imatinib and various functional monomers were established, and select the best monomers for MIPs synthesis, ^{1}H-NMR titrations of 4 mM imatinib with increasing amounts of the synthesized fluorescent functional monomers **2**, **3**, **4**, **11** (fluorescein O-acrylate) and **12** (N-acryloyl EDANS) (**Scheme 5.3**) were performed in DMSO-d_6. The chemical shifts variations of the observed protons of irinotecan, before and after the adding of ten equivalents of each monomer are reported in **Figure 5.1**.

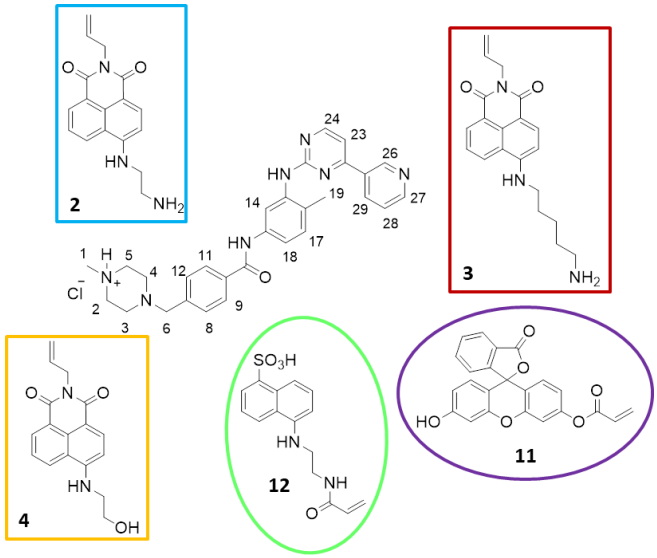

Scheme 5.3: Chemical structure of imatinib hydrochloride and of the functional monomers employed for ^{1}H-NMR investigations. Compounds **2**, **3** and **4** are 1,8-naphtalimide derivatives and their synthesis has been described in the previous chapter.

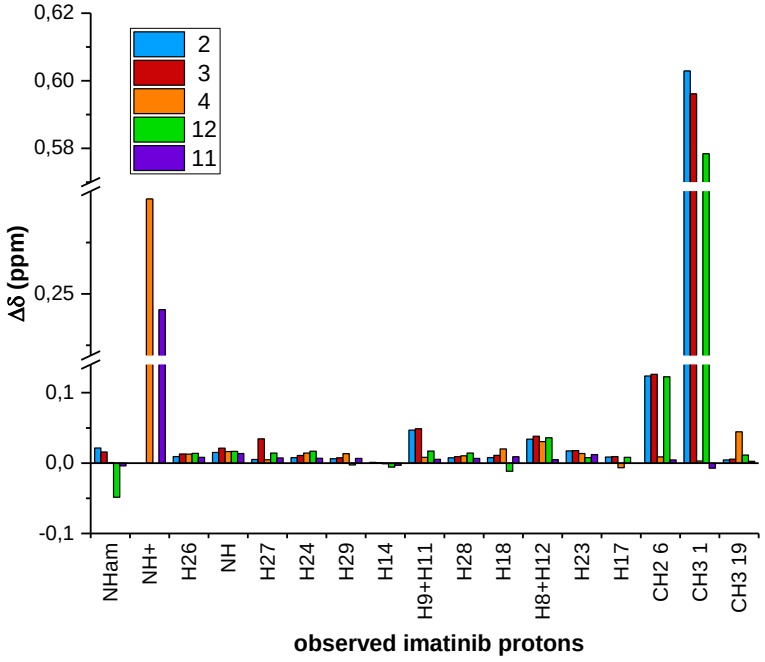

Figure 5.1: Variation of chemical shift of observed irinotecan protons before and after the adding of 10 equivalents of the functional monomers **2**, **3**, **4**, **11** and **12**.

In the histogram of **Figure 5.1**, most of irinotecan protons are shown to be shifted to higher fields, indicating that monomer-template complexes were probably formed. In general, protons that showed the highest shift were methylene *H26* and methyl *H1*, when N-acryloyl EDANS (**12**) and both naphtalimide monomers **2** and **3** were added to imatinib, suggesting, respectively, that an ionic pair has been probably established and a proton transfer occurred from imatinib protonated piperazinic moiety to the amino terminal of compounds **2** and **3**. This was confirmed by the apparent disappearance of the NH^+ signal already after adding the first amounts of these monomers. Finally, also the piperazine NH^+ signal was highly shifted when monomer **4** and fluorescein O-acrylate were added to the template, suggesting that an ionic pair or strong hydrogen bond could have been established. It is important to underline that monomer **12** is for sure present in a salt form, as it contains a sulfonic acid group, which is a very strong acid.

Focus on each single ^{1}H-NMR titration is reported in detail in the following paragraphs.

5.3 Fluorescent MIPs for imatinib containing naphtalimide derivatives

The ^{1}H-NMR titrations of imatinib with 1,8-naphtalimidic monomers **2**, **3** and **4** were performed in DMSO-d_6. Chemical shifts variations of the observed imatinib protons are reported in **Figure 5.2**.

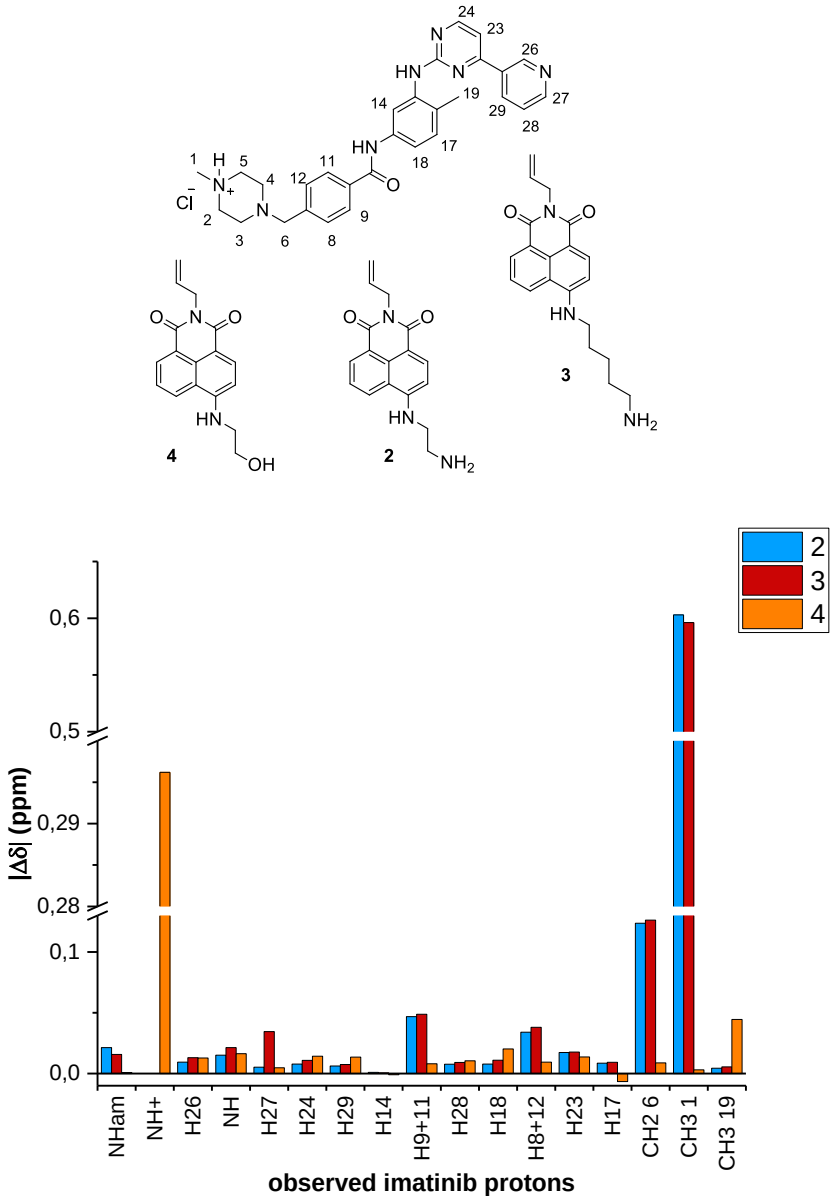

Figure 5.2: Chemical shift variations of observed imatinib protons before and after the adding of 10 equivalents of monomer **2**, **3** or **4**, in DMSO-d_6. Top: chemical structure of imatinib and monomers **2**, **3** and **4**.

In the histogram of **Figure 5.2**, very similar shifts of imatinib protons were observed when monomers **2** and **3** were employed, as these compounds contain the same functional groups, but only a different length of the amino chain in position 4 of the naphtalimide moiety. Monomer **4**, instead, interacted differently with imatinib, as the

entity of the protons shifts obtained were not the same as the ones obtained with monomers **2** and **3**.

Analysing the trends of the signal variation of the mainly shifted imatinib protons, after the adding of monomers **2** and **3**, it seemed that a proton was transferred from piperazine NH^+ to the terminal amino group of both compounds **2** and **3**. A plateau of the trends was reached after the adding of one equivalent of the functional monomers. In **Figure 5.3** these trends, related to imatinib methyl protons *H1*, methylene protons *H6* and aromatic protons *H8*, *H9*, *H11* and *H12*, are reported. The largest shifts entities were observed for the protons *H1* and *H6*, directly connected to the protonated piperazine moiety. As already mentioned, the NH^+ peak apparently disappeared after the adding of 0.5 equivalents of both monomers **2** and **3**, and it was probably shifted to spectrum fields not easily identified, because of a possible overlapping of signals.

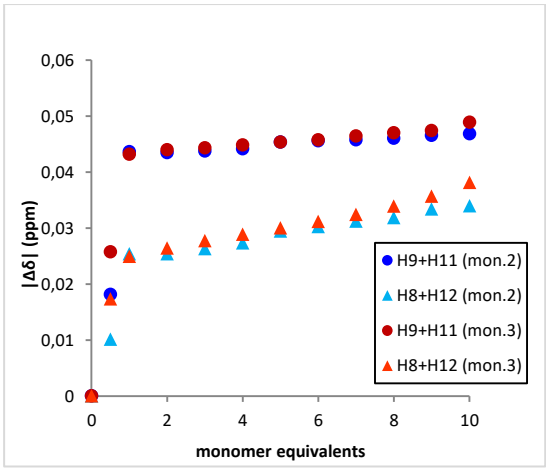

a)

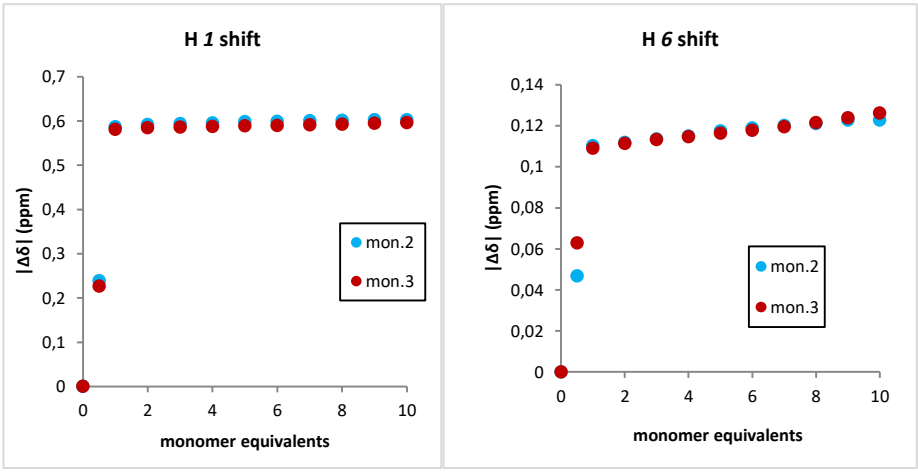

b)

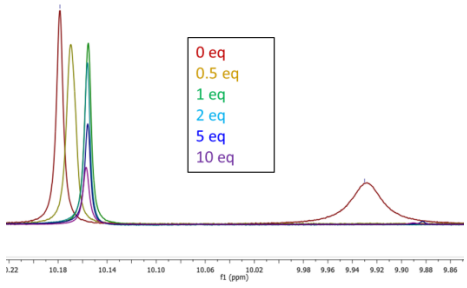

c)

Figure 5.3: Chemical shift variations of imatinib protons *H9+H11* and *H8+H12* (a), methyl *H1* and methylene *H6* (b), upon adding of 1,8-naphtalimidic monomers **2** and **3** in DMSO-d_6. c): apparent disappearance of NH^+ piperazinic signal (right, bbd) after the adding of monomer **2**.

The trends related to the variation of the chemical shifts of *H1*, *H8+H12*, *H6* and *H9+H11*, upon adding of monomer **4** to the template, are reported in **Figure 5.4**. A liner change of chemical shift on adding monomer **4** was observed for all protons, indicating that the equilibrium between free and bound imatinib did not reached a saturation point, but was continuously shifted to the complex form within the available concentration range. This different type of interactions could be due to the absence of an amino terminal group in monomer **4**, as a protons transfer cannot occur.

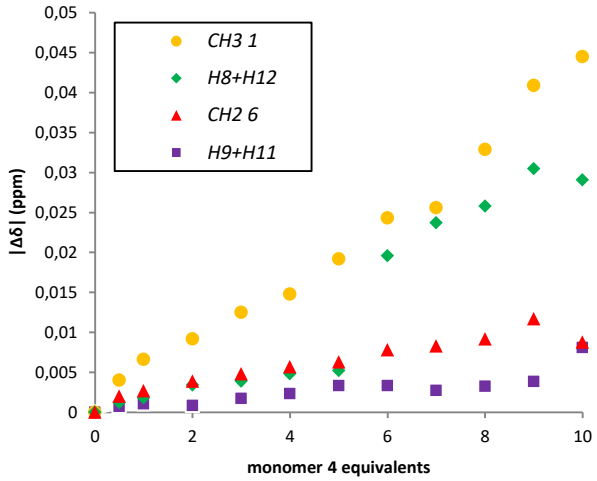

Figure 5.4: Variations of chemical shifts of imatinib protons methyl *H1*, methylene *H6*, aromatic *H8+H12* and *H9+H11*, while monomer **4** was added to the template in DMSO-d_6.

Since monomers **2** and **3** showed a very similar behaviour towards imatinib, we decided to design imprinted polymers using only monomer **2**, as a previous experience on this fluorophore was already achieved for irinotecan MIPs. A MIP containing monomer **4** was also prepared, in order to see if these different interactions with imatinib, observed at NMR titrations, can positively affect the rebinding capacities of the MIPs.

Synthesis of *MIP Q*

The first MIP imprinted with imatinib was designed using 15% (mol) of monomer **2**, also employed for irinotecan, 15% of allyl amine as co-monomer, 70% of EGDMA and 18% of AIBN. Compound **2** was selected as functional monomer, rather than monomer **4**, because a shorter amino chain in position 4 of the naphtalimide moiety, having less degrees of freedom, could be an advantage for the binding pockets formation, imprinted with the template. The choice to use allylamine as co-monomer was due to

the fact that it possess primary amino group able to form hydrogen bonds and its reactivity is similar to monomer **2**, as they both contain an N-allyl group, and should not compete with monomer **2** during polymerization.[4] The molar ratio between template and fluorescent functional monomer employed was 1.2 : 1, respectively, and the critical monomer concentration was fixed at 1%. The polymerisation was performed for 48 hours at 70 °C in DMSO. Compositions, yields and dimensions obtained by DLS measurements are reported in **Table 5.1** for both *MIP Q* and *NIP Q*.

Polymer	Functional monomer (15%)	Co-monomer (15%)	Cross-linker (70%)	Yield	Size distribution by Number (nm)	PDI
MIP Q	2	allyamine	EGDMA	75%	17.5±4.6	0.800
NIP Q	2	allyamine	EGDMA	69%	5.3±0.4	1.00

Table 5.1: Compositions, yields and size of *MIP Q* and *NIP Q*, measured by DLS of 0.25 $mgmL^{-1}$ DMSO solutions of polymers, filtrated on 0.45 µm PTFE filter and sonicated.

Obtained yields were consistent with the previous ones, related to MIPs for irinotecan containing 15% of monomer **2**; *MIP Q* nanoparticles resulted quite larger (17 nm) than corresponding *NIP Q* (5 nm), suggesting that the presence of the template probably favours the formation of big binding cavities, not present in the corresponding NIP.

UV-Visible measurements

To evaluate the amount of fluorophore **2** incorporated during polymerization, UV-Visible absorbance measurements of *MIP Q* and *NIP Q* were performed in DMSO. The results are reported in **Table 5.2**.

Nanogel	Amount of mon. 2 incorporated incorporated/mg of polymer (nmol/mg)	Percentage of monomer 2 incorporated during polymerisation
MIP Q	74.5	9.4%
NIP Q	63.7	8.0%

Table 5.2: Concentration of monomer **2** contained by *MIP Q* and *NIP Q* (nmol/mg) and percentage of fluorophore **2** incorporated during polymerisation.

It is very interesting to notice that, comparing the concentrations of monomer **2** contained by *MIP Q* and *NIP Q* with the previous results of MIPs for irinotecan designed with 15% of compound **2**, the values obtained (**Table 5.2**) are almost two folds higher; this can confirm that employing a co-monomer as allylamine, having a polymerisable moiety with the same reactivity of fluorophore **2**, helps the incorporation of this latter one in the polymer matrix, without competing with it, as the previous acrylamide or

methacrylic acid co-monomers. However, its incorporation in the polymer, remains very low (around 10%), probably because the cross-linker remains the main competitor for reactivity, containing even two reactive groups. Maybe, using a cross-linker having allyl groups rather than acryloyl ones, could have helped even more fluorophore **2** incorporation in the polymers matrix.

HPLC rebinding assays

The rebinding capacity of *MIP Q* and *NIP Q* in water was investigated through the already mentioned HPLC test. 1 $mgmL^{-1}$ nanogels suspensions in 50 µM water solution of imatinib were prepared and incubated for 24 hours. Samples of residual drug solutions were analysed at HPLC, after separation of polymers by spinning. The results obtained are reported in **Figure 5.5**.

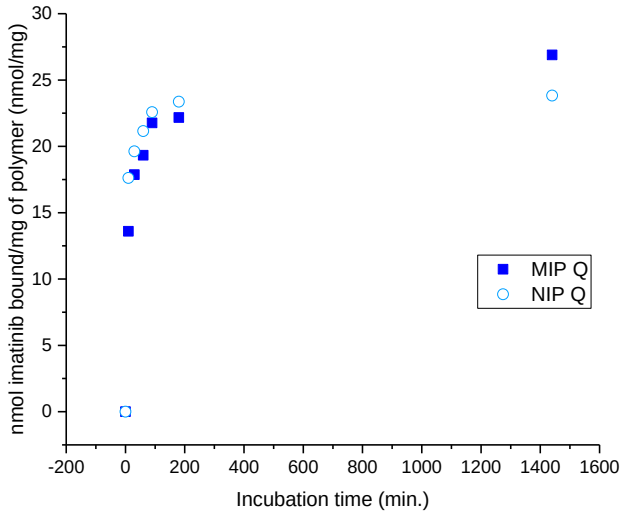

Figure 5.5: Binding kinetics of *MIP Q* and *NIP Q* in water.

The binding kinetics of *MIP Q* and *NIP Q* in water (**Figure 5.5**) showed both apparent first order trends, where a plateau was reached after three hours of incubation, indicating that saturation of binding sites was probably achieved. The kinetics were very similar, and *MIP Q* demonstrated little specificity only after 24 hours. The rebinding values are consistent with the ones obtained with MIPs for irinotecan containing 15% of naphtalimide dye; however, specificity for imatinib was not observed with *MIP Q*.

Fluorescence measurements

Although specificity was not achieved, a fluorescence titration of 60 μgmL^{-1} *MIP Q* with imatinib was directly performed in 3:1 methanol:water mixture, following the results obtained for irinotecan in such environment. Stern-Volmer analysis was made and the related plot is reported in **Figure 5.6**. The imatinib concentration range explored took into consideration its therapeutic range, particularly its minimal concentration for drug efficacy, that is around 2 µM (1002 $ngmL^{-1}$).[5]

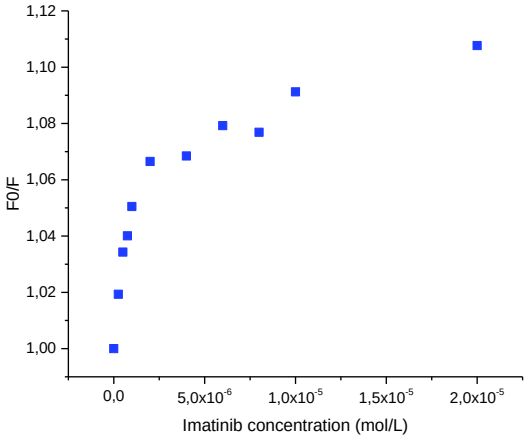

a)

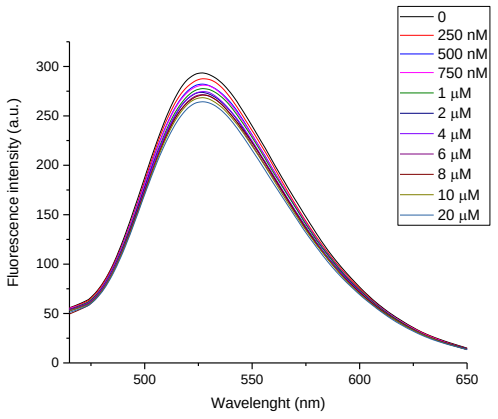

b)

Figure 5.6: a): Stern-Volmer plot related to *MIP Q* fluorescent titration with imatinib in 3:1 methanol:water. MIP Q was filtered on 0.45 µm PTFE filter, as some aggregates were present in the solution. b): emission spectra of the MIP at increasing concentrations of imatinib.

Also in this case, the Stern-Volmer plot showed a bimodal trend, with a higher slope value below 1 µM and a decrease of *MIP Q* sensitivity to the drug at micromolar concentrations, between 1 and 20 µM.

Nanogel	Concentration range	K_{SV} [10^4 $Lmol^{-1}$]	k_q [10^{12} $Lmol^{-1}s^{-1}$]
MIP Q	0 – 1 µM	4.87	5.87
	1 – 20 µM	0.271	0.326

Table 5.3: Stern-Volmer constants (K_{SV}) values and corresponding bimolecular quenching constant (k_q), related to *MIP Q* titration with imatinib in 3:1 methanol:water.

The values of Stern-Volmer constants (**Table 5.3**) were in the 10^4 and 10^3 $Lmol^{-1}$ order in the nanomolar and micromolar range, resulting very similar to the ones obtained for MIPs imprinted with irinotecan, containing 15% of the same monomer. However, despite a static quenching was observed, as bimolecular quenching constants were both higher than diffusion limit ($1 \cdot 10^{10}$ $Lmol^{-1}s^{-1}$), fluorescence quenching was not very efficient (**Figure 5.6**), hence improvements on MIPs design and synthesis had to be done.

Allylamine effectively favoured monomer **2** incorporation, but did not significantly improve MIP performance and specificity for imatinib. A new polymer imprinted with imatinib was therefore designed using the naphalimide derivative **4** as functional monomer.

Synthesis of *MIP R*

A second imprinted polymer containing the functional monomer 1,8-naphtalimide derivative **4** was prepared, since some interactions with imatinib were observed at ^{1}H-NMR titration, different to the ones seen with monomers **2** and **3**. *MIP R* was designed using 30% of compound **4**, 70% of EGDMA and 5% of AIBN. The choice to avoid the adding of a co-monomer was due to the necessity to favour its incorporation in the polymer matrix, favouring a possible enhancement of fluorescence quenching upon binding to the drug, and also to the fact that a co-monomer could react faster than it, as previously seen, favouring the formation of less specific binding cavities. The amount of AIBN was decreased from 18 to 5%, as a higher amount of monomer **4**, less reactive than cross-linker, was used. Composition, yield and size of polymer particles obtained are reported in **Table 5.4**.

Polymer	Functional monomer (30%)	Cross-linker (70%)	Yield	Size distribution by Number (nm)	PDI
MIP R	**4**	EGDMA	56%	33.6±2.0	0.392
NIP R	**4**	EGDMA	62%	26.7±5.9	0.980

Table 5.4: Composition, yield and particles size of *MIP R* and *NIP R*, obtained by DLS measurements of 0.25 $mgmL^{-1}$ solution in DMSO, after filtration on 0.45 µm and sonication. The reaction was performed for 24 hours at 70 °C in DMSO.

Yields of polymers *S* resulted not particularly high. This was probably due to the lower reactivity of monomer **4** or to the less amount of AIBN employed (5%), since also for the previous *MIP P*, imprinted for irinotecan, designed with 30% of monomer **2** and 5% of AIBN, the yield was around 50%. The size of the particles was around 30 nanometer. Employing compound **4** rather than **2** in polymer design, the diameter of the nanoparticles was about two folds higher than MIPs for irinotecan, prepared following the same conditions here reported, except for template and fluorophore.

UV-Visible measurements

To know the amount of functional monomer **4** incorporated by polymers, UV-Visible measurements of *MIP* and *NIP R* solutions in DMSO were carried out. Concentrations of compound **4** were calculated using the molar extinction coefficient (at 444 nm) obtained from the corresponding calibration curve performed in DMSO.

Nanogel	Amount of mon. 4 incorporated/mg of polymer ($nmolmg^{-1}$)	Percentage of mon. 4 incorporated during polymerisation
MIP R	50.6	3.8%
NIP R	36.7	2.8%

Table 5.5: Concentration of monomer **2** contained by *MIP R* and *NIP R* ($nmolmg^{-1}$) and percentage of fluorophore **4** incorporated during polymerization.

Despite the amount of fluorophore was increased from 15 to 30%, less incorporation of the functional monomer than in the previous nanogels *R* was obtained.

HPLC rebinding assays

The rebinding studies of *MIP R* and *NIP R* were performed in water, following the already mentioned HPLC experiment. The concentrations ($nmolmg^{-1}$) of imatinib bound to the polymers over time are reported in **Figure 5.7**.

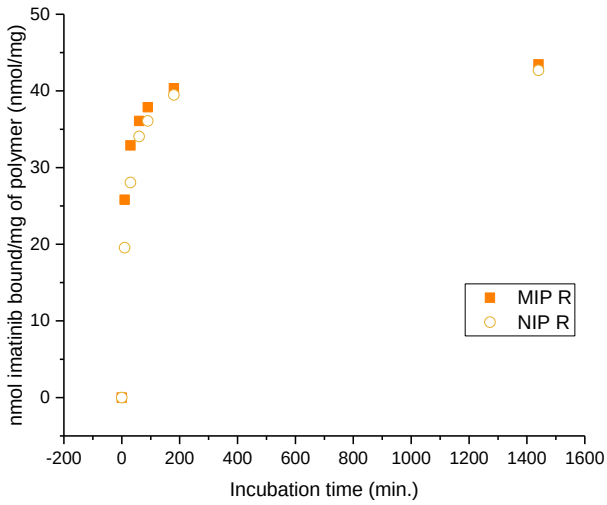

Figure 5.7: Binding kinetics of *MIP R* and *NIP R* in water.

Binding kinetics of *MIP R* and *NIP R* in water showed a trend similar to the previous obtained for polymers *R*, where a plateau was reached after three hours of incubation, indicating saturation of binding sites. The amount of imatinib bound was, instead, very high and almost two folds higher than polymers *R* and fourth set of MIPs for irinotecan (containing 30% of monomer **2**). However, in general, specificity was not achieved neither with *MIP R*, except at short incubation times (10 and 20 minutes) where *MIP R* showed higher binding capacity than corresponding *NIP*.

Fluorescence measurements

Fluorescence titration of 60 μgmL^{-1} *MIP R* with imatinib was performed in 3:1 methanol:water mixture, employing excitation and emission wavelengths of respectively 448 and 530 nm. The related Stern-Volmer plot is reported in **Figure 5.8**.

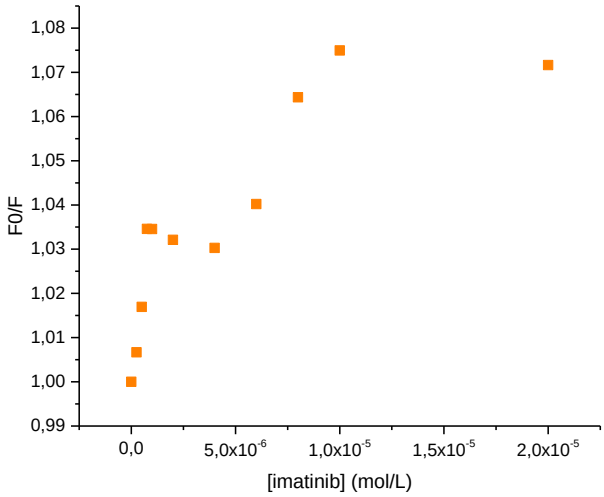

Figure 5.8: Stern-Volmer plot of 60 µgmL^{-1} *MIP R* titration with imatinib in 3:1 methanol:water.

The plot obtained by Stern-Volmer analysis showed a different trend than previous ones, with a high slope value below 1 µM, a sort of plateau between 1 and 4 µM, without decreasing a fluorescence intensity, and finally a quenching of fluorescence between 4 and 10 µM. Related values of Stern-Volmer constants and apparent bimolecular quenching constants, calculated using the emission lifetime of monomer **2**.

Nanogel	Concentration range	K_{SV} [10^4 Lmol^{-1}]	k_q [10^{12} Lmol^{-1}s^{-1}]
MIP R	0 – 1 µM	3.88	4.67
	4 – 10 µM	0.790	0.952

Table 5.6: Stern-Volmer constants and corresponding bimolecular quenching constants values, related to *MIP R* 60 µgmL^{-1} fluorescence titration with imatinib in 3:1 methanol:water mixture.

The bimolecular quenching constants values for *MIP R* were both higher than diffusion limit, confirming that a static quenching occurred, and a *MIP R* – imatinib complex was formed. However, *MIP R* quenching efficiency was not very high upon binding to the anticancer drug and since specificity also was not achieved, it was decided to use no longer 1,8-naphtalimide derivatives as fluorescent dyes to be incorporated in the polymer matrix. Fluorescein was therefore employed to prepare a new set of fluorescent MIPs imprinted with imatinib.

5.4 Fluorescent MIPs for imatinib containing fluorescein O-acrylate

New fluorescent MIPs for imatinib were prepared using a different functional monomer than 1,8-naphtalimide derivatives, as the previous results did not lead to specific and sensitive MIP for the anticancer drug, particularly within its therapeutic range. A new set of polymers was designed employing fluorescein O-acrylate (**11**, **Figure 5.9**) as functional monomer, since it is a very fluorescent molecule, emitting in the visible range (around 510 nm),[6] at wavelengths very far from residual proteins of plasma, avoiding their interference. This monomer may also improve nanogels solubility in water, favouring their binding to the anticancer drug in aqueous environments as human plasma.

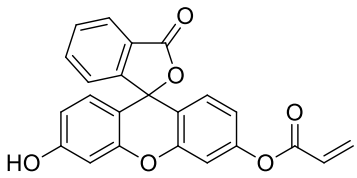

Figure 5.9: Chemical structure of fluorescein O-acrylate (**11**).

Before listing the polymers prepared, a focus on the ^{1}H-NMR titration of imatinib with fluorescein O-acrylate in DMSO-d_6 is reported.

*^{1}H-NMR titration of imatinib with **11***

The variation of chemical shift of the observed imatinib protons is reported in **Figure 5.10**.

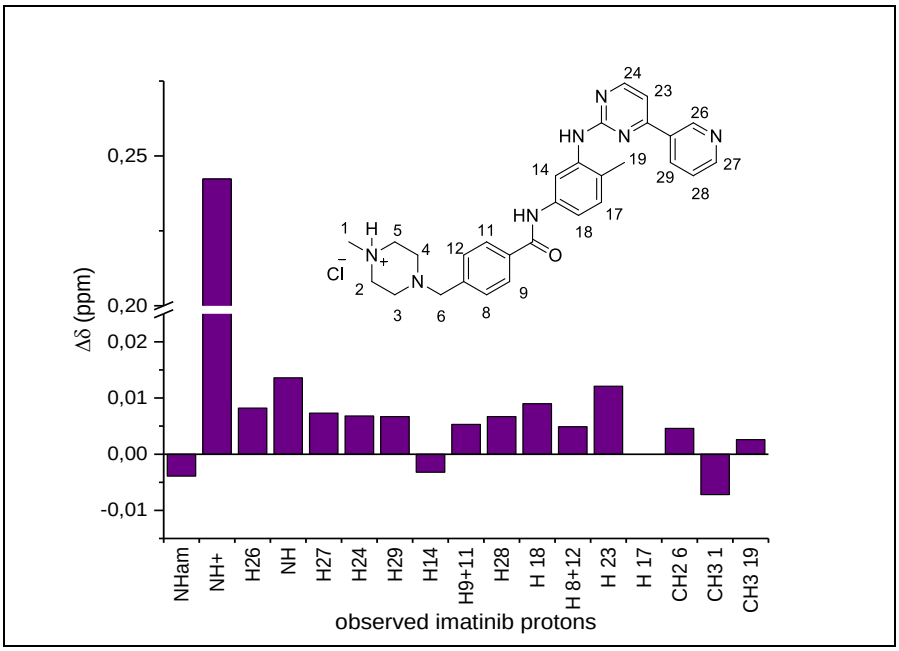

Figure 5.10: Variation of chemical shifts of observed imatinib protons (4 mM), before and after the adding of 10 equivalents (40 mM) of **11** in DMSO-d_6.

The majority of the observed imatinib protons were shifted to higher fields, and the most shifted proton was piperazinic *NH$^+$*, that resulted highly shielded upon adding of fluorescein O-acrylate. The trend of this shift is reported in **Figure 5.11 (a)**: a plateau of the curve was not observed, indicating that the equilibrium between free and bound imatinib was continuously shifted to the bound form, while fluorescein O-acrylate was added.

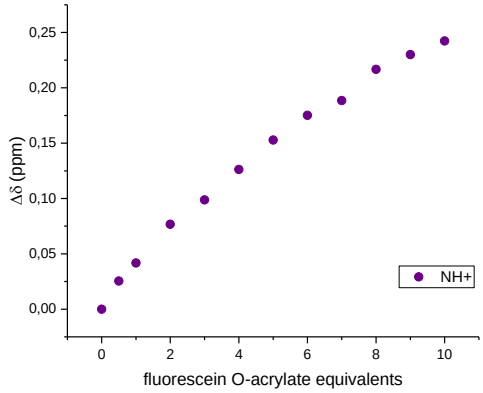

a)

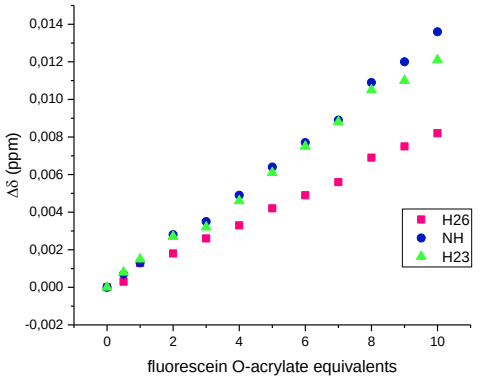

b)

Figure 5.11: Chemical shifts variation of imatinib protons *NH*$^{+}$, *H26*, *NH* and *H23*, upon binding to **11**.

In **Figure 5.11** the variations of imatinib aromatic protons *H26* and *H23*, and amine *NH* are reported, showing a linear correlation between chemical shift and equivalents of functional monomer added, as previously seen for the piperazine *NH*$^{+}$.

Synthesis of *MIPs S*, *T*, *U* and *U-UV*

MIPs S, *T*, *U* and *U-UV* were designed employing 30% of fluorescein O-acrylate, 70% of various cross-linkers, EGDMA, divinylbenzene (DVB) or MBA, and 5% of AIBN. Molar ratio between imatinib and fluorescein O-acrylate was fixed at 1.2 : 1 respectively, following the standard protocol. Reactions were carried out in DMSO and the C_m was

fixed 1%. Relative compositions, yields, reaction conditions and particle dimensions are reported **Table 5.7**.

Polymer	Functional monomer (30%)	Cross-linker (70%)	Yield	Reaction conditions	Size distribution by Number (nm)	PDI
MIP S	**11**	EGDMA	92%	24h, Δ 70 °C	19.3±1.6	0.249
MIP T	**11**	DVB	71%	24h, Δ 70 °C	6.8±0.7	0.188
MIP U	**11**	MBA	93%	24h, Δ 70 °C	*	-
MIP U-UV	**11**	MBA	43%	6 h, UV 40 °C	*	-
NIP S	**11**	EGDMA	69%	24h, Δ 70 °C	10.5±0.6	0.278
NIP T	**11**	DVB	46%	24h, Δ 70 °C	2.2±1.1	0.742
NIP U	**11**	MBA	3%	24h, Δ 70 °C	*	-
NIP U-UV	**11**	MBA	94%	6 h, UV 40 °C	*	-

Table 5.7: Compositions, yields and particles dimensions of *MIPs* and *NIPs S*, *T*, *U* and *U-UV*, obtained by DLS measurements 0f 0.25 $mgmL^{-1}$ polymer solutions in DMSO, after filtration on 0.45 µm PTFE filter and sonication. PDI stays for Poly Dispersion Index. *the DLS data were not available at the time of submission of this thesis as their measurement was still ongoing.

Yields of MIPs containing fluorescein were much higher than imprinted polymers prepared with 30% of 1,8-naphtalimide derivatives, confirming that employing a higher reactive group as O-acrylate rather than N-allyl, higher polymer yields are obtained, hence higher monomer incorporation in the polymer matrix was expected. Yields of relative NIPs were, instead, lower, particularly when MBA was employed as cross-linker (*NIP U*), except for *NIP U-UV* obtained by photo-activating AIBN, indicating that imatinib probably played an important role during polymerisation, favouring the polymer matrix formation. Since yields of NIPs obtained by thermo-activation of AIBN resulted quite low, compared to corresponding MIPs, *MIP* and *NIP U* reactions were replicated by photo-activating radical initiator (*MIP* and *NIP U-UV*), under UV irradiation at 360 nm for six hours at 40 °C. Corresponding yields resulted very good and high, particularly for *NIP U-UV*. This is probably due to the different source employed or lower reaction temperature, that is for sure favourable for imatinib-fluorescein complex form. Polymers particles, measures by DLS, were all in the nanometer scale, below 20 nm; employing a cross-linker as divinylbenzene (*MIP* and *NIP T*) nanoparticles resulted smaller, showing diameters even around 2 nm.

UV measurements

To know the amount of fluorescein incorporated by each polymer, UV-visible absorbance measurements of polymers were performed in water, as fluorescein does not absorb in DMSO, while in water its absorbance is very high. It was interesting to see that MIPs showed a different absorption spectrum rather than corresponding NIPs (**Figure 5.12a**), suggesting that the presence of a protonated template as imatinib probably affected polymers binding cavities formation, favouring one (or more) fluorescein tautomeric form rather than other ones.

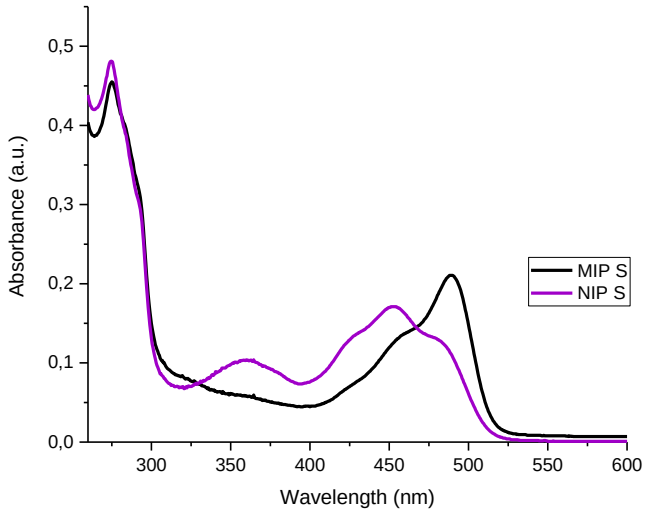

a)

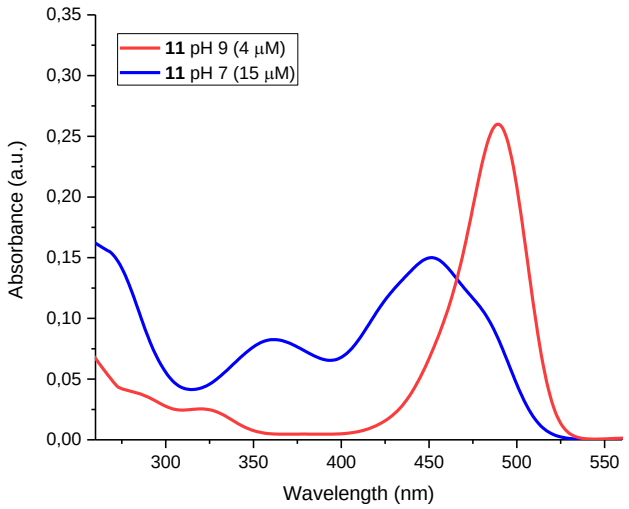

b)

Figure 5.12: a): UV-Visible absorbance spectra of 50 μgmL^{-1} *MIP S* and *NIP S* in water at pH 7 (same spectra trends were obtained for *MIP T* and *NIP T*); b): UV-Visible absorbance spectra of 15 μM **11** at pH 7 and 4 μM at pH 9 in water.

Fluorescein, indeed, can exist in seven prototropic forms in aqueous solution, and relative absorption spectra are strongly affected by the presence of these forms.[7,8]

Fluorescein O-acrylate, however, can exist in only six prototropic forms (**Figure 13**), as the dianionic form cannot be present, because of O-acryloyl group.

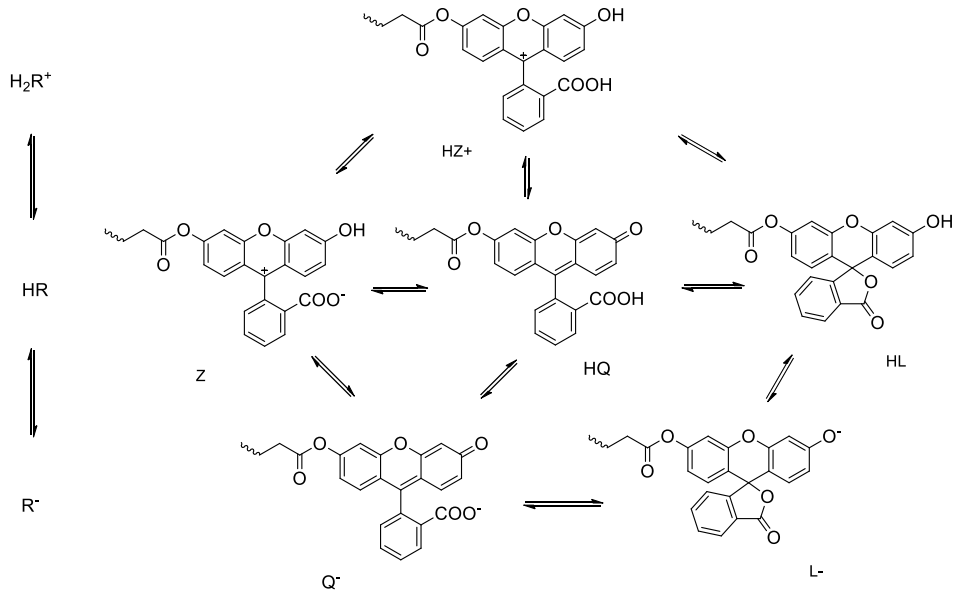

Figure 5.13: Tautomeric forms of fluorescein O-acrylate (**11**): monoprotonated (HR^+) form, that corresponds to monoprotic acid HZ^+; neutral form (HR), which exists in solution as a mixture of three tautomers, zwitterion (Z), quinonoid (HQ) and colorless lactone (HL); anionic form (R^-), that includes phenate tautomer (L^-) and carboxylate form (Q^-).

In general, it is difficult to understand from the absorption spectra, which fluorescein forms are mainly present in aqueous solution, because of overlapping absorption spectra and relative small differences in pK_a values of ionisable groups.[7] Mchedlov-Petrossyan *et al.*[9] analysed the absorption spectra of methyl fluorescein and identified the related tautomeric forms mainly present in water at different values of pH. Methyl fluorescein, indeed, can show six prototropic forms, and it can be considered a more similar structure to **11** rather than free fluorescein. They distinguished three limiting spectra, corresponding to cation (H_2R^+), neutral (HR) and monoanion forms (R^-) (**Figure 5.14).**

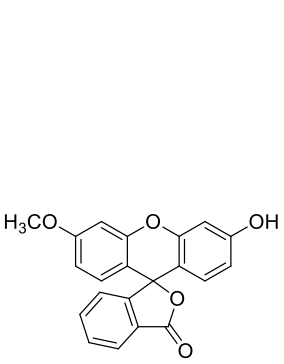

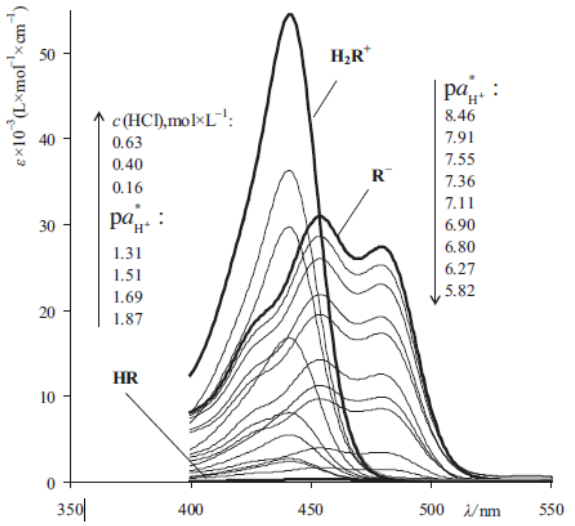

Fig. 2. Absorption spectra of fluorescein methyl ether in 50 mass% aqueous ethanol at different $pa^*_{H^+}$ and limiting dye forms.

Figure 5.14: Methyl Fluorescein chemical structure and absorption spectra of fluorescein methyl ether at different pH and limiting dye forms. (the spectra were recorder in 50% aqueous ethanol).[9]

From the analysis of Mchedlov-Petrossyan *et al.*[9] it is possible to notice that the anion form (R^-) spectrum, that shows two intense bands with maximum at 450 and 490 nm, can be easily compared to the previous spectra of the polymers *S* (**Figure 5.12a**) and the ones of fluorescein O-acrylate at neutral and basic pH (**Figure 5.12b**). *NIP S* spectrum showed a more intense band at 450 nm, while *MIP S* a maximum absorbance at 490 nm. It seemed that in *NIP S* the equilibrium between neutral and anionic form is probably more shifted to neutral forms, while in *MIP S* the predominant form of **11** seemed to be the anionic form, exposing a maximum at 490 nm, hence corresponding to an equilibrium mainly shifted to the anionic form. These hypothesis can be supported by the fact that in *MIP S* anions can be more stabilized by the presence of imatinib, acting as counter-ion and affecting also the global pK_a of the polymer; while in *NIP S*, as imatinib is not present, equilibrium is probably mainly shifted to the neutral forms, more stable in the absence of a protonated template.

To evaluate the amount of fluorescein contained by the polymers, different fluorescein calibration curves were employed, as different spectra were observed for each MIP and

NIP (**Figure 5.12**). For MIPs, it was employed the molar extinction coefficient obtained of fluorescein O-acrylate in water at pH 9, while for NIPs that measured at pH 7.

Nanogel	Amount of mon. 11 incorporated/mg of polymer (nmol/mg)	Percentage of mon. 11 incorporated during polymerisation
MIP S	187.9	15.9%
MIP T	262.0	18.1%
MIP U	614.2	45.7%
MIP U-UV	963.2	71.6%
NIP S	254.7	21.6%
NIP T	276.7	19.1%
NIP U	730.3	54.3%
NIP U-UV	989.3	73.6%

Table 5.8: Amount of **11** incorporated during polymerisation and contained by polymers *S*, *T*, *U* and *U-UV*, obtained by UV-Visible measurements of 50 μgmL^{-1} nanogel solutions (for *MIPs*) and 10 gmL^{-1} (for *NIPs*) in water.

Differently from previous nanogels prepared with naphtalimide derivatives, polymers containing fluorescein showed very high dye incorporation (**Table 5.8**). The highest percentage (around 72%) of incorporated monomer **11** was observed for *MIP* and *NIP U-UV*, prepared by photo-activating the radical initiator. This can be explained by the lower temperature (40 °C) employed for polymerisation under UV irradiation, rather than usual 70 °C, that could have favoured **11** reactivity. However, incorporation of monomer **11** was increased using a cross-linker as MBA (*MIP* and *NIP U*) rather than EGDMA (*MIP* and *NIP S*) or DVB (*MIP* and *NIP T*), which showed lower concentrations of fluorescein inside their polymer matrix.

HPLC rebinding assay

Rebinding capacity of MIPs and NIPs containing fluorescein was investigated through the already described HPLC experiment. 1 $mgmL^{-1}$ polymers suspensions in 50 µM aqueous solution of imatinib were incubated for 24 hours. Since all polymers resulted slightly soluble in water, moreover at that high concentration, an equilibrium dialysis measure was performed, and dialysis tubes were employed to separate polymers from free imatinib solution, that had to be analysed at HPLC.

The concentrations (nmol/mg) of imatinib bound to each nanogel over time are reported in **Figure 5.15**.

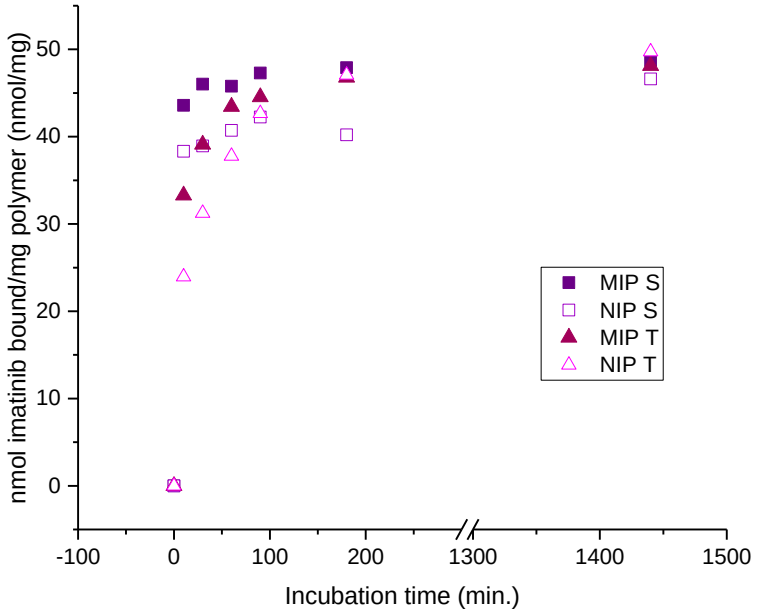

Figure 5.15: Imatinib rebinding kinetics of *MIPs* and *NIPs S* and *T* in water.

The faster binding kinetic was shown by *MIP S*, which captured 43 nmolmg^{-1} of imatinib already after 10 minutes. This concentration was also close to the one corresponding to saturation of binding sites available, as after 90 minutes a plateau was observed (with 47 nmol/mg of imatinib bound. *MIP S* showed also some specificity, particularly at shorter incubation times. After 24 hours, instead, a different behaviour between *MIP S* and *NIP S* was not seen anymore. *MIP T* showed high specificity for the anticancer drug only at the beginning at the experiment. After 90 minutes, *NIP T* captured quite the same imatinib amount of *MIP T* (42.7 vs 44.5 nmolmg^{-1}, respectively), indicating that many non-specific cavities were present also inside *MIP T* matrix.

In general, it seemed that these MIPs containing fluorescein as functional monomer made more accessible their specific binding sites at shorter incubation times, showing all very fast binding kinetics. The previous MIPs for irinotecan, instead, containing fluorophore **2** (belonging to the fourth set of MIPs), behaved in a completely different way, showing slower binding kinetics and achieving specificity at longer incubation times.

Fluorescence measurements

Rebinding capacities of *MIPs S* and *T* were also studied at fluorescence. 20 μgmL^{-1} MIPs solutions in 3:1 methanol:water mixture were titrated with increasing concentrations of imatinib in water. Unfortunately, both imprinted polymers did not show any significant variation of fluorescence intensity upon binding, probably because of methanol, as it is usually a very disadvantageous environment for rebinding of molecularly imprinted polymers.

However, to further investigate MIPs rebinding capacity, fluorescence titrations of 20 μgmL^{-1} MIP solutions with imatinib were performed in water.

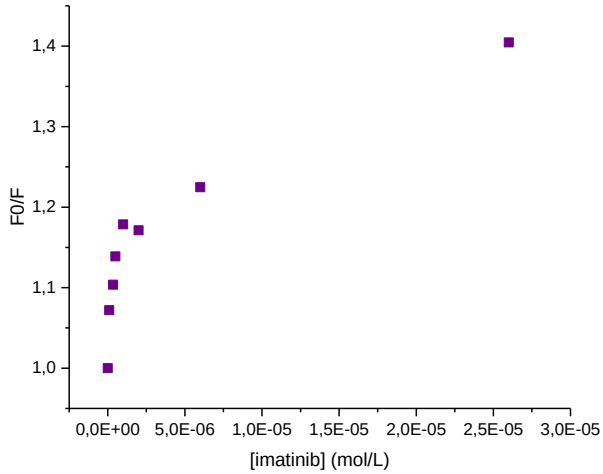

Figure 5.16: Stern-Volmer plot of 20 μgmL^{-1} *MIP S* titration with imatinib in water, using excitation and emission wavelength of 487 nm and 513 nm, respectively.

20 μgmL^{-1} *MIP S* was titrated with imatinib in water and related Stern-Volmer plot is reported in **Figure 5.16**. A bimodal trend of the plot was observed as usual for our MIPs, showing a higher slope value at imatinib concentrations below 1 µM, and a lower one in the micromolar range. Values of Stern-Volmer constants and bimolecular quenching constants are reported in **Table 5.9**.

Nanogel	Concentration range	K_{SV} [10^4 $Lmol^{-1}$]	k_q [10^{12} $Lmol^{-1}s^{-1}$]
MIP S	0 – 1 µM	15.94	38.32
	1 – 26 µM	0.930	2.24

Table 5.9: Values of Stern-Volmer constants and corresponding bimolecular quenching constants, calculated using fluorescein lifetime, as reported in literature (4.16 ns),[10] related to 20 μgmL^{-1} *MIP S* fluorescence titration with imatinib in water.

MIP S performance in water was very good, particularly at concentrations in the nanomolar range, as the value of the bimolecular quenching constant was in the order of 10^{13} $Lmol^{-1}s^{-1}$. Unfortunately, *MIP S* sensitivity decreased at micromolar imatinib concentrations, and a less efficient quenching was observed. Nevertheless, the overall change of emission was among the largest observed.

5.5 Fluorescent MIPs for imatinib containing N-acryloyl EDANS

^{1}H-NMR titration of imatinib with N-acryloyl EDANS

To investigate on non-covalent interactions established between imatinib and N-acryloyl EDANS (**12**), ^{1}H-NMR titration of template (4 mM) with increasing amount of the fluorescent functional monomer (from 3 to 58 mM) was performed in DMSO-d_6. Variations of imatinib protons chemical shifts are reported in **Figure 5.17**.

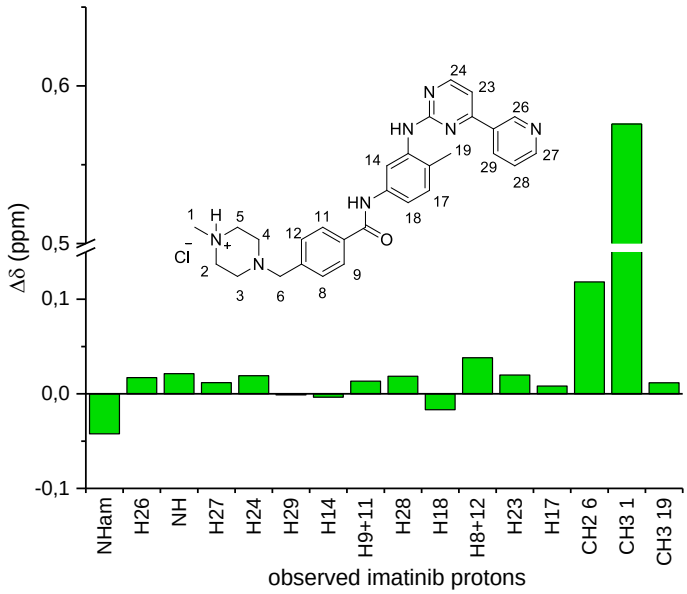

Figure 5.17: Chemical shift variations of observed imatinib protons before and after the adding of 14.5 equivalents of **12**, in DMSO-d_6.

Imatinib protons mainly shifted upon adding of monomer **12** belong to the protonated piperazine moiety, suggesting that an ionic pair between imatinib (cation) and EDANS (anion) could have been established. Moreover, NH^+ signal apparently disappeared immediately after the first adding of the functional monomer, supporting even more this idea. Trends of chemical shift variations of some imatinib protons are reported in **Figure 5.18**.

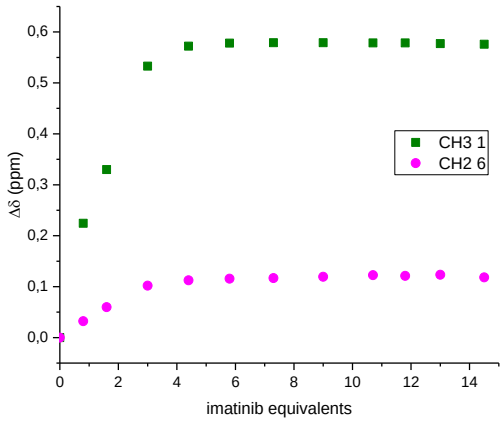

Figure 5.18: Chemical shifts variation of imatinib protons *H1* (methyl), *H6* (methylene), upon adding of **12**.

The largest entity of chemical shift variation was observed for methyl *H1* and methylene *H6* (**Figure 5.18**), suggesting that the piperazine moiety was involved in a quite strong interaction with imatinib, leading probably to the formation of an ionic pair. Unfortunately it was not possible to monitor the other piperazinic protons upon adding of **12**, as overlapping of signal occurred. An interesting plateau was reached by both *H1* and *H6* trends at 3 equivalents of monomer **12** added, indicating that the equilibrium between free and bound template was no longer affected by further monomer adding than 3 equivalents (12 mM **N-acryloyl EDANS**).

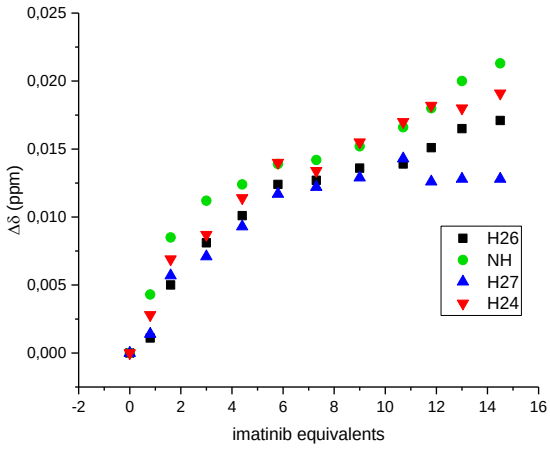

a)

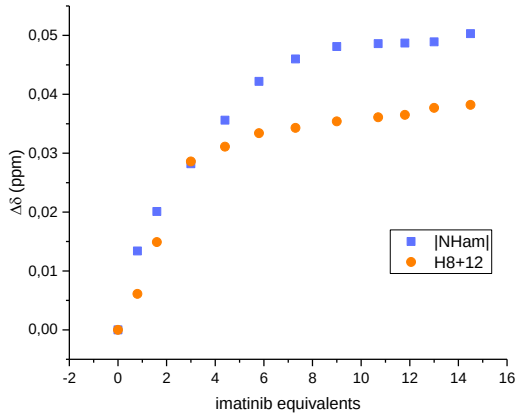

b)

Figure 5.19: Chemical shifts variation of imatinib protons NH, aromatic protons *H26*, *H27*, *H24* (**a**), amidic *NH* and aromatic *H8+12* (**b**), upon adding of **12**. Amidic NH was reported as absolute value, as it was shifted, conversely to other protons, to lower fields.

Trends of chemical shift variation similar to *H1* and *H6* (**Figure 5.18**) were the ones observed for aromatic *H27* (**Figure 5.19a**), *H8+H12* and amidic *NH* (**Figure 5.19b**), that reached a plateau after 6 (*H27*) and 8 (*NHam*, *H8+H12*) monomer equivalents added, respectively, suggesting that these protons could be affected by more than one kind of interaction.

Other interesting curves were obtained for the aromatic *H24*, *H26* and amine *NH* (**Figure 5.19a**), which all showed a bimodal trend, reaching a plateau at 6 equivalents (*H24*, *H26* and *NH*), but then increasing after the adding of 10 equivalents, suggesting that other interactions have been probably established.

Synthesis of *MIPs V*, *W* and *W-UV*

A first set of imprinted polymers for imatinib containing EDANS as fluorescent monomer was designed employing 30% of functional monomer and 70% of different cross-linker (EGDMA or MBA). Molar ratio between imatinib and monomer **12** was fixed at 1.2 : 1; AIBN and C_m employed were 5% and 1%, respectively. Reactions were carried out in DMSO for 24 hours for radical initiator thermo-activation or 6 hours when UV irradiation was used for photo-initating AIBN. Compositions, yields, reaction conditions and particles sizes are reported in **Table 5.10**.

Polymer	Functional monomer (30%)	Cross-linker (70%)	Yield	Conditions	Size Distribution by Number (nm)	PDI
MIP V	**12**	EGDMA	90%	70 °C, 24 h	9.1±2.1	0.369
MIP W	**12**	MBA	95%	70 °C, 24 h	9.0±1.5	0.643
MIP W-UV	**12**	MBA	88%	40 °C, 6 h (UV irradiation)	*	-
NIP V	**12**	EGDMA	93%	70 °C, 24 h	5.1±0.2	0.413
NIP W	**12**	MBA	5%	70 °C, 24 h	12.7±2.3	0.858
NIP W-UV	**12**	MBA	21%	40 °C, 6 h (UV irradiation)	*	-

Table 5.10: Compositions, yields, conditions of polymerisation and size dimensions of *MIPs* and *NIPs V*, *W*, *W-UV*; DLS measurements of 0.25 $mgmL^{-1}$ nanogel solutions were performed in DMSO, after filtration on 0.45 µm PTFE filter and sonication. *the DLS data were not available at the time of submission of this thesis as their measurement was still ongoing.

The yields resulted very high and particles sizes were all around 10 nm, as the previous MIPs. *NIP W*, designed with 30% of **12** and 70% of MBA was obtained with a very low yield (5%) when polymerisation was initiated by heath (70 °C), while a better yield was achieved when UV irradiations were employed to activate radical initiator (*NIP W-UV*, 21%). These results suggest that for *NIP W-UV* synthesis a lower reaction temperature is favoured (40 vs 70 °C), but combination of **12** and MBA without the presence of the template disfavours NIP formation. This could be explained by the different charge state of the polymerisation mixtures, that should be strongly negative when the template is not added (NIP), as only N-acryloyl EDANS is present, while charges should be neutralized when imatinib is added (MIP), as it actually is a counter-ion for EDANS.

UV-Visible measurements

To know the amount of EDANS contained and incorporated during polymerisation by each nanogel, UV-Visible measurements were performed in DMSO. The EDANS molar extinction coefficient was previously obtained by a calibration curve in DMSO and corresponded to 10812 $Lmol^{-1}cm^{-1}$ at 338 nm. This value was employed to calculate the concentration of fluorophore in the polymer matrix using Lambert-Beer equation.

The obtained results are reported in **Table 5.11**.

Nanogel	Amount of EDANS incorporated/mg of polymer (nmol/mg)	Percentage of EDANS incorporated during polymerisation
MIP V	515.6	40.5%
MIP W	509.9	34.5%
MIP W-UV	510.0	34.8%
NIP V	140.6	11.0%
NIP W	437.3	29.8%
NIP W-UV	114.7	7.8%

Table 5.11: Percentage of EDANS incorporated during polymerisation and contained by polymers *V*, *W* and *W-UV*, obtained by UV-Visible measurements of 0.05 $mgmL^{-1}$ nanogel solutions in water (except for *NIP W-UV*, which a solution of 0.2 $mgmL^{-1}$ was prepared for).

The amounts of fluorophore incorporated by polymers containing EDANS were very high, compared to MIPs for irinotecan containing 30% of monomer **2**. However, incorporation of **12** by NIPs resulted quite low, even if UV irradiation was employed for polymerisation (*NIP W-UV*). This can indicate that the presence of imatinib increases N-acryloyl EDANS reactivity, perhaps because its negative charge is neutralized by the protonated form of imatinib, in MIP polymerisation mixture.

HPLC rebinding assays

Rebinding capacity of polymers containing EDANS was studied through HPLC experiments, except for *NIPs W and W-UV*, because not enough amount of them was available for the assay. Equilibrium dialysis measures were performed: all polymers suspensions in water were kept in dialysis tube during incubation, as they were soluble in water. Results are reported in **Figure 5.20**.

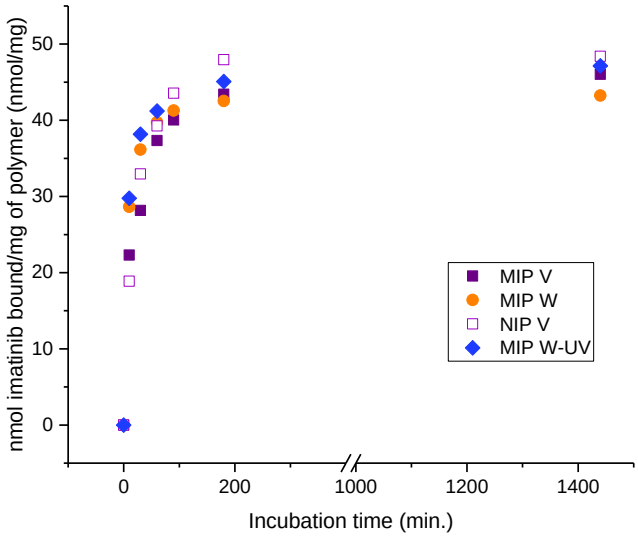

Figure 5.20: Binding kinetics of *MIP V*, *MIP W*, *MIP W-UV* and *NIP V* in water, obtained by HPLC experiments.

All polymers showed very high rebinding capacity towards imatinib. The faster binding kinetics were observed for *MIPs W* and *W-UV*, that bound about 30 $nmolmg^{-1}$ of imatinib already after 10 minutes of incubation. *MIP V* showed little specificity only after ten minutes of incubation, but during the whole experiment *NIP V* captured more drug than corresponding *MIP V*. All three polymers reached saturation of binding sites after three hour of incubation, as shown by the plateau of relative binding kinetics in **Figure 5.20**. It is also important to notice that *MIPs W* and *W-UV* showed quite the same binding kinetic, indicating that MIP performance was not highly affected by thermo-activation or photo-activation of radical initiator in the synthesis; *MIP W-UV* showed, however, just a higher rebinding capacity than *MIP W* at long incubation times.

Fluorescence measurements

Before MIPs fluorescence titrations with imatinib were carried out, UV-Visible absorbance spectra of imatinib at different concentrations were performed in both water and 3:1 methanol:water mixture, in order to investigate on the possible inner filter effect caused by imatinib in these solvents, as excitation wavelength of EDANS (around 335 nm) are not so far from the anticancer drug absorbance. In this way, it was

possible to correct, particularly for micromolar imatinib concentrations, all MIPs fluorescence intensities measured, using the following **Equation 5.1**, excluding an eventual error of observed quenching interpretation.[11]

$$F_{corr} = F_{obs} \cdot 10^{\frac{\varepsilon_{\lambda ex} \cdot l \cdot c}{2}}$$

(**Eq. 5.1**)

Where F_{corr} and F_{obs} are respectively the corrected and observed fluorescence intensities, $\varepsilon_{\lambda ex}$ the molar extinction coefficient of quencher (imatinib) at the excitation wavelength employed, in the same solvent of fluorescence measurements ($Lmol^{-1}cm^{-1}$), *l* is the length of optical pathway (cm) and *c* the molar concentration of quencher ($molL^{-1}$).

Fluorescence titrations of 20 μgmL^{-1} *MIP V* and *MIP W* with imatinib where performed in 3:1 methanol:water mixture, but again as with the previous series, no quenching of polymers fluorescence was observed, suggesting that methanol was a very disadvantageous environment for these polymers performances.

Therefore, fluorescence titrations of *MIPs V* and *W* with imatinib were carried out in water.

To 20 μgmL^{-1} *MIP W* in water increasing amount of imatinib were added, from 150 nM to 6 µM, using excitation and emission wavelengths of 337 and 498 nm, respectively. The results were corrected using **Equation 5.1** and plotted using Stern-Volmer analysis (**Figure 5.21**).

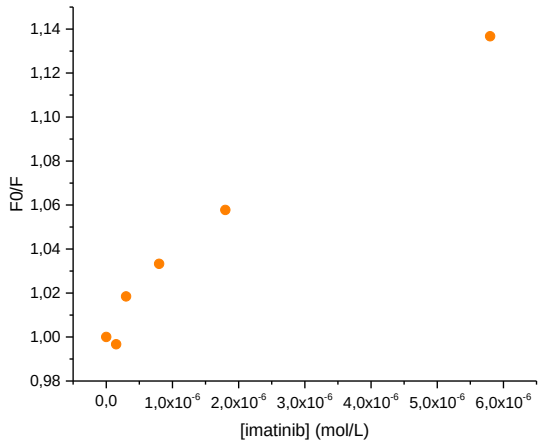

Figure 5.21: Stern-Volmer plot of 20 μgmL^{-1} *MIP W* fluorescence titration with imatinib in water.

Differently from almost all the other MIPs studied, the Stern-Volmer plot of *MIP W* in water (**Figure 5.21**) showed a simple linear correlation between imatinib concentration and *F0/F*, suggesting that only one population of binding sites specific for imatinib, was active in the polymer matrix, at the explored range of concentrations. The value the Stern-Volmer constant, was $2.32 \cdot 10^{4}$ $Lmol^{-1}$, and the related bimolecular quenching constant was $1.83 \cdot 10^{12}$ $Lmol^{-1}s^{-1}$, calculated using the EDANS fluorescence lifetime reported in literature (12.7 ns);[12] the obtained value confirmed that a static quenching occurred.

To further investigate the behaviour of *MIP W* and *MIP W-UV* in a wider range of imatinib concentrations, fluorescence titrations of each nanogel were performed in water, from 1 nM to 100 µM. The amount of polymers was decreased to 6 $\mu g mL^{-1}$, to see if MIP sensitivity could be improved. The Stern-Volmer plots obtained are reported in **Figure 5.22**.

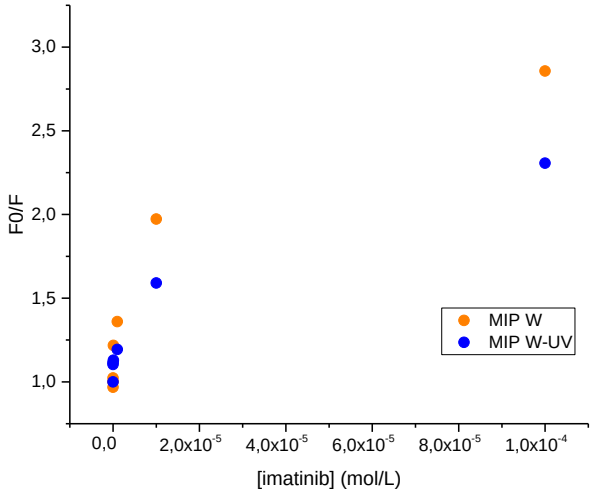

a)

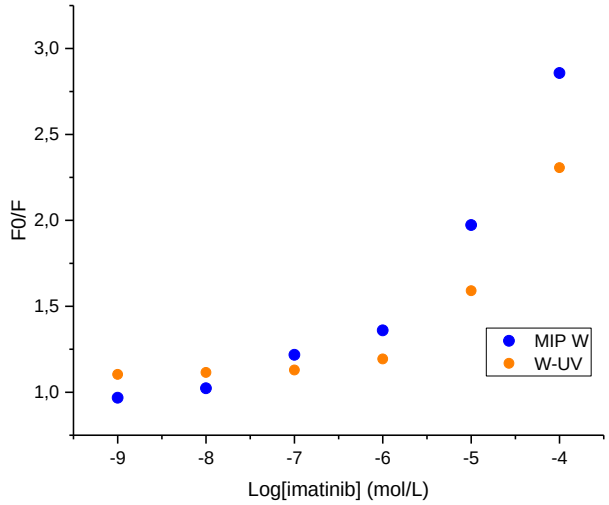

b)

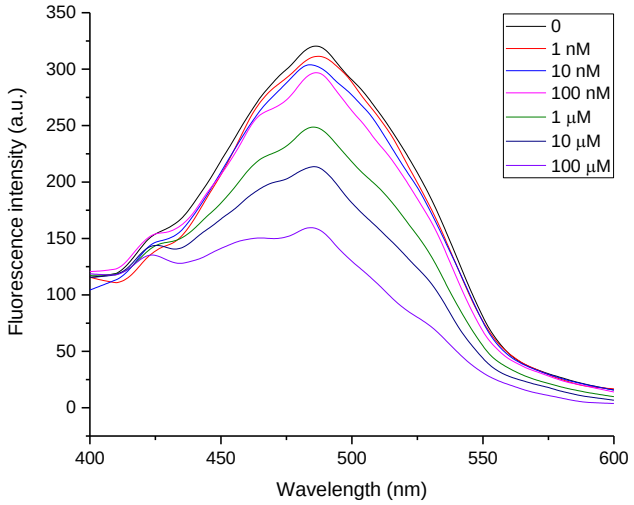

c)

Figure 5.22: a): Stern-Volmer plots of 6 μgmL^{-1} *MIPs W* and *W-UV* in water, within a large concentration range; b) SemiLog scale of 6 μgmL^{-1} *MIPs W* and *W-UV* Stern-Volmer plots in water; c) Fluorescence emission quenching of 6 μgmL^{-1} *MIP W-UV* in water upon adding of increasing amounts of imatinib.

The efficiency of *MIPs W* and *W-UV* fluorescence quenching upon imatinib adding was very high, as seen in the emission scans reported in **Figure 5.22c).**

From the Stern-Volmer plots reported in (**Figure 5.22a**) a bimodal linear trend was observed for both nanogels, showing a higher value of the slope at concentrations below 10 µM. The related values of Stern-Volmer constants and bimolecular quenching constants are reported in **Table 5.12**.

Nanogel	K_{sv} [$\cdot 10^4$ $Lmol^{-1}$]	k_q [10^{12} $Lmol^{-1}s^{-1}$]
MIP W	9.02	7.10
MIP W-UV	5.00	3.93

Table 5.12: Stern-Volmer constants an related bimolecular quenching constants of 6 μgmL^{-1} MIP W and MIP W-UV fluorescence titrations with imatinib in water.

It is very interesting to notice that, decreasing *MIP W* concentration, a higher sensitivity was actually achieved, as the value of the Stern-Volmer, compared with the previous one of 20 μgmL^{-1} *MIP W* ($2.32 \cdot 10^4$ $Lmol^{-1}$) was even three folds higher ($9.02 \cdot 10^4$ $Lmol^{-1}$). *MIP W-UV*, however, resulted less sensitive than the related MIP prepared by thermo-activation, showing a Stern-Volmer constant of $5.00 \cdot 10^4$ $Lmol^{-1}$. The observed bimolecular quenching constants had values of 10^{12} order, hence the quenching was confirmed as static.

MIP W showed very promising properties, as good affinity and sensitivity were achieved lowering the concentration of the polymer in water. However, these nanogels were not stable in 3:1 methanol:water mixtures, leading to difficulties to study their behaviour in plasma treated samples.

Synthesis of *MIP X*

Since all the previous polymers containing EDANS showed very low stability in methanol (as this solvent is usually employed for plasma processing), a new polymer for imatinib was designed. This MIP provided the incorporation of a very small amount of the co-monomer NIPAM, which should establish less interactions as possible with the template molecule, avoiding to hinder monomer **12** reactivity, and should favour MIP stability, thanks to its solubility in polar media.

MIP X was designed fixing the molar ratio between imatinib and **12** at 1 : 2 respectively, as ^{1}H-NMR titration suggested that an amount of functional monomer higher than one molar equivalent could shift even more the equilibrium towards bound imatinib. An

excess of **12**, as already proven by MIPs for irinotecan containing 30% of monomer **2**, can also favour the formation of more specific cavities for the template, containing for example two monomers per pocket. The percentage of **12** employed (in mol) was 36%, while co-monomer NIPAM was 4% and 60% of MBA as cross-linker; the decision to decrease the amount of cross-linker was done because it usually reacts faster than other monomers, interfering with their reactivity. AIBN and C_m were fixed at 5% and 1%, respectively. Reaction was carried out in DMSO at 70 °C.

Polymer	Functional monomer	Co-monomer	Cross-linker	Yield	Size Distribution by Number (nm)	PDI
MIP X	**12** (36%)	NIPAM (4%)	MBA (60%)	66%	6.9±0.3	0.830
NIP X	**12** (36%)	NIPAM (4%)	MBA (60%)	21%	8.6±2.1	0.425

Table 5.13: Composition, yield and particles dimensions, measured at DLS, of *MIP X* and *NIP X*. DLS measurements of 0.25 μgmL^{-1} were performed in DMSO, after filtration on 0.45 µm and sonication.

The size of *MIP* and *NIP X* nanoparticles were around 8 nm, consistently with the previous ones. Instead, the yields were lower than previous *MIPs V* and *MIP W*, containing **12** as well. This could be due to the lower percentage of cross-linker and larger amount of functional monomer employed, and their different reactivity, as already proved. A particularly low yield was observed for *NIP X*, hence, some ^{1}H-NMR investigations on conversion of functional monomer and cross-linker in presence or absence of template were performed.

NMR investigations of monomers conversion

Two polymerisation mixtures with or without imatinib, were prepared on a small scale in DMSO-d_6, maintaining the same compositions reported in **Table 5.13**; the ^{1}H-NMR spectra of each mixture were recorded before thermo-initiating the polymerisation and after 24 hours of reaction. An external standard (2-Bromo-6-methoxynaphtalene) was added to each mixture before recording the NMR spectrum. The conversions of MBA and monomers after polymerisation are reported in **Table 5.14**.

Polymer	Monomers	Conversion after 24 h (%)
MIP X	**12**	66
	NIPAM	82
	MBA	86
NIP X	**12**	74
	NIPAM	92
	MBA	94

Table 5.14: NMR conversions of **12**, NIPAM and MBA after 24 hours of polymerisation in presence (*MIP X*) and absence (*NIP X*) of imatinib.

The experiments showed that in the presence of imatinib, a 10% higher conversion of all mixture components (**Table 5.14**) was observed, suggesting that a protonated template as counter-ion probably plays a quite important role during polymerization. Yields obtained for polymers containing **12** (*MIPs* and *NIPs V*, *W* and *W-UV*), were much higher than *MIP X* (more than 90% versus 66%). This could be due to the 1 : 2 template : functional monomer molar ratio employed, which did not make enough imatinib available as counter-ion to all the anionic N-acryloyl EDANS, leading to less reactive polymerisation mixture.

UV-Visible measurements

To know the amount of EDANS incorporated by polymers *X*, UV-Visible absorbance measurements of DMSO nanogel solutions were performed.

Nanogel	Amount of EDANS incorporated/mg of polymer (nmol/mg)	Percentage of EDANS incorporated during polymerisation
MIP X	488.5	28.5%
NIP X	155.4	9.1%

Table 5.15: Percentage of edans incorporated during polymerisation and contained by polymers MIP X and NIP X, obtained by UV-visible measurements of 50 μgmL^{-1} solutions in DMSO.

MIP X showed much higher incorporation of monomer **12** in its matrix than corresponding *NIP X* (**Table 5.15**); this was probably due to the lowest reactivity of N-acryloyl EDANS in the absence of imatinib. Comparing these results with the previous ones, related to *MIPs* and *NIPs V*, *W* and *W-UV*, a very similar amount of incorporated EDANS was obtained, around 500 $nmolmg^{-1}$ in MIPs and 150 $nmolmg^{-1}$ in NIPs. Hence, using **12** as functional monomer seemed to lead to MIPs containing a concentration of fluorophore about three folds higher than corresponding NIPs. This result confirmed the NMR experiment previously reported, where the MIP polymerisation mixture showed higher incorporation of monomer **12** rather than NIP. Moreover, it is important to remember that EDANS conversions measured at NMR, were higher because

polymerisation mixtures analysed included also all the oligomers, that are always removed through dialysis.

HPLC rebinding assay

Due to the low availability of *NIP X*, the rebinding measures were carried out on the MIP, by equilibrium dialysis as previously described. *MIP X* specificity was, however, studied subsequently at fluorescence. The rebinding kinetic is reported in **Figure 5.23**, compared to the previous ones related to *MIPs V* and *W*.

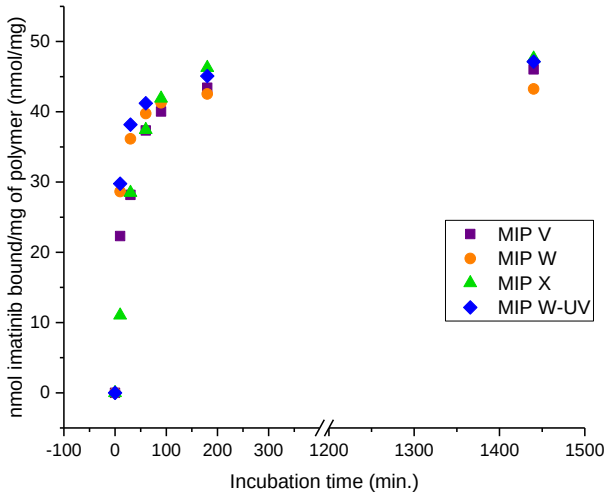

Figure 5.23: Binding kinetics of *MIPs V*, *W*, *W-UV* and *X* towards imatinib in water, obtained by HPLC experiments.

The rebinding kinetic of *MIP X* in water showed a very similar trend to *MIPs V*, *W* and *W-UV*, as saturation of all polymers binding sites was observed after about three hours of incubation and circa same amount of imatinib (45 $nmolmg^{-1}$) was captured by them. *MIP X* only showed a slower binding kinetic at shorter incubation times (after 10 and 30 minutes), indicating maybe that specific sites were not immediately accessible to the anticancer drug.

Fluorescence measurements

As already mentioned, all values of *MIP X* fluorescence intensities were corrected using **Equation 5.1**, in order to consider the inner filter effect caused by imatinib.

The first *MIP X* fluorescence titration was performed in 3:1 methanol:water, to evaluate if polymer performance, compared to previous MIPs containing EDANS, was improved using *MIP X* in this media. Unfortunately, *MIP X* did also not show any variation of its fluorescence intensity, excluding the possibility to use this polymer in plasma samples treated with methanol; other conditions have been therefore evaluated to extract the drug from plasma samples and exploit *MIP X* performance.

MIP X binding capability was therefore studied in water, to see if any fluorescence variation occurred upon binding to imatinib. 20 μgmL^{-1} *MIP X* in water was titrated with increasing concentration of imatinib. The explored concentration range took into account the information about the imatinib therapeutic range, particularly its lower limit of efficacy, that is around 2 $\mu molL^{-1}$. The titration was also repeated after filtration of colloidal *MIP X* solution in water (on 0.20 µm PTFE filters), to see if after removing eventual aggregates, MIP performance was improved, as a more homogeneous solution can be obtained. The related Stern-Volmer plots are reported in **Figure 5.24a**.

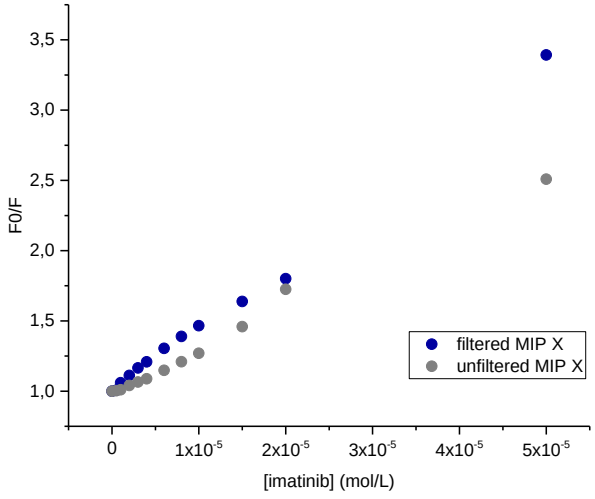

a)

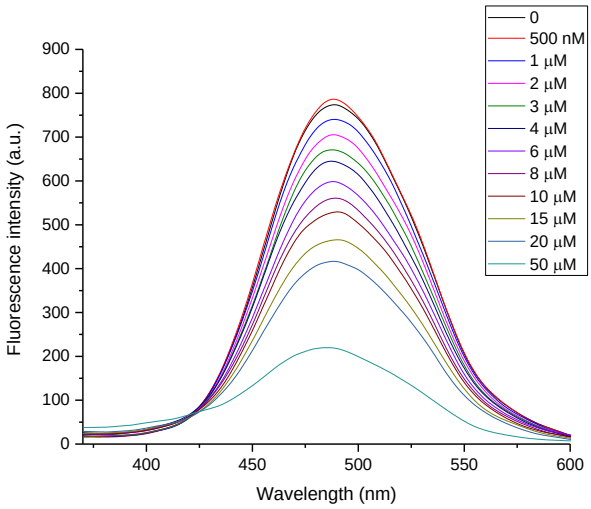

b)

Figure 5.24: a): Stern-Volmer plots of 20 μgmL^{-1} *MIP X* fluorescence titration with imatinib in water without (grey) and with (blue) filtering polymer solution on 0.20 μm filter; b): emission spectra related to the titration.

A very large change in emission occurred for both the measures (**Figure 5.24b**). *MIP X* filtration resulted very effective, as a higher value of the Stern-Volmer slope was obtained, confirming that removal of bigger aggregates favoured imatinib accessibility to MIP nanoparticles binding sites. A good linearity of the Stern-Volmer plot was observed for *MIP X* titration after filtration, and the Stern-Volmer constant value was $4.67 \cdot 10^4$ Lmol^{-1} and relative bimolecular quenching constant resulted $3.68 \cdot 10^{12}$ Lmol^{-1}s^{-1}, confirming that a static quenching occurred.

To study *MIP X* specificity, 20 μgmL^{-1} fluorescence titration of *NIP X* with imatinib was performed in water, after solution filtration (**Figure 5.25**).

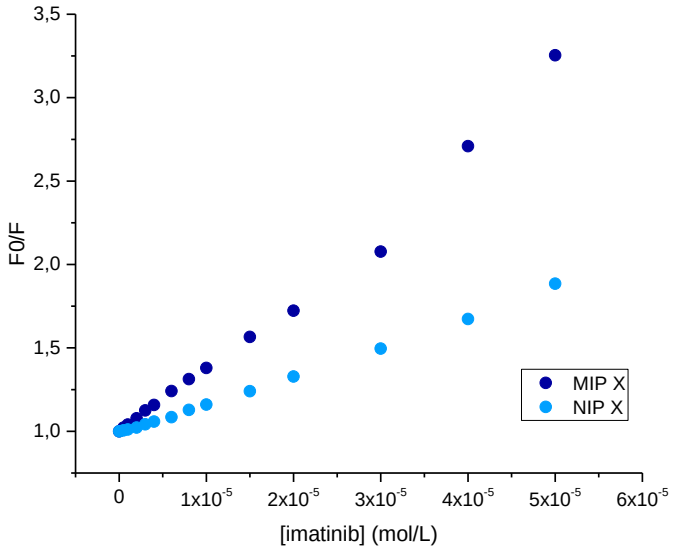

Figure 5.25: Stern-Volmer plots of 20 µgmL^{-1} fluorescence titrations of *MIP X* and *NIP X* with imatinib in water, after polymer solutions filtration on 0.20 µm PTFE filter.

MIP X specificity for imatinib was proven by *NIP X* fluorescence titration with imatinib, as a lower value of the Stern-Volmer constant was obtained ($1.74 \cdot 10^4$ Lmol^{-1}), corresponding to more than a half of K_{SV} observed for *MIP X*. According to these results, *MIP X* is the best material obtained for imatinib, thanks to the very large change in emission, the linearity and the specificity in comparison with the *NIP*.

Different concentrations of *MIP X* in water were titrated with imatinib, in order to find the best one for MIP performance. The explored MIP X concentrations were 10, 20, 40 and 60 µgmL^{-1} (**Figure 5.26**).

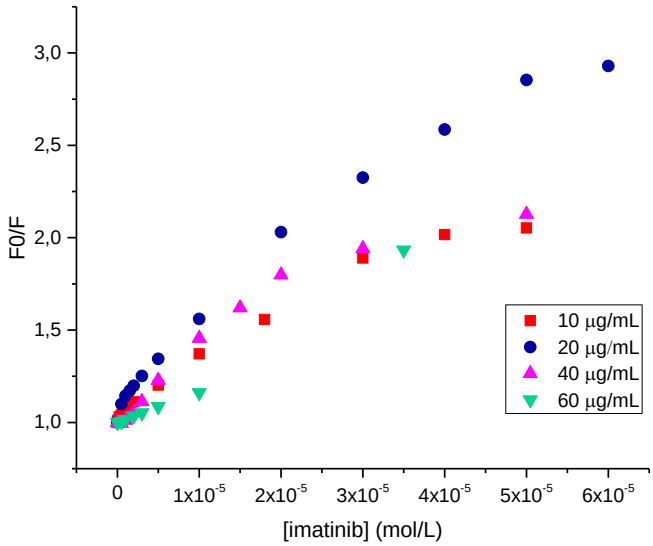

Figure 5.26: Stern-Volmer plots of *MIP X* 10, 20, 40 and 60 µgmL^{-1}in water with imatinib. All *MIP* solutions were filtered on 0.20 µm filters before starting the titrations.

Stern-Volmer analysis of *MIP X* fluorescence titrations with imatinib showed that the best MIP performance was obtained using a 20 µgmL^{-1} polymer concentration of, as the highest quenching of fluorescence upon adding of imatinib was observed using this polymer concentration. Using 10 µgmL^{-1} *MIP X* concentration, however, the Stern-Volmer plot obtained was not so far from the curve corresponding to 20 µgmL^{-1} at nanomolar concentrations range. Hence, for further investigations, the optimal *MIP X* concentration could be in the range between 10 and 20 µgmL^{-1}, as an higher amount of polymer probably leads to aggregation and produced a not very efficient fluorescence quenching upon binding to imatinib.

20 µgmL^{-1} *MIP X* titration with imatinib was repeated three times (**Figure 5.27**), to verify *MIP X* response variability and then eventually evaluate if it is possible to use this titration as calibration curve for an analytical method for drug quantification in real human plasma samples.

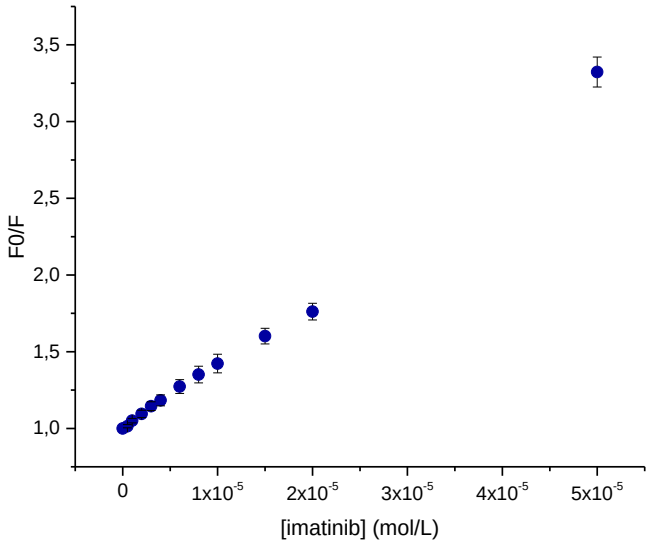

Figure 5.27: Stern-Volmer plot of 20 µgmL^{-1} *MIP X* fluorescent titration with imatinib in water, repeated three times.

The value of Stern-Volmer constant obtained was $4.78 \cdot 10^4 \pm 0.141 \cdot 10^4$ Lmol^{-1} and related bimolecular quenching constant resulted $3.76 \cdot 10^{12}$ Lmol^{-1}s^{-1}, confirming that a static quenching occurred. The intercept of the graph was 0.961 ± 0.0246, with an error of 2.56%, while r^2 was 0.992. The average precision of the plot, defined as the average of the standard deviations on each single point, was 4.37%. On the basis of the standard deviation, the estimated LOD corresponded to $1.66 \cdot 10^{-6}$ molL^{-1} imatinib concentration.

A triplicate of fluorescence titrations of *MIP X* with imatinib in water was performed also at 10 µgmL^{-1} MIP (**Figure 5.28**).

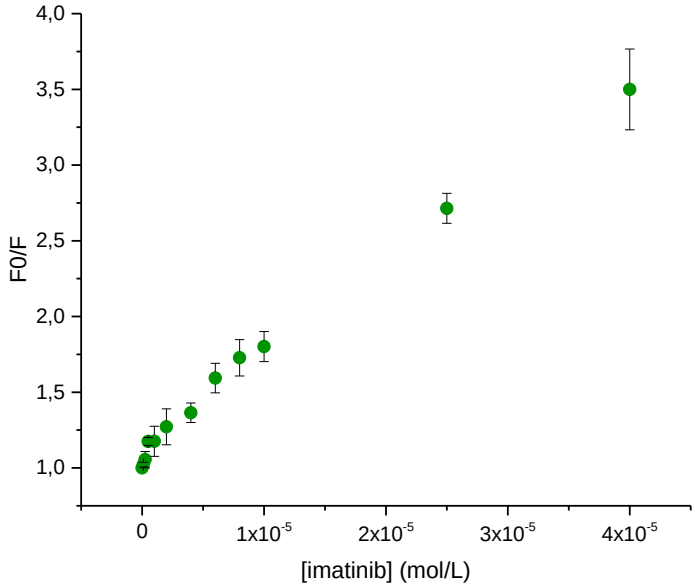

Figure 5.28: Stern-Volmer plot of 10 µgmL^{-1} *MIP X* fluorescence titration with imatinib in water.

The Stern-Volmer constant obtained using 10 µgmL^{-1} *MIP X* concentration was even higher ($6.17 \cdot 10^4 \pm 0.21 \cdot 10^4$ Lmol^{-1}) than the one observed with 20 µgmL^{-1} ($4.78 \cdot 10^4 \pm 0.14 \cdot 10^4$), hence a static quenching surely occurred. The intercept of the graph was 1.12 ± 0.03, with an error of 2.64%, while r^2 was 0.989. The average precision of the plot, defined as the average of the standard deviations on each single point, was 3.35%, a lower value than the previous one, obtained with 20 µgmL^{-1} *MIP X*. On the basis of the standard deviation, the estimated LOD corresponded to $10.55 \cdot 10^{-6}$ molL^{-1} imatinib concentration, resulting higher than the previous one and indicating that a lower *MIP X* sensitivity was observed at this concentration.

Since in the final real sample, *MIP X* should operate in a denaturating environment, obtained by precipitating or just defolding proteins of plasma samples by adding an organic solvent as methanol or DMSO, as previously described in **Chapter 4**, *MIP X* performance was investigated in 3:1 DMSO:water mixture, as in methanol it already showed very low activity and acetonitrile could not be used because imatinib is not soluble in it.

MIP X 20 μgmL^{-1} was titrated with increasing amount of imatinib in 3:1 DMSO:water, using excitation and emission wavelengths of 355 and 465 nm, respectively (**Figure 5.29**).

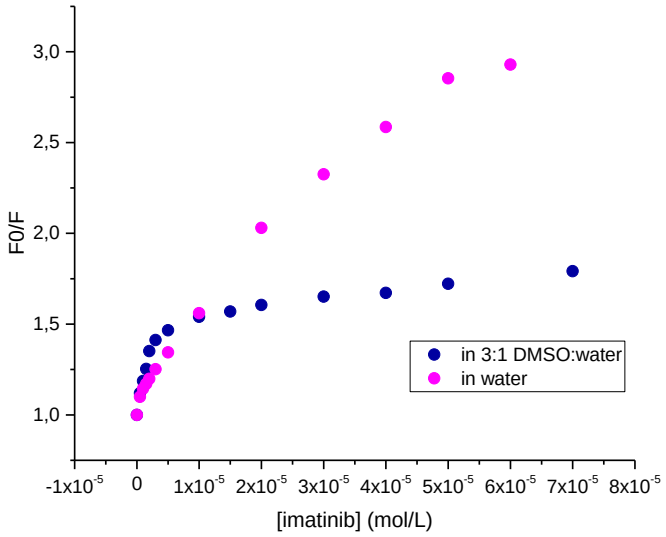

Figure 5.29: Stern-Volmer plots of 20 μgmL^{-1} *MIP X* titration with imatinib in 3:1 DMSO:water and water.

MIP X performance in 3:1 DMSO:water mixture got worse, particularly at micromolar concentrations, where MIP fluorescence quenching was not very efficient upon imatinib binding. Conversely to results in water, in 3:1 DMSO:water a bimodal trend of the plot was observed, with higher slope value below 5 μM and a lower one at higher imatinib concentrations (**Table 5.16**).

Nanogel	Concentration range	K_{SV} [10^4 Lmol^{-1}]	k_q [10^{12} Lmol^{-1}s^{-1}]
MIP X	0 – 5 μM	9.06	7.13
	5 – 70 μM	0.457	0.360

Table 5.16: Stern-Volmer constants and related bimolecular quenching constants of *MIP X* fluorescence titration with imatinib in 3:1 DMSO:water.

Despite the less efficient fluorescence quenching observed at imatinib concentrations higher than 5 μM, a higher value of bimolecular quenching constant ($7.13 \cdot 10^{12}$ Lmol^{-1}s^{-1}) than the one obtained in water ($3.58 \cdot 10^{12}$ Lmol^{-1}s^{-1}) was observed, indicating that *MIP X* sensitivity, at concentrations below 5 μM, was a bit higher in 3:1 DMSO:water, rather than water alone. However, this environment was not very favourable for imatinib rebinding, hence it was not considered anymore for further studies with *MIP X*.

5.6 Trials in plasma

Since *MIP X* performance was not satisfactory in both methanol and DMSO media, a different approach for plasma treatment was considered. One aliquot of human plasma was processed with three volumes of methanol. After proteins precipitation and separation by centrifugation, as above mentioned, the supernatant was evaporated at a high vacuum centrifuge, keeping the temperature not higher than 37 °C, in order to remove the methanol. The residual plasma was then suspended using a volume of water equal to the 3:1 methanol:plasma initial mixture, hence diluting in water three or nine times the regenerated plasma.

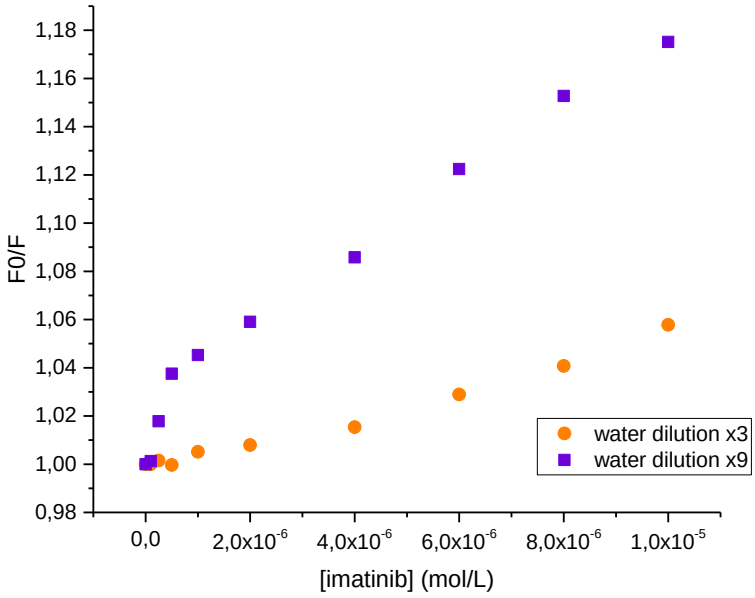

Figure 5.30: Stern-Volmer plots of 10 gmL^{-1} *MIP X* fluorescence titration with imatinib in regenerated plasma diluted with three volumes (x3, orange) or ten volumes (x9, purple) of water.

The Stern-Volmer plots in diluted plasma (**Figure 5.30**) showed that *MIP X* performance was not totally lost in a complex matrix as plasma, mostly by dilution of the regenerated plasma with nine volumes of water, leading to less interference of the plasma proteins. The corresponding constants obtained by Stern-Volmer analysis are reported in **Table 5.17**.

Nanogel	Solvent	K_{SV} [10^4 $Lmol^{-1}$]	k_q [10^{12} $Lmol^{-1}s^{-1}$]
***MIP X* (10 μgmL^{-1})**	in water	5.69	4.48
	in 3:1 water:plasma(R)	0.600	0.471
	in 9:1 water:plasma(R)	1.68	1.32

Table 5.17: Stern-Volmer constants and related bimolecular quenching constants values of 10 gmL *MIP X* fluorescence titration with imatinib in different media, 3:1 water: (R) regenerated plasma and 9:1 water: regenerated (R) plasma.

The values of the bimolecular quenching constants demonstrated that, despite the polymer performance got worse in the presence of unfolded plasma proteins, a fluorescence static quenching of *MIP X* upon binding to imatinib occurred and confirmed that this plasma processing, involving first the treatment with an organic solvents and then the re-suspension in water, was a practicable approach. Unfortunately, all the analytical parameters were not evaluated yet, because further system investigations would be performed exploring more diluted conditions.

[1] Szakács Z., Béni S., Varga Z., Örfi L., Kéri G., Noszál B., *Acid-Base Profiling of Imatinib (Gleevec) and Its Fragments* , J. Med. Chem. (2005), 48: 249-255

[2] Bürger H.M., Manley P.W., Mutz M., *Salt forms of 4-(4-methylpiperazin-l-ylmethyl)-n-[4-methyl-3-(4-pyridin-3-yl)pyrim-idin-2-yl amino)phenyl]-benzamid* (2005), WO 2005/075454 A2

[3] Guo J., Xu C., Li X., Chen S., *A Simple, Rapid and Sensitive FRET Assay for Botulinum Neurotoxin Serotype B Detection*, PLoS One. (2014) 9(12): e114124

[4] Karim K., Breton F., Rouillon R., Piletska E.V., Guerreiro A., Chianella I., Piletsky S.A., *How to find effective functional monomers for effective molecularly imprinted polymers?*, Adv. Drug Del.Rev. (2005) 57: 1795– 1808

[5] Hübner Martins D., Comparsi Wagner S., Vianna dos Santos T., de Lima Feltraco Lizot L., Venzon Antunes M., Capra M., Linden R., *Monitoring imatinib plasma concentrations in chronic myeloid leukemia*, Rev Bras Hematol Hemoter. (2011) 33(4):302-306

[6] Sjoback R., Nygren J., Kubista M., *Absorption and fluorescence properties of fluorescein*, Spectr. Chim. Acta Part A (1995) 51:L7-L21

[7] Klonis N., Sawyer W.H., *Spectral Properties of the Prototropic Forms of Fluorescein in Aqueous Solution, Journal of Fluorescence*, Vol. 6, No. 3, 1996

[8] Zanker V., Peter W., *Die prototropen Formen des Fluoresceins*, Chem. Bet. (1958) 91: 572-580

[9] Mchedlov-Petrossyan N.O., Cheipesh T.A., Shekhovtsov S.V., Redko A.N., Rybachenko V.I., Omelchenko I.V., Shishkin O.V., *Ionization and tautomerism of methyl fluorescein and related dyes*, Spectrochim. Acta Part A: Molec.and Biomolec. Spectr. (2015) 150: 151–161

[10] Zhang X.F., Zhang J., Liu L., *Fluorescence Properties of Twenty Fluorescein Derivatives: Lifetime, Quantum Yield, Absorption and Emission Spectra*, J. Fluoresc. (2014) 24:819–826

[11] Lakowicz J.R., *Principles of Fluorescence Spectroscopy*, Third Edition, Springer (2006), ISBN-13: 978-0387-31278-1

[12] Petersen K.J., Peterson K.C., Muretta J.M., Higgins S.E., Gregory D. Gillispie G.D., Thomas D.D., *Fluorescence lifetime plate reader: Resolution and precision meet high-throughput*, Rev. Sci. Instrum. (2014) 85(11): 113101

6. Experimental Section

6.1 Instrumentation

Flash-chromatography purifications were carried out using Merck silica gel 60 (230-240 Mesh). Thin layer chromatography (TLC) was performed on Merck plastic sheets pre-coated with 0.25 mm silica gel 60F-254. TLC plates were examined under UV light.

Microwave assisted reactions were performed on CEM Discover® synthesizer, working in pressurized mode and under magnetic stirring. Variable microwaves power was employed, in order to keep temperature at a fixed value (85 °C) during the whole reaction.

Nuclear magnetic resonance ^{1}H-NMR, ^{13}C-NMR, bidimensional gCOSY and gHSQCAD spectra were recorded on a Varian 500 MHz spectrometer.

Mass spectrometry (MS) spectra were collected on a Esquire 400 (Bruker Daltonics) spectrometer, using electrospray ionization (ESI) source.

High performance liquid chromatography (HPLC) analysis were run on an Agilent series 1100 liquid chromatograph equipped with an Agilent 1100 series variable wavelength detector and a Phenomenex reverse phase Kinetex® column (5 µm, C18, 100 Å, 250x4.6 mm).

Fluorescence measurements were performed with a CARY Eclipse (Varian) spectrometer, keeping the temperature at 25.0 °C.

UV-visible spectra were recorded on a UV-1800 spectrometer (Shimadzu).

Particles size were measured by Dynamic Laser Light Scattering (DLLS) on a Zetasizer nano-S (Malvern) instrument.

TEM images were recorded with a Camera Olympus QUEMESA and software RADIUS (EMSIS) on a TEM Philips EM208 electron microscopy operating at 100 kV.

6.2 Materials and methods

Chemicals and solvents were purchased from Sigma Aldrich. Anhydrous dichloromethane was prepared by drying the solvent over $CaCl_2$. When anhydrous conditions were required, reaction flasks were flame-dried and immediately placed under a flux of argon.

Glass Wheaton® vials used for the polymer synthesis were purchased from Sigma Aldrich. Spectra/Por3 dialysis membrane having MWCO of 3500 Da was purchased from Spectrumlabs. PTFE syringe filters with pore size of 0.45 µm were purchased from VWR, and before filtering DMSO solutions, filters were pre-treated with 1:1 mixture of methanol:isopropyl alcohol and washed with DMSO.

AIBN was recrystallized before synthesising the polymers, following a procedure already employed by our research group.[1]

Pure irinotecan·HCl·3H_2O and Imatinib base were purchased from Bepharm.

Human plasma (pool) was achieved by CRO - National Cancer Institute of Aviano.

6.3 Synthesis of polymerisable monomers

Synthesis of 1,8-naphalimide derivatives

2-allyl-6-bromo-1H-benzo[de]isoquinoline-1,3(2H)-dione (compound 1a)[2]

312 mg of 4-bromo-1,8-naphtalic anhydride (1.13 mmo, 1eq) and 7 mL of ethanol were heated up to 55 °C under stirring; 89 µL of allylamine (68 mg, d = 0.761 gmL^{-1}, 119 mmol, 1 eq) were added to the mixture, which was then refluxed for four hours, and the reaction was monitored by TLC using 1:1 dichloromethane:ethyl acetate as eluent. After cooling to room temperature, the solid was filtered under vacuum, washed with cold ethanol and dried at room temperature for one night. 239 mg of a brown powder were obtained, with 67% yield. *^{1}H-NMR* (δ, ppm, 500 MHz, $CDCl_3$): 4.79 (d, 2H, ^{3}J= 6 Hz), 5.21 (dd, 1H, $^3J_{cis}$= 10 Hz, ^{2}J= 1 Hz), 5.32 (dd, 1H, $^3J_{trans}$= 17 Hz, ^{2}J= 1 Hz), 5.98 (m, 1H), 7.85 (t, 1H, ^{3}J= 8 Hz), 8.04 (d, 1H, ^{3}J= 8 Hz), 8.42 (d, 1H, ^{3}J= 8 Hz), 8.57 (d, 1H, ^{3}J= 8.5 Hz), 8.66 (d, 1H, ^{3}J = 7.3 Hz) *^{13}C-NMR* (δ, ppm, 500 MHz, $CDCl_3$): 42.68, 117.97, 122.30, 123.17, 128.25, 129.21, 130.55, 130.83, 131.28, 131.50, 132.07, 132.32, 133.54, 163.47, 163.49 *ESI-MS* (m/z): 338.4 + 340.3 ($[M+Na]^+$), 355.2 + 357.2 ($[M+K]^+$)

2-allyl-6-chloro-1H-benzo[de]isoquinoline-1,3(2H)-dione (compound 1b)[2]

200 mg of 4-chloro-1,8-naphtalic anhydride (0.860 mmol, 1 eq) were added to 7 mL of ethanol and the resulting mixture was heated up under magnetic stirring; at 55 °C 64 µL of allyl amine (49 mg, d = 0.761 gmL^{-1}, 0.853 mmol, 1 eq) were added. The mixture was

refluxed for four hours and the reaction was monitored by TLC using a 1:1 dichloromethane:ethyl acetate mixture as mobile phase. After cooling to room temperature, the solid was filtered, washed with cold ethanol and dried under vacuum. 142 mg (yield 61%) of light brown powder were obtained. *^{1}H-NMR* (δ, ppm, 500 MHz, $CDCl_3$): 4.80 (d, 2H, ^{3}J= 6 Hz), 5.22 (dd, 1H, $^{3}J_{cis}$= 10 Hz, ^{2}J= 1 Hz), 5.32 (dd, 1H, $^{3}J_{trans}$= 17 Hz ^{2}J= 1 Hz,), 5.99 (m, 1H), 7.83 (d, 1H, $^{3}J_{ortho}$= 8 Hz), 7.86 (t, 1H, $^{3}J_{ortho}$= 7.8 Hz), 8.51 (d, 1H, $^{3}J_{ortho}$= 8 Hz), 8.61 (dd, 1H, $^{3}J_{ortho}$= 8.5 Hz, $^{4}J_{meta}$= 1 Hz), 8.67 (dd, 1H, $^{3}J_{ortho}$= 7 Hz, $^{4}J_{meta}$= 1 Hz) *^{13}C-NMR* (δ, ppm, 500 MHz, $CDCl_3$): 42.66, 117.95, 121.66, 123.17, 127.55, 128.02, 129.29 (2C), 129.52, 130.90, 131.40, 132.10, 132.29, 139.32, 163.35, 163.61 (2CO) *ESI-MS* (m/z): 272.3 and 274.3 $[M+H]^+$, 294.3 and 296.3 $[M+Na]^+$

2-allyl-6-((3-aminoethyl)amino)-1H-benzo[de]isoquinoline-1,3(2H)-dione (mon. 2)

– *"traditional" procedure*

To a mixture of 107 mg of **1b** (0.392 mmol, 1 eq) and 6 mL of ethanol, 50 µL of ethylene diamine (45 mg, d= 0.90 gmL^{-1}, 0.748 mmol, 2 eq) were added; the mixture was refluxed for 24 hours and monitored by TLC, using 1:1 dichloromethane:ethyl acetate as mobile phase. As **1b** was not totally consumed after 24 hours, other 23 total equivalents (600 µL, 540 mg) were added over another day. After 51 hours of reflux, reaction was stopped, and solvent was removed from the resultant solution to obtain an orange oil. 5 mL of water were then added to the mixture and the solid was filtered under vacuum on a Gooch (porosity III), washed with cold water and dried at room temperature. 113 mg of orange powder were obtained (97% yield).

– *"microwave assisted" procedure*

Reaction of 200 mg of **1b** (0.736 mmol, 1 eq) and 1.5 mL of ethylenediamine (1.35 g, d= 0.90 gmL^{-1}, 22.5 mmol) was assisted by microwaves. The mixture was heated up to 85 °C for 2 hours and the reaction was monitored by TLC using a 1:1 dichloromethane:ethyl acetate mixture as mobile phase. Then 12 mL of water were added and the mixture was cooled overnight at 4 °C. The resulting solid was filtered under vacuum, washed with cold water and dried at 60 °C for two days. 199.7 mg of pure compound **2** were obtained as orange solid (92% yield).

^{1}H-NMR (δ, ppm, 500 MHz, DMSO-d_6): 2.87 (d, 2H, ^{3}J= 6.4 Hz), 3.38 (d, 2H, ^{3}J= 5.2 Hz), 5.07 (dd, 2H, ^{3}J= 6.1 Hz, ^{2}J= 1.3 Hz), 5.10 (s, 1H), 5.92 (m, 1H), 6.82 (d, 1H, $^{3}J_{ortho}$= 8.5 Hz), 7.69 (t, 1H, $^{3}J_{ortho}$= 7.8 Hz), 8.26 (d, 1H, $^{3}J_{ortho}$= 8.5 Hz), 8.43 (d, 1H, $^{3}J_{ortho}$= 7.3 Hz), 8.72 (d, 1H, $^{3}J_{ortho}$= 8.4 Hz) *^{1}H-NMR* (δ, ppm, 500 MHz, $CDCl_3$): 3.18 (s, 2H), 3.41 (d, 2H, ^{3}J= 4 Hz), 4.79 (d, 2H, ^{3}J= 4Hz), 5.18 (d, 1H, $^{3}J_{cis}$= 10 Hz), 5.29 (d, 1H, $^{3}J_{trans}$= 17 Hz), 6.00 (m, 1H), 6.19 (bbd, 1H), 6.705 (d, 1H, $^{3}J_{ortho}$= 8.4 Hz), 7.62 (t, 1H, $^{3}J_{ortho}$= 7.6 Hz), 8.18 (d, 1H,

$^{3}J_{ortho}$= 8.3 Hz), 8.46 (d, 1H, $^{3}J_{ortho}$= 8.2 Hz), 8.59 (d, 1H, $^{3}J_{ortho}$= 7.1 Hz) *^{13}C-NMR* (δ, ppm, 500 MHz, $CDCl_3$): 40.30, 42.31, 44.99, 104.62, 110.29, 117.12, 120.65, 123.16, 124.85, 126.49, 130.06, 131.42, 132.87, 134.81, 149.93, 164.03, 164.61 (2CO) *ESI-MS* (m/z): 296.4 $[M+H]^+$

2-allyl-6-((5-aminopentyl)amino)-1H-benzo[de]isoquinoline-1,3(2H)-dione (mon. 3)

300 mg of **1b** (1.00 mmol) and 670 µL of 1,5-diaminopentane (585 mg, d=0.873 gmL^{-1}, 5.72 mmol) were dissolved in 30 mL of ethanol. The mixture was refluxed for 24 hours. To monitor the reaction, TLC was performed using 1:1 dichlorometane:ethyl acetate as mobile phase. 2 equivalents of 1,5-diaminopentane (234 µL, 204 mg, 2.00 mmol) were added after 24 hours and other 3 equivalents (351 µL, 306 mg, 3 mmol) after 48 hours; the reaction was completed after 96 hours. The solvent was removed under reduced pressure to obtain an orange oil. 35 mL of water were added and an orange solid was left to precipitate for one night at 4 °C. The solid was filtered on a Gooch (porosity III), washed with cold water and dried at 60 °C overnight. 342 mg of a yellow solid (**3**) was obtained (yield 92%). *^{1}H-NMR* (δ, ppm, 500 MHz, DMSO-d_6): 1.41 (m, 4H), 1.70 (t, 2H, ^{3}J= 6.6 Hz), 2.54 (t, 2H, ^{3}J= 6.0 Hz), 3.36 (s, 2H), 4.61 (d, 2H, ^{3}J= 5 Hz), 5.065 (d, 1H, ^{3}J= 4.3 Hz), 5.09 (s, 1H,), 5.915 (m, 1H), 6.76 (d, 1H, ^{3}J= 8.6 Hz), 7.67 (t, 1H, ^{3}J= 7.8 Hz), 7.77 (bbd, 1H), 8.25 (d, 1H, ^{3}J= 8.5 Hz), 8.42 (d, 1H, ^{3}J= 7.3 Hz), 8.71 (d, 1H, ^{3}J= 8.4 Hz) *^{13}C-NMR* (δ, ppm, 500 MHz, DMSO-d_6): 24.08, 27.79, 33.11, 41.29, 41.62, 42.93, 103.79, 107.27, 115.95, 121.74, 120.14 (2C), 124.22, 128.72, 129.53 (3C), 130.73, 133.31, 134.39, 150.79, 162.58 (CO), 163.47 (CO) *ESI-MS* (m/z): 338.5 ($[M+H]^+$)

2-allyl-6-((2-hydroxyethyl)amino)-1H-benzo[de]isoquinoline-1,3(2H)-dione (mon. 4)

271 mg of **1b** (1.00 mmol, 1 eq) were mixed with 600 µL of 2-aminoethanol (607 mg, d=1.012 g/mL, 9.94 mmol, 9 eq) in 15 mL of ethanol. The mixture was refluxed for 24 hours and the reaction monitored with TLC using 1:1 dichloromethane:ethyl acetate as mobile phase. Other 8 equivalents of 2-aminoethanol (485 µL, 489 mg) were added after 24 hours, 12 equivalents after 48 hours and 6 equivalents (363 µL, 366 mg) after 72 hours. The reaction was stopped when **1b** was totally consumed, after 96 hours of refluxing. The solvent was removed under reduced pressure and an orange oil was obtained. 20 mL of water were added to precipitate an orange solid, that was filtered on Gooch III, washed with cold water and dried at 60 °C for one night. 293 mg of **4** as orange solid were obtained (yield 99%). *^{1}H-NMR* (δ, ppm, 500 MHz, CD_3OD): 3.60 (t, 2H, ^{3}J= 5.7 Hz), 3.88 (t, 2H, ^{3}J= 5.7 Hz), 4.72 (d, 2H, ^{3}J= 6.5 Hz), 5,13 (d, 1H, $^{3}J_{cis}$= 10.3 Hz), 5.19 (d, 1H, $^{2}J_{trans}$= 17.2 Hz), 5.96 (m, 1H), 6.83 (d, 1H, ^{3}J= 8.5 Hz), 7.64 (t, 1H, ^{3}J= 8.4 Hz),

8.34 (d, 1H, ^{3}J= 8.5 Hz), 8.49 (d, 1H, ^{3}J= 7.3 Hz), 8.52 (d, 1H, ^{3}J= 8.4 Hz) *^{13}C-NMR* (δ, ppm, 500 MHz, CD_3OD): 42.99, 60.82, 62.91, 105.22, 109.48, 117.07, 121.96, 123.36, 125.56, 129.41, 131.32, 132.31, 134.00, 136.00, 152.80, 165.39 (CO), 165.92 (CO). *ESI-MS* (m/z): 297.1 $[M+H]^+$, 319.1 $[M+Na]^+$, 295.1 $[M-H]^-$.

2-allyl-6-(ethylamino)-1H-benzo[de]isoquinoline-1,3(2H)-dione (mon. 5)

150 mg of **1b** (0.552 mmol) and 1.85 mL (excess) were stirred under microwave at 85 °C for 4 hours; reaction was monitored by TLC, using an eluent mixture of 4:1 ethylacetate:dichlorometane. After cooling to room temperature, 20 mL of water where added to the orange solution obtained; the precipitated solid was filtered under vacuum, washed with cold water and dried at room temperature. 127 mg of orange powder (monomer **5**, 82% yield) were obtained. *^{1}H-NMR* (δ, ppm, 500 MHz, DMSO-d_6): 1.31 (t, 3H, ^{3}J= 7.2 Hz), 3.42 (quint., 2H, ^{3}J= 7.2 Hz), 4.62 (d, 2H, ^{3}J= 5.2 Hz), 5.07 (m, 1H), 5.10 (m, 1H), 5.93 (m, 1H), 6.77 (d, 1H, ^{3}J= 8.5 Hz), 7.68 (t, 1H, ^{3}J= 8.4 Hz), 7.76 (t, 1H, ^{3}J= 5.2 Hz), 8.27 (d, 1H, ^{3}J= 8.5 Hz), 8.43 (d, 1H, ^{3}J= 7.3 Hz), 8.71 (d, 1H, ^{3}J= 8.4 Hz) *^{13}C-NMR* (δ, ppm, 500 MHz, DMSO-d_6): 13.67, 37.50, 41.28, 103.77, 107.37, 115.95, 120.13, 121.74, 124.22, 128.72, 129.50, 130.72, 133.29, 134.39, 150.63, 162.58, 163.46 *ESI-MS* (m/z): 281.1 $[M+H]^+$, 303.1 $[M+Na]^+$, 279.0 $[M-H]^-$.

2-allyl-6-((3-succinimidoil-aminoethyl)amino)-1H-benzo[de]isoquinoline-1,3(2H)-dione (mon. 6)

A mixture of 50 mg of **2** (0.169 mmol, 1 eq) and 480 µL of triethylamine (348 mg, d= 0.725 gmL^{-1}, 3.44 mmol) in 20 mL of anhydrous THF was stirred at room temperature for 15 minutes. When compound **2** was totally dissolved, 20 mg of succinic anhydride (0.370 mmol, 2.2 eq) were added. The mixture was stirred at room temperature under argon atmosphere for 30 minutes, and under ambient conditions for 3 hours and 30 minutes, monitoring the reaction by TLC, using 1:1 dichloromethane: ethyl acetate as mobile phase. 10 mL of water were then added to the mixture and the pH was brought to 1-2 with 37% HCl to precipitate an orange solid. The mixture was poured in ice bath for 30 minutes and the solid was filtered on Gooch (porosity III), washed with cold water and dried at room temperature. 49 mg of an orange solid were obtained (yield 73%). *^{1}H-NMR* (δ, ppm, 500 MHz, DMSO-d_6): 2.34 (t, 2H, ^{3}J= 6.7 Hz), 2.45 (t, 2H, ^{3}J= 6.7 Hz), 3.39 (q, 2H, ^{3}J= 6.0 Hz), 3.44 (q, 2H, ^{3}J= 5.7 Hz), 4.62 (d, 2H, ^{3}J= 5.2 Hz), 5.07 (m, 1H), 5.10 (m, 1H), 5.92 (m, 1H), 6.85 (d, 1H, ^{3}J= 8.5 Hz), 7,71 (t, 1H, ^{3}J= 8.4 Hz), 7.85 (t, 1H, ^{3}J= 5.2 Hz), 8.16 (t, 1H, ^{3}J= 5.6 Hz), 8.29 (d, 1H, ^{3}J= 8.5 Hz), 8.44 (dd, 1H, ^{4}J= 0.91 Hz, ^{3}J= 7.3 Hz), 8.62 (d, 1H, ^{3}J= 8.4 Hz), 12.06 (s, 1H) *^{13}C-NMR* (δ, ppm, 500 MHz, DMSO-d_6):

29.12, 30.06, 37.45, 41.33, 42.73, 103.77, 107.71, 115.98, 120.18, 121.81, 124.45, 128.57, 129.49, 130.83, 133.28, 134.33, 150.71, 162.60, 163.47, 171.93, 173.84 *ESI-MS* (m/z): 396.2 $[M+H]^+$, 418.1 $[M+Na]^+$, 393.9 $[M-H]^-$.

N-(tert-Butoxycarbonyl)-1,2-diaminoethane

6.13 mL of ethylenediamine (5.51 g, d= 0.899 gmL^{-1}, 91.7 mmol, 9 eq) were dissolved in 90 mL of chloroform; the solution was cooled to 0 °C, under stirring. Small aliquots of a cold solution of di-tert-butyl dicarbonate in chloroform (2.11 g, 9.67 mmol, 1 eq, in 40 mL of $CHCl_3$) were added to the mixture, avoiding to exceed 2-3 °C. The reaction mixture was then left stirring at room temperature for 12 hours. The mixture was finally washed with Brine (6x20 mL), water (1x20 mL), and then dried on anhydrous sodium sulfate; the solvent was removed under reduced pressure to get a colourless oil (1.57, yield 93%). *^{1}H-NMR* (δ, ppm, 500 MHz, $CDCl_3$): 1.23 (bbd, 2H), 1.44 (s, 9H), 2.79 (t, 2H, ^{3}J= 5.7 Hz), 3.17 (q, 2H, ^{3}J= 5.9 Hz), 4.85 (bbd, 1H) *^{13}C-NMR* (δ, ppm, 500 MHz, $CDCl_3$): 20.56 (3C), 31.39 (1C), 42.05 (1C), 43.58 (1C), 146.49 (C=O) *ESI-MS* (m/z): 161.1 $[M+H]^+$, 183.0 $[M+Na]^+$.

Tert-butyl (2-(6-chloro-1,3-dioxo-1H-benzo[de]isoquinolin-2(3H)-yl)ethyl)carbamate (compound 7)

A mixture of 1.01 g of **1b** (4.34 mmol, 1 eq) and 696 mg (4.34 mmol, 1 eq) of N-(tert-Butoxycarbonyl)-1,2-diaminoethane was refluxed in 50 mL of ethanol for 12 hours. After cooling to room temperature, the mixture was put in an ice-bath and precipitation occurred; a beige solid was filtered on Gooch (porosity III), washed with cold ethanol and dried at 60 °C for a night. 838 mg of compound **7** were obtained (yield 51%).

^{1}H-NMR (δ, ppm, 500 MHz, DMSO-d_6): 1.20 (s, 9H), 3.26 (q, 2H, ^{3}J= 5.9 Hz), 4.12 (t, 2H, J= 5.7 Hz), 6.80 (t, 1H, ^{3}J= 6.2 Hz), 8.00 (t, 1H, ^{3}J= 8.2 Hz), 8.03 (d, 1H, ^{3}J= 7.9 Hz), 8.42 (d, 1H, ^{3}J= 7.9 Hz), 8.57 (d, 1H, ^{3}J= 7.3 Hz), 8.59 (d, 1H, ^{3}J= 8.6 Hz) *^{13}C-NMR* (δ, ppm, 500 MHz, DMSO-d_6): 28.02 (3C), 37.62, 39.92, 77.43, 121.80, 123.08, 127.62, 128.42, 128.56, 129.82, 130.68, 131.61, 137.18, 155.74, 162.92 (CO), 163.20 (CO) *ESI-MS* (m/z): 397.1 $[M+Na]^+$, 413.0 $[M+K]^+$.

Tert-butyl (2-(6-((2-aminoethyl)amino)-1,3-dioxo-1H-benzo[de]isoquinolin-2(3H)-yl)ethyl)carbamate (compound 8)

A mixture of 200 mg of **7** (0.533 mmol) and 2 mL of ethylenediamine (1.8 g, 30.0 mmol) was stirred at 85 °C under microwaves for three hours. 15 mL of water were then added to the mixture and the solid was left to precipitate at 4 °C for a night. The precipitate was filtered under vacuum, washed with cold water and dried at room temperature. 198 mg of an orange solid were obtained (yield 93%). ^{1}*H-NMR* (δ, ppm, 500 MHz, DMSO-d_6): 1.26 (s, 9H), 2.89 (t, 2H, ^{3}J= 6.4 Hz), 3.21 (q, 2H, ^{3}J= 6.4 Hz), 3.39 (t, 2H, ^{3}J= 6 Hz), 6.78 (d, 1H, ^{3}J= 6.4 Hz), 6.83 (t, 1H, ^{3}J= 6 Hz), 7.66 (t, 1H, ^{3}J= 8.0 Hz), 8.23 (d, 1H, ^{3}J= 8.5 Hz), 8.39 (d, 1H, ^{3}J= 7.2 Hz), 8.69 (d, 1H, ^{3}J= 8.3 Hz) ^{13}*C-NMR* (δ, ppm, 500 MHz, DMSO-d_6): 28.13 (3C), 38.03, 39.08, 39.71, 46.09, 77.38, 103.70, 107.91, 120.09, 122.06, 124.09, 128.42, 129.52, 130.46, 134.03, 150.64, 155.63, 163.08 (CO), 163.94 (CO) *ESI-MS* (m/z): 399.2 $[M+H]^+$, 421.2 $[M+Na]^+$, 397.1 $[M-H]^-$, 433.0 $[M+Cl]^-$

Tert-butyl (2-(6-((2-acrylamidoethyl)amino)-1,3-dioxo-1H-benzo[de]isoquinolin-2(3H)-yl)ethyl)carbamate (compound 9)

100 mg of **8** (0.251 mmol, 1 eq) and 105 µL of triethylamine (76 mg, d= 0.728 gmL^{-1}, 0.755 mmol, 3 eq) were dissolved in 10 mL of anhydrous dichloromethane under stirring for 30 minutes at room temperature, under argon atmosphere. The mixture was then cooled to 0 °C and small aliquots of 2 mL solution of acryloyl chloride (24 µL, 27 mg, d= 1.114 gmL^{-1}, 1.2 eq) in anhydrous dichlorometane were added, drop by drop, avoiding to exceed 5 °C. The mixture was then stirred for one hour under argon atmosphere and 12 hours at ambient conditions. 5 mL of dichloromethane and 15 mL of water were then added to the mixture, and organic phase was extracted with dichloromethane (2x15 mL), washed with brine (45 mL) and dried on anhydrous sodium sulfate; solvent was removed under reduced pressure to give 84.1 mg of an orange solid (yield 75%). ^{1}*H-NMR* (δ, ppm, 500 MHz, DMSO-d_6): 1.25 (s, 9H), 3.22 (q, 2H, ^{3}J= 6.1 Hz), 3.48 (q, 4H, ^{3}J= 6.2 Hz), 4.09 (t, 2H, ^{3}J= 6.0 Hz), 5.62 (dd, 1H, $^{3}J_{cis}$= 10.0 Hz, ^{2}J= 2.2 Hz), 6.13 (dd, 1H, $^{3}J_{trans}$= 17.1 Hz, ^{2}J= 2.2 Hz), 6.23 (dd, 1H, $^{3}J_{trans}$= 17.0 Hz, $^{3}J_{cis}$= 10.1 Hz), 6.84 (t, 1H, ^{3}J= 5.3 Hz), 6.86 (d, 1H, ^{3}J= 8.7 Hz), 7.69 (t, 1H, ^{3}J= 7.5 Hz), 7.84 (bbd, 1H), 8.25 (d, 1H, ^{3}J= 8.5 Hz), 8.40 (bbd, 1H), 8.43 (d, 1H, ^{3}J= 7.5 Hz), 8.61 (d, 1H, ^{3}J= 8.5 Hz) ^{13}*C-NMR* (δ, ppm, 500 MHz, DMSO-d_6): 28.13, 37.42, 38.03, 39.31, 42.58, 77.39, 103.61, 108.25, 120.12, 122.18, 124.32, 125.45, 128.22, 129.54, 130.56, 131.59, 134.01, 150.35, 155.65, 163.11, 163.95, 165.37 *ESI-MS* (m/z): 453.2 $[M+H]^+$, 475.2 $[M+Na]^+$, 451.2 $[M-H]^-$, 487.1 $[M+Cl]^-$

N-(2-((2-(2-aminoethyl)-1,3-dioxo-2,3-dihydro-1H-benzo[de]isoquinolin-6 yl)amino)ethyl) acrylamide (monomer 10)

10 mL of dichloromethane were added to 83.5 mg of compound **9** (0.184 mmol, 1 eq) and the mixture was stirred at room temperature for 20 minutes; 800 µL of trifluoroacetic acid (1.19 g, d= 1.489 gmL^{-1}, 10.4 mmol, excess) were then added, and mixture was stirred for two hours at room temperature. Solvent and residual TFA were removed under reduced pressure and washings with diethyl ether (x5) were performed to favour TFA evaporation. The red solid obtained was dissolved in 10 mL of 1 M KOH (pH 10); the product was extracted from aqueous phase with ethyl acetate (6x10 mL), and dried on sodium sulfate anhydrous. Solvent was removed under reduced pressure to get 41.4 mg of an orange powder (yield 63%). *^{1}H-NMR* (δ, ppm, 500 MHz, DMSO-d_6): 3.12 (m, 2H), 3.49 (quint., 4H, ^{3}J= 4.9 Hz), 4.28 (t, 2H, ^{3}J= 6 Hz), 5.63 (dd, 1H, $^{3}J_{cis}$= 10.0 Hz, ^{2}J= 2.2 Hz), 6.13 (dd, 1H, $^{3}J_{trans}$= 17.1 Hz, ^{2}J= 2.2 Hz), 6.23 (dd, 1H, $^{3}J_{trans}$= 17.1 Hz, $^{3}J_{cis}$= 10.0 Hz), 6.90 (d, 1H, ^{3}J= 8.7 Hz), 7.73 (t, 1H, ^{3}J= 8.3 Hz), 7.78 (bbd, 2H), 7.95 (t, 1H, ^{3}J= 5.2 Hz), 8.29 (d, 1H, ^{3}J= 8.5 Hz), 8.42 (t, 1H, ^{3}J= 5.2 Hz), 8.44 (d, 1H, ^{3}J= 7.3 Hz), 8.66 (d, 1H, ^{3}J= 8.5 Hz) *^{13}C-NMR* (δ, ppm, 500 MHz, DMSO-d_6): 37.20, 37.41, 37.89, 42.62, 103.75, 107.94, 120.14, 122.08, 124.44, 125.51, 128.58, 129.67, 130.77, 131.56, 134.27, 150.71, 163.44, 164.44, 165.41 *ESI-MS* (m/z): 353.1 $[M+H]^{+}$

6.3 Fluorescent MIPs for irinotecan

Irinotecan-hydrochloride ^{1}H-NMR characterization

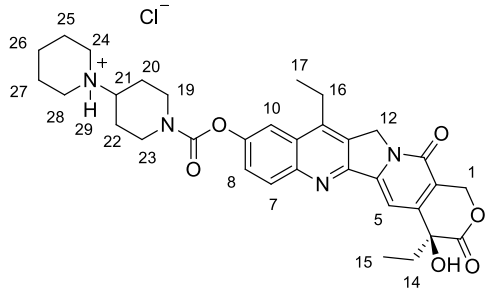

^{1}H-NMR (δ, ppm, 500 MHz, DMSO-d_6): 0.88 (t, 3H, ^{3}J= 7.4 Hz, H15), 1.30 (t, 3H, ^{3}J= 7.7 Hz, *H17*), 1.44 (m, 1H, *H26ax*), 1.73 (d, 2H, ^{2}J= 12.3 Hz, *H26eq*, *H20ax*), 1.84 (m, 7H, *H25*, *H27*, *H22ax*, *H14*), 2.16 (m, 2H, *H20eq*, *H22eq*), 2.97 (m, 3H, *H19ax*, *H24ax*, *H28ax*), 3.13 (m, 1H, *H23ax*), 3.19 (q, 2H, ^{3}J= 7.8 Hz, *H16*), 3.42 (d, 2H, ^{2}J= 12.2 Hz,

H24eq, *H28eq*), 3.48 (m, 1H, *H21*), 4.21 (d, 1H, ^{2}J= 12.4 Hz, *H23eq*), 4.41 (d, 1H, ^{2}J= 11.7 Hz, *H19eq*), 5.35 (s, 2H, *H12*), 5.44 (s, 2H, *H1*), 6.52 (s, 1H, *OH*), 7.32 (s, 1H, *H5*), 7.68 (dd, 1H, $^{3}J_{ortho}$= 9.1 Hz, $^{3}J_{meta}$= 2.5 Hz, *H8*), 7.99 (d, 1H, $^{4}J_{meta}$= 2.5 Hz, *H10*), 8.19 (d, 1H, $^{3}J_{ortho}$= 9.1 Hz, *H7*), 9.88 (bbd, 1H, NH^{+})

^{1}H-NMR titrations

To investigate on interactions between template and functional monomers, ^{1}H-NMR titrations of 4 mM irinotecan (2.0 mg, 3 µmol, in 750 µL) with increasing amounts of functional monomers **2**, **3**, **5**, **6, 11** and **10** (from 2 mM to 40 mM, except for monomer 10 added from 1 mM to 10 mM) were performed in DMSO-d_6. An ^{1}H-NMR spectrum (64 scans, 500 MHz) was recorded after every adding.

Synthesis of MIPs

1 eq of each functional monomer (2eq for the fourth set of MIPs) and 1.2 eq of irinotecan (1 eq for the fourth set of MIPs) were dissolved in 2 mL of DMSO. The solution was stirred for one hour at room temperature; eventual co-monomer, cross-linker and recrystallized radical initiator (AIBN) were dissolved in a certain volume of DMSO and added to the pre-polymerization complex, in order to reach a total volume of DMSO corresponding to the 99% in weight (99.9% for only *MIP P*) of the total amount of monomers and cross-linker employed, as C_m was fixed at 1% in weight (0.1% for only *MIP P*). The mixture was then poured in a Wheaton® glass bottle and argon was bubbled inside it, in order to remove all the oxygen; the bottle was tight closed and two cycles of vacuum-Argon flushing were carried out. The mixture was finally kept at 70 °C for at least 24 hours (except for MIP Q prepared by photo-activation, under UV irradiation for 6 hours). For some MIPs, the corresponding NIPs were prepared, following the same procedure, except for the adding of template. At the end of polymerization, a viscous clear solution was obtained and transferred in a dialysis tube; dialysis was performed against water for one day (changing the solvent at least 3 times per day), against 7:3 mixture of methanol:acetic acid for two days (changing the mixture once per day), and against water for two days (changing the solvent three times per day). The polymers suspensions in water were freeze-dried to get a thin powder or fluffy material.

Some polymers were further washed, as they contained a significant amount of irinotecan entrapped in the matrix, by adding 1 mL of methanol to 1 or 2 mg of polymer; after vortex stirring and centrifugation at 15000 rpm for ten minutes, the supernatant was removed. This washing process was repeated until the template was

not anymore detected in the supernatant, under UV lamp. Once irinotecan was removed, a washing step in water was performed and polymers were finally suspended in water, left under magnetic stirring for one night and freeze-dried.

The amounts of each reagent employed for MIPs synthesis and final yields are reported in **Table 6.1** and related NIPs in **Table 6.2**.

MIP	Irinotecan [mg]	Funct. mon. [mg]	Co-monomer [mg]	Cross-linker [mg]	AIBN [mg]	DMSO [mL]	Yield [mg]
A	41.0	**2** 10.0	MAA 6.1	EGDMA 46.2	17.0	5.61	57
B	41.0	**2** 15.0	MAA 12.2	EGDMA 59.5	4.2	7.88	40.5
C	41.0	**2** 30.0	MAA 5.7	MBA 25.6	4.0	5.52	38.5
D	41.0	**2** 15	MAA 4.3	EGDMA 46	17	5.92	48
E	41	**2** 15.0	AA 3.5	EGDMA 46.2	17.0	5.87	35
F	41	**2** 15.0	NIPAM 5.7	EGDMA 46.2	17.0	6.06	46
G	41	**2** 15.0	AA 3.5	EGDMA 46.2	17.0	5.85	34
H	41.0	**2** 15.0	AA 3.6	MBA 36.3	17.0	4.96	41
I	41.0	**5** 14.0	MAA 4.3	EGDMA 46.2	17.0	5.85	50.5
J	41.0	**6** 20.0	NIPAM 5.7	EGDMA 46.2	17.0	6.52	51
K	41.0	**10** 23.0	NIPAM 11.4	MBA 26.0	4.1	5.46	42
L	41.0	**2** 30.0	-	EGDMA 46.2	17.0	6.89	58
M	41.0	**2** 30	-	EGDMA 46	17.0	6.89	40
N	41.0	**2** 30	-	EGDMA 46	4.7	6.89	46.5
O	41.0	**2** 30.0	-	EGDMA 46.2	9.4	6.93	50
P	20.5	**2** 15.0	-	EGDMA 23.3	8.5	34.95	13
L-UV	41.0	**2** 30.0	-	EGDMA 46.2	17.0	6.89	48

Table 6.1: Amount of template, functional monomer, co-monomer, AIBN and DMSO used for each MIP synthesis and corresponding yield in milligrams.

NIP	Funct. mon. [mg]	Co-monomer [mg]	Cross-linker [mg]	AIBN [mg]	DMSO [mL]	Yield [mg]
A	**2** 10.0	MAA 6.1	EGDMA 46.2	17.0	5.61	65
B	**2** 15.0	MAA 12.2	EGDMA 59.5	4.2	7.88	35
C	**2** 30.0	MAA 5.7	MBA 25.6	4.0	5.52	49
D	**2** 15.0	MAA 4.3	EGDMA 46.2	17.0	5.92	37
E	**2** 15.0	AA 3.5	EGDMA 46.2	17.0	5.87	27
F	**2** 15.0	NIPAM 5.7	EGDMA 46.2	17.0	6.06	33
I	**5** 14.0	MAA 4.3	EGDMA 46.2	17.0	5.85	50
J	**6** 20.0	NIPAM 5.7	EGDMA 46.2	17.0	6.52	48
K	**10** 23.0	NIPAM 11.4	MBA 26.0	4.1	5.46	34
L	**2** 30.0	-	EGDMA 46	17.0	6.89	32
M	**2** 30.0	-	EGDMA 46	17.0	6.89	40
O	**2** 30.0	-	EGDMA 46.2	9.4	6.93	50

Table 6.2: Amount of template, functional monomer, co-monomer, AIBN and DMSO used for each NIP synthesis and corresponding yield in milligrams.

Dynamic Laser Light Scattering (DLS)

For each MIP or NIP a 0.25 $mgmL^{-1}$ solution in DMSO was prepared, sonicated for 30 minutes and filtered on 0.45 µm PTFE filter; 1 mL of each polymer solution was then poured in a 3 mL quartz cuvette having 1 cm light path.

Transmission Electron Microscopy (TEM)

MIP L was suspended in distilled water (0.2 mgmL-1) and sonicated for 30 minutes. This solution was then diluted 40 times with distilled water and sonicated for 1 hour. A drop of this solution was then placed on an amorphous carbon coated grid and left it to dryness at room temperature for one night; TEM images of the MIP L were finally recorded.

UV-Visible measurements

Calibration curves of monomer **2**, **5**, **6** and **10** were performed in DMSO in order to calculate monomers concentration inside polymers matrix, using Lambert-Beer Law. The following DMSO solutions were prepared for monomers **2**, **5** and **6**: 5, 10, 20, 30, 40, 50 and 60 µM; while for monomer **10** the DMSO concentrations were 50, 70, 100, 250 and 375 µM.

The following list reports the values of molar extinction coefficient obtained for each monomer, measured at 25 °C in DMSO:

- 12504 $Lmol^{-1}cm^{-1}$ at 442 nm (monomer **2**);
- 19197 $Lmol^{-1}cm^{-1}$ at 444 nm (monomer **5**);
- 21815 $Lmol^{-1}cm^{-1}$ at 442 nm (monomer **6**);
- 1423 $Lmol^{-1}cm^{-1}$ at 444 nm (monomer **10**).

For each *MIP* and *NIP* 0.3 and 0.6 $mgmL^{-1}$ solutions in DMSO were prepared, by dilution of 1 $mgmL^{-1}$ mother solution, except for *MIP K* and *NIP K*, as 1 $mgmL^{-1}$ mother solution in DMSO was directly measured, after filtration on 0.45 µm PTFE filter, as even after sonication nanogels aggregated and more diluted solutions did not absorb light.

UV-Visible absorbance measurement of 500 µL of each nanogel DMSO solution was performed using 1 mL black quartz cuvette with 1 cm of light path.

HPLC rebinding assay

1 $mgmL^{-1}$ suspension of each polymer in 50 µM irinotecan aqueous solution was incubated for 24 hours at room temperature, under magnetic stirring. An aliquot (200 µL) of each suspension was taken after 10, 30, 60, 90, 180 and 1440 minutes of incubation; polymer was separated by unbound irinotecan by centrifugation at 15000 rpm for 10 minutes, and supernatant was analysed at HPLC. By subtraction of unbound irinotecan to initial irinotecan concentration it was possible to obtained the bound drug concentration and get the binding kinetic of each polymer. Because of their slightly solubility in water, *MIP H*, *MIP K* and *NIP K* suspensions were poured in dialysis tube to allow separation of polymers from unbound irinotecan solution. Aliquots of the solution outside the dialysis tube were directly analysed at HPLC, skipping the centrifugation step.

Isocratic elution was performed using a flux of 1 $mLmin^{-1}$, an eluent consisting of 75% of water with 0.05% TFA and 25% of acetonitrile with 0.05% TFA and absorbance wavelength at 363 nm.

Fluorescence measurements

Polymers binding capabilities were studied through fluorescence titrations with increasing amounts of irinotecan in various media. 400 µL of each polymer solution were poured in a quartz cuvette with light path of 0.5 cm; irinotecan solutions employed for titrations were prepared in the same media in which polymers were dissolved, and 2 µL of each solution were added to each polymer, with a maximum of 20 additions; irinotecan solutions in 3:1 methanol:water were kept in ice-bath while titrations were performed, to avoid its degradation. At least 5 minutes were waited after each drug addition, before fluorescence measurements. The specific conditions of the performed experiments are divided by sets of nanogels prepared.

- *First set of polymers*: 60 µgmL^{-1} solutions of *MIP C*, *MIP D* and *NIP D* in a 3:1 mixture of DMSO:water were obtained by diluting a 1 mgmL^{-1} mother solution of each nanogel in DMSO. Excitation and emission wavelength employed were 448 and 520 nm, respectively, using excitation slit of 5 nm and emission slit of 10 nm (except for *MIP C* that 5 nm slits were used for both excitation and emission wavelengths). 60 µgmL^{-1} *MIP D* solution in 3:1 methanol:water was also obtained by dilution of 1 mgmL^{-1} *MIP D* solution in DMSO, and excitation and emission wavelength employed were 448 and 525 nm, respectively, setting 5 and 10 nm of excitation and emission slits.

- *Second set of polymers*: 60 µgmL^{-1} solutions of *MIP E* and *NIP E* in DMSO and *MIP E* and *MIP F* in 3:1 methanol:water were prepared by diluting a mother solution 1 mgmL^{-1} of each nanogel, using the appropriate solvent. Fluorescence measurements of all polymers were performed using 448 and 520 nm of excitation and emission wavelengths, setting the slits at 5 and 10 nm, for excitation and emission beam, respectively.

- *Third set of polymers*: 60 µgmL^{-1} *MIP I* solution in 3:1 DMSO:water was prepared by diluting 1 mgmL^{-1} *MIP I* solution in DMSO; 448 and 525 nm were employed as excitation and emission wavelengths, respectively, setting the excitation and emission slits at 10 and 5 nm. 100 µgmL^{-1} *MIP J* DMSO solution was prepared by diluting a 1 mgmL^{-1} DMSO mother solution; 448 and 520 nm as excitation and emission wavelengths were employed, respectively, setting the slits at 5 and 2.5 nm. 20 µgmL^{-1} MIP K solution in 3:1 DMSO:water was obtained diluting its 1 mgmL^{-1} mother solution, using 445 and 530 nm as excitation and emission wavelengths and slits at 5 nm, for both excitation and emission beams.

- *Fourth set of polymers*: 60 μgmL^{-1} *MIPs L*, *M* and *O* in 3:1 methanol:water were prepared by dilution of 1 mgmL^{-1} DMSO solution of each nanogel; for all three titrations with irinotecan, 448 and 525 nm were employed as excitation and emission wavelengths, respectively, and slits were fixed at 5 nm for both beams. 30 μgmL^{-1} *MIP L* and *MIP O* solutions in 3:1 methanol:water were prepared as well by dilution of 1 mgmL^{-1} DMSO mother solutions; 448 and 525 nm were used as excitation and emission wavelengths, with slits at 5 and 10 nm, respectively.

6.5 Irinotecan MIPs investigations in human plasma

Plasma samples processing

Pooled plasma was processed using three different organic solvents: methanol, acetonitrile and DMSO. Methanol and acetonitrile produced the same effect: denaturation and precipitation of most of the proteins (mainly albumin), while DMSO unfolded proteins without precipitating them; however a precipitate was obtained also using DMSO, corresponding probably to anticoagulants.

- *Treatment with methanol/acetonitrile*: 3 volumes of solvent were added to 1 volume of plasma in a 2 mL centrifuge tube. After vortexing for 2 minutes, the mixture was centrifuged for ten minutes at 13000 rpm at 4 °C; supernatant was separated from precipitate and one or more centrifugation runs were performed again until supernatant resulted totally clear. Supernatant solutions were readily employed or stored at -80 °C.

- Treatment with DMSO: 3 volumes of solvent were added to 1 volume of plasma in a 2 mL centrifuge tube. After vortexing for 2 minutes, the mixture was centrifuged for ten minutes at 13000 rpm at 25 °C. Supernatant was separated from precipitate and one or more centrifugation runs were performed again until a clear solution was obtained. Supernatant solutions were readily employed or stored at -20 °C.

MIP L fluorescence titrations in processed plasma

400 μL of 60 μgmL^{-1} MIP L solution in 3:1 methanol: plasma or 3:1 acetonitrile:plasma or 3:1 DMSO:plasma (obtained by diluting 1 mgmL^{-1} DMSO nanogel mother solutions) were poured in a quartz cuvette with 0.5 cm of light path. 448 and 525 nm were set as

excitation and emission wavelength, respectively, using 5 nm of both beams slits (except for 3:1 DMSO:plasma, where 10 and 5 nm were used as excitation and emission slits, respectively). Irinotecan solutions were prepared in 3:1 solvent:water mixtures, depending if solvent used for plasma processing was methanol, DMSO or acetonitrile. While each titration was performed, the solutions of the anticancer drugs were kept in ice-bath, except for the ones prepared in 3:1 DMSO:water.

MIP L fluorescence titration in 3:1 acetonitrile:water

60 μgmL^{-1} *MIP L* solution in 3:1 acetonitrile:water was prepared by dilution of 1 $mgmL^{-1}$ *MIP L* mother solution in DMSO. Excitation and emission wavelengths used were 448 and 525 nm, respectively, setting both slits at 5 nm. Irinotecan solutions added were prepared in 3:1 acetonitrile:water.

6.6 Fluorescent MIPs for imatinib

Template preparation[3]

1-methyl-4-(4-((4-methyl-3-((4-(pyridin-3-yl)pyrimidin-2-yl)amino)phenyl)carbamoyl)benzyl)piperazin-1-ium chloride (Imatinib-HCl)

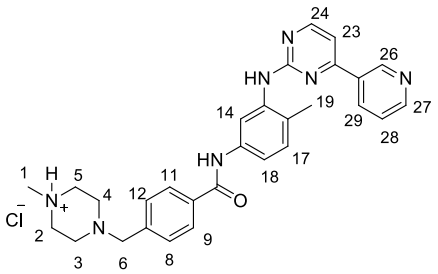

5 mL of ethanol were added to 810 mg of imatinib base (1.64 mmol); after stirring for ten minutes at room temperature, 136 µL of 37% HCl (163 mg, d=1.2 g/mL, 1.64 mmol) were added to the mixture, that was left to stir for other 20 minutes. The solvent was then removed under reduced pressure and the sticky solid obtained was recrystallized in a mixture of 1:1 ethanol:ethyl acetate, and also in isopropyl alcohol. The obtained yellow solid was filtered under vacuum and washed with diethyl ether to yield 541 mg of imatinib hydrochloride (62%). *^{1}H-NMR* (δ, ppm, 500 MHz, DMSO-d_6): 2.22 (s, 3H,

H19), 2.36 (bbd, 4H, *H3*, *H4*), 2.73 (s, 3H, *H1*), 2.88 (bbd, 2H, *H2ax*, *H5ax),* 3.01 (bbd, 2H, *H2eq*, *H5eq*), 3.63 (s, 2H, H6), 7.21 (d, 1H, ^{3}J= 8.2 Hz, H17), 7.425 (d, 1H, ^{3}J= 8.1 Hz, *H23*), 7.46 (dd, 2H, ^{3}J= 8.3 Hz, ^{4}J= 2.1 Hz, *H8*, *H12*), 7.48 (dd, 1H, ^{3}J= 8.5 Hz, ^{4}J= 2.1 Hz, *H18*), 7.52 (dd, 1H, ^{3}J= 8.0 Hz, ^{4}J= 4.8 Hz, *H28*), 7.95 (d, 2H, ^{3}J= 8.1 Hz, *H9, H11*), 8.08 (d, 1H, ^{4}J= 1.9 Hz, *H14*), 8.47 (dt, 1H, ^{3}J= 8.0 Hz, ^{4}J= 2.1 Hz, *H29*), 8.51 (d, 1H, ^{3}J= 5.1 Hz, *H24*), 8.68 (dd, 1H, ^{3}J= 4.8 Hz, ^{4}J= 1.6 Hz, *H27*), 8.98 (s, 1H, NH), 9.27 (d, 1H, ^{4}J= 2.2 Hz, H26), 9.82 (bbd, 1H, *NH*$^{+}$), 10.18 (s, 1H, *NHam*) *^{13}C-NMR* (δ, ppm, 500 MHz,DMSO-d_6): 17.65 (*C19*), 41.89 (*C1*), 52.76 (C3+C4), 60.50 (*C6*), 62.00 (C2+C5), 107.52 (*C23*), 116.77 (*C18*), 117.27 (*C14*), 119.27 (C_{quat}) 123.77 (*C28*), 127.69 (*C9+C11*), 128.76 (*C8+C12*), 130.02 (*C17*), 132.20 (C_{quat}), 134.40 (*C29*), 137.12 (C_{quat}), 137.79 (C_{quat}), 148.19 (*C26*), 151.37 (*C27*), 159.47 (*C24*), 161.17 (C_{quat}), 161.59 (C_{quat}), 163.05 (C_{quat}), 165.06 (*CO*)

Synthesis of N-acryloyl edans[4]

2,5-dioxopyrrolidin-1-yl acrylate (N-acryloxysuccinimide)

1.02 g of N-Hydroxysuccinimide (8.90 mmol, 1 eq) and 1.24 mL of triethylamine (900 mg, d= 0.728 gmL^{-1}, 8.90 mmol, 1 eq) were mixed in 10 mL of anhydrous dichlorometane under argon atmosphere; the mixture was cooled to 0 °C and 3 mL of a solution of acryloyl chloride in anhydrous dichloromethane (0.75 mL, d= 1.11 gmL^{-1}, 835 mg, 1 eq) was added drop by drop over about 30 minutes, avoiding to exceed 5 °C. The reaction mixture was then stirred for 20 minutes at 0 °C and for one hour at room temperature, always under argon flux. The mixture was filtered and washed with cold water (2x8 mL) and cold Brine (2x8 mL) and dried on sodium sulfate anhydrous. Solvent was not completely removed under reduced pressure, in order to get about 1 mL of organic phase. 3 mL of a solution of 6:1 hexane:ethyl acetate were added to the mixture, that was then stirred at 0 °C for 20 minutes. The obtained solid was filtered and washed with cold hexane. 690 mg of a white powder were obtained with 46% yield. *^{1}H-NMR* (δ, ppm, 500 MHz, $CDCl_3$): 2.86 (s, 4H), 6.17 (dd, 1H, $^{3}J_{cis}$= 10.5 Hz, ^{2}J= 0.5 Hz), 6.32 (dd, 1H, $^{3}J_{trans}$= 17 Hz, $^{3}J_{cis}$= 11 Hz), 6.70 (dd, 1H, $^{3}J_{trans}$= 17 Hz, ^{2}J= 0.5 Hz) *^{13}C-NMR* (δ, ppm, 500 MHz, $CDCl_3$): 25.76 (2C), 123.10, 136.33, 161.18 (CO), 169.16 (2CO) *ESI-MS* (m/z): 192 [M+Na]$^{+}$

5-((2-acryloylaminoethyl)amino)naphthalene-1-sulfonic acid (12, N-acryloyl EDANS)

A mixture of 199 mg of EDANS (0.75 mmol, 1eq), 1.79 g of sodium bicarbonate (1.79 g, 21.3 mmol) and 152 mg of N-acryloxysuccinimide (0.90 mmol, 1 eq) in 150 mL of water was stirred for 24 hours at room temperature. 200 mL of acetone were added to the mixture to precipitate most of sodium bicarbonate salt; after filtration under vacuum,

solvents were removed under reduced pressure and a dark brown sticky solid was obtained. The product was purified by gravity chromatography using 6:4 dichloromethane:methanol as mobile phase; 206.4 mg of pure **12** as brown powder were obtained (86%). *^{1}H-NMR* (δ, ppm, 500 MHz, DMSO-d_6) 3.22 (t, 2H, ^{3}J= 6 Hz), 3.49 (t, ^{3}J= 6 Hz, 2H), 5.60 (dd, 1H, $^{3}J_{cis}$= 10 Hz, ^{2}J= 2 Hz), 6.13 (dd, 1H, $^{3}J_{trans}$= 17 Hz, ^{2}J= 2 Hz), 6.20 (t, 1H, ^{3}J= 5 Hz), 6.25 (dd, 1H, $^{3}J_{trans}$= 17 Hz, $^{3}J_{cis}$= 10 Hz), 6.56 (d, 1H, ^{3}J= 8 Hz), 7.25 (dd, 1H, ^{3}J= 8 Hz), 7.31 (dd, 1H, ^{3}J= 7 Hz, ^{3}J= 8 Hz), 7.91 (d, 1H, ^{3}J= 6 Hz), 8.09 (d, 1H, ^{3}J= 8 Hz), 8.10 (d, 1H, ^{3}J= 8 Hz), 8.45 (t, 1H, ^{3}J= 5 Hz) *^{13}C-NMR* (δ, ppm, 500 MHz, DMSO-d_6): 38.12, 43.51, 102.40, 115.66, 122.10, 122.60, 124.14, 125.18, 126.03, 129.41, 131.6, 131.76, 135.09, 164.79 (CO) *ESI-MS* (m/z): 319.0 $[M-H]^-$

^{1}H-NMR titrations

^{1}H-NMR titrations of 4 mM imatinib-HCl (2.0 mg, 3 μmol, in 750 μL) were performed in DMSO-d6 by adding increasing amounts of functional monomers **2**, **3**, **4**, **11** (fluorescein O-acrylate) and **12** (N-acryloyl EDANS). Compounds **2**, **3**, **4** and **11** were added from 2 to 40 mM, while **12** from 2 to 56 mM. After each addition an ^{1}H-NMR spectrum was recorded (64 scans, 500 MHz).

Synthesis of MIPs

1 eq of each functional monomer (2eq for only *MIP X*) and 1.2 eq of imatinib-HCl (1 eq for *MIP X*) were dissolved in 2 mL of DMSO. The solution was stirred for one hour at room temperature; eventual co-monomer, cross-linker and recrystallized radical initiator (AIBN) were dissolved in a certain volume of DMSO and added to the pre-polymerization complex, in order to reach a total volume of DMSO corresponding to the 99% in weight of the total amount of monomers and cross-linker employed, as C_m was fixed at 1% in weight. The mixture was then poured in a Wheaton® glass bottle and argon was bubbled inside it, in order to remove all the oxygen; the bottle was tight closed and two cycles of vacuum-Argon flushing were carried out. The mixture was finally kept at 70 °C for at least 24 hours (except for *MIPs* and *NIPs U-UV* and *W-UV*, prepared by photo-activation, under UV irradiation at 360 nm for 6 hours). For each MIP a corresponding NIPs was prepared, following the same procedure, except for the adding of template. At the end of polymerization, a viscous clear solution was obtained and transferred in a dialysis tube; dialysis was performed against water for one day (changing the solvent at least 3 times per day), against 7:3 mixture of methanol:acetic acid for two days (changing the mixture once per day), and against water for two days

(changing the solvent three times per day). The polymers suspensions in water were freeze-dried to get a thin powder or fluffy material.

The amounts of each reagent employed for MIPs synthesis and final yields are reported in **Table 6.3** and related NIPs in **Table 6.4**.

MIP	Imatinib [mg]	Funct. mon. [mg]	Co-monomer [mg]	Cross-linker [mg]	AIBN [mg]	DMSO [mL]	Yield [mg]
Q	30.0	**2** 15.0	allylamine 3.0	EGDMA 46.2	17.0	5.85	48
R	31.8	**4** 29.6	-	EGDMA 46.2	4.6	6.83	44
S	31.8	**11** 19.3	-	EGDMA 23.0	2.3	3.82	39
T	31.8	**11** 19.3	-	DVB 15.2	2.3	3.10	24
U	31.8	**11** 19.3	-	MBA 18.0	2.3	3.33	35
U-UV	31.8	**11** 19.3	-	MBA 18.0	2.3	3.33	16
V	31.8	**12** 16.0	-	EGDMA 23.2	2.3	3.12	35
W	31.8	**12** 16.0	-	MBA 18.0	2.3	3.06	36
W-UV	31.8	**12** 16.0	-	MBA 18.0	2.3	3.06	30
X	16.0	**12** 19.0	NIPAM 0.6	MBA 15.0	2.6	3.12	21

Table 6.3: Amount of template, functional monomer, co-monomer, AIBN and DMSO used for each MIP synthesis and corresponding yield in milligrams.

NIP	Funct. mon. [mg]	Co-monomer [mg]	Cross-linker [mg]	AIBN [mg]	DMSO [mL]	Yield [mg]
Q	**2** 15.0	allylamine 3.0	EGDMA 46.2	17.0	5.85	45
R	**4** 29.6	-	EGDMA 46.2	4.6	6.83	47
S	**11** 19.3	-	EGDMA 23.0	2.3	3.82	29
T	**11** 19.3	-	DVB 15.2	2.3	3.10	16
U	**11** 19.3	-	MBA 18.0	2.3	3.33	1.1
U-UV	**11** 19.3	-	MBA 18.0	2.3	3.33	35
V	**12** 16.0	-	EGDMA 23.2	2.3	3.12	36
W	**12** 16.0	-	MBA 18.0	2.3	3.06	1.7
W-UV	**12**	-	MBA			

	16.0		18.0	2.3	3.06	7.4
Z	**12**	NIPAM	MBA			
	19.0	0.6	15.0	2.6	3.12	7.3

Table 6.4: Amount of functional monomer, co-monomer, AIBN and DMSO used for each NIP synthesis and corresponding yield in milligrams.

Dynamic Laser Light Scattering (DLS)

For each MIP or NIP a 0.25 $mgmL^{-1}$ solution in DMSO was prepared, sonicated for 30 minutes and filtered on 0.45 µm PTFE filter; 1 mL of each polymer solution was then poured in a 3 mL quartz cuvette having 1 cm light path.

UV-Visible measurements

Calibration curves of monomer **2**, **4** and **EDANS** were performed in DMSO in order to calculate monomers concentration inside polymers matrix, using Lambert-Beer Law. The following DMSO solutions were prepared for monomers **2** and **4**: 10, 20, 30, 40, 50, 60 and 70 µM; while for **EDANS** the prepared solutions had concentrations of 5, 10, 15, 25, 30 and 50 µM.

The following list reports the values of molar extinction coefficient obtained for each monomer, measured at 25 °C in DMSO:

- 12504 $Lmol^{-1}cm^{-1}$ at 442 nm (monomer **2**);
- 15507 $Lml^{-1}cm^{-1}$ at 444 nm (monomer **4**);
- 10452 $Lmol^{-1}cm^{-1}$ at 341 nm (**EDANS**).

Calibration curve of **11** was, instead, obtained measuring different aqueous solutions in water at pH 7 and pH 9. All the solution were prepared by diluting a millimolar mother solution in DMSO, as the monomer is not soluble in water at that high concentration, while following dilutions in water to get concentration of micromolar order, were obtained without assisting to precipitation in water. Solutions of **11** in water at pH 7 analysed had the following concentrations: 5, 10, 15, 25, 30 and 50 µM, while working at pH 9 the solutions prepared were 1, 2, 4, 6, 8 and 10 µM, as fluorescein anion form showed higher absorbance.

The value of molar extinction coefficient obtained for 11 at pH 7 was 12750 $Lmol^{-1}cm^{-1}$ at 452 nm, while at pH 9 84374 $Lmol^{-1}cm^{-1}$ at 492 nm measured at 25 °C.

For *MIPs* and *NIPs Q* and *R* 300 and 600 μgmL^{-1} solutions in DMSO were prepared by diluting 1 $mgmL^{-1}$ mother solution; for *MIPs* and *NIPs X* and *W* DMSO solutions of 75 and 150 μgmL^{-1} were prepared from 1 $mgmL^{-1}$ mother solution in DMSO, while for *MIP V* and *NIP V* 100 and 200 μgmL^{-1} DMSO solutions were prepared. Concentrations of

MIPs and *NIPs S*, *T*, *U* and *U-UV*, containing **11**, were 25 and 50 μgmL^{-1} in water, by diluting 1 $mgmL^{-1}$ DMSO mother solutions.

UV-Visible absorbance measurement of 500 µL of each nanogel DMSO solution was performed using 1 mL black quartz cuvette with 1 cm of light path.

HPLC rebinding assay

1 $mgmL^{-1}$ suspension of each polymer in 50 µM imatinib aqueous solution was incubated for 24 hours at room temperature, under magnetic stirring. The suspensions (except for *MIP Q* and *NIP Q*) were kept in dialysis tube to allow separation of polymers from unbound irinotecan solution. Aliquots (200 µL) of the solution outside the dialysis tube were taken after 10, 30, 60, 90, 180 and 1440 minutes of incubation were directly analysed at HPLC, skipping the centrifugation step.

For *MIP Q* and *NIP Q* an aliquot (200 µL) of each suspension was taken after the above mentioned incubation times; polymers were separated by unbound irinotecan by centrifugation at 15000 rpm for 10 minutes, and supernatants were analysed at HPLC. By subtraction of unbound irinotecan to initial irinotecan concentration it was possible to obtained the bound drug concentration and get the binding kinetic of each polymer.

Isocratic elution was performed using a flux of 1 $mLmin^{-1}$, an eluent consisting of 85% of water with 0.05% TFA and 15% of acetonitrile with 0.05% TFA, and absorbance wavelength at 270 nm.

Fluorescence measurements

Polymers binding capabilities were studied through fluorescence titrations with increasing amounts of imatinib in various media. 400 µL of each polymer solution were poured in a quartz cuvette with light path of 0.5 cm; imatinib solutions employed for the titrations were prepared in the same media in which polymers were dissolved, and 2 µL of each solution were added to each polymer, with a maximum of 20 additions; irinotecan solutions in water or 3:1 methanol:water were kept in ice-bath while titrations were performed, to slow down drug degradation. At least 5 minutes were waited after each drug addition, before fluorescence measurement. The specific conditions of the experiments are divided by type of fluorescent monomer employed for nanogels synthesis.

- *MIPs containing 1,8-naphtalimide derivatives*: 60 gmL^{-1} *MIP Q* and *MIP R* solutions in 3:1 methanol:water mixtures were prepared by diluting 1 $mgmL^{-1}$

mother solutions in DMSO. *MIP Q* was filtered on 0.45 µm PTFE filter before starting the titration, and excitation and emission wavelengths employed for it were 453 and 525 nm, setting the excitation and emission slits at 5 and 10 nm, respectively; while, for *MIP R* excitation and emission wavelengths used were 448 and 530 nm, respectively, setting both slits at 5 nm.

- *MIPs containing fluorescein*: 20 µgmL^{-1} *MIP S* solution in water was obtained by diluting 1 mgmL^{-1} DMSO mother solution; excitation and emission wavelengths were fixed at 487 and 513 nm, setting both slits at 5 nm.

- *MIPs containing EDANS*: all the following solutions were prepared by diluting 1 mgmL^{-1} DMSO nanogel solution with the appropriate solvent. For 20 µgmL^{-1} *MIP W* titration in water excitation and emission wavelengths employed were 337 and 498 nm, respectively, setting both slits at 5 nm. For 10 µgmL^{-1} *MIPs W* and *W-UV* titrations in water excitation and emission wavelengths were fixed at 335 and 487 nm, respectively, using excitation and emission slits of 3 and 7 nm (MIP W) and 3 and 7 nm (MIP W-UW). For *MIP X* and *NIP X* titrations in water the excitation and emission wavelengths were fixed at 335 and 485 nm, respectively, adjusting the slits upon polymer concentrations, from 5 nm for both slits (60 µgmL^{-1} *MIP X*) to 10 and 20 nm, for excitation and emission beams, respectively (for *MIP X* 10 µgmL^{-1}).

Trials in plasma

Pooled plasma was processed with methanol as previously described; 3:1 methanol:plasma supernatants were then evaporated at high vacuum centrifuge at 37 °C. The obtained dried plasma was then suspended in water at the same initial volume of 3:1 methanol:water samples. This "regenerated" plasma was then further diluted with 3 or 9 volumes of water for dissolving *MIP X.*

400 µL of 10 µgmL^{-1} *MIP X* solution in regenerated plasma diluted 3 or 9 times was titrated with increasing amount of imatinib solutions (from 100 nM to 15 µM), prepared in water and kept in ice-bath while the experiment was carried out. The excitation and emission wavelengths employed were 333 and 485 nm, respectively, setting the excitation and emission slits at 5 and 8 nm.

[1] Pellizzoni E., *Molecularly Imprinted polymeric nanoparticles for the Therapeutic Drug Monitoring of Anticancer Drugs*, PhD Thesis in Nanotechnology (2015)

[2] Konstantinova T.N., Meallier P., Grabchev I., *The synthesis of some 1,8-naphtalic anhydride derivatives as dyes for polymeric materials*, Dyes and Pigm. (1993) 22: 191-198

[3] Bürger H.M., Manley P.W., Mutz M., *Salt forms of 4-(4-methylpiperazin-l-ylmethyl)-n-[4-methyl-3-(4-pyridin-3-yl)pyrim-idin-2-yl amino)phenyl]-benzamide*, WO 2005/075454 A2 (2005)

[4] Miyata T., Uragami T., Okawa K., *Stimulus responsive gel with optical characteristic molecule introduced therein, external stimulus measuring apparatus making use of the same, and method of measuring external* stimulus, WO 2006/118077 (2006)

7. Conclusions

In this thesis project, a set of six 1,8-naphtalimide fluorophores and one polymerisable derivative of EDANS have been prepared and characterized, in order to get fluorescent functional monomers to be incorporated in the Molecularly Imprinted Polymers, for both irinotecan and imatinib. The synthesis of the naphtalimide derivatives was optimized, thanks to the support of the microwaves, for the nucleophilic aromatic substitution, that allowed to obtain pure compounds in a very short reaction time and high yields. Besides the newly synthesized fluorescent functional monomers, fluorescein O-acrylate was also considered.

The interactions of the fluorescent compounds and fluorescein O-acrylate, with each anticancer drug were studied through ^{1}H-NMR titrations, in order to select the best monomer-template matches for the pre-polymerisation complexes.

Twenty-two different fluorescent MIPs were prepared, sixteen imprinted with irinotecan and six with imatinib, following a high dilution radical polymerisation approach, in order to obtain MIPs with high sensitivity, specificity, good yields, optimal optical response and compatibility with the final environment in which the polymer should operate. To optimize all these parameters, the following variables were taken into consideration: composition, incorporation of a co-monomer and reaction conditions. A long empirical work was carried out to improve MIPs performance, through optimization of the above mentioned factors, also on the basis of the template features.

The results obtained showed that, using imatinib and irinotecan as templates (maybe because they are both cations), the incorporation of a co-monomer was not favourable, as a competition with the fluorescent functional monomer was observed. Good MIPs sensitivity was obtained, but specificity remains an open issue for the molecular imprinting of these anticancer agents. MIPs selectivity was implicitly faced off, as plasma is a complex matrix and already contains almost all the possible interfering materials; hence, the investigations of MIP performance in human plasma allowed to account for the selectivity of the polymeric materials.

Finally, after solving various aspects of human plasma samples preparation, also due to the different drug solubility in the usually employed organic solvents, a favourable conclusion was achieved: among the examined solvents, methanol was excluded from samples treatment, and another solvent, anyhow employed for clinical analysis, was used, namely acetonitrile. In 3:1 acetonitrile:plasma conditions, it was possible, for *MIP L* (imprinted for the irinotecan), to develop a proof of concept of an analytical method, showing good robustness, precision and an acceptable Limit of Detection (9 nM).

As to MIPs designed to detect imatinib, the main issues were the incompatibility of *MIP X* with methanol and DMSO, and the drug insolubility in acetonitrile; a method that required two steps was however developed, and an interesting proof of concept was achieved, showing very high *MIP X* fluorescence variations, upon binding to the imatinib, and satisfactory sensitivity. Further studies should be performed on the robustness and accuracy of this method, by investigating *MIP X* performance at lower imatinib concentrations, in the nanomolar range.

Acknowledgments

I would like to thank:

The italian association AIRC for funding this project, and Dr. Giuseppe Toffoli (CRO) for giving me the possibility to attend this Ph.D. course

Prof Marina Resmini (Queen Mary University of London), and her research group, for the precious time she spent with me, her advices and help for the MIPs synthesis

My research group, in particular Giorgia, Elena, Anggy, Valentina and Sara, for supporting me and making laboratory life a wonderful experience

Professor Felluga, Benedetti, Milani and all the members of the Department of Chemical and Pharmaceutical Science

Walter, Giacomo and Luca, for their contributions to this thesis

Alois Bonifacio and Stefano Fornasaro of the Department of Engineering, for all the MIPs-SERS trials

Matjaz, Jasmina and Ales (Cobik)

Special thanks to Cristina, for her support and kindness, and to Federico, for his limitless patience and positivity, for improving my little knowledge in Chemistry and giving me the possibility to experience a real scientific research.

Finally, I want to thank all the people who helped me for taking care of my baby, during the last year of my Ph.D.; a very big special thank goes to Gabriele and Giacomo for bearing and loving me every day, reminding me how beautiful and unique life can be.